



The
University
Of
Sheffield.

Synthesis of [^{13}C]-labelled Combretastatin A1P

By

Rebecca Christina Collins

A thesis submitted in partial fulfilment of the requirements for the degree of
Doctor of Philosophy

The University of Sheffield
Faculty of Science
Department of Chemistry

Submission Date: September 2015

Contents

Declaration	iv
Acknowledgements	v
Abbreviations	vi
Abstract	xi
1. Introduction	1
1.1. Cancer treatment	1
1.2. Vascular Disrupting Agents	2
1.2.1. Tubulin and microtubules	4
1.2.2. Tubulin Inhibitors	5
1.3. Combretastatins	7
1.3.1. Combretastatins as vascular disrupting agents	9
1.4. Combretastatin Analogues	10
1.5. Synthesis of combretastatins	12
1.5.1. Synthesis of combretastatins by the Wittig reaction	12
1.5.2. Synthesis of combretastatins by Cross coupling reactions	14
1.5.3. Synthesis of combretastatins by Selective Reduction of diarylalkynes	18
1.5.4. Synthesis of pro-drugs CA1P and CA4P	20
1.6. Combretastatin A1P metabolism	21
1.7. Molecular Imaging	27
1.8. Enhancing MR signal by hyperpolarisation	28
1.9. Applications of hyperpolarised MR	30
1.10. Hyperpolarisation considerations and techniques	32
1.10.1. Brute Force	33
1.10.2. Optical pumping	33
1.10.3. Para-Hydrogen induced polarisation	34
1.10.4. Dynamic nuclear polarisation	35
1.11. Dissolution-DNP experiment	35
1.12. Hyperpolarised substrates	37
1.12.1. ¹³ C DNP probe development	38
1.13. Project Aims	40

2. Synthesis of [¹³C]-Combretastatin A1P	41
2.1. <i>T</i> ₁ times of CA1P	41
2.2. Synthesis of core aromatic species	42
2.3. Synthesis of CA1P <i>via</i> Selective Reduction of diarylalkyne	50
2.4. Synthesis of CA1P <i>via</i> the Wittig reaction	73
2.5. Synthesis of [¹³ C]-CA1P	89
2.6. Synthesis of [¹³ CD ₃]-CA1P	94
3. Conclusions	99
4. Experimental	103
4.1. General	103
4.2. Synthesis towards [¹² C]-CA1P	105
4.3. Synthesis towards [¹³ C]-CA1P	146
5. References	159

Declaration

The thesis records the work carried out in the Department of Chemistry, University of Sheffield, UK and Singapore Bioimaging Consortium (SBIC), Agency of Science, Technology and Research (A*STAR), Singapore between October 2011 and September 2015 and is original except where acknowledged by reference.

No part of this work is being, nor has been, submitted for a degree, diploma or any other qualification at any other university.

Acknowledgements

First and foremost, a huge thanks goes to Dr. Simon Jones for giving me the opportunity to take up a PhD within his research group. I am extremely grateful for all his help, support and advice during my time in Sheffield. Thanks also goes to everyone from E26 over the years with a special mention going to Jonny, Dr. Reeder, Jenna, Matt, Bryony, Dan J, Dan C, Claire, Ashlie and Esther for their support, entertainment and knowledge.

A big thank you goes to all the technical staff in the Department of Chemistry. In particular Rob Hansen (HPLC), Sue Bradshaw (nOe-NMR), Jenny Louth (elemental analysis), Simon Thorpe and Sharon Spey (Mass Spec.). I am also very grateful for the work done by Dr. Ed Cochrane on the $^{13}\text{CD}_3$ synthesis.

From the medical school, I would like to thank Prof. Gill Tozer and Prof. Martyn Paley for their feedback and support. As well as Dr. Steven Reynolds, for his help with NMR and T_1 experiments. I would like to thank SBIC, A*STAR and my supervisor Dr. Weiping Han for the opportunity to spend a year in Singapore. From SBIC a special thanks goes to Dr. Ed Robins for giving me the opportunity to work alongside his group and provide me with valuable lab space and guidance. I would also like to thank Dr. Anna Haslop for her support and encouragement.

Outside of the PhD, I would like to thank my family and George. For their constant love and support, for keeping me sane and making me smile.

Abbreviations

18-C-6	18-Crown-6 (1,4,7,10,13,16-hexaoxacyclooctadecane)
Å	ångström
Ac	Acetyl
aq.	Aqueous
A- ^{ta} Phos	Bis(di- <i>tert</i> -butyl(4-dimethylaminophenyl)phosphine)
atm	atmospheric
ATP	Adenosine triphosphate
B ₀	External magnetic field strength
9-BBN	9-Borabicyclo[3.3.1]nonane
BDPA	α,γ -bisdiphenylene- β -phenylallyl
Bn	Benzyl
Bu	Butyl
<i>c</i>	Concentration
CA1	Combretastatin A1
CA1MPA	Combretastatin A1 monophosphate A
CA1MPB	Combretastatin A1 monophosphate B
CA1G1	Combretastatin A1 monoglucuronide 1
CA1G2	Combretastatin A1 monoglucuronide 2
CA1P	Combretastatin A1 phosphate
CA4	Combretastatin A4
CA4P	Combretastatin A4 phosphate
CAN	Ceric ammonium nitrate
cat.	Catalytic
conc.	Concentrated
d	doublet
Da	Dalton
DCM	Dichloromethane
dd	doublet of doublets
DDQ	2,3-Dichloro-5,6-dicyano-1,4-benzoquinone
DIPEA	<i>N,N</i> -Diisopropylethylamine
DMAP	4-Dimethylaminopyridine

DMDO	Dimethyldioxirane
DME	Dimethoxyethane
DMF	Dimethylformamide
DMS	Dimethylsulfide
DNA	Deoxyribonucleic acid
DNP	Dynamic nuclear polarisation
dppf	1,1'-Bis(diphenylphosphino)ferrocene
dt	Doublet of triplets
eq.	Equivalents
ESI	Electrospray ionisation
Et	Ethyl
ETDA	Ethylenediaminetetraacetic acid
FDA	Food and Drug Administration (USA)
FT-IR	Fourier transform infrared spectroscopy
g	Gram
G	Giga
GI ₅₀	Concentration where 50% of cell growth is inhibited
GTP	Guanosine-5'-triphosphate
h	Hour
ħ	Planck's constant over 2π
HP	Hyperpolarised
HPLC	High performance liquid chromatography
Hz	Hertz
IC ₅₀	Concentration where 50% of activity is inhibited
<i>i</i> Pr	Isopropyl
JMOD	<i>J</i> -Modulated spin echo
k_B	Boltzmann constant
L	Litre
LC	Liquid chromatography
LC-DAD-MS	Liquid chromatography with ultraviolet diode-array-detector
LC-ESI-MS	Liquid chromatography with electrospray ionisation mass spectrometry
LC-MS	Liquid chromatography mass spectrometry

LC-UV	Liquid chromatography with ultraviolet detector
m	metre, milli or multiplet
M	mol dm ⁻³
<i>m</i> CPBA	<i>meta</i> -Chloroperoxybenzoic acid
Me	Methyl
MEOP	Metastable-exchange optical pumping
mol	moles
min	minutes
MOM	Methoxymethyl
MR	Magnetic resonance
MRI	Magnetic resonance imaging
MRS	Magnetic resonance spectroscopy
MRSI	Magnetic resonance spectroscopy imaging
MS	Mass spectrometry
n	Nano
N_{α}	Population of the α spin state
N_{β}	Population of the β spin state
NaHMDS	Sodium bis(trimethylsilyl)amide
NCS	<i>N</i> -chlorosuccinimide
NIS	<i>N</i> -iodosuccinimide
NMP	1-Methyl-2-pyrrolidone
NMR	Nuclear magnetic resonance
nOe	Nuclear Overhauser effect
nuc	Nucleophile
<i>O</i>	Ortho
<i>P</i>	Polarisation
Pa	Pascal
pent.	Pentuplet
PET	Positron emission tomography
PG	Protecting group
Ph	Phenyl
PHIP	Parahydrogen-induced polarisation
ppm	Parts per million

Pr	Propyl
P_{th}	Polarisation at thermal equilibrium
Rad	Radian
R_f	Retention factor
rt	Room temperature
s	singlet
SAR	Structure-activity-relationship
sat.	Saturated
SEOP	Spin-exchange optical pumping
SM:P	Starting material:Product
SNR	Signal-to-noise ratio
SPECT	Single photon emission computed tomography
t	Triplet
<i>t</i>	Tertiary
T	Tesla
<i>T</i>	Temperature
T_1	Longitudinal (or spin-lattice) relaxation time
TBAF	Tetra- <i>n</i> -butylammonium fluoride
TBS	<i>Tert</i> -butyldimethylsilyl
td	Triplet of doublets
TEMPO	2,2,6,6-tetramethyl-piperdine-1-oxyl
Tf	Trifluoromethanesulfonate
TFA	Trifluoroacetic acid
THF	Tetrahydrofuran
TLC	Thin Layer Chromatography
TMEDA	<i>N,N,N',N'</i> -tetramethylethylenediamine
TMS	Trimethylsilyl
UV	Ultraviolet
UV-vis	Ultraviolet-visible spectroscopy
Vis	visible light
VDA	Vascular disrupting agent
vs.	Versus
VTA	Vascular targeting agent
w/w	weight/weight

μ	Micro
δ	Chemical shift
γ	Gyromagnetic ratio

Abstract

Combretastatin A1P **9** is an anti-cancer drug that works as a vascular disrupting agent. CA1P **9** binds to tubulin causing irreversible microtubule destabilisation and results in the destruction of endothelial cells that line tumour blood vessels. The high cytotoxicity of CA1P **9** *in vivo* is thought to be due to the formation of *ortho*-quinone species. Whilst quinone-glutathione adducts have been detected by LC-MS in murine urine and blood, these *ortho*-quinone metabolites have not been directly observed *in vivo*. However, these short-lived metabolites can be imaged *in vivo* using hyperpolarised MRS. Hyperpolarisation is a technique that increases the sensitivity of magnetic resonance techniques and allows for the detection of ^{13}C -labelled compounds and their downstream metabolic products in real-time *in vivo*. Therefore to investigate the *ortho*-quinone metabolites of CA1P **9**, a route for the synthesis of ^{13}C -labelled CA1P [^{13}C]-**153** was developed (Scheme 1).

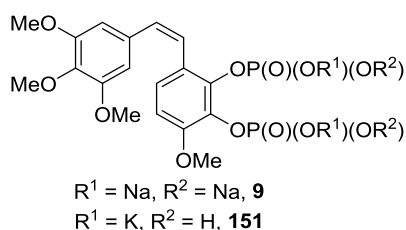
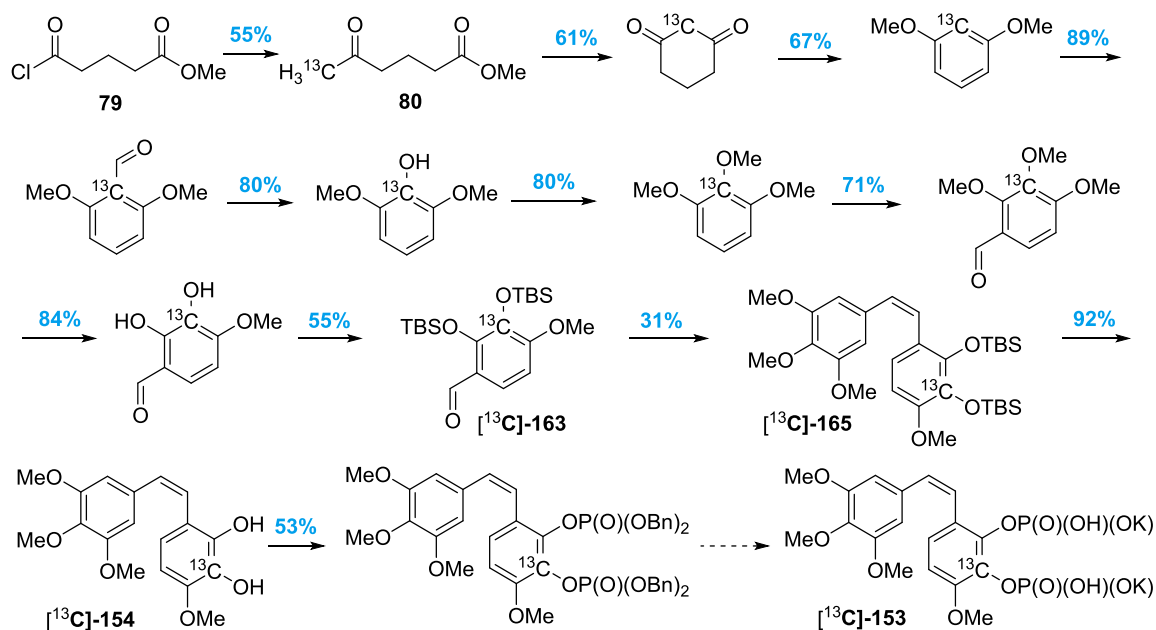


Figure 1: Tetrasodium **9** and dipotassium **151** combretastatin A1P.

The location of the ^{13}C label was chosen at a site with a long T_1 relaxation time in order to maximise the lifetime of the hyperpolarisation. For economic reasons, the route was first developed using ^{12}C material. Attempts were first made to develop a route for the synthesis of CA1P by the selective reduction of a diarylalkyne. This strategy was envisioned to be high yielding and 100% *Z*-selective. Unfortunately, difficulties were had in finding efficient regioselective iodination conditions for a suitable ^{13}C -labelled precursor which would be used in the formation of the diarylalkyne *via* a Sonogashira reaction. Therefore a Wittig strategy was employed for the synthesis of CA1P [^{13}C]-**153**.



Scheme 1: Route towards the synthesis of ^{13}C -labelled combretastatin A1P [^{13}C]-**153**.

The synthesis started with the regioselective insertion of a ^{13}C label into an aromatic ring. This was achieved by [^{13}C]-methylcuprate addition to the acid chloride **79**, and the resulting ketone [^{13}C]-**80** was cyclised then aromatised. A hydroxyl group was then inserted into the 2-position *via* a formylation and Baeyer-Villiger oxidation. CA1 [^{13}C]-**154** was then synthesised by a Wittig reaction with the aldehyde component [^{13}C]-**163** synthesised from the core aromatic species containing the ^{13}C label. The Wittig reaction preceded with an *E/Z* ratio of 18:82 and the resulting *Z*-isomer [^{13}C]-**165** was deprotected to reveal CA1 [^{13}C]-**154**. Conversion of CA1 [^{13}C]-**154** to its prodrug [^{13}C]-**153** was attempted, replicating the conditions established in the ^{12}C synthesis, however the small scale of the reaction prevented the clean isolation of CA1P [^{13}C]-**153**. The ^{12}C -synthesis of CA1P **151** involved 13 steps and had an overall yield of 1.2%.

Chapter 1: Introduction

1.1. Cancer treatment

Cancer is a broad group of diseases defined by uncontrolled cell growth. In humans there are over 200 known types of cancer that have the potential to affect every organ in the body and can develop in almost every type of cell. The complexity of the diseases means they can be hard to treat, making cancer the leading cause of death in the developed world. The GLOBOCAN 2012 project estimates there were 14.1 million diagnoses and 8.2 million deaths due to cancer in 2012 worldwide.¹

Understanding how cancer cells differ from normal cells is fundamental in developing selective treatments for cancers. Hanahan and Weinburg proposed six hallmarks of cancer in their 2011 review:²

1. *Self-sufficiency in growth signals*: Normal cell growth is controlled by appropriate growth factors. Tumour cells have shown a reduced dependence on exogenous growth stimulation caused by having the ability to generate their own growth signals which leads to uncontrolled growth. This ability also disrupts the important homeostatic mechanisms that dictate normal cell behaviour.
2. *Insensitivity to anti-growth signals*: Normal cells have a number of growth-inhibitor signals which are there to maintain cellular quiescence and tissue homeostasis. Tumour cells either disrupt or ignore these signals allowing for uncontrolled growth.
3. *Limitless replicative potential*: Normal cells have an intrinsic cell-autonomous programme that limits their multiplication *i.e.* once a cell has replicated a certain number of times it will stop replicating. Tumour cells have a way to overcome this and therefore have limitless replicative potential.
4. *Evading apoptosis*: Normal cells undergo apoptosis (programmed cell death) when damaged or old, whereas tumour cells acquire a resistance to apoptosis. 50% of cancers show a mutation in the p53 gene which is a gene that suppresses cell growth. This mutation results in the formation of the p53 protein without the DNA damage sensor a key component that starts the apoptosis mechanism.

5. *Tissue invasion and metastasis:* Normal cells produce a chemical that allows cells to adhere to each other. Cancer cells do not produce these substances and, therefore, can “float away” to other regions of the body *via* the blood supply or lymph fluid where they can form tumours in different locations where nutrients and space are not as limiting.
6. *Sustained angiogenesis:* Normal tissue undergoes angiogenesis when growing or repairing damaged tissue. In cancer tissue angiogenesis is deregulated, allowing new blood vessels to form even when growth or repair is unnecessary.

Other significant differences between normal and healthy cells include:

7. *Rate of growth:* Cancer cells reproduce rapidly before cells have a chance to mature and differentiate and, therefore, remain immature and non-specialised.
8. *Energy source:* Normal cells are in an aerobic environment, so get the majority of their energy from the ATP produced in the Krebs cycle, and a smaller amount from the ATP produced *via* glycolysis. Cancer cells however have a lot higher rates of glycolysis even in regions of high oxygen concentration. This is known as the Walburg effect.
9. *Communication:* Normal cells stop growing when they encounter another cell and there is no more free space (contact inhibition). Cancer cells do not have the ability to communicate with other cells through chemical signals, and therefore can invade nearby tissue.

Along with surgery and radiation therapy, chemotherapy is a common treatment of cancer. Traditional chemotherapy drugs target cells that rapidly divide; a key property of cancer cells. However, these drugs are often non-selective so will also damage fast-growing healthy cells, causing side-effects; for example, cells in hair follicles (hair loss) and blood-forming cells in bone marrow (low blood count). Therefore, the ability to differentiate between malignant cancer cells and healthy cells is vital to increase the effectiveness of treatment and reduce side effects.

1.2. Vascular disrupting agents

Tumours are not just a collection of tumour cells; they are complex structures surrounded by a “tumour microenvironment” which includes a network of blood vessels, immune cells and fibroblast cells. An important difference between normal and cancerous tissue

is their vasculature. Oxygen and nutrients supplied by the blood supply are crucial for cell function and survival. The blood supply also provides the main route for metastatic spread. Almost all cells in the tissue reside within 100 μm of a capillary blood vessel, so disruption of the blood supply in solid tumours will deprive the tumour of vital nutrients. Furthermore, the build-up of toxic waste could result in cell death and tumour degeneration.

The differences in the vasculature of normal and tumour cells can be exploited, and led Denekamp to propose a vascular targeting approach to cancer therapy for solid tumours in 1982.³ Anti-cancer drugs that target the vascular system of tumours are known as vascular targeting agents (VTAs). VTAs can be divided into two groups; anti-angiogenic drugs and vascular disrupting agents. Anti-angiogenic drugs work by preventing angiogenesis, the formation of new blood vessels. They are known as cytostatic drugs because they hinder the growth of new tumour cells, thereby stabilising the tumour and preventing metastasis. However, this means that the already established cancer cells and tumour vasculature will remain undamaged and, therefore, anti-angiogenesis drugs will need to be used in conjunction with other chemotherapeutic methods for effective treatment. Unlike anti-angiogenesis drugs, vascular disrupting agents (VDAs) selectively target existing tumour blood vessels rather than preventing the production of new ones. Disrupting existing vasculature will cause rapid occlusion of blood flow to the tumour, depriving the tumour of oxygen and nutrients. VDAs target endothelial cells that line the vasculature throughout the entire tumour and, therefore, have the potential to affect every cell in the tumour. This strategy has the advantage over the traditional treatment of targeting abnormal tumour cells where the drug often cannot reach the core of the tumour. These drugs take advantage of the many differences between normal and tumour vasculature.

An important difference between tumour and normal tissue is the cytoskeleton of their vascular endothelial cells. A cell cytoskeleton is made up of three components; microfilaments (actin filaments), intermediate filaments and microtubules. The ratios of these components vary for normal and tumour cells. The structure and shape of normal cells are supported by a scaffold of microtubules as well as a well-defined actin cytoskeleton due to the dense band of actin microfilaments.⁴ Tumour cells, however, rely

heavily on a tubulin-microtubule cytoskeleton. This causes the endothelial cells in normal vasculature to be mature, regular and well-defined whereas the tumour endothelial cells are structurally disorganised and irregular, relying more on a tubulin cytoskeleton to maintain their shape. As well as differences in the cytoskeleton, the endothelial cells lining blood vessels in tumours proliferate at a much higher rate than those in normal tissue, so they have a significantly increased rate of mitosis.⁵ The mitotic spindle is a key component in mitosis and is a collection of spindle fibres that form during mitosis. During mitosis, the two daughter chromosomes align themselves along the mitotic spindle, which is used to pull the duplicated chromosomes apart to opposite poles. The mitotic spindle is made up of microtubules which form from the polymerisation of α - and β -tubulin.

1.2.1. Tubulin and microtubules

Microtubules are cytoskeletal protein polymers and play essential roles within eukaryotic cells. These include maintaining cell shape, cell division, motility, signalling and intracellular organelle transport.⁶ Microtubules are long, hollow, cylindrical tubes that are approximately 25 nm in diameter and 200 nm – 25 μ m in length. They are composed of two protein subunits: α - and β - tubulin. These subunits polymerise to form α , β -heterodimers which assemble head-to-toe into long protein fibres called protofilaments. It is these protofilaments that form the backbone of the microtubules. The microtubules have polarity due to the head-to-toe assembly of the heterodimers: the α -tubulin end is negatively charged and the β - tubulin end is positively charged. They can undergo highly-regulated rapid assembly and disassembly by reversible association and dissociation of α,β - heterodimers to either end of the microtubule. The microtubule polymerisation occurs through a nucleation-elongation mechanism. This starts with the slow formation of a microtubule nucleus and is followed by fast elongation by reversible, non-covalent addition of tubulin subunits. Microtubules are highly dynamic and alternate between periods of growing and shrinking by the addition or removal of tubulin subunits at the ends of the microtubule. The energy required is provided by the hydrolysis of the GTP-tubulin complex when it adds to the microtubule.

The dynamics of microtubules are crucial for mitosis since the mitotic spindle is made up of microtubules. The mitotic spindle plays a role in all stages of mitosis. At first, the cytoskeletal microtubule network is dismantled, then a spindle-shaped collection of microtubules are formed by polymerising tubulin and this forms the mitotic spindle. Next, the chromosomes are attached to the spindle and line up along the metaphase plate whilst still being attached to the microtubules. These chromosomes then separate and the two chromatids migrate to the opposite spindle poles when the microtubules shorten, and in the final stage the mitotic spindle is dismantled. The rapid dynamics of the microtubules are vital in the delicate movement of the chromosomes, as well as the assembly and disassembly of the mitotic spindle.

1.2.2. Tubulin inhibitors

Microtubules play an essential role in mitosis, and a characteristic of cancer cells is that they divide more frequently and, therefore, have an increased rate of mitosis. Their importance in mitosis makes microtubules a significant target for anti-cancer drugs since their disruption will prevent cell division and cause cell death by apoptosis. There are a large number of compounds which bind to tubulin and, therefore, inhibit cell proliferation and a number have progressed into clinical use. Many of these compounds are derived from natural products and have been isolated from a broad range of species including bacteria, plants and sponges. The majority of anti-mitotic drugs bind to soluble tubulin or to tubulin in the microtubules. At high concentrations these anti-mitotic compounds depolymerise microtubules, but at low concentrations they work by suppressing or stabilising microtubule dynamics without changing microtubule mass, resulting in mitotic disruption and subsequently cell death.⁷ Tubulin-binding agents can be broadly classified as either microtubule-stabilising drugs (*e.g.* taxanes and epothilones) or as microtubule-destabilising (*e.g.* vincristine, colchicine or combretastatins) and are known to bind to specific sites on the tubulin dimer. They generally bind to one of three main binding sites on tubulin; the paclitaxel site, the *vinca* domain or the colchicine site, the latter being associated with vascular targeting agents.

Tubulin polymerisation promoters (or microtubule-stabilisers) are a class of drugs that work by promoting the assembly of tubulin into microtubules and, therefore, interferes

with the breakdown of the mitotic spindle at the end of mitosis, which ultimately leads to cell death. Taxanes are a type of tubulin polymerisation promoter an example of which is paclitaxel **1** (Taxol®) which was approved for medical use in 1992 and has continued to be routinely used to treat a number of solid tumours such as ovarian, breast, lung, bladder and prostate (Figure 2).⁸ Other tubulin polymerisation promoters that have the same mechanism of action include a group of natural products called epothilones. A large number of epothilones have been advancing in clinical trial and ixabepilone **2** has recently, in 2007, been approved by the FDA for the treatment of breast cancer.⁸

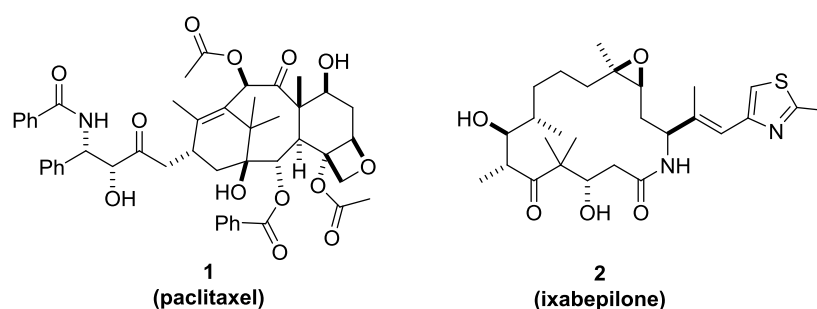


Figure 2: Tubulin polymerisation promoters.

Tubulin polymerisation inhibitors (or microtubule-destabilisers) work by preventing tubulin assembly into microtubules. The most studied inhibitors are the *vinca* alkaloids which were isolated from the *Catharanthus roseus* leaves and were found to have anti-cancer properties in the 1950s.⁹ The *vinca* alkaloid vinblastine **3** was the first tubulin inhibitor to go into clinical trials and is currently used to treat bladder and other cancers (Figure 3). Vadimezan **4** is another vasculature disrupting agent advanced to human clinical trials.

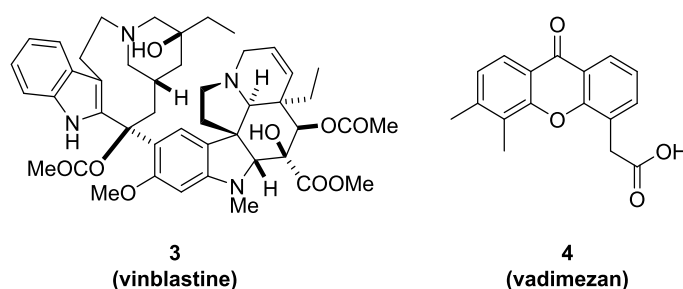


Figure 3: Tubulin polymerisation inhibitors.

Colchicine **5** is also a compound that depolymerises microtubules at high concentrations but stabilises them at low concentrations (Figure 4). Colchicine **5** inhibits microtubule depolymerisation sub-stoichiometrically so is likely to bind to the microtubule ends rather

than free tubulin. Colchicine **5** unfortunately has a low therapeutic ratio and high toxicity which has prevented it from proceeding further in clinical trials. However, the recent AstraZeneca compound ZD6126 **6**, a colchicine analogue, has made it into clinical trials as a vascular disrupting agent.¹⁰ ZD6126 **6** structurally resembles colchicine **5** but differs by containing a benzenoid ring instead of the tropolone ring in colchicine. ZD6126 **6** is a water-soluble pro-drug which is converted to active *N*-acetylcolchinol *in vivo*. The final class of microtubule-destabilisers are the combretastatins, they bind to β -tubulin at the “colchicine binding site” but with a higher affinity than colchicine. Microtubule-binding agents are classically known for their anti-mitotic properties, however agents such as combretastatins have shown rapid anti-vascular effects and are being investigated as potential vascular disrupting agents.

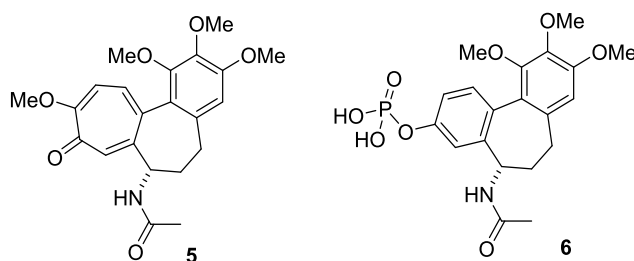


Figure 4: Colchicine **5** and the vascular disrupting agent ZD6126 **6**.

1.3. Combretastatins

Combretastatins were first isolated from the bark of the South African bush willow tree *Combretum caffrum* by Pettit and co-workers in the late 1980s (Figure 5).¹¹ Of the 17 isolated compounds, combretastatin A4 **7** was shown to be the most potent against a panel of tumour cells, with CA1 **8** about one fifth as potent. Combretastatins have been shown to be highly selective towards tumour vasculature and cause significant tumour damage with minimal side effects. This has led to extensive studies of CA1 **8** and CA4 **7** as potential anti-cancer drugs.

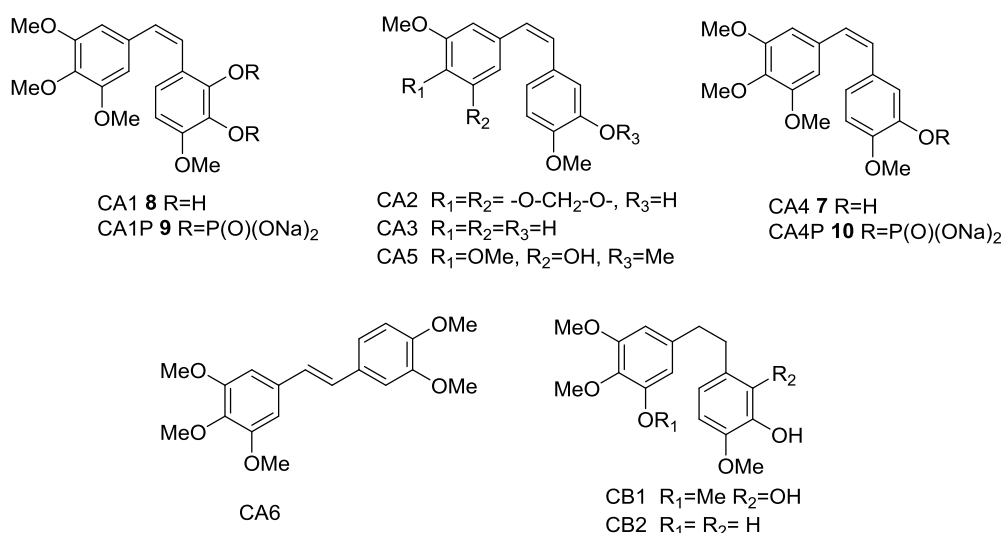


Figure 5: Structures of combretastatins isolated from *Combretum caffrum* and two combretastatin prodrugs CA1P **9** and CA4P **10**.

Combretastatins A1 **8** and A4 **7** show potent biological activity, however they have poor pharmacokinetic properties due to their low water solubility and high lipophilicity. To improve bioavailability, the phosphate pro-drugs CA1P **9** and CA4P **10** were formulated. Interestingly, although CA4 **7** is more potent than CA1 **8** against human cancer cells lines *in vitro*, at equal doses the corresponding prodrug CA4P **10** is less active than CA1P **9** in *in vivo* preclinical tumour growth delay studies. CA1 **8**, CA4 **7** and their corresponding pro-drugs show a wide variety of biological activity against human cancer cell lines (Table 1).^{12–14} CA4P **10** was the first combretastatin to go into clinical trials, entering phase I studies under the trade name Zybrestat™, and was shown to selectively reduce tumour blood flow at well-tolerated doses. CA4P **10** is currently in phase II clinical trials for the treatment of cervical, colorectal, lung, prostate, ovarian and thyroid cancers.¹⁵ The prodrug CA1P **9** (OXi4503) is currently undergoing Phase I human clinical trials for the treatment of primary and secondary hepatic tumours and has completed Phase I trials for the treatment of advanced solid tumours.

Compound	Tubulin Inhibition IC ₅₀ (μM)	Leukaemia P388 GI ₅₀ (μg/mL)	Pancreas BXP-3 GI ₅₀ (μg/mL)	CNS SF265 GI ₅₀ (μg/mL)	Lung-NSC NCI-H460 GI ₅₀ (μg/mL)	Colon KM20L2 GI ₅₀ (μg/mL)	Prostate DU-145 GI ₅₀ (μg/mL)
CA4	1.2 ^a	0.0003 ^b	0.39 ^b	<0.001 ^b	0.0006 ^b	0.061 ^b	0.0008 ^b
CA4P	>40 ^a	0.0004 ^b	0.23 ^b	0.036 ^b	0.029 ^b	0.034 ^b	0.0072 ^b
CA1	1.9 ^a	0.25 ^c	4.4 ^c	-	0.74 ^c	0.061 ^c	0.17 ^c
CA1P	>40 ^a	<0.01 ^c	1.5 ^c	0.036 ^c	0.038 ^c	0.53 ^b	0.034 ^c

^a From reference 12, ^b From reference 13, ^c From reference 14.

Table 1: Tubulin inhibition and human cancer cell line growth inhibition of CA1, CA1P, CA4 and CA4P.

1.3.1. Combretastatins as vascular disrupting agents

Combretastatins have been shown to rapidly disrupt the vascular network in tumours, which leads to secondary cell death. They destabilise microtubules, inducing death in proliferating endothelial cells by damaging mitotic spindles. Combretastatins A1 **8** and A4 **9** structurally resemble the antimitotic agent colchicine **5** and are also classed as tubulin binding agents, and in particular, tubulin polymerisation inhibitors.⁶ Upon administration, the CA1P prodrug **9** undergoes enzymatic dephosphorylation by endogenous non-specific phosphatases to the active metabolite CA1 **8**. Free CA1 **8** rapidly binds to β - tubulin in the α,β - tubulin heterodimer at the same site as colchicine **5**, known as the colchicine binding site, in the endothelial cells that line tumour vasculature. CA4 **7** has been shown to bind with a higher affinity to the colchicine binding site than colchicine **5** itself and unlike colchicine **5**, CA4P **10** is active well below its maximum tolerated dose.

The binding of CA1 **8** or CA4 **7** to tubulin suppresses the microtubule dynamics of the mitotic spindle, causing disruption to the mitotic spindle. As this will now not satisfy the spindle checkpoint the cell will undergo mitotic arrest.^{16,17} Combretastatins in particular target tumour vascular endothelial cells and destruction causes coagulation and thrombus formation to occur. This is followed by loss of blood flow, depriving the tumour of oxygen and nutrients which will result in secondary cell death due to malnutrition.^{18–20} CA1P **9** shows severe haemorrhagic necrosis in tumours after treatment and has seen almost 94% tumour necrosis within 24 hours of treatment.²¹

Treatment with CA4P **10** has been shown to result in a reduction of blood flow within the tumour and also results in haemorrhagic necrosis. It has a wide therapeutic window, since these results can be observed at doses of one tenth of the maximum tolerated dose, which is in contrast to other related tubulin-binding agents.²² However, CA4P **10** induces little growth retardation when administered as a single dose near the maximum tolerated dose, which has been attributed to the survival of a narrow rim of peripheral tumour cells. The existence of this “viable rim” at the end of treatment can result in rapid proliferation and revascularisation of the tumour. However, these cells can be treated with additional chemotherapy, since the tumour periphery is easily accessed by other high molecular

weight drugs. A common explanation for the existence of the “viable rim” is due to these cells receiving oxygen and nutrients from the surrounding undamaged normal tissue. However, this “viable rim” that remains after treatment with CA4P **10** is significantly smaller following treatment with CA1P **9**.

CA1P **9** has been shown to be more effective at producing tumour growth delays than CA4P **10**.²¹ At a 100 mg/kg dose, CA1P **9** induced significant retardation of tumour growth, whereas CA4P **10** showed no significant growth retardation with a single dose up to 400 mg/kg.²³ Therefore CA1P **9** has more potent antivasular effects when used as a single agent than CA4P **10**. The structural difference between CA1P **9** and CA4P **10** is the presence of an extra phosphoryl-protected hydroxyl group on one of the phenyl rings and clearly has a strong influence on the anti-tumour activity. It is possible that the extra phosphate group influences the pharmacokinetic, distribution and release profile of the active CA1 **8**. Once administered both CA1P **9** and CA4P **10** are dephosphorylated to CA1 **8** and CA4 **7** respectively by non-specific phosphatases.

1.4. Combretastatin analogues

The simplicity of the combretastatin skeleton has generated a vast number of analogues. Since CA4 **7** had the most potent *in vitro* antitumour activity of the combretastatins isolated by Pettit *et al.*, it has been used as a lead compound for the development of VDA drugs. However, both combretastatin A1 **8** and A4 **7** show little anti-neoplastic effects *in vivo* due to poor pharmacokinetics caused by low water solubility and high lipophilicity. As a result, more water soluble derivatives have been synthesised in order to improve water solubility and perhaps even increase cytotoxicity. Numerous water-soluble phosphate salts of CA1 **8** have been synthesised including lithium, potassium, caesium, magnesium, calcium, manganese, zinc, piperazine, 3-pyridinecarboxamide, morphine, (+)-and (-)-cinchonane-9-ol and benzeneacetonitrile salts.²⁴ These analogues were evaluated as potential pro-drugs, and the tetrasodium phosphate analogue **9** was found to have the best water solubility and is currently undergoing clinical trials (CA1P, OXi4503).

Structure activity relationship (SAR) studies provide information on the functional groups responsible for the biological activity and by synthesising analogues of a bioactive lead, a compound with higher potency could be found. SAR analysis of combretastatins and

their analogues by Pettit *et al.* shows that the correct alkene geometry of the combretastatin is essential for its cytotoxic activity; the *Z*-isomer has significantly greater cytotoxic activity than the corresponding *E*-isomer.^{11,25} The trimethoxybenzene (Ring A) moiety has also been shown to be essential for its activity.²⁶ A growing library of combretastatin analogues have been synthesised; these analogues typically include Ring A alterations, bridge-modifications, and/or Ring B alterations (Figure 6).

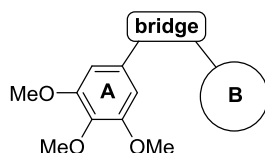


Figure 6: Analogues of CA1 **8** and CA4 **7** typically include Ring A with a modified bridge and/or Ring B alteration.

The search for more water-soluble derivatives that have similar or greater cytotoxic activity has led to the discovery of several analogues that are currently in human clinical trials (Figure 7). Ohsumi and co-workers synthesised a number of CA4 **10** analogues and evaluated their cytotoxicity effects against murine colon 26 adenocarcinoma and their inhibitory activity on tubulin polymerisation.²⁷ They proposed that the introduction of a nitrogen containing group into CA4 **10** could increase its water solubility. Replacement of the hydroxyl group in the C3 position with an amino group resulted in a noticeable increase in water solubility and *in vivo* antitumour activity against murine solid tumours. This has led to the analogue AC-7739 **11** being taken to pre-clinical development. Other analogues in pre-clinical development include Oxi6196 **12**, where the combretastatin bridge has been modified, and Oxi8006 **13** where Ring A has been altered. There are also a number of combretastatin analogues that have progressed to human clinical trials. Ombrabulin (AC-7700 or AVE8062) **14** is a water soluble analogue of CA4 **7** developed by Ohsumi and is currently in Phase I clinical trials for the treatment of advanced staged soft-tissue sarcoma and metastatic non-small cell lung cancer.^{28,29} Ombrabulin **14** is the prodrug and the serine group is cleaved by aminopeptides *in vivo* to reveal the active compound. In a similar fashion to CA1 **8** and CA4 **7**, Ombrabulin **14** binds to tubulin in tumour cells, depolymerising microtubules and causing vascular blood flow shutdown. Other analogues currently in human clinical trials include Crolibulin **15** and BNC 105P **16**.

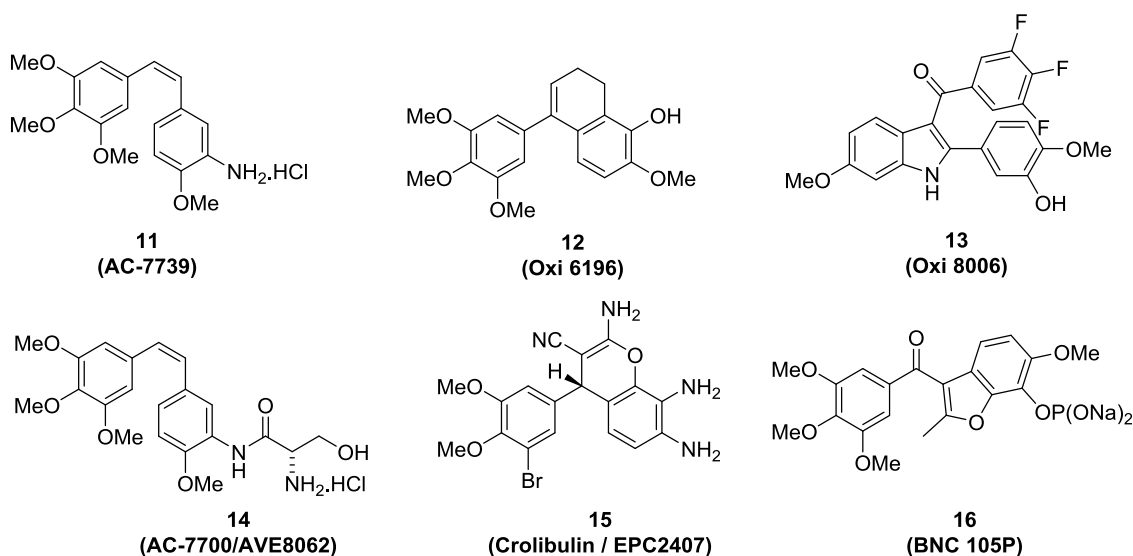


Figure 7: CA4 7 analogues in pre-clinical trials: Oxi8006, Oxi6196 and AC-7739 and human clinical trials: Crolibulin, BNC 105P and AC-7700.

1.5. Synthesis of combretastatins

Combretastatin molecules share several common features. They have two aromatic rings; a 1,2,3-trimethoxy ring (A ring) and 2,3-substituted ring or 2,3,4-substituted (Ring B). These rings are linked by a *Z*-ethene bridge; which has been shown to have much higher biological activity than the *E*-isomer. Therefore a convenient and stereoselective route for the preparation of combretastatins is needed. CA1 8 differs from CA4 7 by only one hydroxyl group on the B ring and this causes them to have different biological activities (Table 1, Figure 8).

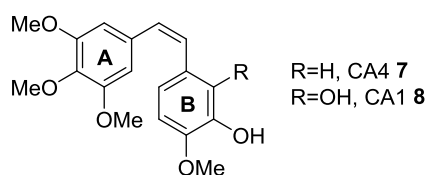
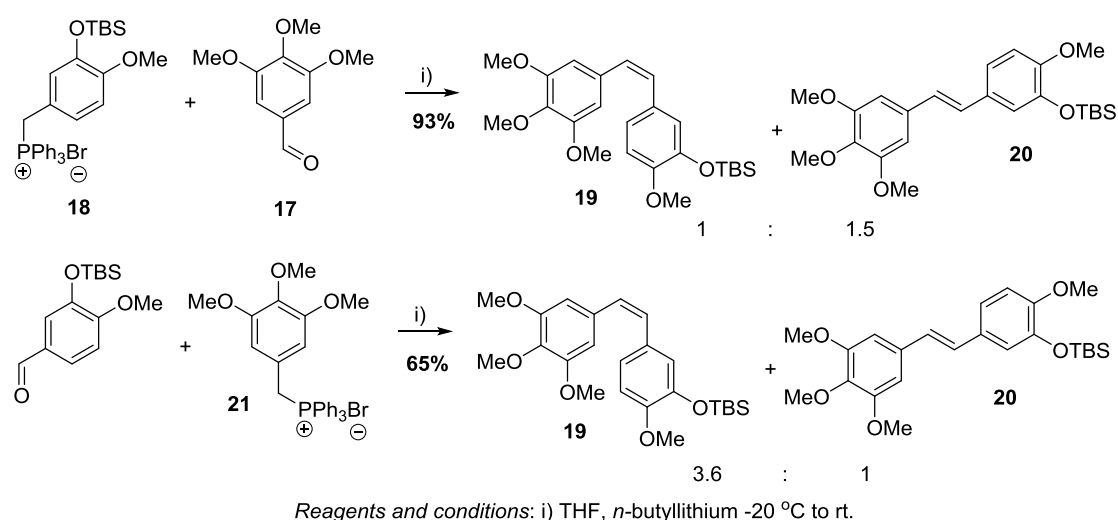


Figure 8: Combretastatins CA1 8 and CA4 7.

1.5.1. Synthesis of combretastatins by the Wittig Reaction

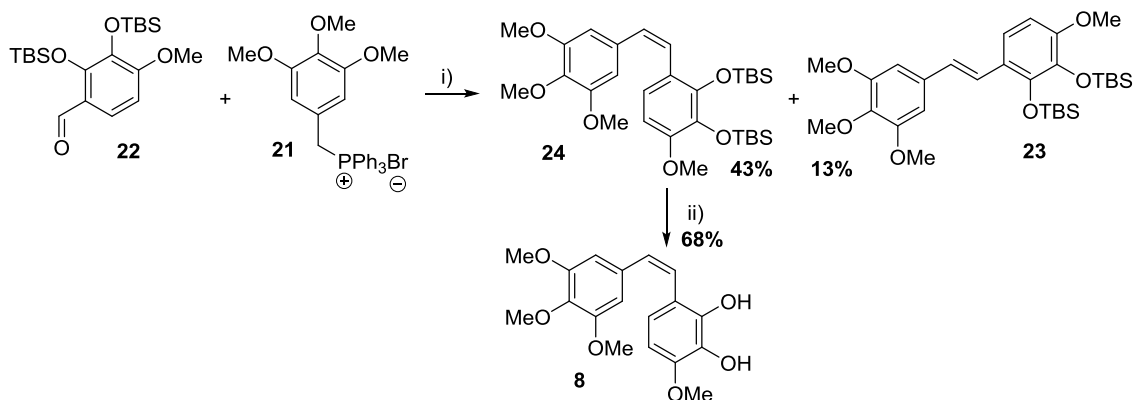
The formation of the *Z*-alkene through the Wittig reaction between an aldehyde and phosphonium ylide is the key step in many synthesis of CA1 8 and CA4 7. In the 1980s the Pettit group first isolated and synthesised combretastatins A1 8 and A4 7, which they

achieved using the Wittig reaction.^{30–32} The reaction of 3,4,5-trimethoxybenzaldehyde **17** with the ylide derived from phosphonium bromide **18** with *n*BuLi afforded a mixture of TBS-protected stilbenes **19** and **20** in a yield of 93% with an *E/Z* ratio of 1.5:1 (Scheme 2). By reversing the components of the Wittig reaction the *E/Z* selectivity was improved to 1:3.6 and the TBS-protected stilbenes **19** and **20** were synthesised in a yield of 65%.³⁰ Subsequent separation by column chromatography and deprotection of the silyl ether with tetrabutylammonium fluoride afforded the desired *Z*-CA4 **7**. Despite the latter method giving a lower overall reaction yield for both isomers, the yield for TBS protected *Z*-CA4 **19** after separation was higher.



Scheme 2: Synthesis of TBS-protected *Z*-CA4 **19** using the Wittig reaction.

Combretastatin A1 **8** has also been successfully synthesised through the Wittig reaction. Pettit and Lippert treated the phosphonium salt **21** with *n*-butyllithium which formed the corresponding ylide *in situ*.²⁴ To this ylide, benzaldehyde **22** was added and resulted in a mixture of the *E*- and *Z*-isomers **23** and **24**. The desired *Z*-isomer **24** was isolated after column chromatography and recrystallisation in a 43% yield and underwent desilylation with potassium fluoride and hydrobromic acid in dimethylformamide to reveal CA1 **8** in 68% yield.

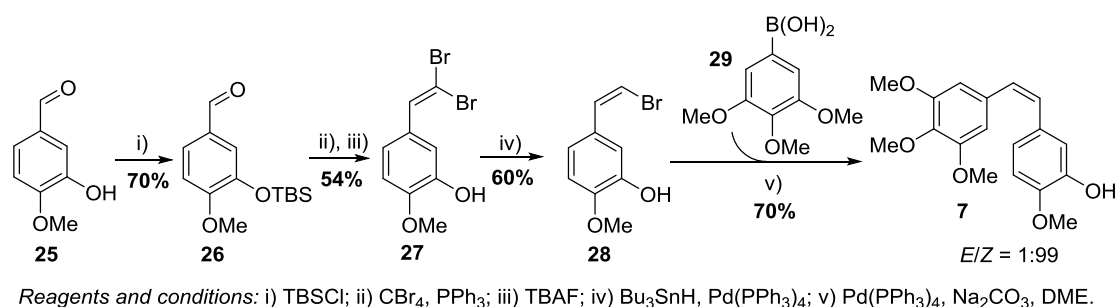


Reagents and conditions: i) THF, *n*-butyllithium -20 °C to rt; ii) KF, DMF, HBr, 18 h.

Scheme 3: Synthesis of CA1 **8** using the Wittig reaction.

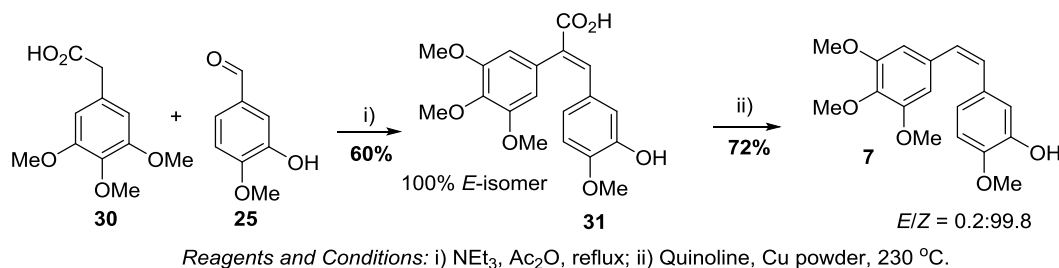
1.5.2. Synthesis of combretastatins by Cross coupling reactions

A disadvantage of the Wittig reaction is the low selectivity and the need for laborious chromatography separations which results in an overall low yield for the desired *Z*-isomer, thus a more stereoselective route is desirable.³⁰ Hadfield and co-workers sought to develop a method with improved stereoselectivity that was also amenable to large-scale production. They developed two methods, the first of which uses the commonly used Suzuki cross coupling reaction (Scheme 4).³³ A Corey-Fuchs Wittig-like bromination of silyl protected 3-hydroxy-4-methoxybenzaldehyde **26** followed by deprotection yielded the dibromoalkene **27** in satisfactory yield, 54%. Stereoselective reduction of dibromoalkene **27** using tributyltin hydride and tetrakis(triphenylphosphine)palladium (0) afforded the (*Z*)-vinyl bromide **28** in good yield. The Pd-catalysed Suzuki cross-coupling of (*Z*)-vinyl bromide **28** with 3,4,5-trimethoxyphenylboronic acid **29** under basic conditions, employing tetrakis(triphenylphosphine)palladium (0) as the catalyst afforded the *Z*-isomer of CA4 **7** with excellent stereoselectivity (*Z*:*E* = 99:1) and good yield. The overall yield from the starting material isovanillin **25** is 16% which is comparable to the overall yields observed using the Wittig reaction.³¹



Scheme 4: Synthesis of CA4 **7** using Suzuki cross coupling.

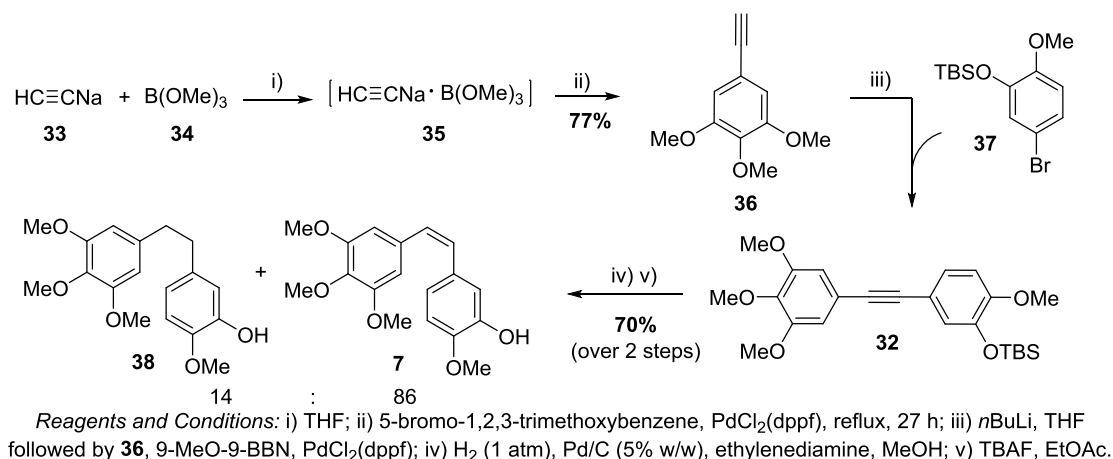
The second method developed by Hadfield and co-workers is a two-step stereoselective synthesis of combretastatin A4 **7** using a Perkin condensation of 3,4,5-trimethoxyphenylacetic acid **30** and 3-hydroxy-4-methoxybenzaldehyde **29** (Scheme 5).³³ The resulting cinnamic acid **31**, which was formed as a single isomer, was then decarboxylated using copper and quinoline to yield combretastatin A4 **7** in an overall yield of 42% yield. Crude GC analysis showed a *Z*:*E* ratio of 88:12, but following recrystallisation this increased to 99.8:0.2. This shows that this is an efficient stereoselective method for the synthesis of *Z*-CA4 **7**, avoiding the use of protecting groups and column chromatography, and is more efficient than the Hadfield's Suzuki method which had an overall yield of 16% from isovanillin **29**.



Scheme 5: Synthesis of CA4 **7** via a Perkin condensation.

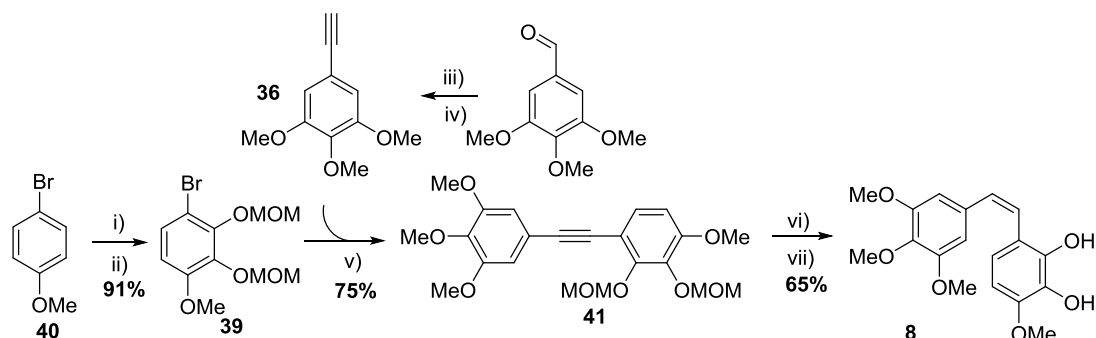
Palladium catalysed cross coupling reactions are of central importance in organic chemistry for forming carbon-carbon bonds. Suzuki-Miyaura, Sonogashira and Negishi reactions have been the key step in many syntheses of combretastatins.^{33–35} The Suzuki-Miyaura cross coupling of an aryl boronic acid and a vinyl halide is the most common cross-coupling reaction used for the synthesis of combretastatins.^{33,34} Fürstner and Nikolakis developed a stereoselective method for the synthesis of CA4 **7** through a Lindlar-based semi-hydrogenation of a diarylalkyne **32** which was synthesised through two consecutive Suzuki-type cross coupling reactions (Scheme 6).³⁶ The addition of

sodium acetylide **33** to B(OMe)₃ **34** led to a mixture of borate complexes **35** and the subsequent reaction with 5-bromo-1,2,3-trimethoxybenzene in the presence of catalytic PdCl₂(dppf) yielded the corresponding aryl acetylene **36** in good yield. This acetylene **36** underwent 9-MeO-9-BBN-mediated Suzuki-type cross coupling with the bromide **37** and afforded the diarylalkyne **32**. Z-Selective semi-hydrogenation with a Lindlar catalyst (5% Pd/C, ethylenediamine) provided the silyl-protected CA4 **19** in 80% yield. Deprotection using tetrabutylammonium fluoride led to combretastatin A4 **7** in high yield. Despite the reaction being Z-selective, over-reduction caused the formation of the corresponding alkane **38** in a ratio of 86:14 (Z-combretastatin A4 **7**: alkane **38**) and separation through flash chromatography was needed.



Scheme 6: Synthesis of CA4 **7** via two consecutive Suzuki-type cross coupling reactions.

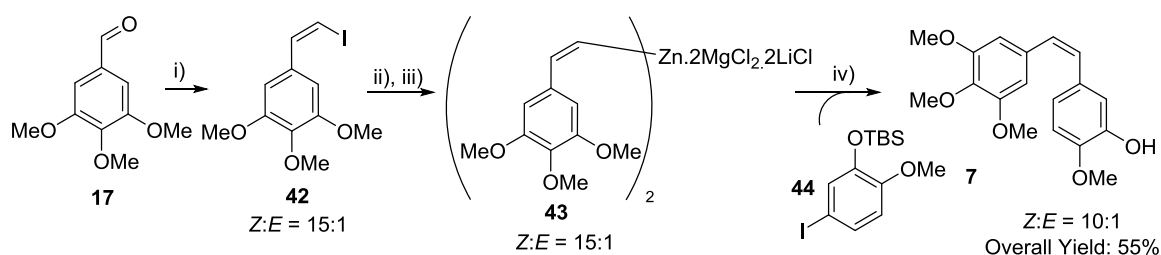
Another synthesis of combretastatins using Suzuki-Miyaura cross-coupling was reported by Hudlicky and co-workers.³⁴ The aryl bromide component **39** of the Suzuki reaction was generated by the bio-oxidation of 4-bromoanisole **40** using the biocatalyst *E. coli* JM109 (pDTG602) followed by MOM protection. The coupling of *p*-bromomethoxycatechol **39** with the alkynyl-boronic ester of trimethoxyphenylacetylene **36** under Suzuki-Miyaura conditions yielded acetylene **41** (Scheme 7). Comparative studies on the reduction of the diarylalkyne **41** to the Z-MOM protected alkene showed the superior use of hydroboration over using Lindlar's catalyst providing the required MOM-protected Z-olefin in an 84% yield. Subsequent deprotection using dilute hydrochloric acid yielded CA1 **8** with an overall yield of 44% over 5 steps.



Reagents and conditions: i) JM109 (pDTG602) 1.0-1.5 g/L; ii) MOMCl, DCM, EtN(*i*Pr)₂; iii) CBr₄, PPh₃, DCM, 0 °C; iv) *n*BuLi, THF; v) a) *n*BuLi, B(O*i*Pr)₃, DME:THF/10:1, -78 °C; b) Pd(PPh₃)₄, 90 °C, 5-6 h; vi) (C₆H₁₁)₂BH, 0 °C, 1 h then 20 °C 30 min, HOAc, 0 °C, 4 h; vii) 3N HCl:THF/1:1.

Scheme 7: Synthesis of CA1 **8** via Suzuki-Miyaura coupling.

Knochel and co-workers reported a mild yet stereoselective synthesis of CA4 **7** using the Negishi cross-coupling reaction.³⁷ The 3,4,5-trimethoxy- β -iodostyrene **42** intermediate was prepared with excellent stereoselectivity from the commercially available 3,4,5-trimethoxybenzaldehyde **17** and Zhao's reagent in the presence of NaHMDS. The iodostyrene **42** first underwent iodide-magnesium exchange with *i*PrMgCl.LiCl, then subsequent Mg-Zn transmetalation by addition of 1 M ZnCl₂ in a THF-NMP mixture to afford the organozinc reagent **43** with no loss in stereoselectivity. The organozinc reagent **43** was then subjected to *in situ* Negishi cross-coupling with 1-iodo-2,3-OTBS-4-methoxybenzene **44** in the presence of the palladium catalyst (A-^{ta}Phos)₂PdCl₂. The resulting combretastatin A4 **7** was obtained with very good stereoselectivity (*Z*:*E* = 10:1).

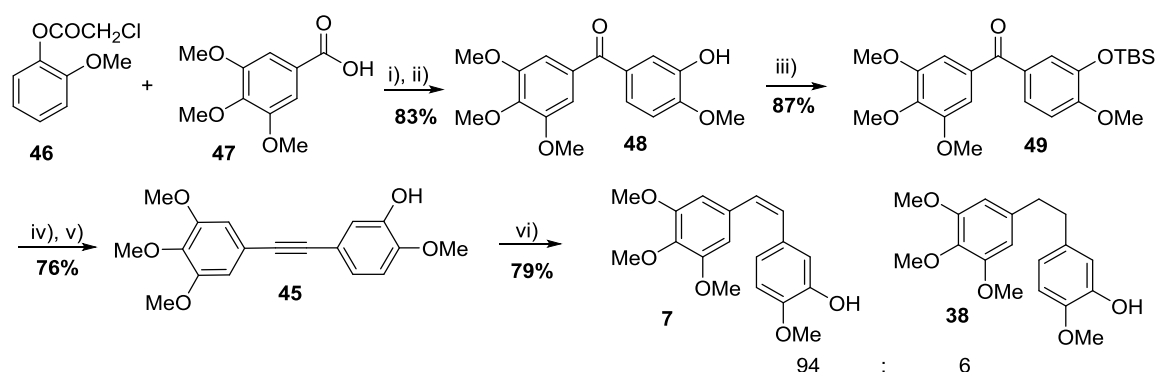


Reagents and conditions: i) ¹PPh₃⁺CH₂I⁻, NaHMDS, THF; ii) *i*PrMgCl.LiCl, -40 °C, 15 min; iii) ZnCl₂, NMP, -40 °C, 1 min; iv) (A-^{ta}Phos)₂PdCl₂ (2 mol%), rt.

Scheme 8: Synthesis of CA4 **7** through employment of the Negishi cross-coupling reaction.

1.5.3. Synthesis of combretastatins by selective reduction of diarylalkynes

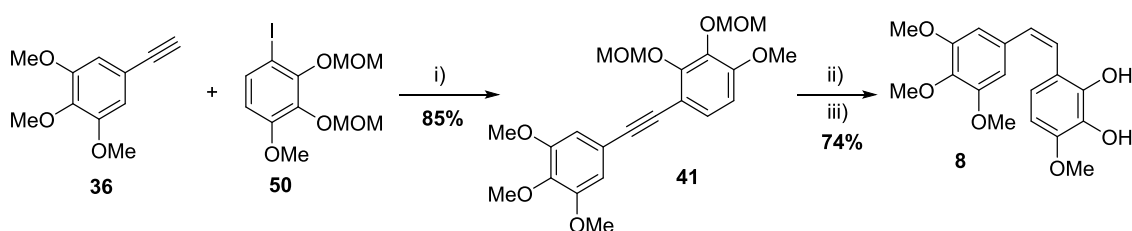
Many syntheses of *Z*-combretastatins are achieved through the reduction of the corresponding diarylalkyne, with methods including using Lindlar's catalyst,³⁸ alkyne hydroboration,³⁴ and the hydrolysis of a Ti(II)-alkyne complex.³⁹ Petrov *et. al.* developed a route that uses the Colvin rearrangement to generate the diarylalkyne intermediate **45** (Scheme 9).³⁸ Acylation of protected-anisole **46** with 3,4,5-trimethoxybenzoic acid **47** in the presence of Eaton's reagent followed by deprotection of the chloroacetyl group afforded the phenstatin precursor **48** in high yield. In the key step, the Colvin rearrangement was carried out with the TBS-protected phenstatin **49** and trimethylsilyldiazomethane employing *n*BuLi as the base. Final deprotection using tetrabutylammonium fluoride yielded the desired diarylalkyne intermediate **45** in excellent yield. The partial hydrogenation of the diarylalkyne was then studied. Preliminary experiments for the hydrogenation of diarylalkyne **45** used Pd/C as the catalyst in the presence of ethylenediamine in methanol and resulted in the formation of fully hydrogenated corresponding alkane **38**. Hydrogenation of TBS-protected alkyne over Lindlar catalyst (Pd/CaCO₃) with quinoline as an additive in hexanes formed the desired combretastatin **19** with a ratio of 82:18 (combretastatin:alkane). However better results were obtained by the partial hydrogenation of the deprotected alkyne **45** in a 1:1 solvent mixture of hexanes and toluene, giving the combretastatin **7** in a 94:6 ratio with its corresponding alkane **38**.



Reagents and Conditions: i) MeSO₃H/P₂O₅, 40 °C, 4 h; ii) KOAc, MeOH, reflux, 15 min; iii) TBSCl, DMAP, Et₃N, DCM, rt, 12 h; iv) TMSCHN₂, *n*BuLi, THF, -78 °C to rt; v) TBAF, EtOAc, rt, 10 min; vi) H₂, Lindlar catalyst, quinoline, hexane-toluene

Scheme 9: Synthesis of combretastatin A4 **7** via the Colvin Rearrangement.

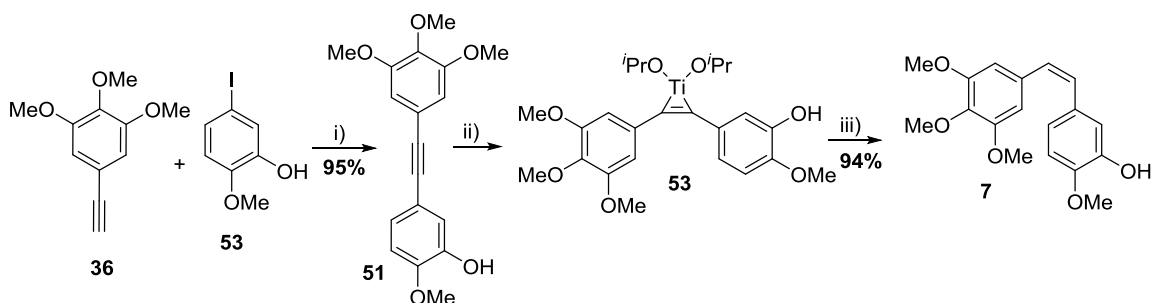
Hansen and co-workers reported the synthesis of combretastatin A1 **8** via the selective reduction of a diarylalkyne **41** which was synthesised by the Sonogashira reaction.³⁵ The Sonogashira coupling between a MOM protected iodide **50** and 3,4,5-trimethoxyphenylacetylene **36** in the presence of Pd(PPh₃)₄, CuI and *n*-propylamine afforded the diarylalkyne **41** in good yield. Hydroboration under the conditions reported by Hudlicky and co-workers yields the desired *Z*-olefin, subsequent deprotection yields the desired CA1 **8** in high yield with no isomerisation of the *Z*-olefin (Scheme 10).³⁴



Reagents and Conditions: i) Pd(PPh₃)₄, *n*-PrNH₂, CuI, Δ; ii) a) BH(C₅H₁₁), THF, 0 °C; b) AcOH; iii) HCl, THF.

Scheme 10: Synthesis of Combretastatin A1 **8** via a Sonogashira Reaction.

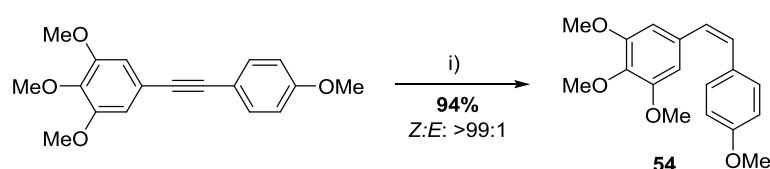
Lara-Ochoa synthesised CA4 **7** by formation of a diarylalkyne **51** followed by the hydrolysis of the corresponding thermally stable Ti(II)-alkyne complex **52**.³⁹ The diarylalkyne **51** was synthesised through the coupling of a 3,4,5-trimethoxyphenylacetylene **36** with 5-iodo-2-methoxyphenol **53** using Pd(OAc)₂ and triphenylphosphine and heating at reflux in pyrrolidine, following the method developed by Nwokogu (Scheme 11).⁴⁰ Generation of the thermally stable Ti(II)-alkyne complex **52** from diarylalkyne **51** using *n*BuLi and Ti(O*i*Pr)₄ results in the two aryl rings formed in the a *cis* configuration. Subsequent hydrolysis of the Ti(II)-alkyne complex yields the stilbene CA4 **7** with the desired *Z*-geometry in good yields and high purity.



Reagents and conditions: i) Pd(OAc)₂, PPh₃, pyrrolidine, reflux; ii) *n*BuLi, Ti(O*i*Pr)₄, -78 °C to 50 °C; iii) H₂O.

Scheme 11: Synthesis of CA4 **7** through the hydrolysis of a Ti(II)-alkyne complex **52**.

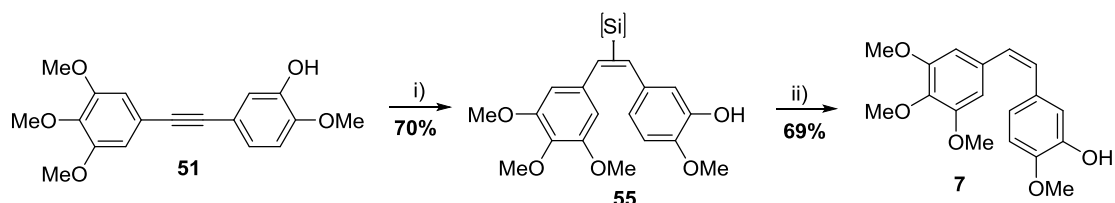
Hua and co-workers undertook studies in the semi-hydrogenation of internal alkynes to *Z*-alkenes.⁴¹ DMF/KOH was shown to be an efficient hydrogen source in the Pd(OAc)₂ catalysed transfer semi-hydrogenation of various functionalised alkynes to *Z*-alkenes in high yields and excellent chemo- and stereoselectivity. They also applied these conditions towards the synthesis of a CA4 analogue **54**.



Reagents and conditions: i) Pd(OAc)₂ (2.0 mol %), KOH (1.5 eq.), DMF, 145 °C, 6 h.

Scheme 12: Synthesis of CA4 analogue **55** by semi-hydrogenation with DMF/KOH.

A further example of the synthesis of CA4 **7** from the diarylalkyne **51** is the reduction *via* the platinum-catalysed hydrosilylation of the alkyne **55** with a silicon hydride reagent followed by a fluoride-mediated deprotection (Scheme 13).⁴²

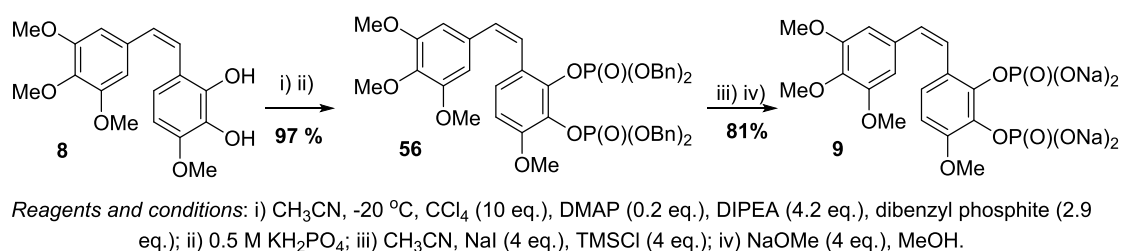


Reagents and conditions: i) HSiOEtMe₂ (4.0 eq.), PtO₂ (7%), 60 °C, 2 h; ii) TBAF (1.1 eq.), 60 °C, 1 h, THF.

Scheme 13: Synthesis of CA4 **7** through a hydrosilylation/protodesilylation sequence.

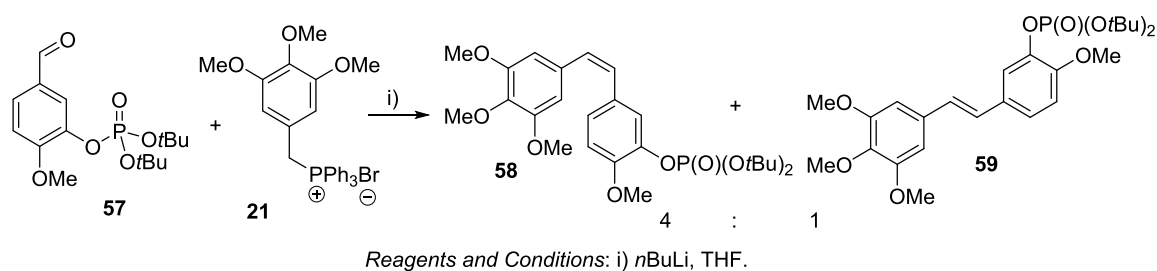
1.5.4. Synthesis of prodrugs CA1P and CA4P

Having a range of methods to syntheses CA1 **8** and CA4 **7**, the combretastatins need to be converted into their corresponding prodrugs as this will improve the water solubility and bioavailability. The synthesis of phosphate pro-drug CA1P **9** from CA1 **8** can be achieved *via* a dibenzylphosphate intermediate **56** (Scheme 14). Treatment of CA1 **8** with dibenzyl phosphite in the presence of carbon tetrachloride, DMAP and DIPEA afforded tetrabenzylphosphate **56** in excellent yields. Debonylation of the benzylphosphate **56** using TMSCl resulted in a tetra-TMS-phosphate ester followed by quenching with excess NaOMe afforded the tetrasodium salt **9**.



Scheme 14: Synthesis of prodrug CA1P **9**.

An alternate strategy for the synthesis to the prodrug CA4P **10** based on the Wittig reaction was developed by Bedford *et. al.*⁴³ 3-Hydroxy-4-methoxybenzaldehyde was converted to the phosphate triester **57** before coupling with 3,4,5-trimethoxybenzyl triphenylphosphonium bromide **21** via the Wittig reaction (Scheme 15). The two CA4 phosphate bis-*t*-butyl ester isomers **58** and **59** were formed in an *E:Z* ratio of 1:4. After separation the *Z*-isomer was converted into the potassium salt of CA4.



Scheme 15: Synthesis of potassium salt of CA4 via the Wittig reaction.

1.6. Combretastatin A1P metabolism

Metabolic studies on pro-drug CA1P **9** revealed up to 14 metabolites being observed in the blood plasma.⁴⁴ Some of the CA1P **9** metabolites reported include monophosphates, monoglucuronides, bisglucuronides as well as the active drug CA1 **8** (Figure 9). It is believed that partial enzymatic dephosphorylation of CA1 **8** could lead to the two monophosphate isomers CA1MPA **60** and CA1MPB **61**.⁴⁵ Glucuronidation, the addition of glucuronic acid to a substrate by enzymatic conjugation, is a mechanism to convert exogenous compounds into more water-soluble metabolites for excretion and could lead to the two monoglucuronide isomers CA1G1 **62** and CA1G2 **63**.⁴⁶ In order for further biological evaluation in support of the ongoing human clinical development of CA1P **9**, Pinney and co-workers were able to prepare regioisomeric monophosphate and monoglucuronide isomers of CA1 **8**.^{45,46} All isomers were synthesised using the Wittig

reaction and the two vicinal phenols were distinguished by using different protecting groups. Biological evaluation however, showed the monophosphate derivatives to be inactive as inhibitors of tubulin assembly ($IC_{50} > 40 \mu M$). The two monoglucuronide isomers also showed low cytotoxicity compared to CA1P **9** against selected human cancer cell lines, with CA1G1 **62** being slightly more potent than CA1G2 **63**.

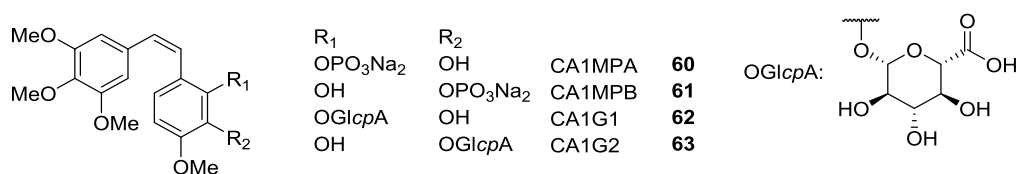
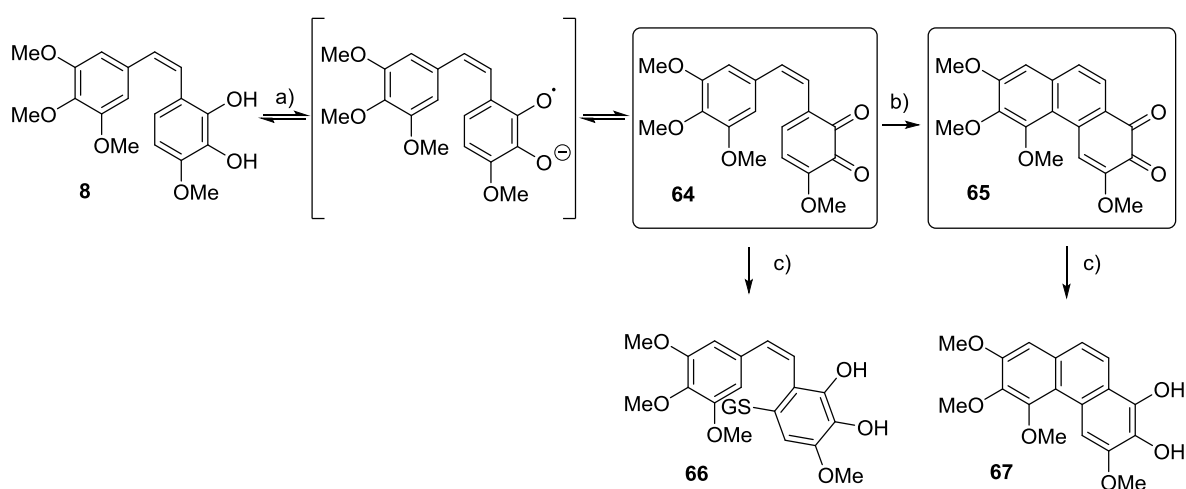


Figure 9: CA1P **9** metabolites.

It is widely thought that the increased anti-tumour activity of CA1 **8** compared with CA4 **7** is due to the formation of *ortho*-quinone intermediates.⁴⁴ Quinones are known to be highly reactive intermediates that cause a number of damaging effects *in vivo* through different mechanisms.⁴⁷ Quinones act as Michael acceptors and can cause cellular damage through alkylation of essential proteins, DNA, and other biological nucleophiles. They are also highly redox active and can undergo a redox cycle with their semiquinone radicals to form reactive oxygen species including superoxide, hydrogen peroxide and the hydroxyl radical which can lead to oxidative stress within cells.

Folkes and co-workers investigated the oxidative metabolism of CA1 **8** and the potential for the resulting quinone intermediates to bind to nucleophiles and enhance oxidative stress *via* free radicals (Scheme 16).⁴⁸ CA1 **8** was oxidised to the *ortho*-quinone **64** by treatment with iron (III) chloride and sulfuric acid in ethanol. The reaction was quenched after one minute to prevent over-oxidation. A 50:50 mixture of the *ortho*-quinone **64** and unreacted CA1 **8** was obtained and its presence was confirmed by LC-MS and UV-vis absorbance. The *ortho*-quinone **64** was observed to be unstable in aqueous solution and is believed to result in electrocyclic ring closing to form a second *ortho*-quinone species **65**. However in a solution of acetonitrile the *ortho*-quinone **64** was said to be stable for 24 hours. The first *ortho*-quinone **64** was also observed by oxidation of CA1 **8** with H₂O₂/horseradish peroxidase compound I, lactoperoxidase, tyrosinase and human promyelocytic leukaemia cells (HL-60). This shows the potential for oxidation of CA1 **8** to *ortho*-quinone **64** *in vivo*. Leaving the reaction of CA1 **8** and iron (III) chloride and

sulfuric acid for a longer period gave a second *ortho*-quinone species **65**; this species was found to be more stable as it was isolated in a pure form after flash column chromatography on silica. Formation of the second ring-closed *ortho*-quinone was not observed without the prior formation of the initial *ortho*-quinone. The *ortho*-quinones **64** and **65** were treated with glutathione, an antioxidant. The first *ortho*-quinone **64** formed a quinone-glutathione adduct **66**, the regioselectivity of which was not confirmed but it is believed that the glutathione adds to the most electropositive site on the B ring. In contrast when the second *ortho*-quinone **65** was treated with glutathione, reduction occurred resulting in a hydroquinone **67** being formed.

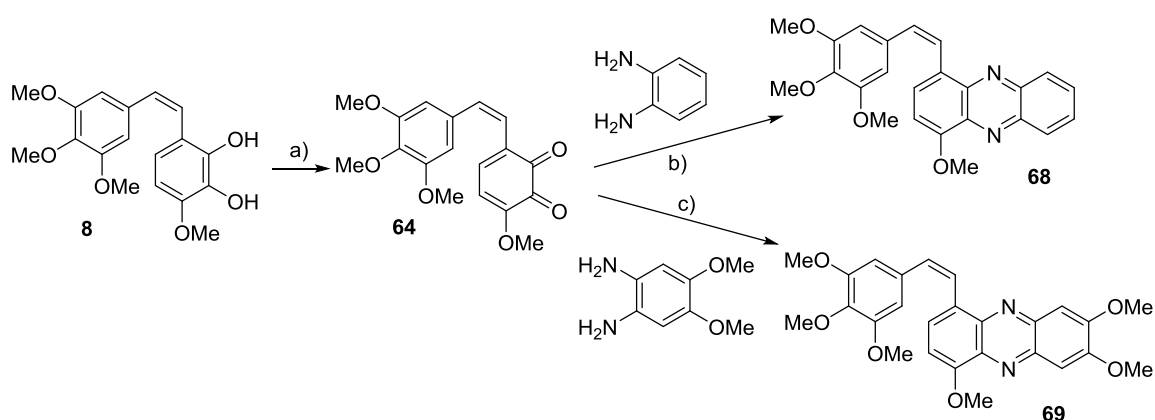


Reagents and conditions: a) FeCl_3 (4 mM), H_2SO_4 (1 mM), EtOH (1%, 0.8 mM), 1 min; b) (From CA1) FeCl_3 (8 mM), H_2SO_4 (2 mM), EtOH (1%, 0.8 mM), 45 min; c) glutathione.

Scheme 16: Synthesis of the *ortho*-quinones **64** and **65** from CA1 **8** their reaction and with the antioxidant glutathione.

CA1P **9** was injected into mice with subcutaneous dorsal CaNT tumours, and after two hours blood and tissue were removed and analysed by HPLC. They found HPLC retention characteristics and MS fragmentation patterns identical to the quinone-glutathione adduct **66** as well as free CA1 **8**. It is thought that glutathione-*S*-transferases catalyses this transformation *in vivo*. Folkes and co-workers showed that CA1 **8** is more susceptible to oxidative metabolism which results in the formation of free radicals. These free radicals can stimulate oxidative stress by increasing superoxide and hydrogen peroxide formation. This shows that CA4P **10** and CA1P **9** have different pharmacological properties and gives a suggestion as to why CA1P **9** has a larger antitumour effect than CA4P **10** *in vivo*.

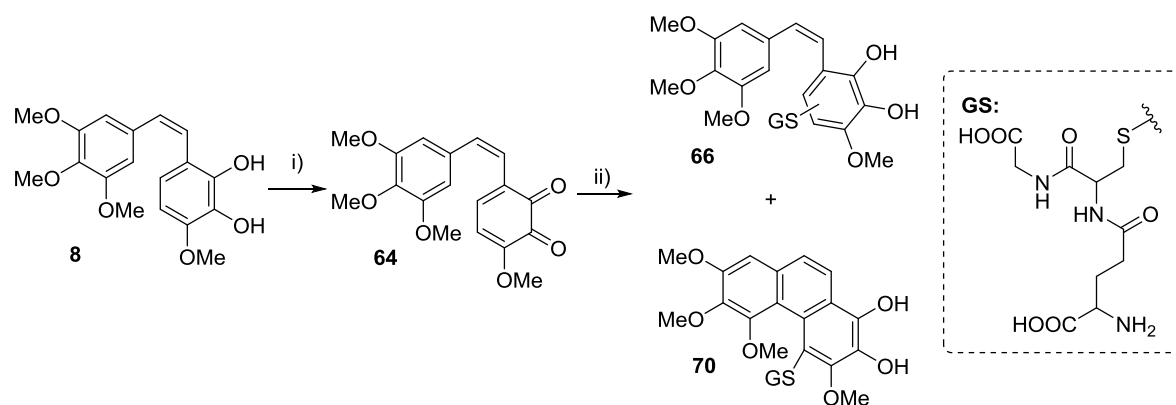
Pettit and co-workers were also able to confirm the presence of *ortho*-quinone intermediates by trapping them as stable phenazine derivatives (Scheme 17).⁴⁹ Treatment of CA1 **8** with sodium periodate and tetrabutylammonium bromide in dichloromethane for ten minutes, was followed by extraction and removal of solvent which revealed the *ortho*-quinone **64**. However, the blue *ortho*-quinone rapidly turned black due to decomposition after just 5-10 minutes. They, therefore, trapped the *ortho*-quinone as a pyrazine **68** and dimethoxyphenylenediamine-derived phenazine derivative **69**. Pettit commented on the remarkable instability of the *ortho*-quinone intermediate **64** and suggested it can be attributed to the extended π -system.



Reagents and conditions: a) NaIO₄, Bu₄NBr, DCM, 0 °C; b) MeOH, 0 °C, 2 h 25%; c) MeOH, 0 °C, 2 h, 29%.

Scheme 17: Synthesis of the *ortho*-quinone metabolite **64** of CA1 **8** and its trapping as phenazine derivatives.

Aprile and co-workers investigated the *in vivo* metabolic fate of CA1 **8** through LC-UV and LC-MS analysis (Scheme 18).⁵⁰ They also managed to prepare the first *ortho*-quinone **64**, by the treatment of CA1 **8** with a polymer supported oxidant, (polystyrylmethyl)-trimethylammonium metaperiodate, in dichloromethane at room temperature. The *ortho*-quinone **64** was isolated following removal of solvent and its identity confirmed by LC-DAD-UV, LC-ESI-MS and ¹H NMR spectroscopy. Like Folkes and co-workers, they also investigated the reaction of the *ortho*-quinone with the thiol-containing nucleophile glutathione. However, in contrast to the studies by Folkes, they observed two quinone-glutathione adducts **66** and **70**.



Reagents and conditions: i) (polystyrylmethyl)-trimethylammonium metaperiodate, DCM, rt; ii) MeOH, glutathione, 2 min.

Scheme 18: Two quinone-glutathione adducts **68** and **70** from reacting *ortho*-quinone **64** with glutathione.

Aprile and co-workers went on to analyse the metabolites of CA1 **8** found in CA1-treated rat urine by LC-ESI-MS/MS (Figure 10). Based on these observations, they proposed the structure of metabolic compounds which had undergone a number of phase I and phase II metabolic pathways. These include aromatic hydroxylation, *O*-demethylation, glucuronidation, sulfation and glutathionylation of the *ortho*-quinone. The cytotoxicity of the *ortho*-quinone species was investigated in a neuroblastoma cancer cell line and compared to CA1 **8**, and found to have comparable IC₅₀ values (3.5 and 3.3 nM vs. 1.3 nM).⁵⁰ Further investigations into whether this cytotoxicity was due to the inhibition of tubulin polymerisation were undertaken and it was found that the second *ortho*-quinone **65** retained the ability of inhibiting tubulin polymerisation but the first *ortho*-quinone **64** did not, even at high concentrations. This was thought to be due to the unstable nature of the first *ortho*-quinone **64**, but this contrasts with the observation of cytotoxicity which requires the compound to act over a number of hours. This suggests that the cytotoxic activity of *ortho*-quinone **64** is caused by something other than tubulin polymerisation inhibition *i.e.* the production of cytotoxic free radicals.

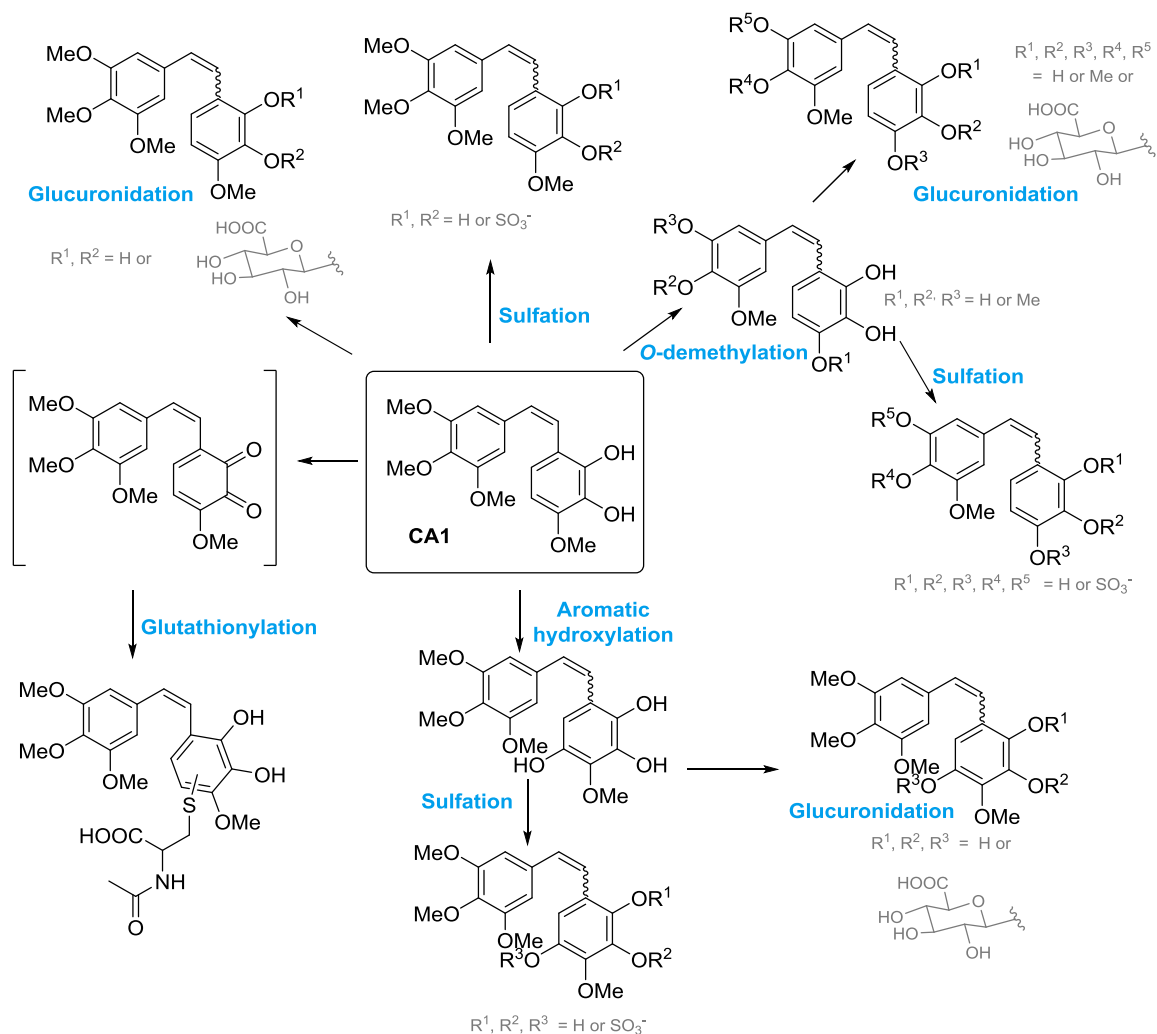


Figure 10: Proposed *in vivo* metabolic pathway of CA1 **8** determined by LC-ESI-MS/MS analysis of CA1 **8** treated rat urine.

To support the free radical mechanism for the enhanced antitumour activity observed by CA1 **8** compared to CA4 **7**, Rice and co-workers investigated tumour necrosis in KHT sarcoma-bearing mice treated with CA4P **10** and the *E*- isomer of CA1P.⁵¹ The *E*-isomer should lack the antitubulinic activity as it is well reported that the *Z*-configuration of the stilbene backbone is essential in binding to tubulin, but as the *E*-isomer still contains a 1,2-diol that can be oxidised to an *ortho*-quinone and induce some cytotoxic activity. Their work showed that tumour necrosis of mice treated with both CA4P **10** and *E*-CA1P was greater than with treatment of CA4P **10** alone. These results suggest that the primary source of the antitumour effect of CA1 **8** is its tubulin binding capacity but the generation of cytotoxic species also contributes to its overall activity.

1.7. Molecular imaging

Molecular imaging is a way to non-invasively visualise, characterise and quantify molecular processes or pathways *in vivo* at a cellular and sub-cellular level. There are a variety of methods used in molecular imaging including: positron emission tomography (PET), single photon emission computed tomography (SPECT), optical imaging, Raman spectroscopy and magnetic resonance imaging (MRI).

The development of MRI, which evolved from nuclear magnetic resonance (NMR), is one of the major advances in biomedical imaging in the last 30 years. MRI is now considered critical in the workup (diagnosis, monitoring *etc.*) of patients with a wide range of diseases and disorders. While MRI provides morphometric information about the organs and diseases studied, magnetic resonance spectroscopy (MRS) is used to study metabolites in the tissue. Magnetic resonance spectroscopy imaging (MRSI) offers metabolic data which is processed and displayed as density maps of several metabolites. MRS provides insight into the biochemistry and function of the tissue and has been commonly used for clinical scans of the brain and prostate gland.^{52,53} Unlike traditional MRI which detects changes in the density of bulk water, MRS detects multiple small, endogenous metabolites within cells or extracellular spaces associated with several metabolic pathways.

Clinical use of MRI is currently restricted to studying the ^1H nucleus under normal thermal equilibrium conditions. This is because the ^1H nucleus has a high natural abundance, resulting in high concentrations in the body. Other nuclei that are also found in relevant metabolites within the body that have MR-active isotopes include ^{13}C , ^{18}O , ^{14}N and ^{31}P ; however, these are difficult to observe at thermodynamic equilibrium. This is due to their low natural abundance and/or low gyromagnetic ratios. These metabolites are present in concentrations $\sim 10,000$ times lower than that of tissue water protons, and it is not possible to image them at clinical magnetic field strengths. Despite these limitations, a small number of non- ^1H nuclei have been studied in human using MRS; ^{31}P has been used to study high energy metabolites and lipid metabolism,^{54–57} and ^{23}Na has been used to study stroke and neurodegenerative diseases of the brain.

Entry	Nucleus	Spin	Natural abundance	γ (relative to ^1H)	Biomedical application
1	^1H	1/2	99.98	1	Total body MRI/MRSI
2	^{13}C	1/2	1.11	0.2515	Metabolic tracer injection using MRSI
3	^{15}N	1/2	0.37	0.1013	Metabolic tracer injection using MRSI
4	^{17}O	5/2	0.04	0.1355	Oxidative metabolism using MRSI
5	^{23}Na	3/2	100	0.2645	Neurodegeneration and cardiac imaging using MRSI
6	^{31}P	1/2	100	0.4048	Bioenergetics and pH using MRSI

Table 2: Biomedical applications of NMR active nuclei under thermal equilibrium.

The use of biomarkers or molecular probes with MR techniques allows information to be gained not only on the tissue morphology but also the tissue biochemistry. However, a major limitation of MRS is low sensitivity; this has been overcome by a technique called hyperpolarisation, where the spin polarisation of a nucleus is enhanced beyond that seen at thermodynamic equilibrium. ^{13}C – MRS has long been used in the investigation of static metabolic processes *in vivo* and recently, with the arrival of hyperpolarisation techniques, ^{13}C – MRS/MRSI can now measure the dynamics of metabolic conversions *in vivo*. These hyperpolarisation techniques can increase sensitivity up to 10,000-fold allowing for detection of ^{13}C -labelled compounds and their downstream metabolic products in real-time *in vivo*.

1.8. Enhancing MR signal by hyperpolarisation

The signal-to-noise ratio is a measure of sensitivity and is proportional to the gyromagnetic ratio γ of the nucleus under study, concentration c of nuclear spins, and the polarisation P . The gyromagnetic ratio is an inherent property of the nucleus and is the ratio of the nucleus' magnetic dipole moment to its angular momentum. The basis of any magnetic resonance technique is the interaction between the magnetic field in the MR machine and the nuclei spins of molecules in the body. When placed in a magnetic field, the spins align themselves with the magnetic field, as such they can either lie in the same direction as the magnetic field or opposed to it. The population of these spins in the two possible states is not equal and is referred to as the polarisation. For a spin $\frac{1}{2}$ nucleus, such as ^1H or ^{13}C , the population (or polarisation) of the two allowed energy levels is

given by the Boltzmann distribution. In normal clinical magnetic field strengths and temperature, this population difference is very small, but there are slightly more nuclei the α spin state (Figure 11a). This difference (albeit very small) is what allows a signal to be detected.

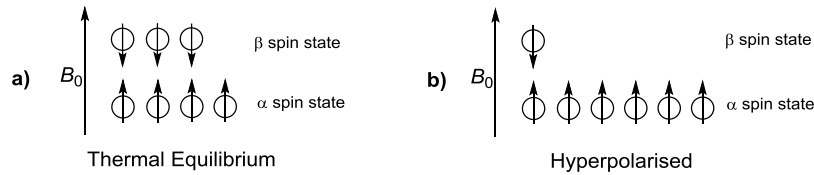


Figure 11: Pictorial representation of hyperpolarisation: an increase in the population difference between the α and β spin states.

The population difference is dependent on many factors, including the strength of the magnetic field, temperature, the abundance of the NMR-active nucleus and the gyromagnetic ratio of the nucleus under study (Equation 1). Different nuclei will have different sensitivities due to their different gyromagnetic ratios; for ^1H , $\gamma = 26.75 \cdot 10^7 \text{ rad T}^{-1} \text{ s}^{-1}$ and for ^{13}C , $\gamma = 6.72 \cdot 10^7 \text{ rad T}^{-1} \text{ s}^{-1}$. So the ^1H nuclei will have higher polarisation at thermal equilibrium than ^{13}C nuclei. The abundance of nuclei in a sample also affects the sensitivity; ^1H has a natural abundance of 99.9%, whereas the natural abundance of ^{13}C is only 1.1% with the remainder being the NMR-inactive ^{12}C . This means only a small percentage of ^{13}C nuclei can become polarised by the external magnetic field B_0 and are therefore available to produce an NMR signal or image. For these reasons, clinical *in vivo* imaging techniques are usually limited to the ^1H nucleus. To improve the sensitivity (or polarisation), the population difference between the lower and upper energy levels needs to be increased (Figure 11b).

$$\text{a) } P = \frac{N_{\alpha} - N_{\beta}}{N_{\alpha} + N_{\beta}} \quad \text{b) } P_{th} = \tanh\left(\frac{\gamma\hbar B_0}{2k_B T}\right)$$

Equation 1: a) Definition of polarisation P (where N_{α} is the population of the α spin state, N_{β} is population of the β spin state) and b) definition of the thermal polarisation P_{th} (where \tanh refers to the hyperbolic tangents, B_0 is the external magnetic field strength, γ is the gyromagnetic ratio, T is temperature, \hbar is Planks constant, k_B is Boltzmann's constant).

Hyperpolarisation methods are used to increase the sensitivity of magnetic resonance techniques and can result in signals being increased by more than a factor of 10^5 compared to thermal equilibrium.⁵⁸ Hyperpolarisation is the general term for a method that

enhances the spin polarisation difference of populations of nuclei in a magnetic field (Figure 11b). It involves transferring the polarisation from a highly polarised species to the spin of a nucleus in the molecule of interest. This will create an artificial non-equilibrium distribution of nuclei spins and result in increased polarisation and, therefore, sensitivity.

1.9. Applications of hyperpolarised MR

Hyperpolarisation techniques have been utilised in solid-state research for a number of years but recently due to the advances in the dissolution methods, injectable hyperpolarised solutions can be generated which are suitable for *in vitro* and *in vivo* studies. The signal enhancement caused by hyperpolarisation allows less sensitive nuclei such as ^{13}C to be studied using magnetic resonance imaging (MRI), allowing molecules to be observed *in vivo* that were previously inaccessible.

The hyperpolarisation of ^{13}C -labelled cell metabolites allows them to be imaged *in vivo* and more importantly their metabolic conversion can be measured in real-time. Therefore, the visualisation of metabolism through enzymatic conversions can be achieved non-invasively. Most major diseases are linked to metabolic alterations, so by being able to visualise the flux of metabolic pathways enables a greater understanding of these diseases. It also provides essential information on the biodistribution, uptake and local environment of specific metabolites. Hyperpolarised MR works well for studying processes that are fast, short-lived and dynamic since their study is difficult under thermal equilibrium conditions.

The most well studied hyperpolarised metabolite is $[1 - ^{13}\text{C}]$ pyruvate, as it lies on an intersection of important metabolic pathways. By hyperpolarising $[1 - ^{13}\text{C}]$ pyruvate, its conversion to $[1 - ^{13}\text{C}]$ lactate, $[1 - ^{13}\text{C}]$ alanine, and $[^{13}\text{C}]$ bicarbonate can be monitored (Figure 12). The ratio of the converted metabolites will vary depending on the status of the cell, for instance tumours rely more heavily on the pyruvate-to-lactate pathway than normal cells which rely more on the pyruvate-to-alanine pathway. Therefore hyperpolarised $[1 - ^{13}\text{C}]$ pyruvate can be used a diagnostic tool or to monitor the change in tumour metabolism after treatment with anti-tumour agents. $[1 - ^{13}\text{C}]$ pyruvate is not the only metabolite that is studied, others include the isomers $[2 - ^{13}\text{C}]$ pyruvate and $[1,2$

$-^{13}\text{C}_2$]pyruvate, $[1 - ^{13}\text{C}]$ lactate, $[1 - ^{13}\text{C}]$ alanine, $[1,4 - ^{13}\text{C}_2]$ fumarate, $[5 - ^{13}\text{C}]$ glutamine, $[1 - ^{13}\text{C}]$ urea and $[2 - ^{13}\text{C}]$ fructose.⁵⁹

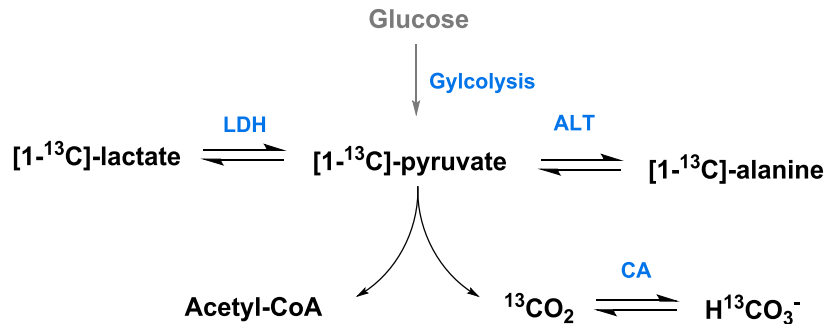


Figure 12: Metabolic pathway of $[1 - ^{13}\text{C}]$ -pyruvate where LDH = lactate dehydrogenase, ALT aminotransferase = and CA = carbonic anhydrase.

MR experiments with hyperpolarised $[1 - ^{13}\text{C}]$ pyruvate can show whether the tumour is responding to treatment by showing there is a metabolic change in the tumour. However it does not show whether the treatment has destroyed any tumour cells. For instance a decrease in $[1 - ^{13}\text{C}]$ -lactate can indicate a loss of cells within the tumour but could also be the result of metabolic change caused by a decrease in LDH activity or change in substrate concentration. A method that directly detects cell death is highly sort after since cell death after treatment is a good prognostic indicator to treatment. The formation of $[1,4 - ^{13}\text{C}_2]$ malate from $[1,4 - ^{13}\text{C}_2]$ fumarate has been shown to be a sensitive marker of tumour cell death *in vivo*.⁶⁰ Fumarate is an intracellular metabolite, and there is no detectable uptake of hyperpolarised $[1,4 - ^{13}\text{C}_2]$ fumarate when administered extracellular in viable cells. However in dying cells the plasma membrane permeability barrier has been damaged allowing for the uptake of $[1,4 - ^{13}\text{C}]$ fumarate into the cell and subsequent hydration to $[1,4 - ^{13}\text{C}]$ malate. Therefore the detection of $[1,4 - ^{13}\text{C}]$ malate indicates cell necrosis.

The microenvironment of tumours have a huge influence on the tumour aggressiveness, treatment response and metastatic spread. Most tumours are associated with an acidic extracellular pH compared with normal tissue, so monitoring the extracellular pH can provide information on prognosis and response to treatment. The extracellular pH of tumour can be imaged using the ratio of the signal intensities of hyperpolarised $\text{H}^{13}\text{CO}_3^-$ and hyperpolarised $^{13}\text{CO}_2$ using the Henderson-Hasselbalch equation (Equation 2).⁶¹ Hyperpolarised $\text{H}^{13}\text{CO}_3^-$ can also be used as a generic biomarker for detecting the

presence of disease since the majority of pathological states (such as tumours, ischaemia, infection, hypoxia, and inflammation) are accompanied by low extracellular tissue pH or changes in the acid-base balance in the tissue.

$$\text{pH} = \text{p}K_a + \log([\text{H}^{13}\text{CO}_3^-]/[^{13}\text{CO}_2])$$

Equation 2: The Henderson-Hasselbalch equation.

The use of hyperpolarised $[1 - ^{13}\text{C}]$ pyruvate in a clinical setting has been achieved in 2010 with a clinical trial looking to detect tumour response to treatment of prostate cancer.⁶² The initial results from this trial confirmed the safety of $[1 - ^{13}\text{C}]$ pyruvate and also saw elevated $[1 - ^{13}\text{C}]$ lactate/ $[1 - ^{13}\text{C}]$ pyruvate ratio in the tumours. Subsequent trials will guide the way for $[1 - ^{13}\text{C}]$ pyruvate to be used as a non-invasive cancer diagnostic and for the monitoring of cancer treatments.

1.10. Hyperpolarisation – Imaging considerations and techniques

Hyperpolarised magnetisation is in non-equilibrium and therefore is not renewable. The polarisation decays to thermal equilibrium at rate T_1 . So after each excited pulse, longitudinal magnetisation will recover to the thermal equilibrium value, not the hyperpolarised value. Therefore the main disadvantage of hyperpolarisation techniques is that the polarisation is relatively short-lived, typically 10 – 30 s for hyperpolarised ^{13}C -compounds *in vivo*. For all hyperpolarisation techniques that will be used *in vivo* the polarised compound has to be brought rapidly to body temperature and field strength, then injected, absorbed and distributed into the biological system without significant loss in polarisation. This restricts the time window for clinical imaging diagnostic imaging to 2 or 3 times the T_1 relaxation time, therefore having a long T_1 relaxation time is essential in order for the lifetime of the polarisation to be sufficiently long to be detected in subsequent imaging experiments. In order to gain any information on metabolism, the hyperpolarised ^{13}C -labelled substrate must also be metabolised quickly. There are four main hyperpolarisation techniques; brute force, optical pumping, parahydrogen induced polarisation, and dynamic nuclear polarisation.

1.10.1. Brute force

The thermal equilibrium polarisation, P , of a nuclei increases with increasing magnetic strength B_0 , and decreasing temperature T (Equation 3). Therefore hyperpolarisation can occur simply through “brute force” by subjecting the sample to a very high magnetic field and very low temperatures. For example, if a sample is cooled to 4 K (using liquid helium) with a field strength of 20 T, the polarisation can be increased by a factor of 1000.⁵⁸ However, in order to obtain polarisation levels high enough to see a significantly increased signal *in vivo*, impractically low temperatures in the mK range is required and very high magnetic fields. These conditions require very high costs therefore the brute force method has been surpassed by other hyperpolarisation techniques.

$$P_{th} = \tanh\left(\frac{\gamma\hbar B_0}{2k_B T}\right)$$

Equation 3: Definition of the thermal polarisation P_{th} where \tanh refers to the hyperbolic tangens, B_0 is the external magnetic field strength, γ is the gyromagnetic ratio for nucleus, \hbar is Planck’s constant over 2π , k_B is the Boltzmann constant and T is the temperature.

1.10.2. Optical pumping

Another technique for hyperpolarisation is optical pumping and is used to hyperpolarise noble gases usually ^3He or ^{129}Xe . Optical pumping allows the polarisation to be increased considerably, typically $\sim 10\%$ for ^{129}Xe and $\sim 50\%$ for ^3He .⁶³ There are two methods used; spin-exchange optical pumping (SEOP) and metastable-exchange optical pumping (MEOP). The most common method, SEOP, uses circularly polarised light to polarise the valence electron of a vapourised alkali metal. The polarisation generated is then transferred to the nuclear spin of a noble gas by collision of the gas molecule with the alkali metal. Rubidium is commonly used as it has only one valence electron, is in high abundance, and is readily vaporised. In contrast to SEOP, MEOP does not require an alkali metal intermediate and the noble gas is polarised directly by a metastable noble gas state. Despite being quicker than SEOP, MEOP is less efficient method for hyperpolarising noble gases. Optical pumping is frequently used to hyperpolarise ^3He or ^{129}Xe for medical imaging of the lung when used with ^3He MRI. ^{129}Xe has the advantage of being soluble in blood so hyperpolarised ^{129}Xe can be used to image the circulatory system and organs. The T_1 relaxation times of noble gases are relatively long compared to other nuclei so will have longer polarisation lifetimes resulting molecules being

polarised for very long periods. This technique however is only applicable to noble gases so has limited applications

1.10.3. Parahydrogen-induced polarisation

Parahydrogen-induced polarisation (PHIP) is a hyperpolarisation technique that is achieved *via* a chemical reaction using parahydrogen.⁶⁴ Molecular hydrogen can exist in two possible states; orthohydrogen where the two proton spins are aligned parallel forming three triplet states or parahydrogen where the two spins are aligned anti-parallel which forms a singlet state. At room temperature the ratio of ortho-H₂: para-H₂ is 3:1. Parahydrogen can be prepared by mixing hydrogen gas with a highly inhomogeneous, locally paramagnetic species (e.g. metal oxides or activated carbon) at a temperature of 4 K, this results in 99.9% parahydrogen.^{65,66} This nuclear ordering or polarisation is achieved at much higher temperatures than by using the brute force method thus making parahydrogen an ideal source of spin order for hyperpolarisation experiments. Once parahydrogen is produced, it is inserted into a carbon-carbon double or triple bond of an asymmetrical precursor molecule through catalytic hydrogenation (Figure 13).⁶⁶ Once the C=C double bond is saturated with parahydrogen, its inherent spin order is transferred to a vicinal heteronucleus, typically a ¹³C nucleus *via* asymmetric coupling. A ¹³C labelled carbonyl group is common among substrates studied using PHIP because it has a relatively long *T*₁ relaxation time and helps with coordination with the hydrogenation catalyst. Typically a α,β -unsaturated carbonyl substrate is used as the PHIP- precursor. Parahydrogen-induced polarisation yields signal-to-noise enhancements of up to 10⁵.

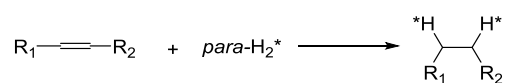


Figure 13: Catalytic hydrogenation of a double bond in a precursor molecule using parahydrogen.

A limitation on this technique is the availability of a corresponding unsaturated asymmetric precursor of the substrate of interest, thus can only be used on a limited class of molecules. Another issue that limits the substrate scope is precursors that undergo keto-enol tautomerism where the more stable equilibrium form of the precursor is the keto form which cannot be hydrogenated (Figure 14a).⁶⁵ These series of compounds cannot be used unless the enol tautomer is stabilised. An ester is commonly used to stabilise the enol form, as the ester can be hydrogenated with parahydrogen then undergo

saponification with sodium hydroxide to produce a carboxylic acid and the desired polarised molecule (Figure 14).

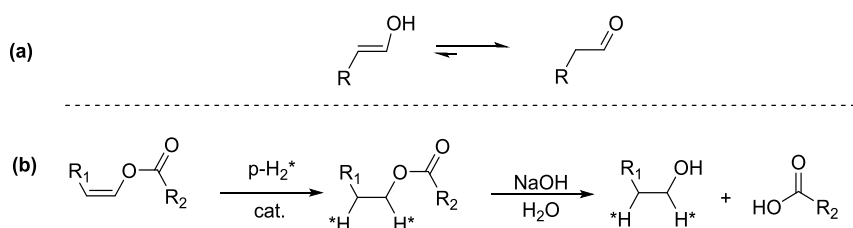


Figure 14: a) Keto-enol tautomerism b) Stabilisation of enol tautomer through formation of an ester, followed by para-hydrogenation and ester hydrolysis.

1.10.4. Dynamic nuclear polarisation

The final hyperpolarisation technique is dynamic nuclear polarisation (DNP) and has emerged as the frontrunner for hyperpolarisation techniques due to high polarisation, large substrate range and wide range of biomedical applications. DNP involves the high spin polarisation of free electrons being transferred to a nuclear spin by microwave irradiation. This enhances the differences between the nuclear energy levels resulting in a dramatically enhanced MR signal by up to 10^5 . Dynamic nuclear polarisation was first predicted by Overhauser in 1953,⁶⁷ and was later observed experimentally in metals by Slichter. Over the years DNP has played an important role in producing solid targets for high-energy physics research, structural biology determination,⁶⁸ and accessing *in vivo* metabolism.^{69,70} The latter process is possible due to the key development from Golman and co-workers where they showed the polarised nuclear spins can be warmed rapidly to room temperature with substantial retention of the polarisation that was present in the frozen solid state therefore producing a hyperpolarised liquid-state.⁷¹ This is achieved by rapidly dissolving the frozen sample in pressurised superheated water ~ 180 °C. Electrons are inherently highly polarised (>90%) due to their large gyromagnetic ratio.

1.11. Dissolution-DNP experiment

DNP works by transferring the polarisation of an electron to the nuclei of interest using microwave irradiation at low temperature and high magnetic field. This is achieved using specialised equipment, a DNP polariser. During a dissolution-DNP experiment there are three main processes; sample preparation, hyperpolarisation and dissolution:

1. *Sample preparation:* The DNP sample consists of the substrate to be hyperpolarised enriched with a MR-active nucleus (*e.g.* ^{13}C), a source of unpaired electron and a solvent. For some substrates a glassing agent, such as glycerol, is used and/or Gd-chelates added to enhance polarisation. Organic free radicals are usually the source of unpaired electron used in DNP experiments. The electron resonance needs to have a linewidth of the same order or lower than the nuclear Larmor frequency, therefore a trityl radical *e.g.* OX063 is commonly used as the free electron source when polarising protons. However when using a trityl radical and ^{13}C , thermal mixing is often the source of polarisation due to the electron resonance being wider than the ^{13}C Larmor frequency. Therefore nitroxide radicals such as TEMPO, BDPA, DPPH or galvinoxyl are often used. The solvent used in DNP experiments is chosen to maximise the concentration of the ^{13}C substrate in the sample to enhance ^{13}C - ^{13}C spin diffusion during polarisation and allowing a more concentrated solution after dissolution. To ensure the homogeneous distribution of the radical, the sample must form an amorphous solid or become “glassy” upon freezing. To achieve this, a co-solvent such as DMSO or glycerol can be added to the aqueous sample. It has been showed that the addition of Gd^{3+} -chelates can increase the polarisation of a sample.⁷² In a recent study, the gadolinium complex 10-(2-hydroxy-propyl)-1,4,7,10-tetraazacyclododecane-1-4-7-triacetic acid (gadoteridol) was added to sample of $[1 - ^{13}\text{C}]$ pyruvate with different radicals; OX063, 4-oxo TEMPO and BDPA. They showed a 300% increase in solid state polarisation with pyruvate and OX063 when adding Gd^{3+} -chelate. This increase has been attributed to the shortening of the electronic spin-lattice relaxation time T_{1e} . However since the Gd-chelates are paramagnetic, they may also shorten the T_1 of the ^{13}C nucleus in the molecule of interest, thus reducing the observable window available.
2. *Hyperpolarisation:* The sample cup is inserted in the polariser and rapidly frozen to ~ 1.2 K (which is achieved by boiling off helium under vacuum at ~ 100 Pa) and is placed in a magnetic field. The electron spin polarisation can then be transferred to the nuclear spins by microwave irradiation at or close to the Larmor frequency, with the solid-state polarisation reaching a plateau at 1-2 hours for a typical sample.

3. *Dissolution*: The dissolution process involves transferring the solid hyperpolarised sample from the polariser to *in vitro* or *in vivo* models in either a MRI or NMR machine whilst retaining the polarisation.⁷¹ It first needs to be rapidly warmed to room temperature which is achieved by rapidly dissolving the frozen sample in pressurised superheated water (180 °C). Several solvents can be employed for dissolution but for biological applications an aqueous buffer is used. A chelating agent (typically ethylene-dinitrotetraacetic acid, or ETDA) is often used to bind paramagnetic ions that might increase the relaxation rate. The solution is then ready for *in vitro* or *in vivo* applications, which usually performed with 1-2 minutes following dissolution to minimise T_1 -dependent loss of signal.

1.12. Hyperpolarisation substrates

There are a number of different techniques used to induce hyperpolarisation, but the hyperpolarisation of substrates for *in vivo* studies has been dominated by a technique called dynamic nuclear polarisation (DNP). In principle any nucleus can be polarised, although attention has largely been focussed on ^{13}C . This is due to its relatively long T_1 times and commercial availability of ^{13}C -labelled cell metabolites. In ^1H -MRS the chemical shift range of metabolites of interest is limited ($\Delta\delta \approx 10$ ppm), which results in crowded spectra resulting in difficult deconvolution of the data. Also, a large number of water and lipid protons relative to the metabolites can overwhelm the spectrum. However, the chemical shift range of ^{13}C metabolites is much larger than ^1H ($\Delta\delta \approx 200$ ppm), which allows for improved resolution of metabolites that would otherwise not be resolved. Also, because the natural abundance of ^{13}C in the body is very low, the background noise created by these nuclei is kept to a minimum since non-enriched metabolites are not generally observable in biological applications. The ^{13}C nucleus has a gyromagnetic ratio that is 25% that of ^1H and its natural abundance is much lower at 1.1%, making it very insensitive, so the MR imaging of endogenous ^{13}C compounds is not possible within reasonable imaging times. However, using hyperpolarised ^{13}C -enriched metabolites, the sensitivity can be increase dramatically. Despite the fact that the vast majority of hyperpolarised experiments (certainly for biological applications) use the ^{13}C nucleus there are a number of other nuclei that have been hyperpolarised (Table 3).

Entry	Nucleus	Natural abundance	γ (relative to ^1H)	Example substrates
1	^1H	99.98	1	H_2O
2	^{13}C	1.11	0.2515	Pyruvate, fructose, urea
3	^{15}N	0.37	0.1013	Choline ⁷³
4	^{29}Si	4.70	0.1987	Nanoparticles ⁷⁴
5	^{89}Y	100	0.1761	DOTA chelates ⁷⁵

Table 3: Nuclei and example substrates that have been hyperpolarised using dissolution-DNP.

1.12.1. ^{13}C DNP probe development

At present hyperpolarised ^{13}C agents can be divided into three categories according to their uses:

1. *Endogenous molecules modified by ^{13}C enrichment:* These molecules are often key biochemicals in metabolic pathways. Not only can these metabolites be imaged but their metabolic products can also be detected in real-time. This provides information that will help better understand and treat metabolic diseases such as cancer and diabetes *e.g.* $[1 - ^{13}\text{C}]$ pyruvate or $[1 - ^{13}\text{C}]$ lactate
2. *Environmental sensors:* These agents can be endogenous or non-endogenous and are used to detect chemical environment *e.g.* $\text{H}^{13}\text{CO}_3^-$ used to detect pH.
3. *Molecules to advance and understand DNP-NMR techniques and technology e.g.* $[2,3 - ^{13}\text{C}_2]$ diacetyl is used to study spin polarisation in the singlet state.

There are many considerations for developing ^{13}C DNP substrates used for *in vitro* and *in vivo* studies. They are generally small molecules (<200 Da) and contain a ^{13}C nucleus with a long T_1 time. In hyperpolarisation studies the T_1 relaxation time determines how long the hyperpolarisation lasts, and therefore the length of useful imaging time. After dissolution, ~37% of the hyperpolarised MR signal remains after $1 \times T_1$ and ~5% after $3 \times T_1$. Therefore, the imaging window after dissolution is usually only $3 - 5 \times T_1$. For this reason, the placement of the ^{13}C nucleus in a DNP probe usually means that it does not have a neighbouring spin $\frac{1}{2}$ nucleus, for example, carboxylate carbons. Therefore, ^{13}C nuclei attached directly to protons are not feasible candidates for DNP probes due to having small T_1 times, however, this can be overcome by substitution of ^1H with ^2H . The majority of ^{13}C DNP substrates usually contain carbonyl groups: carboxylic acids, ketones, amides and esters have all been studied. Of these, carboxylic acids are most popular due to their abundance in endogenous metabolites, water solubility, longer T_1

times, relative ease of ^{13}C -enrichment and because they are often the active functional group in metabolic conversion. Non-carbonyl substrates can also be used in DNP studies, providing they have a sufficient T_1 time.

The placement of a ^{13}C in a carboxyl or carbonyl group, which removes the ^{13}C - ^1H intramolecular dipolar relaxation, is not always possible, especially for aliphatic compounds. However, the polarisation lifetime can still be increased by deuterium enrichment but the ^2H enrichment needs to occur at non-exchangeable sites. Deuterium is a quadrupole nucleus with a spin of 1 therefore it exhibits scalar coupling (J -coupling) with other spin $\frac{1}{2}$ nuclei *e.g.* ^{13}C nuclei where $J_{(^{13}\text{C}-^2\text{H})} \sim 30$ Hz. Using ^{13}C probes with deuterium enrichment has been used on multiple occasions and has been shown to dramatically increase T_1 times (Table 4). The size of the effect is proportional to the strength of the ^1H coupling (with ^{13}C) of the replaced nucleus, the stronger the coupling, the greater the effect. However, ^2H substitution also leads to splitting which can decrease the overall SNR when moving to field strengths where J is large relative to ω . ^2H Substitution can also have an impact on the metabolism in biological systems, due to kinetic isotope effects and may impact the ability to observe certain deuterated ^{13}C metabolites in DNP-NMR by slowing down the rate of metabolic conversion.

Entry	Probe	Non deuterated T_1 time	Deuterated T_1 time
1	[2- ^{13}C , U- ^2H] fructose	16 s (@11.7 T)	34 s (@11.7 T)
2	[U- ^{13}C , U- ^2H] glucose	-	T_1 reported are $^{13}\text{C}_{1-5} \sim 12$ s and $^{13}\text{C}_6 \sim 10$ s.
3	[5- ^{13}C , 4- $^2\text{H}_2$] glutamine	-	Results in \sim two-fold increase in the T_1 time for C_5 .

Table 4: Comparison of T_1 from deuterated and non-deuterated substrates.

Generally DNP probes are small in molecular size (<200 Da). This is due to their ease of synthesis, high aqueous solubility and relevance in fast metabolism. Also the T_1 rate decreases as a function of the increasing correlation time (τ_c) seen with increasing molecular size. The highest reported DNP enhancements are seen with small molecules (<200 Da). ^{13}C DNP probes that are to be used in biological systems (*in vitro* or *in vivo*) are usually limited to those that are water-soluble. The probe also has to be highly soluble

in the solvent as it needs to be polarised at high concentrations in order for effective polarisation to occur. High concentrations are also needed because of the inevitable dilution caused by the dissolution process. The high concentration of the hyperpolarised DNP agents in *in vitro* and *in vivo* experiments means the toxicity of the agents also has to be considered. Therefore, the DNP probe is usually an endogenous metabolite, chemically similar to one, or chemically inert (*e.g.* Gd-chelates). Another limitation of the type of probe that can be used in DNP experiments is the synthetic feasibility of ^{13}C enrichment of a probe that meets the above requirements and is met at reasonable costs.

1.13. Project aims

The aim of this project is to investigate the *ortho*-quinone metabolism of CA1P **9** by synthesising then hyperpolarising a ^{13}C -labelled combretastatin A1P. At first, the location of the ^{13}C label needs to be determined which can be done by finding the carbon atom with the longest T_1 time. Next, a route needs to be developed that incorporates a ^{13}C label into one of the already established syntheses of combretastatins.

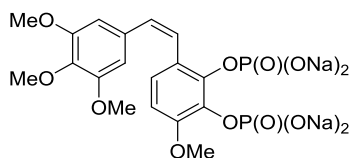


Figure 15: Target molecule to be enriched with a ^{13}C label.

Chapter 2: Synthesis of [¹³C]-Combretastatin

A1P

2.1. T_1 relaxation times of Combretastatin A1P

The synthesis of a hyperpolarised [¹³C]-labelled CA1P substrate first requires the optimum ¹³C labelling site to be determined. The site of the ¹³C nucleus needs to be chosen so it induces the largest hyperpolarisation as well as being synthetically viable. The T_1 value of the ¹³C nucleus dictates the length of hyperpolarisation and therefore the imaging window ($3 - 5 \times T_1$) in which to observe the metabolism of CA1P. This means a long T_1 value is crucial. The T_1 relaxation times of the carbon atoms in CA1P **9** were determined through an Inverse Recovery Sequence (Figure 15, Table 5).ⁱ

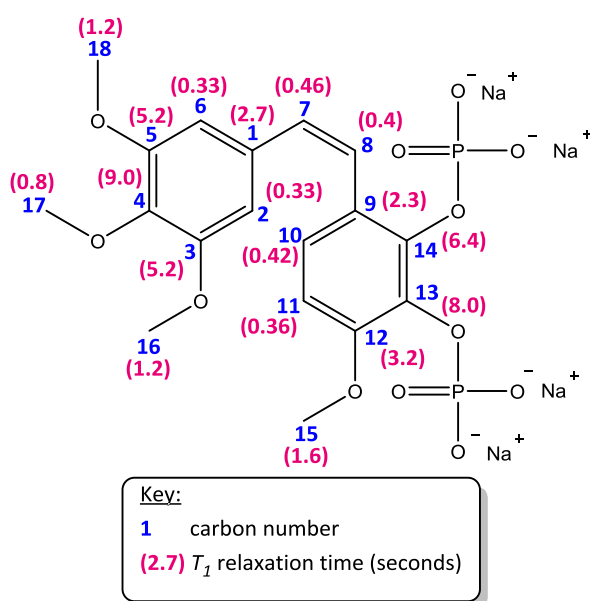


Figure 16: The T_1 values for the ¹³C atoms in CA1P **9** (34 mM in D₂O).

Carbon number	¹³ C (ppm)	T_1 (s)
1	133.75	2.7
2	106.8	0.33
3	152.09	5.2
4	135.68	9.0
5	152.09	5.2
6	106.8	0.33
7	125.8	0.46
8	130.0	0.4
9	124.06	2.3
10	125.0	0.42
11	108.3	0.36
12	151.9	3.2
13	143.56	8
14	134.44	6.4
15	56.1	1.6
16	56.0	1.2
17	60.9	0.8
18	56.0	1.2

Table 5: ¹³C chemical shifts values of CA1P **9** with measured T_1 relaxation values for a 34 mM sample in D₂O.

ⁱ The work finding the T_1 times of CA1P was done by Dr. Steven Reynolds, University of Sheffield, UK.

The longest relaxation time was found to be the carbon in the 4-position in ring A with a value of 9.0 seconds (Figure 15, Table 5, Entry 4). However C₄ is on the opposite side of the molecule to where the oxidative changes occur on the phosphorylated ring during metabolism, therefore any chemical change that occurs during metabolism would produce a small-to-negligible chemical shift change for the signal of the ¹³C label. With the second highest T₁ relaxation time of 8.0 seconds, C₁₃ could be another candidate for ¹³C labelling. Not only does it have a high relaxation time T₁, it is also located on the metabolically active ring, so was chosen as the site for the ¹³C label (Figure 17).

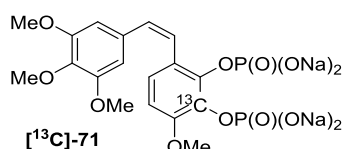
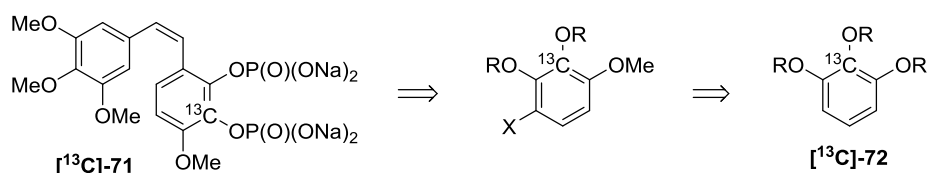


Figure 17: Target ¹³C-labelled molecule.

2.2. Synthesis of core aromatic species

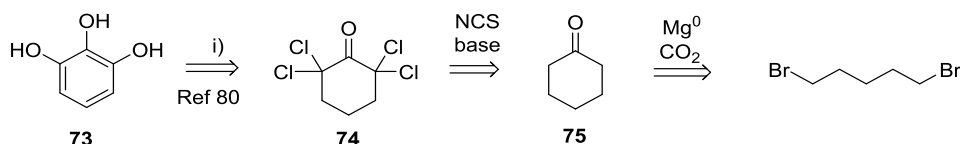
The synthesis of [¹³C]-combretastatin A1P [¹³C]-**71** presented several significant challenges, the first of which is the regioselective insertion of the carbon-13 label into an aromatic species. Since there are no suitable commercially available sources of ¹³C-labelled aromatic compounds, a route needed to be developed to synthesise a 1,2,3-trioxybenzene species **72**, where a ¹³C label is installed in the C₂ position (Scheme 19).



Scheme 19: Retrosynthesis analysis of CA1P **71**.

A common route for the synthesis of 1,2,3-trihydroxybenzene **73** comes from the decarboxylation of gallic acid either using a copper autoclave or by microbes.^{76,77} Pyrogallol **73** can also be synthesised from phenol,⁷⁸ or the deoxygenation of polyhydrobenzenes.⁷⁹ However these routes all require an aromatic precursor which is commonly derived from the enzymatic reactions of glucose. There are a limited number of routes for the synthesis of pyrogallol **73** which involve a non-aromatic simple precursor, one of which is to start from 2,2,6,6-tetrahalocyclohexanone **74** that can be treated with butyrolactone and potassium hydroxide to give pyrogallol **73** (Scheme 20).⁸⁰ 2,2,6,6-

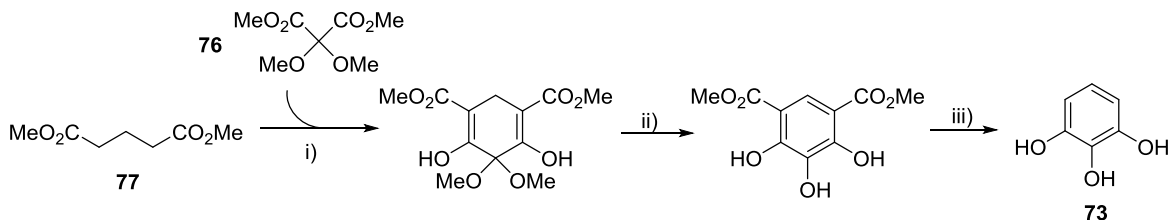
Tetrahalocyclohexanone **74** can be synthesised through chlorination of cyclohexanone **75** which can be synthesised by the double Grignard addition of 1,5-dibromopentane to carbon dioxide. For the ^{13}C -synthesis of the carbon dioxide can be replaced with commercially available ^{13}C -carbon dioxide.



Reagents and conditions: i) Butyrolactone, KOH.

Scheme 20: Retrosynthetic analysis of pyrogallol **73** via 2,2,6,6-tetrachlorocyclohexanone **74**.

The first synthesis of pyrogallol **73** from an aliphatic source was developed by Shipchandler (Scheme 21).⁸¹ It was achieved by the condensation of dimethyl dimethoxymalonate **76** with dimethyl glutarate **77** followed by aromatisation and decarboxylation. However for this synthesis to be viable the ^{13}C label needs to be in the central carbon of the dimethyl dimethoxymalonate **76** which itself is not trivial and would add a number of steps to the synthesis.

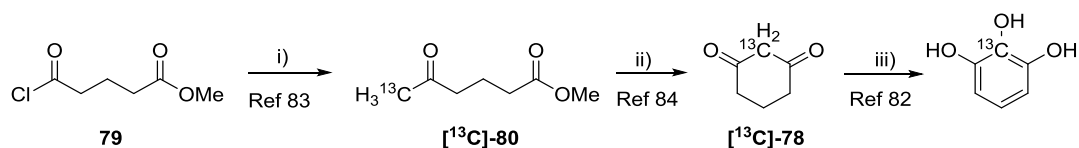


Reagents and conditions: i) NaH; ii) refluxing 48% HBr; iii) 200 °C, MeOH.

Scheme 21: Formation of pyrogallol **73** from aliphatic precursors **76** and **77**.

Another route involves oxidation of the enol form of 1,3-cyclohexanedione using singlet oxygen in the presence of fluoride ions and polymer bound Rose Bengal which was developed by Wasserman and Picket (Scheme 22).⁸² ^{13}C -Labelled 1,3-cyclohexanedione [^{13}C]-**78** can be prepared following the method by Botting and co-workers by the reaction of [^{13}C]-methyl lithium with glutaric acid monomethyl ester chloride **79** which forms ketone [^{13}C]-**80** which is then cyclised to [^{13}C]-cyclohexanedione [^{13}C]-**78** with potassium *tert*-butoxide.^{83,84} This route has the advantage of using [^{13}C]-methyl iodide as the [^{13}C]-label source which is a liquid, commercially available, and easily converted into Grignard reagents or lithiated species. The proposed route also has strong literature

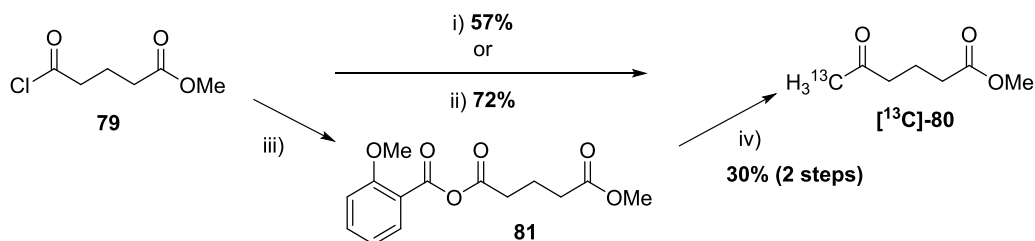
precedence and has only 3 steps, so was chosen as a basis for the synthesis of [^{13}C]-combretastatin A1 [^{13}C]-**71**.



Reagents and conditions: i) MeLi, Et₂O, CuI, 0 °C; ii) KOtBu, THF, 0 °C; iii) Bu₄NF, CHCl₃, O₂, polymer bound Rose bengal.

Scheme 22: Proposed route for the synthesis of [^{13}C]pyrogallol.

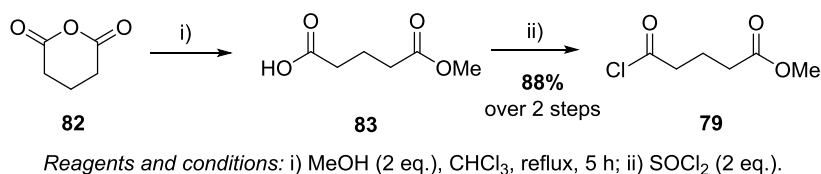
The first step of the synthesis involves the insertion of a $^{13}\text{CH}_3$ unit into glutaric acid monomethyl ether **80**. The transformation of acid chloride **79** to labelled ketone [^{13}C]-**80** has already been achieved in the literature.⁸⁵ Boyce and co-workers first converted monomethyl ester acid chloride **79** to the mixed anhydride **81** which was then reacted with [^{13}C]-methylmagnesium iodide to form [^{13}C]-methyl-5-oxohexanoate [^{13}C]-**80** but in a low 30% yield (Scheme 23). Botting then modified the procedure and reacted acid chloride **79** directly with a cuprate formed from the reaction of [^{13}C]-methyl iodide, lithium metal and copper iodide.⁸³ This gave methyl-5-oxohexanoate [^{13}C]-**80** in an improved yield of 57%. At a later date, the same group repeated the reaction on a larger scale (294 mmol) under identical reaction conditions with a yield of 43%.⁸⁴ The drop in yield highlights a potential problem when scaling up the reaction under these conditions. Finally Yamamoto *et. al.* treated glutaric acid monomethyl ester chloride **79** with di- ^{13}C -methylcadmium which was synthesised from the reaction between cadmium chloride and [^{13}C]-methyl magnesium iodide.⁹⁶ The resulting methyl-5-oxohexanoate [^{13}C]-**80** was formed in a 72% yield. Even though this method produced high yields the drawbacks are the hygroscopic, pyrophoric and highly toxic nature of dimethylcadmium.



Reagents and conditions: i) a) Li, $^{13}\text{CH}_3\text{I}$, Et₂O; b) CuI, 0 °C; c) glutaric acid monomethyl ester chloride **79**, -20 °C, ii) a) $^{13}\text{CH}_3\text{I}$, Mg⁰, ether, reflux; b) CdCl₂; c) glutaric acid monomethyl ester chloride **79**; iii) 2-methoxybenzoic acid, triethylamine, THF, -10 °C; iv) -78 °C, $^{13}\text{CH}_3\text{MgI}$, 30 min.

Scheme 23: Literature results for the synthesis of methyl-5-oxohexanoate [^{13}C]-**80** from glutaric acid monomethyl ester chloride **79**.

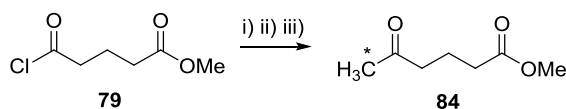
The work in this project began using non-labelled (^{12}C) material to establish and optimise a strategy before using ^{13}C substrates.ⁱⁱ The glutaric acid monomethyl ester chloride **79** starting material was prepared by methanolysis of glutaric anhydride **82** and gave monomethyl glutarate **83** in quantitative yields and was used without further purification. The dropwise addition of thionyl chloride to monomethyl glutarate **83** yielded the acid chloride **79** in an 88% yield after isolation through distillation (Scheme 24).⁸⁶ The acid chloride **79** was then freshly distilled before each experiment.



Scheme 24: Formation of glutaric acid monomethyl ester chloride **79**.

Next, the glutaric acid monomethyl ester chloride **79** was added to the lithium dimethylcuprate formed from the treatment of methyl lithium and copper(I) iodide and this gave methyl-5-oxohexanoate **84** in a 47% yield, which is comparable to the results observed by Botting (Table 6, Entry 1).^{83,84} The reaction was optimised by using commercially available methyl magnesium bromide, but unfortunately this resulted in a lower yield of methyl-5-oxohexanoate **84** (Table 6, Entry 2). For the eventual ^{13}C synthesis the Grignard reagent will need to be synthesised from commercially available sources of ^{13}C ($^{13}\text{CH}_3\text{I}$). Therefore, methyl magnesium iodide was made from magnesium turnings and methyl iodide in diethyl ether, and when the resulting Grignard reagent was treated with acid chloride **79** and copper(I) iodide, the resulting methyl-5-oxohexanoate **84** was formed in a higher yield of 55% (Table 6, Entry 3). Next, the copper source was changed to copper(I) bromide dimethyl sulfide complex as it was expected to form a more stable organocopper reagent. When treated with the three different methyl organometallics an improved yield was observed in each case (Table 6, Entry 4 – 6). The best result was observed when treating glutaric acid monomethyl ester chloride **79** with methyl magnesium iodide and copper(I) bromide dimethyl sulfide complex which gave the desired ketone **84** in a 69% yield (Table 6, Entry 6). It was noticed that when the copper(I) bromide dimethyl sulfide complex was freshly recrystallised from dimethyl sulfide, higher and more consistent yields were observed.

ⁱⁱ *C will denote the eventual location of the ^{13}C label



Reagents and conditions: i) Copper source, THF, 0 °C; ii) MeLi or MeMgBr, THF 1 h; v) glutaric acid monomethyl ester chloride **79**, -10 °C, 1 h.

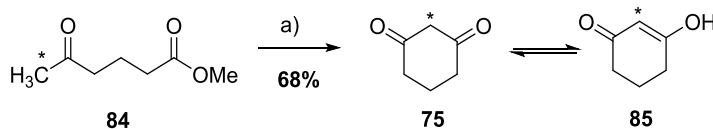
Scheme 25: Transformation of glutaric acid monomethyl ester chloride **79** to methyl-5-oxohexanoate **84**.

Entry	Methyl source	Copper source	Crude mass of methyl-5-oxohexanoate
1	MeLi	CuI	47%
2	MeMgBr	CuI	22%
3	MeMgI ^a	CuI	55%
4	MeLi	CuBr.DMS ^b	50%
5	MeMgBr	CuBr.DMS ^b	62%
6	MeMgI ^a	CuBr.DMS ^b	69%

^a Synthesised from magnesium turnings and iodomethane; ^b Freshly recrystallised from DMS

Table 6: Optimisation of the transformation of glutaric acid monomethyl ester chloride **79** to methyl-5-oxohexanoate **84**.

Previous cyclisations of methyl-5-oxohexanoate **84** to 1,3-cyclohexanedione **75** have been carried out using either potassium *tert*-butoxide or sodium methoxide.⁸³⁻⁸⁵ Botting and co-workers showed that cyclisation using potassium *tert*-butoxide on a 5.22 mmol scale gave an 86% yield, however scaling the reaction up to 14.5 mmol and adding a purification step decreased the yield to 69%.^{83,84} Boyce and co-workers also observed a lower yield of 61% when using sodium methoxide at a larger scale of 41 mmol.⁸⁵ Following the procedure described by Botting, the intramolecular Claisen condensation was carried out on methyl-5-oxohexanoate **84** in dry tetrahydrofuran using potassium *tert*-butoxide as a base (Scheme 26). On a 12.5 mmol scale 1,3-cyclohexanedione **75** was formed in an 68% yield after purification by flash column chromatography. The ¹H NMR spectrum of diketone **75** displayed a mixture of keto **75** and enol **85** tautomers.

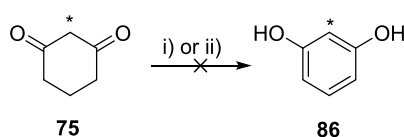


Reagents and conditions: a) i) KOtBu (2 eq.), THF, reflux, 6 h.

Scheme 26: Cyclisation of methyl-5-oxohexanoate **84** to 1,3-cyclohexanedione **75**.

Previously in the Jones group, two attempts were made at the oxidative aromatisation of 1,3-cyclohexanedione **75** to pyrogallol **73**, the first reproducing the work by Wasserman and Pickett.⁸² This process involved oxidising the enol form of 1,3-cyclohexanedione **85** using singlet oxygen in the presence of fluoride ions and polymer bound Rose Bengal, but this failed to give the desired product, just returning starting material. The other method explored used hydrogen peroxide and sodium hypochlorite in the presence of fluoride ions; however this again returned starting material.

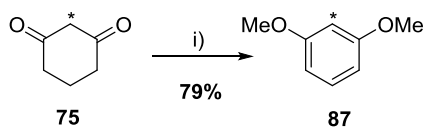
It is known that resorcinol **86** can be synthesised from the aromatisation of 1,3-cyclohexanedione **75** by catalytic dehydrogenation using a palladium on charcoal catalyst in refluxing xylene or toluene.^{83,84} However attempts to reproduce these results were unsuccessful; despite loss of starting material and formation of aromatic signals in the crude ¹H NMR spectrum, formation of the desired resorcinol **86** was not observed (Scheme 27). Another oxidising agent which is known to promote dehydration and aromatisation reactions is 2,3-dichloro-5,6-dicyanobenzoquinone (DDQ) however when 1,3-cyclohexanedione **75** was treated with DDQ in refluxing toluene, a complex mixture was obtained and no resorcinol **86** was observed.



Reagents and conditions: i) Pd/C (10%), xylene, reflux; ii) DDQ, toluene, reflux.

Scheme 27: Attempts at aromatisation of 1,3-cyclohexanedione **75**.

Molecular iodine is another oxidising agent used for the aromatisation of cyclohexenone derivatives and was first used in 1980 by Tamura and Yoshimoto.⁸⁷ The addition of iodine to methanol heated at reflux afforded a variety of anisole derivatives. Later these conditions were applied to 1,3-cyclohexanedione derivatives which were transformed into substituted resorcinols.^{88,89} When these conditions were applied to 1,3-cyclohexanedione **75**, both aromatisation and *O*-methylation were observed and the dimethoxy resorcinol **87** was formed in a 79% yield (Scheme 28).

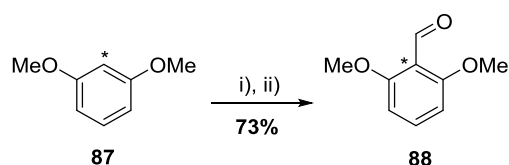


Reagents and conditions: i) I₂, MeOH, reflux.

Scheme 28: Formation of dimethoxy resorcinol **87**.

With a high yielding step into an aromatic species, the next step is to insert a phenol substituent onto carbon-2. This can be achieved by selective formylation in the C-2 position followed by a Baeyer-Villiger oxidation. Initial attempts at selective formylation involved treating 2,6-dimethoxybenzene **87** with paraformaldehyde, magnesium dichloride and triethylamine.⁹⁰ Usually in this reaction the treatment of a phenol and MgCl₂-NEt₃ results in the formation of magnesium phenoxide, which coordinates with the oxygen of the paraformaldehyde and directs the carbon-carbon bond formation to the *ortho*-position.⁹¹ However using these conditions on 2,6-dimethoxybenzene **87** returned only starting material, perhaps due to the methoxy group being unable to coordinate effectively to the magnesium metal. Other known *ortho*-formylation methods include using Reimer-Tiemann conditions of chloroform and sodium hydroxide. Here the chloroform and sodium hydroxide react to form a dichlorocarbene and undergoes attack at the *ortho*-position of the phenol ring. When applying these Reimer-Tiemann conditions to 2,6-dimethoxybenzene **87** no reaction was observed, likely to be due to the absence of a negatively charged phenolate species which increases the nucleophilicity of the aromatic ring.

Vilsmeier-Haack conditions use phosphoryl chloride and dimethylformamide which react to form an electrophilic chloroiminium ion, which goes on to react with arenes to produce an iminium ion intermediate which can be hydrolysed to a benzaldehyde. Despite this being a generic formylation method, it was thought that when applied to 2,6-dimethoxybenzene **87** the two methoxy groups could direct the formylation into the C-2 position. Unfortunately the desired product was not seen when these conditions were used with 2,6-dimethoxybenzene **87**. However, the successful formylation of 2,6-dimethoxybenzene **87** was achieved through the regioselective lithiation with *n*-butyllithium at 0 °C in tetrahydrofuran in the presence of *N,N,N',N'*-tetramethylethylenediamine (TMEDA) followed by treatment with dimethylformamide and acidic workup (Scheme 29).⁹²

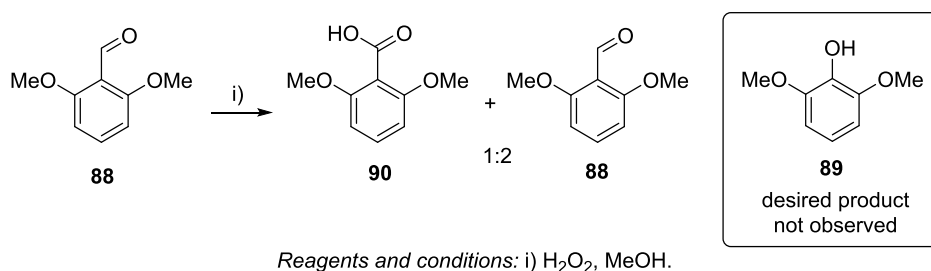


Reagents and conditions: i) TMEDA, *n*BuLi, THF ii) DMF.

Scheme 29: Formylation of 2,6-dimethoxybenzene **87**.

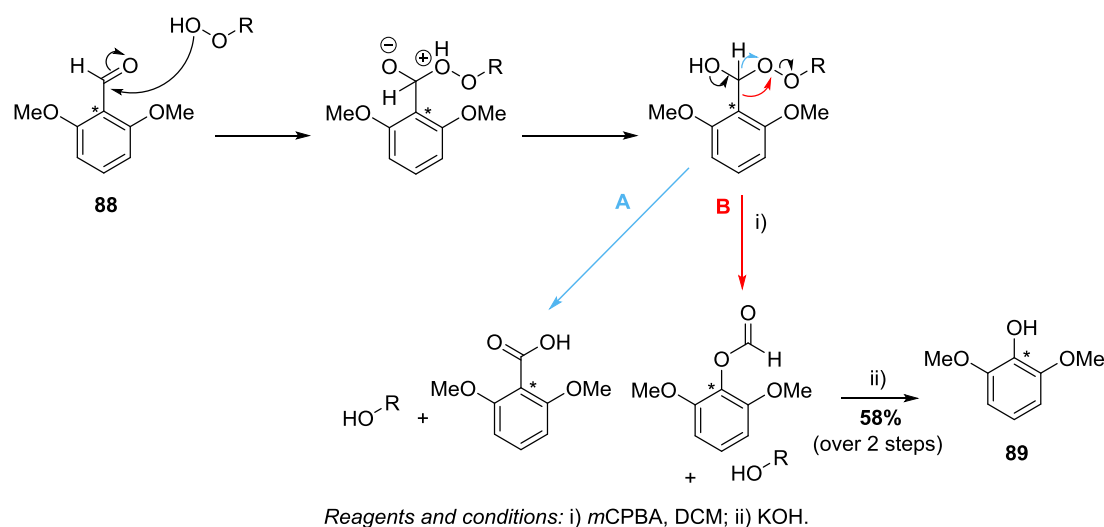
The regioselectivity of the resulting benzaldehyde **88** was confirmed by the splitting pattern in the ^1H NMR spectrum; two aromatic protons signals were observed, a doublet with an integral of two protons and a triplet with an integral of one proton. Haight and co-workers state that although the TMEDA was not essential for metalation it is thought to stabilise the DMF adduct.⁹² The group also found that the addition of aqueous hydrochloric acid in the workup procedure was required to prevent the formation of Cannizzaro reaction by-products, the reduced alcohol and oxidised carboxylic acid, neither of which were observed during the formylation of 2,6-dimethoxybenzene **87**.

The conversion of a benzaldehyde into a phenol can be achieved by a Baeyer-Villiger oxidation reaction using a peroxy acid or hydrogen peroxide species. Therefore, 2,6-dimethoxybenzaldehyde **88** was initially treated with hydrogen peroxide in methanol, but unfortunately this failed to yield the desired phenol **89** and instead gave unreacted starting material and the carboxylic acid **90** in a 2:1 ratio (Scheme 30).⁹³



Scheme 30: Baeyer-Villiger reaction on 2,6-dimethoxybenzaldehyde **88**.

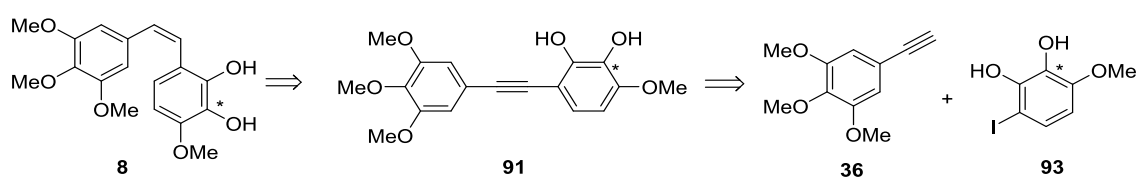
The carboxylic acid **90** was formed through hydride-migration in the rearrangement step of the Baeyer-Villiger reaction (Scheme 31, Route A). In order for the desired phenol **89** to form, aryl group migration is required (Scheme 31, Route B). This was observed after treatment of 2,6-dimethoxybenzaldehyde **88** with *meta*-chloroperoxybenzoic acid in dichloromethane, which gave the formate ester **91** (Scheme 31). Subsequent cleavage of the formate ester **91** with potassium hydroxide gave the desired phenol **89** in a 58% yield.



Scheme 31: Baeyer-Villiger oxidation mechanism.

2.3. Synthesis of CA1P *via* selective reduction of diarylalkyne

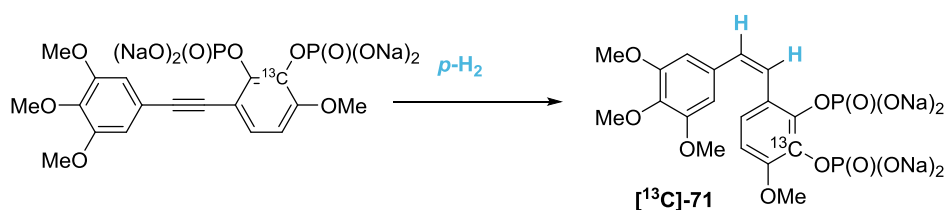
With a route towards a tri-oxygenated benzene species **89** in hand, the synthesis towards CA1 **8** could continue. The selective alkyne reduction strategy seen previously in the synthesis of CA1 **8** and CA4 **7**,^{34,38,39,41} was chosen as it is 100% *Z*-selective, therefore reducing the need for isomer separation and giving potentially higher yields than other reported strategies. It was envisioned that the alkyne **91** needed for the selective reduction could be synthesised by a Sonogashira reaction (Scheme 32).



Scheme 32: Retrosynthesis of CA1 **8** *via* selective hydrogenation and the Sonogashira reaction.

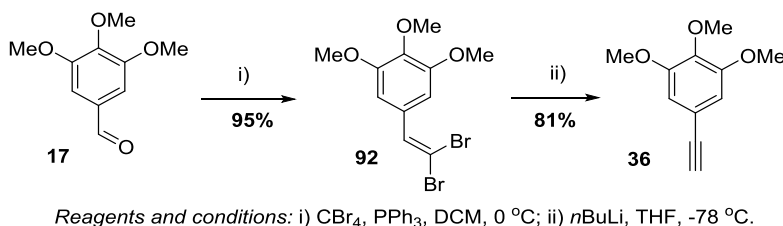
The selective reduction strategy also has the added advantage that it could be applied to a different hyperpolarisation technique called *para*-hydrogen induced polarisation (PHIP).⁶⁴ This technique uses the addition of the naturally polarised *para*-hydrogen to unsaturated precursors through a hydrogenation reaction and this results in a highly hyperpolarised species. Since one of the proposed steps in the synthesis of CA1P **9** is a hydrogenation there is potential to use PHIP to enhance the polarisation (Scheme 33). This could be useful if the hyperpolarisation created by dynamic nuclear polarisation is

insufficient to see a signal, as the hyperpolarisation from *para*-hydrogen could be transferred to the ^{13}C nucleus when used in conjunction with dynamic nuclear polarisation.



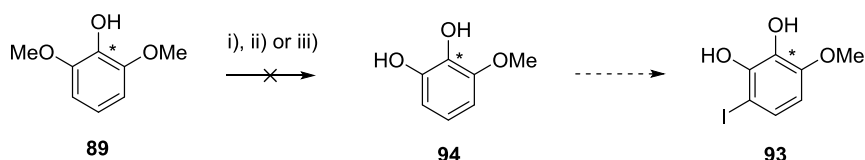
Scheme 33: Theoretical hydrogenation with *para*-hydrogen to generate hyperpolarised [^{13}C]-CAIP **71**.

The synthesis of the terminal alkyne component **36** of the Sonogashira reaction was achieved using a Corey-Fuchs reaction (Scheme 34). The aldehyde **17** was treated with carbon tetrabromide and triphenylphosphine, and formed the dibromoalkene **92** in a 95% yield. Subsequent treatment of the dibromoalkene **92** with *n*-butyllithium gave the alkyne **36** in an 81% yield upon work up and purification.



Scheme 34: Formation of the terminal alkyne **36** component of the Sonogashira reaction.

The synthesis of the iodo-component **93** of the Sonogashira reaction began by attempting to demethylate 2,6-dimethoxyphenol **89** which then can be iodinated (Scheme 35, Table 7). 2,6-Dimethoxyphenol **89** was treated with the demethylating agent boron trichloride but this unfortunately returned starting material (Table 7, Entry 1). Starting material was also recovered when the demethylating reagent was changed to aluminium trichloride (Table 7, Entry 2). The hard acid/soft nucleophile reagent pair of thiourea/aluminium trichloride has been shown to dealkylate alkyl aryl ethers where it is suspected the sulfur atom acts as a weak nucleophile and is capable of cleaving a methoxy group.⁹⁴ Treatment of 2,6-dimethoxyphenol **89** with 1.2 equivalents of both thiourea and aluminium chloride did produce the desired mono-demethylated compound **94** but only with a 46% conversion (Table 7, Entry 3). When the number of equivalents were increased to 2.5 the conversion increased slightly to 60% (Table 7, Entry 4). However no improvement was observed when 4.0 equivalents was used (Table 7, Entry 5).



Reagents and conditions: i) BCl₃, DCM, rt; ii) AlCl₃, DCM, rt; iii) Thiourea, AlCl₃, DCM, reflux.

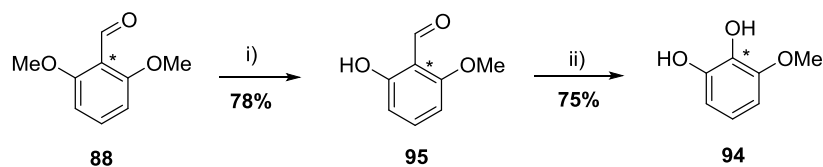
Scheme 35: Strategy 1: Demethylation followed by iodination.

Entry	Conditions	Conversion (%) ^a
1	BCl ₃ (1.2 eq.)	0
2	AlCl ₃ (1.2 eq.)	0
3	AlCl ₃ (1.2 eq.), thiourea (1.2 eq.)	46
4	AlCl ₃ (2.5 eq.), thiourea (2.5 eq.)	60
5	AlCl ₃ (4.0 eq.), thiourea (4.0 eq.)	59

^aFrom analysis of crude ¹H NMR spectrum

Table 7: Attempts at demethylation of 2,6-dimethoxyphenol **89**.

Since the selective demethylation of 2,6-dimethoxyphenol **89** was problematic it was envisioned that demethylation could be performed on the aldehyde **88**. The carbonyl group can aid and direct the demethylation and the remaining aldehyde **95** functionality can then be converted to the phenol **94** via Baeyer-Villiger oxidation (Scheme 36). Boron trichloride was chosen as the demethylating agent as it has previously been shown to effectively cleave methyl ethers in the *ortho* position,²⁴ and when treated with 2,6-dimethoxybenzaldehyde **88** mono-demethylation successfully occurred giving the phenol **95** in an 88% yield after purification. Next, the Baeyer-Villiger reaction of the benzaldehyde **95** was attempted using *meta*-chloroperoxybenzoic acid followed by sodium hydroxide as this was successful in the benzaldehyde to phenol transformation previously observed in the formation of 2,6-dimethoxyphenol **89** (Scheme 31). Unfortunately no conversion to the phenol **94** was observed and instead, 21% conversion to the carboxylic acid was seen which was due to hydride-migration rather than the desired aryl-migration in the rearrangement step of the Baeyer-Villiger reaction (Table 8, Entry 2). Therefore the oxidising agent was changed to hydrogen peroxide under basic conditions, as this has been known to convert similar benzaldehydes to phenols that have methoxy- and hydroxyl-substituents.⁹⁵ Unfortunately this only gave the desired diphenol **94** with 19% conversion (Scheme 36, Table 8, Entry 2). Matsumoto and co-workers reported the acid-catalysed oxidation of a number of benzaldehydes to phenols.⁹³ These conditions, hydrogen peroxide in methanol with catalytic sulfuric acid, were used on benzaldehyde **95** giving the desired diphenol **94** with 100% conversion and a 75% yield.



Reagents and conditions: i) BCl_3 , DCM, 18 h; ii) H_2O_2 , MeOH, H_2SO_4 (cat.).

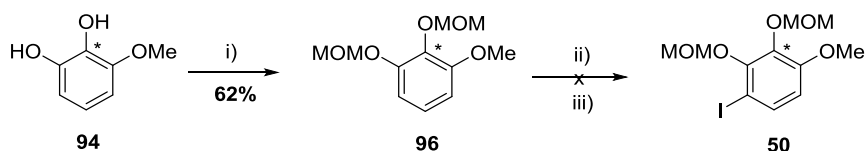
Scheme 36: Strategy 2: Demethylation, Baeyer-Villiger oxidation then iodination.

Entry	Conditions	Conversion (%) ^a
1	<i>m</i> CPBA, DCM then KOH, MeOH	0 ^b
2	H_2O_2 , NaOH	19
3	H_2O_2 , H_2SO_4 (cat.) then NaOH	100

^a From analysis of crude ^1H NMR spectrum ^b 21% conversion to carboxylic acid

Table 8: Attempts at conversion of benzaldehyde **95** to phenol **94**.

With the diphenol **94** in hand, the iodo coupling partner for the Sonogashira reaction needed to be made with the correct regioselectivity by adding an iodine atom in the 6-position. Iodination of diphenol **94** was proposed by firstly deprotonating with *n*-butyllithium then treatment with iodine. Due to the two free phenols being susceptible to deprotonation, the diphenol **94** was protected by treatment with MOMCl and sodium hydride in tetrahydrofuran, which afforded the protected diphenol **96** in a 62% yield (Scheme 37). The MOM protecting group was chosen because it is not only easy to remove but could also potentially direct the lithiation to the 6-position. Unfortunately, after treatment of protected diphenol **96** with *n*-butyllithium followed by addition of iodide, no iodine was incorporated into the molecule, with only starting material being recovered. The deprotonation/lithiation step was repeated but instead of the addition of iodine, the reaction was quenched with deuterium oxide. No deuterium incorporation was observed in the crude ^1H NMR spectrum indicating that deprotonation did not occur.



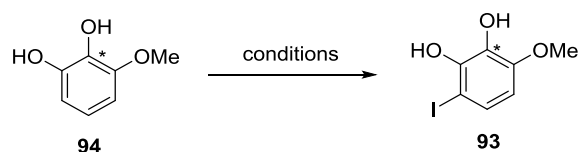
Reagents and conditions: i) NaH, MOMCl, THF, 0 °C; ii) *n*BuLi, THF, -78 °C; iii) I_2 .

Scheme 37: Attempts at the iodination of protected iodide **96**.

Rather than trying to optimise the deprotonation step, different iodination conditions were looked at for the direct treatment of the substrate **94** with an electrophilic source of iodine

(Scheme 38, Table 9). This strategy would also eliminate the need to use protecting groups. The iodination of methoxy-substituted aromatic compounds has been achieved in the literature using *N*-iodosuccinimide, an electrophilic source of iodine.¹¹⁰ However iodination with *N*-iodosuccinimide in acetonitrile at room temperature did not yield the desired iodo compound **93** neither did increasing the reaction temperature to reflux (Table 9, Entries 1 – 2).⁹⁶ Iodine(I) chloride is another source of electrophilic iodine which can be generated *in situ* from *N*-chlorosuccinimide and sodium iodide in acetic acid and has been shown to iodinate electron-rich aromatics.⁹⁷ However when 3-methoxy-benzene-1,2-diol **94** was treated with *N*-chlorosuccinimide and sodium iodide, iodination did not occur (Table 9, Entry 3). The regioselective iodination of a different methoxy-substituted phenol, 2-methoxy-benzene-1,3-diol, has been achieved using iodine and cerium(IV) ammonium nitrate (10 mol%) and when these conditions were applied to the diol **94**, the iodo species **93** was formed but only with 16% conversion of the starting material.⁹⁸ Even though the desired iodoarene **93** was produced, the unsatisfactory yield meant that other iodination conditions were investigated.

The iodination of aromatics has been demonstrated using a superelectrophilic species generated *in situ* from *N*-iodosuccinimide and a variety of catalysts. These include trifluoroacetic acid,⁹⁹ trifluoromethanesulfonic acid,¹⁰⁰ $\text{BF}_3 \cdot \text{H}_2\text{O}$,¹⁰¹ ZrCl_4 ,¹⁰² and $\text{In}(\text{OTf})_3$.¹⁰³ The diphenol **94** was treated with *N*-iodosuccinimide with catalytic trifluoroacetic acid and the desired iodinated species **93** was formed with 10% conversion (Table 9, Entry 5).⁹⁹ Iodination under conditions by Romo was attempted on 3-methoxy-benzene-1,2-diol **94**, using the mild Lewis acid indium(III) trifluoromethanesulfonate as a catalyst (10 mol%) in addition to a stoichiometric amount of *N*-iodosuccinimide.¹⁰³ Under these conditions an improved conversion of 31% to the iodo-compound **93** was observed by ^1H NMR spectroscopy (Table 9, Entry 6). Leaving the reaction for an extended time or increasing the temperature by heating at reflux failed to give the desired iodo compound in a satisfactory yield (Table 9, Entries 7 – 10).



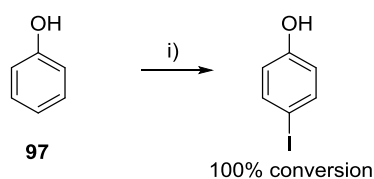
Scheme 38: Attempted iodination of diphenol **94**.

Entry	Conditions	Catalyst	Solvent	Temp.	Time (h)	Conversion (%) ^a	Reference
1	NIS	-	MeCN	rt	18	0 ^b	96
2	NIS	-	MeCN	reflux	18	0 ^b	-
3	NCS, NaI	-	AcOH	rt	18	0	97
4	I ₂ , CAN	-	MeCN	rt	18	16	98
5	NIS	TFA ^c	MeCN	rt	18	10	99
6	NIS	In(OTf) ₃ ^d	MeCN	rt	18	31	103
7	NIS	In(OTf) ₃ ^d	MeCN	rt	24	35	-
8	NIS	In(OTf) ₃ ^d	MeCN	rt	48	45	-
9	NIS	In(OTf) ₃ ^d	MeCN	rt	84	49	-
10	NIS	In(OTf) ₃ ^d	MeCN	reflux	18	0	-

^a Determined from analysis of crude ¹H NMR spectrum ^b degradation of starting material ^c 30 mol% ^d 10 mol%

Table 9: Optimisation for the iodination of 3-methoxy,1,2-benzenediol **94**.

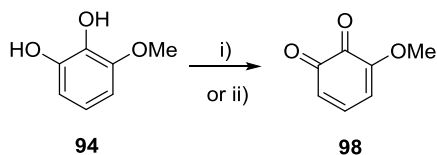
As the consistently low conversion for the iodination reactions were surprising, the NIS/In(OTf)₃ system was applied to an original substrate used in the paper, phenol **97** (Scheme 39). Under identical conditions the reaction proceeded to complete conversion which suggests that the diphenol substrate **94** is incompatible with this reaction.



Reagents and conditions: i) NIS, In(OTf)₃, MeCN, rt, 18 h.

Scheme 39: Iodination of phenol **97**.

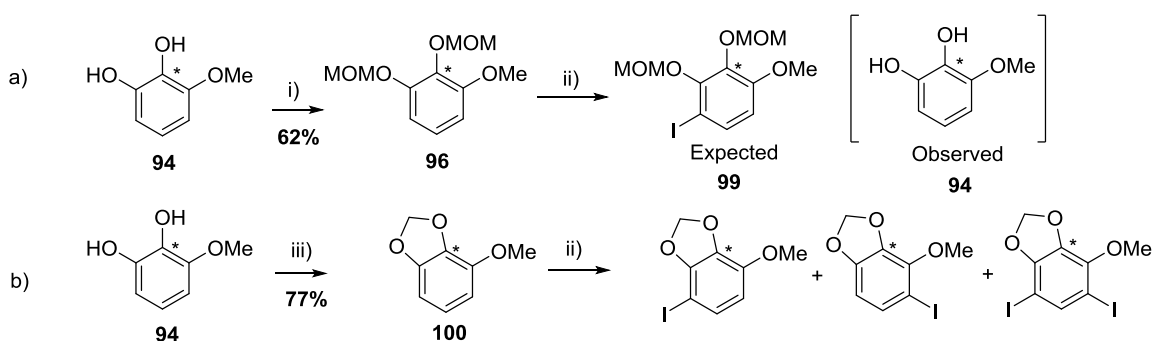
It was thought that the diphenol **94** could be deactivating the catalyst through coordination of the metal and the two phenolic oxygens. To test this hypothesis 0.5 equivalents of the diphenol **94** and 0.5 equivalents of phenol **97** were put into the same reaction vessel with *N*-iodosuccinimide and In(OTf)₃ at room temperature under the conditions reported. No iodination occurred on either substrate suggesting that catalyst inhibition was occurring. 1,2-Diols are known to be oxidised to *ortho*-quinone species in the presence of an oxidising reagent (Scheme 40).^{104,105} Therefore it is possible that the *N*-iodosuccinimide/In(OTf)₃ system could also be acting as an oxidising agent converting the catechol **94** into the 3-methoxy-benzoquinone **98**.



Reagents and conditions: *o*-Chloranil (1.1 eq.), Et₂O, -20 °C, 15 min; ii) Iodosylbenzene (1.1 eq), DCM:MeOH (5:1), rt, 3 min.

Scheme 40: Formation of *ortho*-quinone **98**.

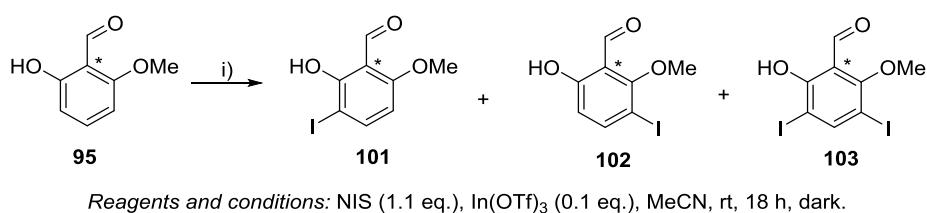
As it was found that iodination of the unprotected diphenol **94** under these conditions cannot occur directly, iodination of a protected diphenol was investigated. At first the MOM protected diphenol **96**, which has been synthesised previously (Scheme 37), was treated with *N*-iodosuccinimide and In(OTf)₃ (Scheme 41a). The crude ¹H NMR spectrum showed that all the starting material had disappeared and that multiple products had formed. The desired protected iodo species **99** was not seen since no MOM peaks were detected, however the diphenol **94** was observed. It was thought the acid sensitive MOM groups were cleaved under these conditions resulting in a reactive aldehyde species which could go on and react to form by-products. As the MOM protecting group was unsuitable, the diphenol **94** was protected as a methylenedioxy group **100** using dibromomethane and caesium fluoride in DMF.¹²⁰ The resulting 1,3-benzodioxole **100** was subjected to the *N*-iodosuccinimide and In(OTf)₃ conditions and three products were formed: the two regioisomers of mono-iodinated product and the di-iodinated product in a 1:1:2 ratio (Scheme 41b). The lack of convincing regioselectivity for the two regioisomers for the mono-iodinated compound is likely due to the fact that the sites of iodination are electronically and sterically very similar.



Reagents and conditions: i) NaH, MOMCl, THF, 0 °C; ii) NIS (1.1 eq.), In(OTf)₃ (0.1 eq.), MeCN, rt, dark; iii) CH₂Br₂, CsF, DMF, 120 °C.

Scheme 41: Attempted iodination of protected diphenols **96** and **100**.

Rather than pursuing different protecting groups that required both an additional protection and deprotection step, iodination on previously synthesised intermediates was examined. Firstly, 2-hydroxy-4-methoxybenzaldehyde **95** was treated with *N*-iodosuccinimide and In(OTf)₃ (Scheme 42). Three products were formed believed to be two mono-substituted products **101** and **102** and a di-substituted product **103** in a 69:21:10 ratio. The major mono-iodinated product **101** was isolated through flash column chromatography with an overall yield of 45%.



Scheme 42: Iodination of 2-hydroxy-4-methoxybenzaldehyde **95**.

The regioselectivity of the major mono-substituted isomer **101** was confirmed through nOe experiments (Figure 18). When the sample was irradiated at a frequency corresponding to the aromatic proton H_a, an enhancement was observed at the signal for the aromatic proton H_b. When the proton H_b was irradiated the signals of both the aromatic proton H_a and the methyl proton H_c were enhanced. Finally when the methyl proton H_c was irradiated, a signal enhancement was observed for the aromatic proton H_b and small enhancement was observed for the aldehyde proton H_d.

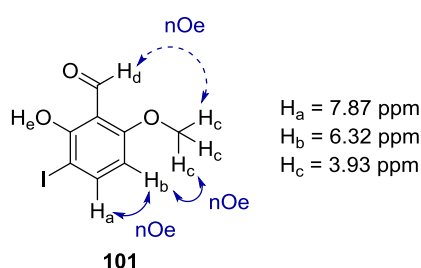
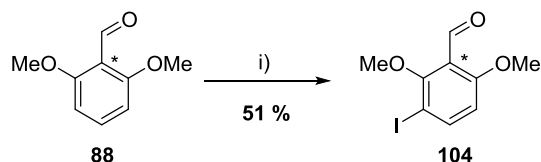


Figure 18: nOe – NMR study confirming the regioselectivity of the iodination to iodobenzaldehyde **101**.

The low overall yield for the iodination of 2-hydroxy-4-methoxybenzaldehyde **95** and the difficulties with both over-iodination and regioselectivity (Scheme 42) led to looking at the iodination on a symmetrical species followed by subsequent desymmetrisation by demethylation. 2,6-Dimethoxybenzaldehyde **88**, which is another previously made intermediate, was subjected to the NIS/In(OTf)₃ iodination conditions (Scheme 43).

Initially after 18 h, starting material **88** and a mono-substituted product **104** was seen in a 2:1 ratio. When the reaction was repeated but the reaction time left for 72 hours, the ratio of the two products was 1:1. When the number of equivalents of *N*-iodosuccinimide was increased from 1.1 to 2.2 and the number of equivalent of In(OTf)₃ was increased from 0.1 to 0.2, 100% conversion was observed. The mono-substituted product **104** was isolated through flash column chromatography with a yield of 51%.



Reagents and conditions: i) NIS (1.1 eq.), In(OTf)₃ (0.1 eq.), MeCN, rt, dark.

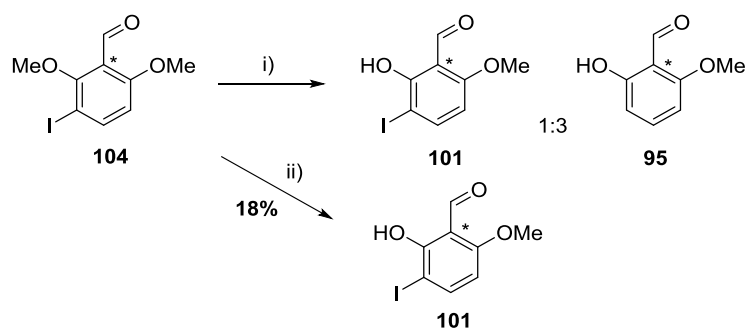
Scheme 43: Iodination of 2,6-dimethoxybenzaldehyde **88** followed by selective demethylation.

Entry	Number of equivalents of NIS	Number of equivalents of In(OTf) ₃	Time (h)	SM:P ratio ^a
1	1.1	0.1	18	2:1
2	1.1	0.1	72	1:1
3	2.2	0.2	18	0:100

^aDetermined from analysis of crude ¹H NMR spectrum

Table 10: Optimisation of the iodination of 2,6-dimethoxybenzaldehyde **88**.

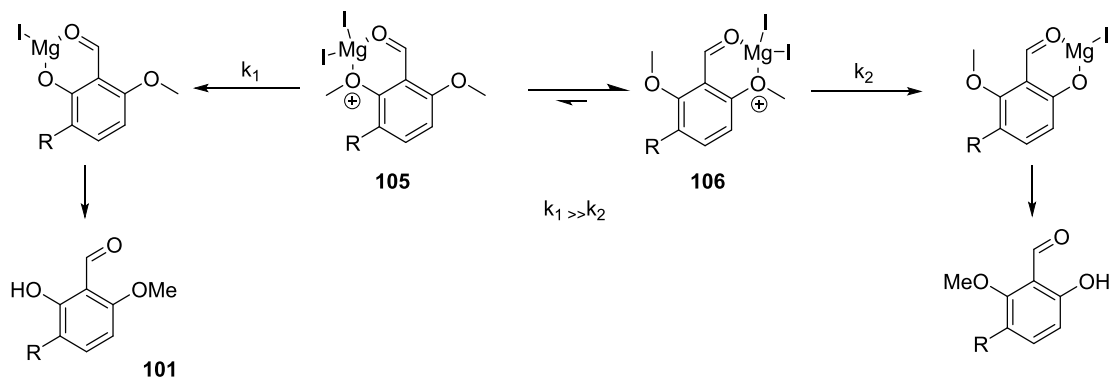
There are only a handful of examples in the literature where the more sterically hindered methoxy group is selectively cleaved on a 1,3-dimethoxycarbonyl compound where either magnesium iodide etherate or boron tribromide was used.¹⁰⁶ Yamahuchi and co-workers were successful in selectively demethylating 2,6-dimethoxybenzaldehydes to their corresponding phenols with magnesium iodide etherate; their examples include the formation of 3-chloro-2-hydroxy-6-methoxybenzaldehyde from 3-chloro-2,6-dimethoxybenzaldehyde.¹⁰⁶ Therefore the selective demethylation of 5-iodo-2,6-dimethoxybenzaldehyde **104** is thought to occur under the same conditions. The magnesium iodide etherate was made *in situ* by treating magnesium turnings with iodine in dry diethyl ether at reflux then leaving the reaction until the brown iodine colour had disappeared. The solution was then added to 5-iodo-2,6-dimethoxybenzaldehyde **104** in toluene and heated at reflux. Analysis of the crude ¹H NMR spectrum showed two products in a 1:3 ratio (Scheme 44). The minor product was the desired 2-hydroxy-4-methoxybenzaldehyde **101**, but unfortunately the major product was the de-iodinated product **95**.



Reagents and conditions: i) Mg^0 , I_2 , Et_2O , rt, 1 h then **104** (1 eq.) in toluene, reflux, 18 h; ii) BCl_3 , DCM, 18 h, rt.

Scheme 44: Demethylation of 5-iodo-2,6-dimethoxybenzaldehyde **104**.

The weak C-I bond had broken, possibly through a radical process caused by magnesium metal, so the reaction was repeated where the excess magnesium used in the formation of the magnesium iodide etherate was allowed to settle before decanting the solution to prevent any excess magnesium from being present in the reaction. The reaction temperature was also lowered from reflux to room temperature, but the ratio of the products did not improve.



Scheme 45: Possible explanation for the regioselectivity of demethylation observed by Yamauchi and co-workers.

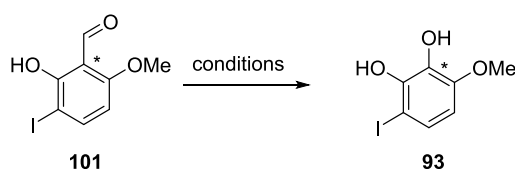
Even though the reaction did not go to completion, the correct regioisomer was formed since the NMR data corresponded to the phenol **101** which was previously formed and its regiochemistry was confirmed by nOe studies (Figure 18). The exact reasons behind the regioselectivity are unknown, however Yamaguchi and co-workers suggest that the 5-halo-2,6-dimethoxybenzaldehyde can form an equilibrium of two chelation isomers **105** and **106** with the magnesium iodide etherate (Scheme 45). This chelation causes the methyl group in adduct **105** to have unfavourable steric interactions with the R group making it less stable than adduct **106**. However in order for the regioisomer **101** to be

formed the next step, the elimination of methyl iodide, must be kinetically more favoured for the unstable isomer **105** than the more stable isomer **106** by having a lower activation barrier.

Since the correct regioselectivity was observed for the demethylation using magnesium iodide etherate, the low overall yield meant that other demethylation conditions were tried. The more traditional demethylating reagent, boron trichloride, was used and successful demethylation iodophenol **104** was formed with 100% conversion to the desired regioisomer which was determined by analysis of the crude ¹H NMR spectrum (Scheme 44). The iodinated product **101** was purified by flash column chromatography but unfortunately the majority of the product degraded on the column and only 18% of the crude product was recovered.

The final step towards synthesising the desired iodo-component **93** for the Sonogashira reaction involved the conversion of the aldehyde **101** to the phenol **93** via a Baeyer-Villiger oxidation (Scheme 46, Table 11). At first the aldehyde **101** was treated with *meta*-chloroperoxybenzoic acid, and this resulted in a 47% conversion of aldehyde **101** to the desired diphenol **93** (Table 11, Entry 1). When the peroxide was changed to hydrogen peroxide there was a slight increase in conversion to 50%. As the reaction with *meta*-chloroperoxybenzoic acid showed a larger amount of unknown by-products in the crude ¹H NMR spectrum, optimisation was carried out using hydrogen peroxide as the oxidant (Table 11, Entries 1 and 2). To try and increase the conversion, the temperature of the reaction was increased from room temperature to 60 °C; however this resulted in decomposition of the starting material (Table 11, Entry 3). The number of equivalents of hydrogen peroxide was also investigated; when increased to 2.5 equivalents the conversion increased to 64% (Table 11, Entry 4). When the number of equivalents was increased further to 5.0 equivalents, no further increase in conversion was observed, therefore the number of equivalents of hydrogen peroxide was kept at 2.5 (Table 11, Entry 5). Next the reaction time was investigated; when the reaction time was decreased from 18 hours to 1 hour a dramatic drop in conversion was observed, and when increased to 90 hours no significant change in conversion was observed, suggesting a reaction time of 18 hours was optimal (Table 11, Entry 6 and 7). A change in solvent from methanol to ethanol saw a large decrease in conversion meaning that methanol was kept as the solvent (Table 11, Entry 8). The reaction conditions were then changed from acid-catalysed to

base-catalysed but the treatment of aldehyde **101** with hydrogen peroxide and sodium hydroxide resulted in return of starting material. When the reaction temperature for base catalysis was increased to 60 °C, the conversion increased slightly to <5% (Table 11, Entries 9 and 10). Since acid was needed for the reaction to proceed, different types of acidic additives were investigated (Table 11, Entries 11-14). The addition of trifluoroacetic acid to the reaction resulted in a small conversion of 6% (Table 11, Entry 12), the addition of acetic acid gave a comparable conversion to that seen with sulfuric acid (Table 11, Entry 13), and the addition of selenium dioxide gave a conversion of 31% (Table 11, Entry 14). A possibility for the low conversion could be due to the oxidation of the 1,2-diphenol product **93** to its corresponding *ortho*-quinone (Scheme 40). Therefore oxygen was eliminated from the reaction by carrying it out under nitrogen and using degassed solvent, but unfortunately the conversion did not improve (Table 11, Entry 15).



Scheme 46: Attempts at the Baeyer-Villiger oxidation on benzaldehyde **101**.

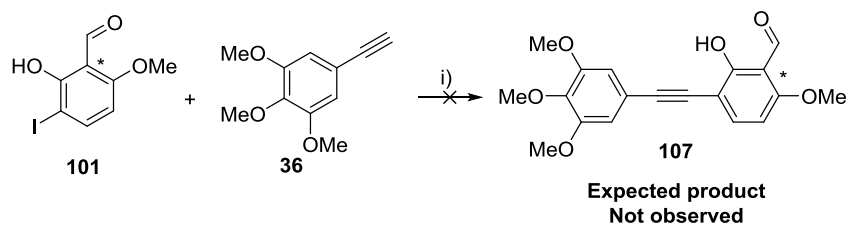
Entry	Peroxide	Eq. of peroxide	Additive ^a	Solvent	Temp.	Time (h)	Conversion (%) ^b
1 ^c	<i>m</i> CPBA	2.0	-	DCM	rt	18	47
2 ^d	H ₂ O ₂	1.3	H ₂ SO ₄	MeOH	rt	18	50
3 ^d	H ₂ O ₂	1.3	H ₂ SO ₄	MeOH	60 °C	18	0 ^f
4 ^d	H ₂ O ₂	2.5	H ₂ SO ₄	MeOH	rt	18	64
5 ^d	H ₂ O ₂	5.0	H ₂ SO ₄	MeOH	rt	18	65
6 ^d	H ₂ O ₂	2.5	H ₂ SO ₄	MeOH	rt	1	7
7 ^d	H ₂ O ₂	2.5	H ₂ SO ₄	MeOH	rt	90	63
8 ^d	H ₂ O ₂	2.5	H ₂ SO ₄	EtOH	rt	18	24
9	H ₂ O ₂	2.5	NaOH ^h	MeOH	rt	18	0 ^g
10	H ₂ O ₂	2.5	NaOH ^h	MeOH	60 °C	18	<5
11 ^d	H ₂ O ₂	2.5	-	MeOH	rt	18	0 ^g
12 ^d	H ₂ O ₂	2.5	TFA	MeOH	rt	18	6
13 ^d	H ₂ O ₂	2.5	AcOH	MeOH	rt	18	60
14 ^d	H ₂ O ₂	5.0	SeO ₂	MeOH	60 °C	18	31
15 ^{d,e}	H ₂ O ₂	5.0	H ₂ SO ₄	MeOH	rt	18	53

^a 0.2% ^b Determined by the ratio of starting material and product peaks in crude ¹H NMR spectra, ^c then treated with KOH ^d then treated with NaOH ^e under N₂, ^f decomposed ^g unreacted starting material ^h 3.0 eq.

Table 11: Optimisation of the Baeyer-Villiger reaction on 3-iodo-2-hydroxy-6-methoxybenzaldehyde **101**.

In summary, the best reaction conditions for the Baeyer-Villiger reaction of aldehyde **101** to diphenol **93** were using 2.5 equivalents of hydrogen peroxide with 0.2% sulfuric acid in methanol at room temperature and leaving the reaction for 18 hours (Table 11, Entry 4). This resulted in a reasonable conversion from the aldehyde **101** to diphenol **93** at 64% but unfortunately attempts at purifying the crude material *via* flash column chromatography showed degradation of the product on the silica meaning no product could be isolated. In order to determine the yield of the reaction, one molar equivalent of *N*-methylmaleimide was added as a NMR reference to the crude material. The ratio between the reference peak and the product peaks in the ¹H NMR spectra was 18% showing that significant material was lost through work up. The reaction was repeated ensuring an acidic environment and doubling the number of extractions but unfortunately failed to improve either the conversion or the yield.

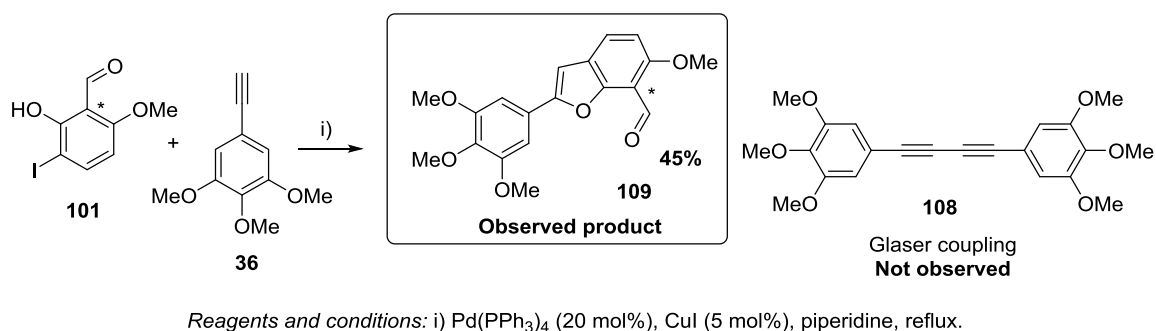
As a result of the poor conversion and failure to isolate 1-iodo-2,3-dihydroxy-4-methoxybenzene **93** from 3-iodo-2-hydroxy-6-methoxybenzaldehyde **101**, it was decided to instead use the iodo-benzaldehyde **101** as the iodo-component for the Sonogashira reaction. The reaction conditions followed those used by Lawrence and co-workers for the synthesis of CA4.¹⁰⁷ Firstly the iodo-benzaldehyde **101** and 5-ethynyl-1,2,3-trimethoxybenzene **36** [made previously (Scheme 34)] were treated with tetrakis(triphenylphosphine)palladium(0) and copper (I) iodide in triethylamine but unfortunately this returned starting material. It was noticed during the reaction that there was significant amount of undissolved starting material, therefore the base, which also acts as the solvent was investigated. The alkyne **36** dissolved in triethylamine but the iodoarene **101** did not. However the iodoarene **101** did partially dissolve in diethylamine and pyrrolidine, and fully dissolved in piperidine. Therefore the base was changed to piperidine, the reaction was also heated to reflux and all the starting material was consumed and a product was isolated in a 60% yield after column chromatography (Scheme 47).



Reagents and conditions: i) Pd(PPh₃)₄ (20 mol%), CuI (5 mol%), piperidine, reflux.

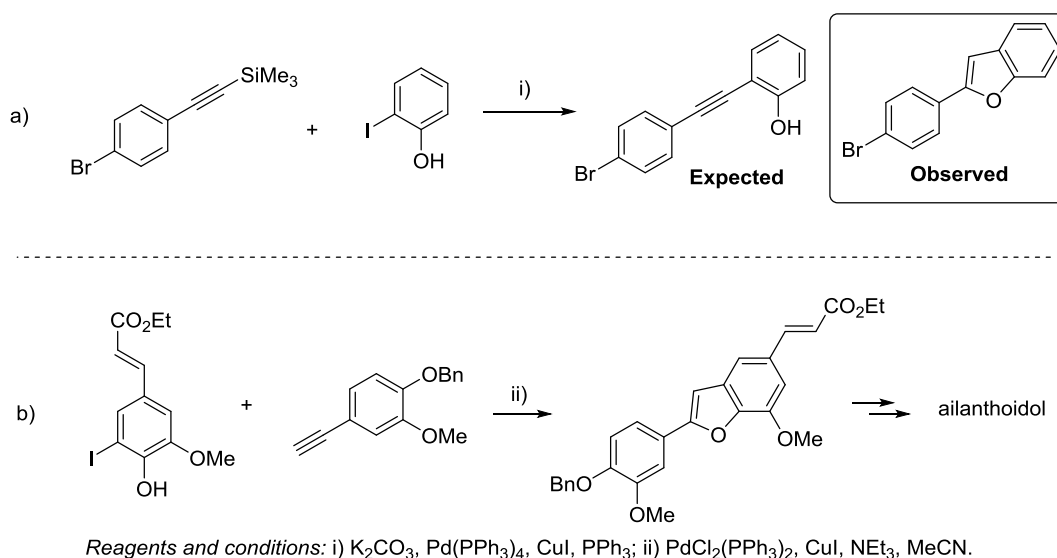
Scheme 47: Sonogashira reaction of aryl iodide **101** and alkyne **36**.

Unfortunately the isolated product was not the desired alkyne product **107**. The expected ¹H NMR spectrum should have 3 singlets in the methoxy region, an alcohol peak, an aldehyde peak and in the aromatic region a singlet with an integral of 2H, and two doublets with an integral of 1H each. However the ¹H NMR spectrum of the product had an additional singlet (1H) in the aromatic region and no OH peak. The ¹³C J-MOD NMR spectrum for the expected product was expected to have 3 CH₃ peaks, 1 deshielded CH₁ peak for the aldehyde, 3 aromatic CH₁ peaks and 9 CH₀ peaks in the aromatic region. However, the ¹³C J-MOD NMR spectrum for the product differs from the expected spectrum by having 4 CH₁ peaks and 8 CH₀ peaks in the aromatic region. Sonogashira reactions using copper are prone to Glaser coupling, where the alkyne component undergoes homocoupling upon oxidation and leads to a symmetrical diyne. In the system with 5-ethynyl-1,2,3-trimethoxybenzene **36** this would lead to the formation of 1,1'-(1,3-butadiyne-1,4-diyl)-bis-(3,4,5-trimethoxybenzene) **108**, however since the ¹H NMR spectrum shows 8 different proton environments the dimerised product can be ruled out as this only has 3 different proton environments. The ¹H NMR spectrum of the product shows an additional aromatic proton and no alcohol proton when compared to the expected compound **107** therefore it was hypothesised that the expected *ortho*-hydroxydiarylalkyne product **107** underwent a ring-closing reaction forming a benzofuran **109** (Scheme 48). The expected ¹H and ¹³C J-MOD NMR spectra for the benzofuran **109** correspond to the NMR spectra gained from the reaction.



Scheme 48: Formation of benzofuran **109** from aryl iodide **101** and alkyne **36**.

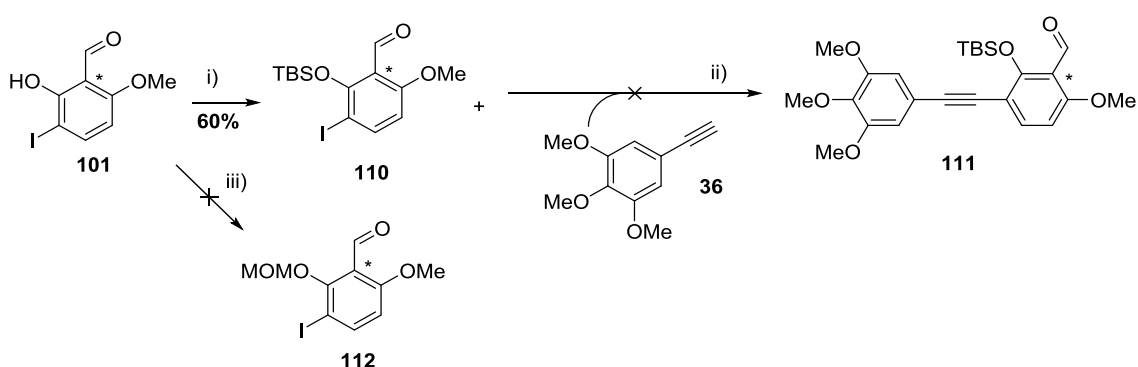
There are a number of reports in the literature of *ortho*-hydroxydiarylalkynes undergoing annulation under palladium catalysis.^{108,109} When investigating phenoxide-mediated Sonogashira coupling of trimethylsilylalkynes and aryl iodides, Shigeta and Konishi found that when using *ortho*-hydroxy-iodoarenes they unexpectedly gave rise to benzofurans (Scheme 49a).¹⁰⁸ This reaction has been utilised by Scammells and co-workers in the synthesis of A₁ adenosine receptor aianthoidol (Scheme 49b).¹⁰⁹



Scheme 49: Examples of benzofuran formation from *ortho*-hydroxydiarylalkynes.

As it was found that having an unprotected alcohol in the *ortho*-position on the iodoarene generates an undesired benzofuran, protection of the alcohol was required. 3-Iodo-2-hydroxy-6-methoxybenzaldehyde **101** was initially protected with a *tert*-butyldimethylsilyl ether protecting group using TBSCl, DMAP and triethylamine (Scheme 50). The Sonogashira reaction with the resulting TBS-protected iodide **110** went to 100% completion but unfortunately no product was observed after purification by flash

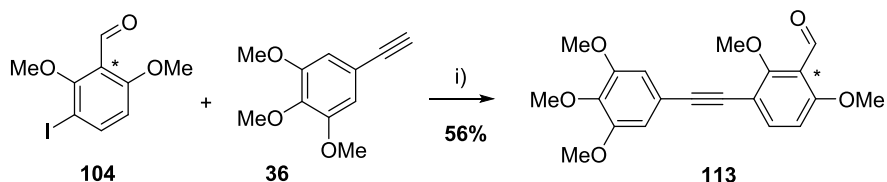
column chromatography; however deprotected iodophenol **101** was seen. In addition, no TBS-protected product **110** was seen when the silica was deactivated using 1% triethylamine. Therefore the crude protected iodoarene **110** underwent the Sonogashira reaction under the same conditions as used on the unprotected system (Scheme 50). Unfortunately the formation of the desired diarylalkyne **111** did not occur, as the crude ^1H NMR spectrum showed loss of the TBS-protecting group suggesting that the TBS-protecting group could be incompatible with these conditions. Next, a methoxymethyl ether protecting group was used; unfortunately only a 16% conversion to the protected product **112** was observed when treating phenol **101** with sodium hydride and MOMCl.



Reagents and conditions: i) NEt_3 , DMAP, DCM then TBSCl; ii) $\text{Pd}(\text{PPh}_3)_4$ (20 mol%), CuI (5 mol%), piperidine, reflux; iii) MOMCl, NaH, THF, 0°C .

Scheme 50: Attempts at the Sonogashira reaction using protected iodoarenes.

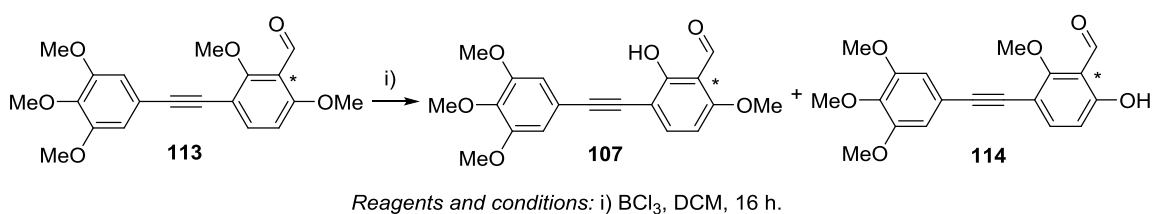
The next protecting group studied was the methyl ether protecting group. This has the added advantage of being an intermediate already synthesised (Scheme 43) and therefore eliminating the need for both an additional protecting and deprotecting step. The Sonogashira reaction between the methyl ether protected iodoarene **104** and the terminal alkyne **36** gave the diarylalkyne **113** in a 56% yield.



Reagents and conditions: i) $\text{Pd}(\text{PPh}_3)_4$ (20%), CuI (5%), piperidine, reflux.

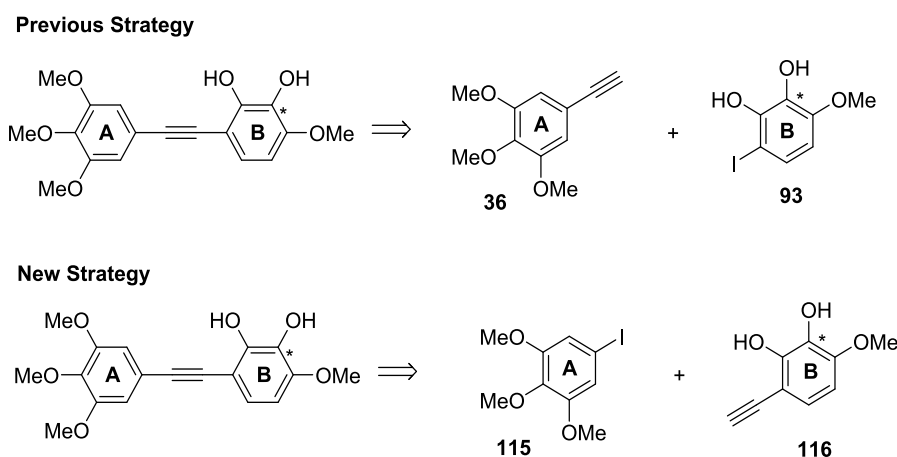
Scheme 51: Sonogashira reaction to synthesise diarylalkyne **113**.

Next, demethylation of the methoxy group in the *ortho* position relative to both the aldehyde and alkyne of the diarylalkyne **113** was required. The reagent of choice was boron trichloride as it had already been shown as an effective *ortho*-demethylating agent. Since there is a hydroxyl group in both *ortho* positions to the benzaldehyde **113**, theoretically demethylation could occur at either site. However there is literature evidence that demethylation can occur on the more sterically hindered methyl ether, and this was also observed previously on the demethylation of 5-iodo-2,6-dimethoxybenzaldehyde **104** (Scheme 44 and Scheme 45). Unfortunately treatment of the diarylalkyne **113** with boron trichloride resulted in two products in a 1:1 ratio presumably the two demethylated products **107** and **114** (Scheme 52).



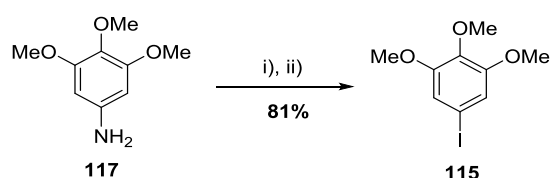
Scheme 52: *Ortho*-demethylation of diarylalkyne **113**

The difficulties in achieving a suitable synthesis for the iodo-species for the Sonogashira reaction led to a different strategy being investigated where the iodo-component **115** contained the trimethoxy A ring and the alkyne component **116** contained the ^{13}C -labelled B ring (Scheme 53).



Scheme 53: Sonogashira strategies for the synthesis of CA1 **8**.

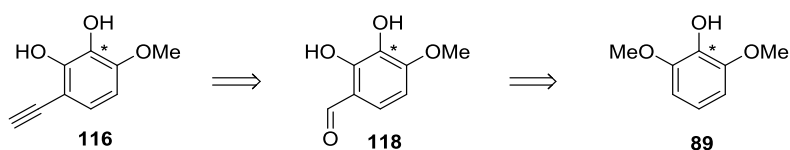
For this new strategy, the iodo component **115** was synthesised from the commercially available 3,4,5-trimethoxyaniline **117** via a Sandmeyer reaction (Scheme 54). The aniline **117** was treated with nitrous acid which was prepared *in situ* from sodium nitrate and sulfuric acid, and this led to a diazonium salt intermediate which when treated with potassium iodide revealed the iodoarene **115** in an 81% yield.



Reagents and conditions: i) H_2SO_4 , NaNO_2 , H_2O , 1 h, 0°C ; ii) KI , H_2O .

Scheme 54: Formation of 1-iodo-3,4,5-trimethoxybenzene **115**.

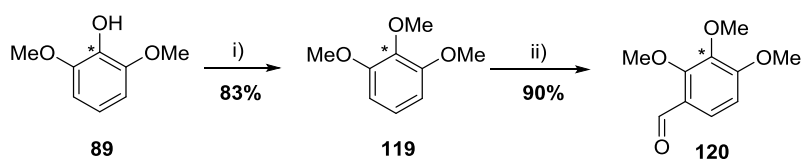
The alkyne component **116** can be derived from 2,3-dihydroxy-4-methoxybenzaldehyde **118** via a Corey-Fuchs reaction and this aldehyde **118** needs to be derived from 2,6-dimethoxyphenol **89** as this will contain the ^{13}C label (Scheme 55).



Scheme 55: Retrosynthesis of the alkyne component for the Sonogashira reaction.

The synthesis towards the alkyne component **116** first began by methylating the phenol **89** to 1,2,3-trimethoxybenzene **119** using sodium hydride and methyl iodide, and this was achieved in a 83% yield (Scheme 56). Next, *ortho*-formylation on 1,2,3-trimethoxybenzene **119** occurred using Rieche formylation conditions, and the resulting 2,3,4-trimethoxybenzaldehyde **120** was isolated in a 90% yield (Scheme 56). The regiochemistry of the benzaldehyde was confirmed by the multiplicities in the crude ^1H NMR spectrum which had two distinct doublets ($J=8.8$ Hz) being observed for the two aromatic protons. The regioselectivity is due to the coordination of the titanium atom to both the oxygen atom of the methoxy group in the substrate and the dichloromethyl methyl ether. This forms a 6-membered titanium complex which influences the direction of the electrophilic substitution. The *C*-formylation occurs exclusively in the 4 or 6 position and since the starting substrate is a symmetrical species, formylation in both position will result in the same product **120**. The coordination of the titanium atom not

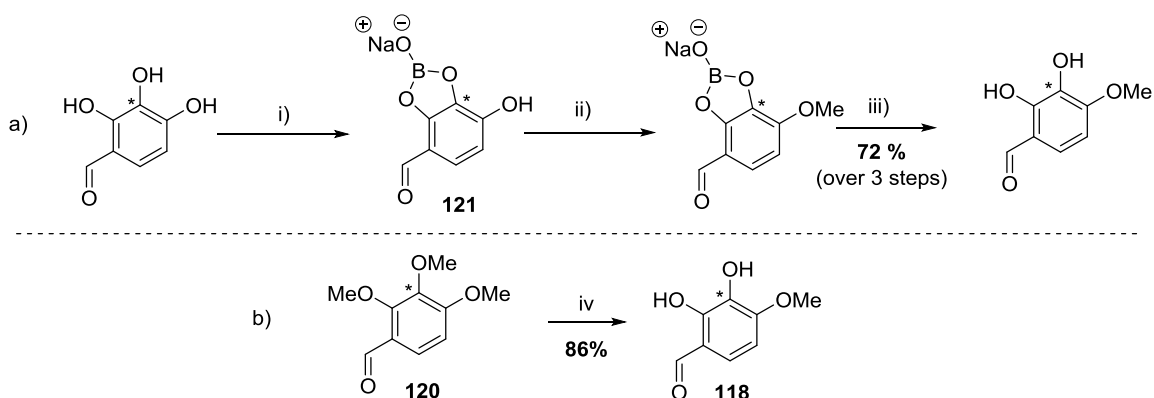
only provides the correct regioselectivity but it also increases the electrophilicity of the dichloromethyl methyl ether.¹¹⁰



Reagents and conditions: i) MeI (3 eq.), 18-C-6, acetone; ii) TiCl₄, Cl₂CHOMe, DCM.

Scheme 56: Methylation of 1,3-dimethoxyphenol **89** followed by Rieche formylation and demethylation.

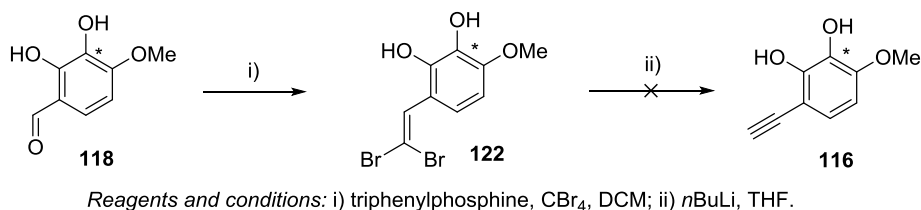
The formation of benzaldehyde **118** has previously been achieved by two different strategies by Pettit and co-workers. The first is the treatment of 2,3,4-trihydroxybenzaldehyde with sodium borate which selectively forms a 2,3-borate ester **121** allowing for the selective methylation of the 4-hydroxy group using dimethylsulfate (Scheme 57a).¹¹ However, more recently Pettit established an alternative route towards 2,3-dihydroxy-4-methoxybenzaldehyde **118** that was not only more atom economical but also more applicable on a larger scale.²⁴ This route involved the demethylation of 2,3,4-trimethoxybenzaldehyde **120** using 2 equivalents of boron trichloride which gave the desired mono-methylated product **118** in an 87% yield.¹¹¹ Due to the latter method being both higher yielding and easier to synthesise from 2,6-dimethoxyphenol **89**, it was proposed to be used as the demethylation method. The selective demethylation of 2,3,4-trimethoxybenzaldehyde **120** with boron trichloride gave 2,3-dihydroxy-4-methoxybenzaldehyde **118** in an 86% yield.



Reagents and conditions: i) sodium borate-decahydrate, H₂O; ii) (MeO)₂SO₂; iii) H⁺/H₂O, iv) BCl₃, DCM.

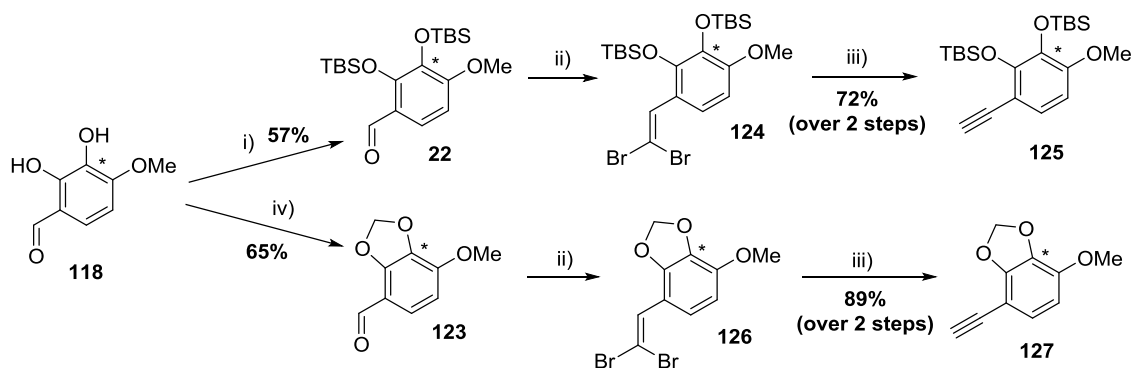
Scheme 57: Pettit's formation of 2,3-dihydroxy-4-methoxybenzaldehyde **118** a) *via* methylation of a 2,3 borate ester b) *via* selective demethylation.

To produce the desired alkyne component **116** needed for the Sonogashira reaction, the benzaldehyde **118** was subjected to Corey-Fuchs conditions (Scheme 58). Treatment of the benzaldehyde **118** with triphenylphosphine and carbon tetrabromide gave the dibromoalkene **122** but unfortunately subsequent treatment with 5 equivalents of *n*-butyllithium failed to give the dehydrohalogenated product **116**.



Scheme 58: Attempts at the Corey-Fuchs reaction on unprotected benzaldehyde **118**.

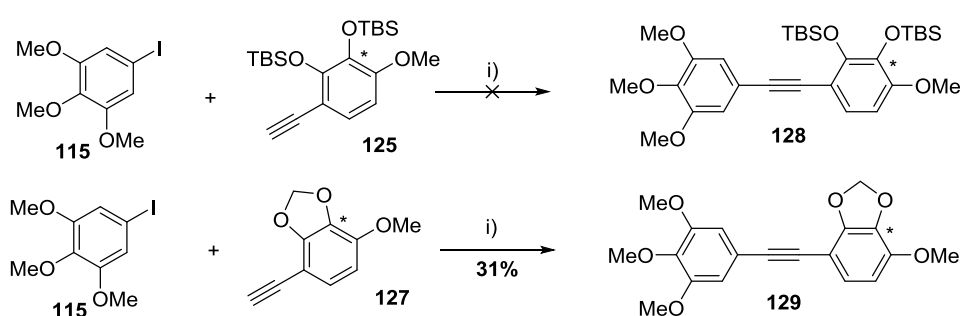
Therefore the diphenol moiety was protected as a *tert*-butyldimethylsilyl ether **22** and 1,3-benzodioxole **123** which subsequently underwent the two-step Corey-Fuchs reaction (Scheme 59). Protection with a TBS group, which was achieved by treating 2,3-dihydroxy-4-methoxybenzaldehyde **118** with using TBSCl, DMAP and triethylamine, the TBS-protected aldehyde **22** was formed in a 57% yield after purification by recrystallisation. This was then converted to the dibromoalkene **124** by treatment with triphenylphosphine and carbon tetrabromide in dichloromethane. Subsequent treatment of the dibromoalkene **124** with *n*-butyllithium followed by purification gave the TBS-protected alkyne **125** in a 72% yield (over 2 steps). 2,3-Dihydroxy-4-methoxybenzaldehyde **118** was also protected as a 1,3-benzodioxole **123**, which was achieved following treatment with potassium fluoride and dibromomethane. The resulting protected-aldehyde **123** was isolated in a 65% yield and treated with carbon tetrabromide and triphenylphosphine and gave the dibromoalkene **126**. Then treatment of this dibromoalkene with *n*-butyllithium revealed the dioxole protected alkyne **127** in an 89% yield (over 2 steps).



Reagents and conditions: i) TBSCl, DMAP, NEt_3 , THF; ii) PPh_3 , CBr_4 , DCM, 74%; iii) $n\text{BuLi}$, THF; iv) K_2CO_3 , CH_2Br_2 , DMF.

Scheme 59: Protection of aldehyde **118** and subsequent Corey-Fuchs reactions.

The protected terminal alkynes **125** and **127** were then treated with 1-iodo-3,4,5-trimethoxybenzene **115**, tetrakis(triphenylphosphine)palladium(0), and copper (I) iodide in piperidine. Unfortunately when using the TBS-protected alkyne **125**, these Sonogashira conditions were unsuccessful in giving the desired diarylalkyne **128** as a large number of peaks were seen in the crude ^1H NMR spectrum, including unreacted starting material and deprotected starting material. As this was also seen before for the Sonogashira reaction between the TBS-protected iodoarene **110** and 5-ethynyl-1,2,3-trimethoxybenzene **36** (Scheme 50) it was concluded that the TBS group is incompatible with these Sonogashira conditions. However when these conditions were applied to the 1,3-benzodioxole protected alkyne **127**, the desired diarylalkyne **129** was formed in a 31% yield (Scheme 60).

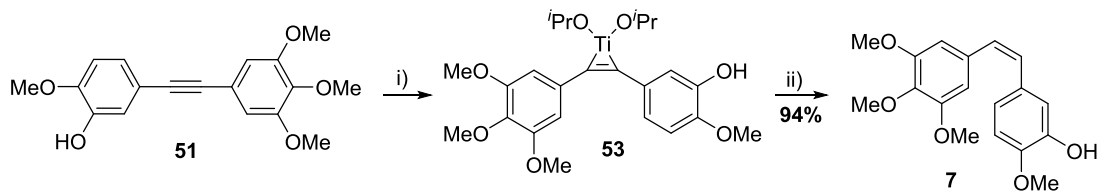


Reagents and conditions: i) $\text{Pd}(\text{PPh}_3)_4$, CuI , piperidine.

Scheme 60: Sonogashira reactions between protected alkynes **125** and **127** with 5-iodo-1,2,3-trimethoxybenzene **115**.

Next, the diarylalkyne **129** needed to be selectively reduced to the *Z*-alkene **130**. During their work to synthesise a different combretastatin, CA4 **7**, Lara-Ochoa and co-workers selectively reduced diarylalkyne **51** by generating a thermally stable $\text{Ti}(\text{II})$ -alkyne

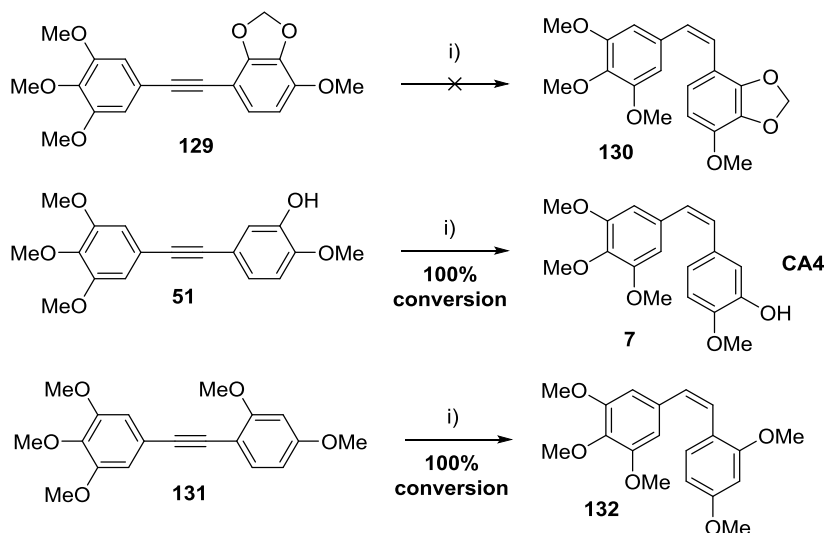
complex **53** using *n*-butyllithium and Ti(O^{*i*}Pr)₄ (Scheme 61).³⁹ The two aryl rings on the Ti(II)-alkyne complex are in a *cis* configuration and after hydrolysis the Z-CA4 **7** is produced in high yields.



Reagents and conditions: i) *n*BuLi, Ti(O^{*i*}Pr)₄, -78 °C to 50 °C; ii) H₂O.

Scheme 61: Formation and hydrolysis of a Ti(II)-alkyne complex **53** for the synthesis of CA4 **7**.

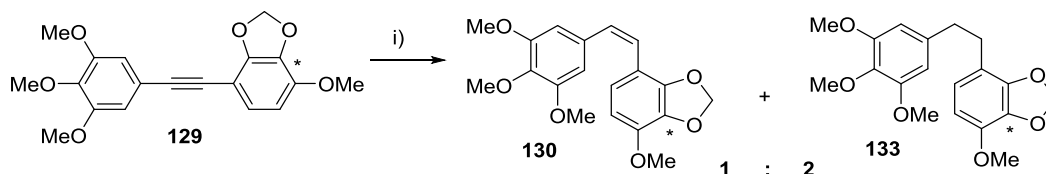
Unfortunately when these conditions were applied to the protected diarylalkyne **129** the isolation of the protected-CA1 species **130** as a single *Z*-isomer was unsuccessful. Attempts at purification of the crude reaction material by flash column chromatography isolated two products with the same *R_f* value. Analysis of the ¹H NMR spectrum suggested these products could be the *Z* and *E*-isomers of the desired alkene. During Eisch's investigations into the reactions of dialkyltitanium (IV) compounds with unsaturated substrates, they observed the unexpected isomerisation of *cis*-stilbene to its *trans*-isomer along with over-reduction to the alkane.¹¹² Therefore it is possible that the desired *Z*-alkene **130** produced from reduction of diarylalkyne **129** can isomerise to the *E*-alkene under these conditions. To check the quality of reagents and procedure, two other diarylalkynes **51** and **131** were reduced using the Ti(O^{*i*}Pr)₄/*n*BuLi conditions. The diarylalkynes **51** and **131** were first synthesised by Sonogashira reactions of 5-iodo-1,2,3-trimethoxybenzene **115** and the corresponding iodoarene. The diarylalkynes were then treated with Ti(O^{*i*}Pr)₄ and *n*BuLi and were both reduced with 100% conversion to the *Z*-alkenes **7** and **132** respectively suggesting that the diarylalkyne **129** is incompatible with these conditions.



Reagents and conditions: i) *n*BuLi, Ti(O*i*Pr)₄, THF.

Scheme 62: Attempts at selective reduction of diarylalkyne **129** using *n*BuLi and Ti(O*i*Pr)₄.

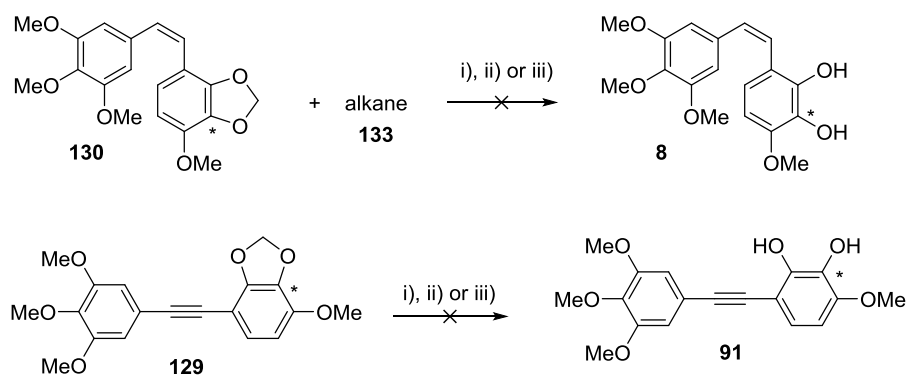
The reduction of diarylalkyne **129** was therefore attempted using the H-cube®, a continuous-flow hydrogenation flow reactor. This time the reduction to the *Z*-alkene **130** occurred, without the formation of the *E*-isomer, but unfortunately despite using a Lindlar catalyst over-reduction to the alkane **133** was also observed.



Reagents and conditions: i) H₂, (H-Cube, 5 mM, 50 °C, atm pressure, 1 mL/min, 5% Pd/CaCO₃/Pb catcart).

Scheme 63: Hydrogenation of diarylalkyne **129** using H-cube® conditions.

Rather than optimising the H-cube® hydrogenation conditions at this stage, the deprotection of the acetonide protecting group was looked at (Scheme 64). Unfortunately a number of different deprotection conditions were attempted including, hydrochloric acid, boron trichloride¹¹³ and *n*-butyllithium,¹¹⁴ and these all failed in deprotecting either the protected alkene **130** or the alkyne **129** as starting material was returned in all cases.



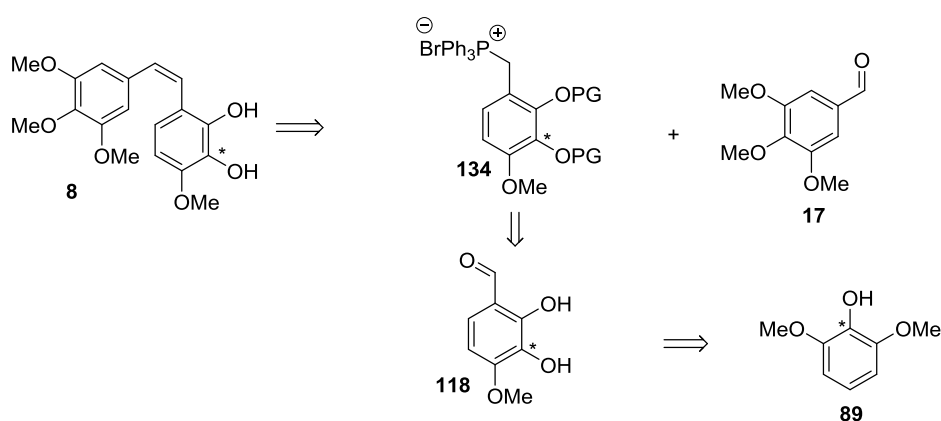
Reagents and conditions: i) HCl, H₂O, reflux; ii) BCl₃ (2 eq.), DCM; iii) *n*BuLi, THF, reflux.

Scheme 64: Attempts at deprotection of alkene **130** and diarylalkyne **129**.

It was at this point that the whole synthesis *via* the Sonogashira reaction, up to this point, was examined and it was found that this already comprised of 12 steps with an overall yield of 1.9%. Due to the cost of the ¹³C starting material and the fact that the remaining steps require a large amount of optimisation, another route towards the synthesis of CA1P **9** was investigated.

2.4. Synthesis of CA1P *via* the Wittig reaction

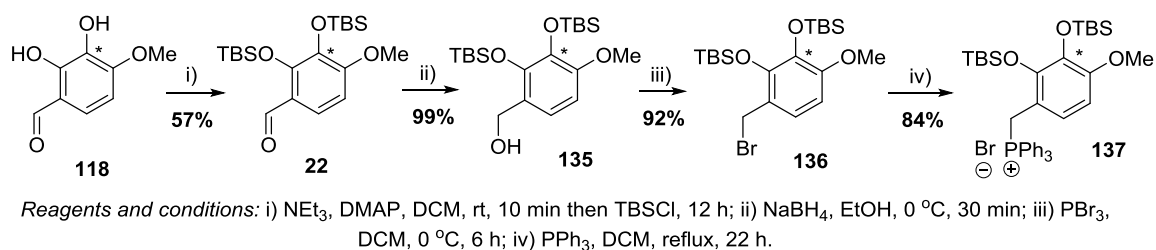
In parallel to synthesising CA1 **8** through the Sonogashira strategy, a Wittig strategy was examined. It was envisioned that CA1 **8** could be synthesised by the Wittig reaction of the commercially available 3,4,5-trimethoxybenzaldehyde **17** and the phosphonium salt **134** (Scheme 65).



Scheme 65: Wittig reaction strategy for the synthesis of CA1 **8**.

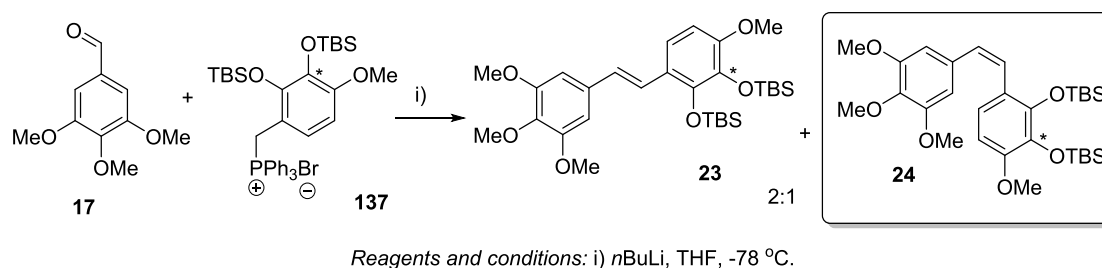
The protected phosphonium salt **134**, which needs to eventually contain the ¹³C label, can be derived from the aldehyde **118**. A route towards the aldehyde **118** has already been

established previously (Scheme 57). At the start of the synthesis of the phosphonium salt **134**, the diphenol functionality of the aldehyde **118** needed to be protected. A *tert*-butyldimethylsilyl ether protecting group was chosen because it is simple to attach and remove, and has been shown to be stable under Wittig reaction conditions.¹¹ Treatment of 2,3-dihydroxy-4-methoxybenzaldehyde **118** with triethylamine and 4-dimethylaminopyridine followed by addition of *tert*-butyldimethylsilyl chloride gave the TBS-protected aldehyde **22** in a 57% yield (Scheme 66). The protected aldehyde **22** was then reduced to the corresponding alcohol **135** using sodium borohydride in a 99% yield and then converted to the bromide **136** using phosphorus tribromide in a 92% yield. Next, the bromide **136** was transformed to the phosphonium salt **137** using triphenylphosphine in refluxing dichloromethane in a 84% yield.



Scheme 66: Synthesis of the Wittig precursor, phosphonium salt **137**.

The aldehyde component of the Wittig reaction, 2,3,4-trimethoxybenzaldehyde **17** is commercially available. The ylide component was formed from the treatment of the phosphonium salt **137** with *n*-butyllithium, and then reacted with the aldehyde **17** to form the protected-CA1 **24** with an *E/Z* ratio of 2.3:1 (determined by ¹H NMR spectroscopy) (Scheme 67). However the separation of the two isomers **23** and **24** by flash column chromatography was problematic due to the isomers having very close *R_f* values.

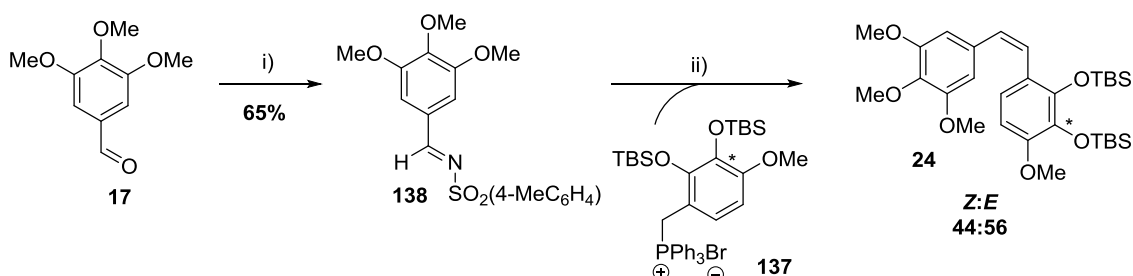


Scheme 67: Wittig reaction between aldehyde **17** and phosphonium salt **137**.

The two *E*- and *Z*-TBS protected CA1 isomers **23** and **24** have previously been separated by recrystallization in ethanol, however when applied to the above system this failed to

separate the desired *Z*-isomer **24** in an acceptable yield.¹¹ This is presumably due to the low proportion of *Z*-isomer **24** in the mixture and the large amount of triphenylphosphine oxide. Therefore a pure mixture of *E*- and *Z*- isomers **23** and **24** was isolated through flash column chromatography before recrystallisation and this led to the *Z*-isomer **24** being isolated in a 21% yield. This low yield of the isolation of the desired *Z*-CA1 **24** was due to the unfavourable selectivity of the Wittig reaction.

There have been a number of modifications aimed at altering the *E/Z* stereoselectivity for the Wittig reaction, the majority of which occur on the phosphonium ylide, for example the Horner-Wadsworth-Emmons, Still-Gennari and Ando modifications. A common modification of semi-stabilised triphenylphosphonium ylides is to replace the phenyl groups with heteroaryl groups or substituted aryl groups. There are fewer modifications on the carbonyl component of the Wittig reaction; however Tian and co-workers recently reported the highly stereoselective olefination of semi-stabilised triphenylphosphonium ylides with *N*-sulfonyl imines.¹¹⁵ It is proposed that the olefination occurs through a Wittig-type reaction pathway involving the cycloaddition to a 1,2-azaphosphetane intermediate, which collapses yielding an alkene and iminophosphorane. The authors employed a sulfonyl electron-withdrawing group to activate the imine and to influence the selectivity. They found that treating *p*-toluenesulfonyl-activated aromatic imines with a variety of benzylidenetriphenylphosphoranes yielded *Z*-alkenes with greater than 99:1 selectivity and in good yields.



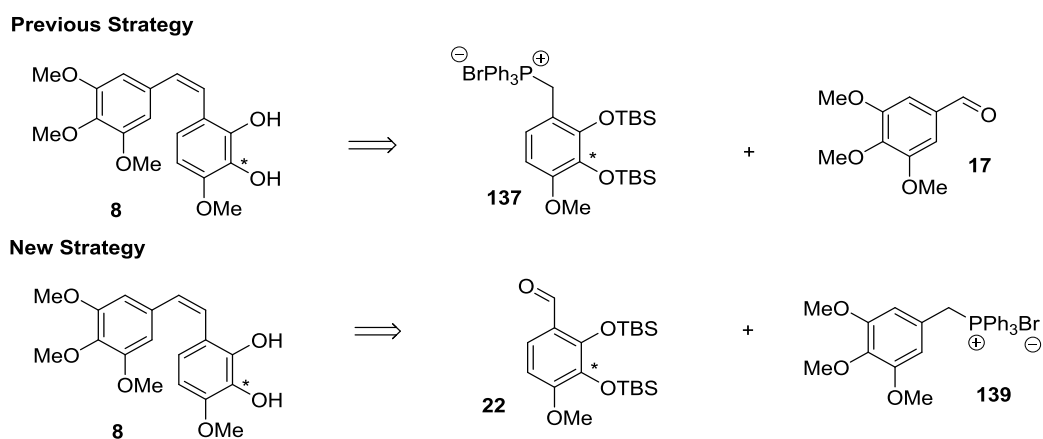
Reagents and conditions: i) *p*-toluenesulfonamide, Si(OEt)₄, 120 °C; ii) LDA, THF, phosphonium bromide **137**, -78 °C, 1 h then *N*-sulfonyl imine **138**.

Scheme 68: Olefination with *N*-sulfonyl imine **138** and phosphonium salt **137**.

It was therefore expected that a higher *Z*-selectivity would occur by converting the 3,4,5-trimethoxybenzaldehyde **17** into the *p*-toluenesulfonyl-activated aromatic imine **138** which would then undergo a Wittig-like reaction with the phosphonium salt **137**. The *N*-

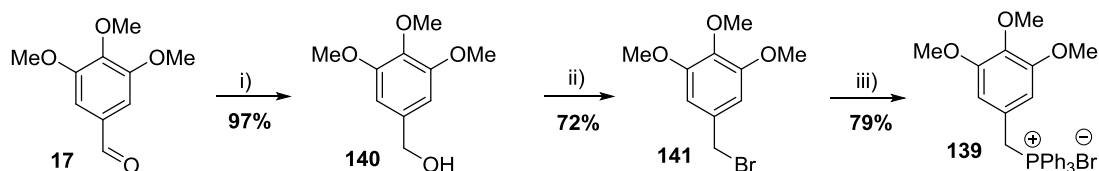
sulfonyl imine **138** was prepared by treating benzaldehyde **17** with *p*-toluenesulfonamide and tetraethyl orthosilicate and heating to 120 °C (Scheme 68). Unfortunately when the *N*-sulfonyl imine **138** was treated with the phosphonium salt **137** under the conditions used by Tian and co-workers, low *Z*-selectivity was observed; instead of the expected >99:1 *Z*-selectivity, a ratio of 44:56 (*Z*:*E*) was found.

As the synthetic route would later be repeated using [¹³C] material, it was important to reduce the number of steps that the label is involved in as much as possible. This could be achieved by switching the components of the Wittig reaction, which also might see an improvement of the *E*:*Z* ratio of the product and allow better separation of the isomers (Scheme 69).



Scheme 69: Second Wittig strategy for the synthesis of CA1 **8**.

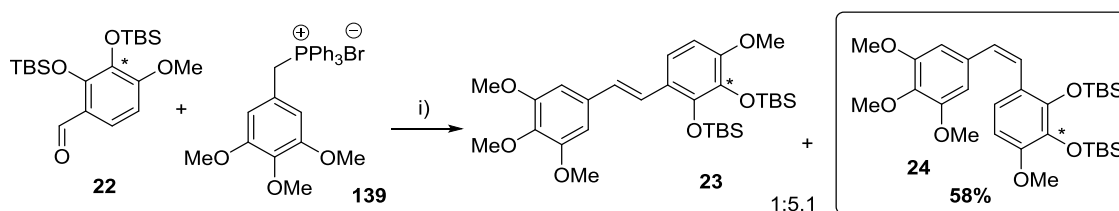
The aldehyde component, 2,3-*bis*-[[[(1,1-dimethylethyl)dimethylsilyl]oxy]-4-methoxy]benzaldehyde **22** had already been synthesised (Scheme 66). The phosphonium salt for ylide component **139** was synthesised from the commercially available 3,4,5-trimethoxybenzaldehyde **17** which was first reduced by sodium borohydride to give the alcohol **140** in a 97% yield after recrystallisation. Next the alcohol **140** was brominated using phosphorus tribromide which gave the bromide **141** in a 72% yield after recrystallisation. Finally the bromide **141** was treated with triphenylphosphine which gave the phosphonium salt **139** in a 79% yield.



Reagents and conditions: i) NaBH₄, EtOH, 0 °C, 30 min; ii) PBr₃, DCM, 0 °C, 6 h; iii) PPh₃, DCM, reflux, 22 h.

Scheme 70: Synthesis of phosphonium salt **139** from the commercially available benzaldehyde **17**.

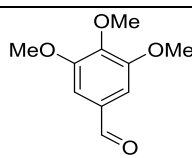
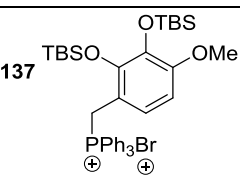
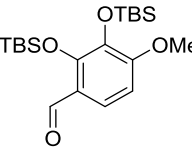
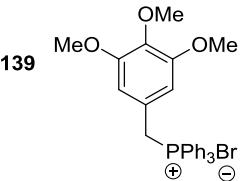
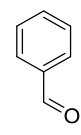
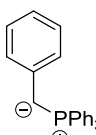
Treatment of the phosphonium salt **139** with *n*-butyllithium at -15 °C formed the ylide *in situ* which was warmed to room temperature then treated with the aldehyde **22** (Scheme 71). Analysis of the crude ¹H NMR spectrum showed the *Z*:*E* ratio of the two isomers **23** and **24** was 2.9:1. Pettit and co-workers observed that the *Z*:*E* ratio is affected by the number of equivalents of *n*BuLi used: when decreasing the number of equivalents from 1.5 to 1.0 they observed an increase in the *Z*:*E* from 3.5:1 to 9:1.¹¹ However, these results could not be reproduced, with the *Z*:*E* ratio remaining the same when only 1.0 equivalent of *n*-butyllithium was used, even when the reaction was repeated under argon and using molecular sieves. However, the temperature of the reaction was shown to affect the *Z*:*E* ratio. The addition of *n*-butyllithium to the phosphonium salt **139** at -15 °C then allowing the mixture to warm to room temperature for 30 minutes, followed by the addition of the aldehyde **22**, gave a *Z*:*E* ratio of 2.9:1. But when the *in situ* generated phosphonium ylide was left at -15 °C (rather than being warmed to room temperature) and the temperature then lowered to -78 °C before the addition of the aldehyde **22**, and then the mixture was warmed to 0 °C, this gave an increase in the *Z*:*E* ratio to 5.1:1. The crude material was first purified using flash column chromatography to remove the triphenylphosphine oxide by-product and gave a clean mixture of the *E*- and *Z*-isomers **23** and **24**. The *Z*- and *E*-isomers **23** and **24** were able to be separated by recrystallisation from ethanol, giving the *Z*-isomer in a 58% yield.



Reagents and conditions: i) *n*BuLi (1.9 M, 1 eq.), THF, -15 °C, then **22**, -78 °C to 0 °C.

Scheme 71: Wittig reaction between aldehyde **22** and phosphonium salt **139**.

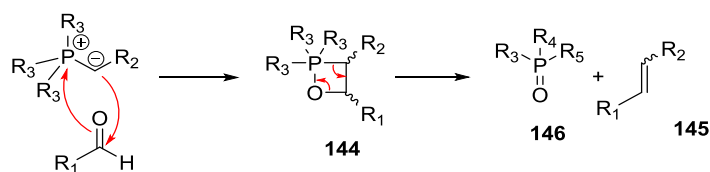
The Wittig reaction between 3,4,5-trimethoxybenzaldehyde **17** and [[2,3-bis[(1,1-dimethylethyl)dimethylsilyl]oxy]-4-methoxyphenyl]methyl]triphenyl phosphonium bromide **137** gave predominately the *E*-alkene whereas the Wittig reaction where the components have been reversed, between 2,3-bis[(1,1-dimethylethyl)dimethylsilyl]oxy]-4-methoxybenzaldehyde **22** and triphenyl[(3,4,5-trimethoxyphenyl)methyl]phosphonium bromide **139**, predominantly gave the *Z* alkene (Table 12). Literature shows that the Wittig reaction between the non-substituted benzylidene triphenylphosphorane **142** and non-substituted benzaldehyde **143** shows no selectivity giving a 1:1 mixture of the *E* and *Z*-isomers.¹¹⁶ This highlights that the substitution on both the aryl aldehyde and benzylide can dramatically shift the selectivity.

Entry	Aldehyde	Ylide or phosphonium salt	<i>Z</i> : <i>E</i> ratio
1	17 	137 	31:69
2	22 	139 	84:16
3 ^a	143 	142 	50:50 ^a

^a Obtained from reference ¹¹⁶

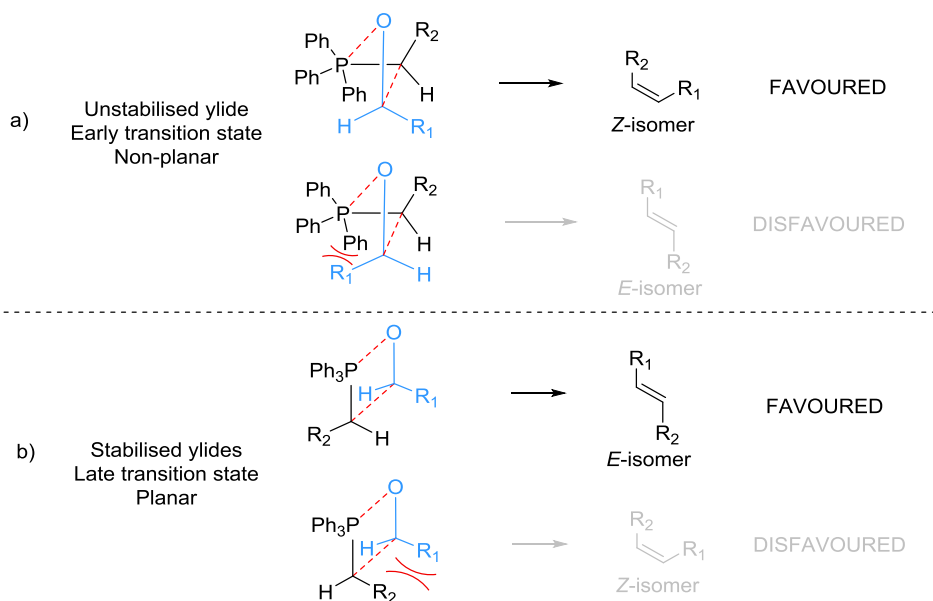
Table 12: Ratios of *Z* and *E* isomers of the Wittig reaction between different semi-stabilised ylides.

The generally accepted mechanism for the Wittig reaction is based on the cycloaddition mechanism proposed by Vedejs.¹¹⁷ The Li salt-free Wittig reactions of non-stabilised, semi-stabilised and stabilised ylides with carbonyls occur under kinetic control where the first step is the irreversible and stereoselective [2+2] cycloaddition between the ylide and aldehyde to give an oxaphosphetane intermediate **144** which then undergoes rapid irreversible and stereospecific cycloreversion to give an alkene **145** and phosphine oxide **146** (Scheme 72). The rate determining step is the oxaphosphetane formation and the *E/Z* ratio of the oxaphosphetane reflects the *E/Z* ratio of the final alkene product.



Scheme 72: Vedejs' [2+2] cycloaddition mechanism for the Wittig reaction.

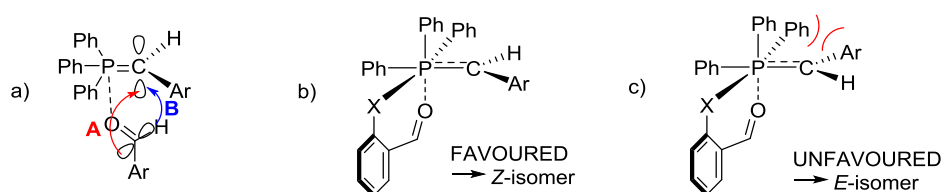
Vedejs argued that the reaction of an unstabilised ylide occurs *via* an early transition state which is therefore reactant-like and non-planar (Scheme 73a), whereas the reaction with a stabilised ylide occurs through a late-stage transition state which is more planar and product-like (Scheme 73b). It is thought that semi-stabilised ylides (*e.g.* benzylides) react similarly to the unstabilised system. The Wittig reaction in the synthesis towards CAIP **9** requires *Z*-selectivity, and in order to enhance *Z*-selectivity, the transition state leading to the *Z*-oxaphosphetane needs to be stabilised or the transition state leading to the *E*-oxaphosphetane should be destabilised.



Scheme 73: a) *Z*-selectivity of unstabilised ylides *via* an early transition state b) *E*-selectivity of stabilised ylides *via* a late transition state.

It has been shown that *ortho*-substitution of benzaldehydes with methoxy or halo groups give predominately *Z*-alkenes.¹¹⁶ Yamataka and co-workers proposed that the selectivity was due to the chelating interaction between the *ortho*-heteroatom and the ylide phosphorus atom. In the initial stage of the Wittig reaction, the aldehyde and ylide are likely to form a σ -complex through a weak interaction between the carbonyl oxygen and

the electron deficient phosphorus atom on the ylide. The stereochemistry of the resulting oxaphosphetane depends on the approach going into the transition state, either through pathway A or B (Scheme 74a). When the benzylide and benzaldehyde have no substituents (Table 12, Entry 3) the C-P-O-C dihedral angle has relatively free rotation and results in a near equal ratio of the two isomers.¹¹⁶ However if there is an *ortho*-methoxy substituent (or heteroatom) on the benzaldehyde, it is believed the σ -complex adopts a different conformation. The phosphorus atom forms a hypervalent octahedral structure where it accepts electrons from both the carbonyl oxygen and the heteroatom in the *ortho*-position of the benzaldehyde (Scheme 74b and c). In the favoured conformation, the aryl group of the ylide is on the same side as the aryl group of benzaldehyde in order to minimise the steric repulsion from the equatorial phenyl groups on the phosphorus; this results in the *Z*-alkene.



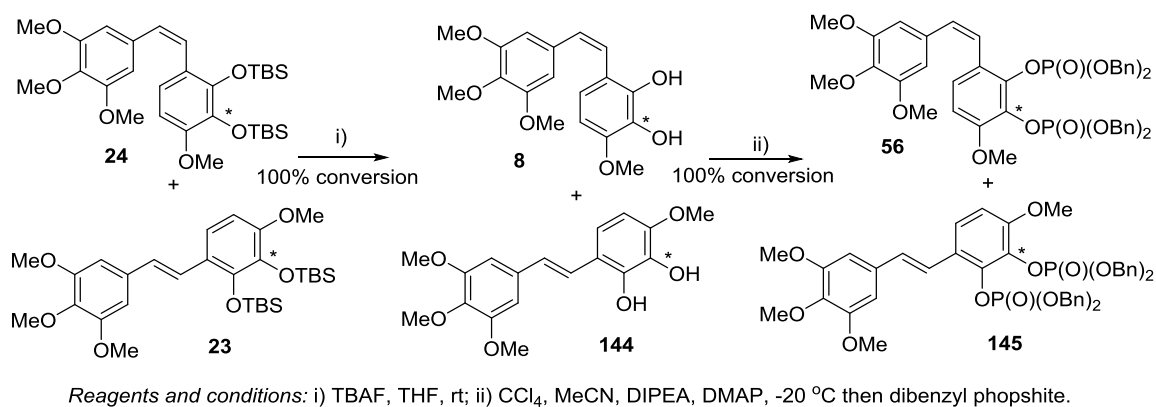
Scheme 74: Initial α -complex formed in the Wittig reaction when there is a) no *ortho* effect b) a favoured octahedral α -complex formed due to the *ortho*-effect and c) an unfavored octahedral α -complex due to steric interactions.

This *ortho*-effect was also observed by Gilheany and Byrne where they observed that having an *ortho* substituent that bears a lone pair considerably increases the proportion of the *Z*-alkene product.¹¹⁸ They also observed that *ortho*-substituted benzylides react with benzaldehydes with moderate *E*-selectivity. No explanation was given for this selectivity but it is likely due to a different geometry of the transition state that favours the *E*-isomer. The observations and explanation by both Yamataka and Gilheany, support the *E/Z* selectivity shown during the Wittig reactions for the synthesis of CA1P (Table 12); the reaction with the highest *Z:E* ratio occurred with a benzaldehyde that has a heteroatom in the *ortho* position and when the benzylide component does not contain a substituent in the *ortho* position (Table 12, Entry 2).

E-selectivity of the Wittig reaction can be increased by the introduction of lithium salts and is commonly employed in the Schlosser-Wittig modification when using unstabilised ylides.¹¹⁹ This lithium salt effect or ‘stereochemical drift’ was first observed by

Maryanoff and co-workers,¹²⁰ and suggests the use of different non-lithium bases could also increase the amount of *Z*-isomer in the product.

The separation of the *E*- and *Z*-isomers **23** and **24** was achieved by recrystallisation from ethanol. On a 3.4 mmol scale the *Z*-isomer **24** was isolated in a 58% yield, however on a smaller 0.25 mmol scale only a 31% yield was obtained. As the latter scale will be used when using [¹³C]-labelled material recovery of the remaining *Z*-isomer from the *E/Z* mixture was considered important. Separation of the CA1-TBS isomers **23** and **24** through flash column chromatography was prevented by their close *R_f* values. Therefore separation of the two isomers at later stages of the synthesis was looked into. An *E/Z* mixture of the TBS-protected alkenes **23** and **24** was treated with tetrabutylammonium fluoride in THF and gave *E*- and *Z*-CA1 **144** and **8** (Scheme 75). Unfortunately, the *R_f* values for these isomers remained too close to separate by flash column chromatography. Therefore *E*-CA1 **144** and *Z*-CA1 **8** were benzylated with dibenzyl phosphite, carbon tetrachloride, DIPEA and DMAP to give the *E*- and *Z*-benzylated isomers **145** and **56**. However, again these isomers were inseparable by flash column chromatography.

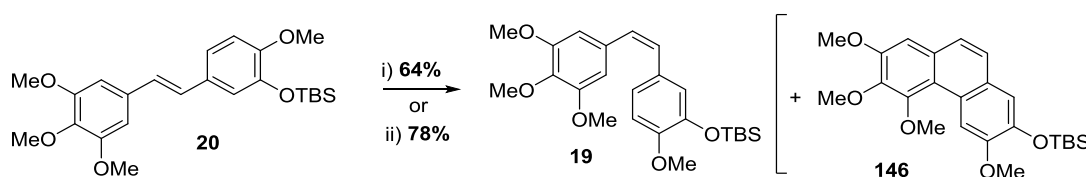


Scheme 75: Deprotection and benzylation of *E*- and *Z*- isomers **23** and **24**.

The isolation of the CA1-TBS *E/Z* isomers **23** and **24** by flash column chromatography was achieved using 10% ethyl acetate: petroleum ether. This was changed to ethyl acetate: toluene as toluene can sometimes improve separation of aromatic species. Unfortunately separation of the *E* and *Z*-CA1-TBS alkenes **23** and **24** was no cleaner, likewise for the *E/Z* mixture of CA1 **144** and **8**, or the *E/Z* mixture of benzylated-CA1 **145** and **56**. Next, the TLC plates were coated with silver nitrate, which is another methodology that can separate non-polar compounds of similar

polarities. Unfortunately the separation for all three sets of *E/Z* isomers (**23/24**, **144/8** and **145/56**) was not improved.

Since separating the *E/Z* isomers effectively was proving difficult, investigations began into converting the undesired *E*-isomer **23** into the desired *Z*-isomer **24**. Photochemical isomerisation using UV irradiation is an attractive method for converting *E*-stilbenes to *Z*-stilbenes and has been used to convert the *E*-isomer of a different combretastatin, CA4, to its *Z*-isomer.³⁰ The *E* to *Z* photochemical isomerisation of *E*-TBS-CA4 **20** was observed in ethanol with UV light (254 nm) by Pettit and co-workers in a 64% yield after column chromatography (Scheme 76).³⁰ However when Lupattelli and co-workers tried to replicate these conditions, they observed significant quantities of a cyclised by-product phenanthrene **146**.¹²¹ They therefore varied the polarities of the solvents used; in low-polarity solvents (*n*-hexane and benzene) the phenanthrene **146** was observed after 5-11 hours. In methanol, 15 mol% of phenanthrene **146** was observed after 4 hours and in other solvents (acetone and acetonitrile) phenanthrene **146** was detected after 16 hours (17 mol%). They also looked at the *E/Z* ratio, and found that this decreased with increasing polarity of the solvent; *n*-hexanes had a *E/Z* ratio of 40:60, whereas methanol had a *E/Z* ratio of 11:89. They therefore used an intermediate solvent, acetone in their isomerisation of *E*-TBS-CA4 **20** to the desired *Z*-isomer **19** (Scheme 76).



Reagents and conditions: i) EtOH, 254 nm, ii) acetone, 254 nm, rt, 44 h.

Scheme 76: *E* to *Z* isomerisation of *E*-TBS-CA4 **20** observed by both Pettit and Lupattelli.

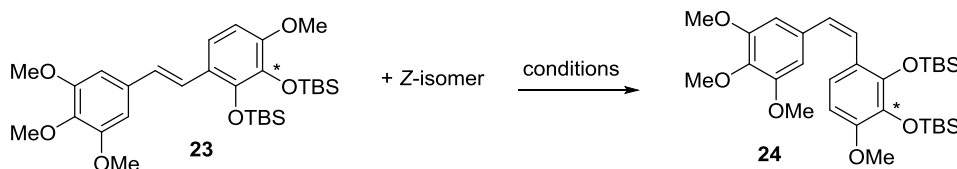
Therefore investigations into converting *E*-CA1-TBS **23** to *Z*-CA1-TBS **24** using UV light began. An *E/Z* mixture (55:45) of CA1-TBS **23** and **24** was irradiated with varying wavelengths of light/UV radiation, in hexane (Table 13, Entries 1-3). However, no significant change in the *Z:E* ratio was observed, and no phenanthrene product was observed. For the isomerisation of *E*-CA4-TBS **23** Lupattelli and co-workers found

higher *E* to *Z* isomerisation occurred with polar solvents, therefore the solvent in the *E*-CA1-TBS **23** system was changed from hexanes to methanol. Unfortunately, no significant increase in the *Z*:*E* ratio was observed (Table 13, Entries 4-6). Iodine is known to catalyse the *Z* to *E* isomerisation of alkenes, therefore catalytic iodine was added to the reaction (Table 13, Entries 7-9).^{122,123} As it is thought that the iodide-catalysed isomerisation occurs through a radical mechanism, it is not surprising that the *E*-isomer was the major product from these reactions.

Entry	Wavelength	Solvent	Additive	<i>Z</i> : <i>E</i> ratio ^a
1	vis	hexane	-	45:55
2	254 nm	hexane	-	49:51
3	365 nm	hexane	-	42:58
4	vis	methanol	-	45:55
5	254 nm	methanol	-	50:50
6	365 nm	methanol	-	43:57
7	vis	hexane	I ₂ ^b	0:100
8	254 nm	hexane	I ₂ ^b	0:100
9	365 nm	hexane	I ₂ ^b	0:100

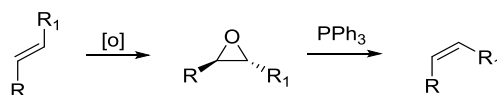
^a *Z*:*E* ratio of the starting material was 45:55. ^b 0.2 mol%.

Table 13: Attempts at isomerisation of *E*-alkene **23** to *Z*-alkene **24**.



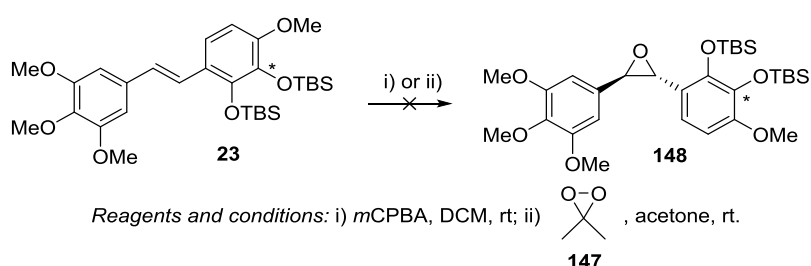
Scheme 77: *E*/*Z* isomerisation of *E*-CA1-TBS **23**

Photoisomerisation of the *E*/*Z* mixture of CA1-TBS **23** and **24** failed to decrease the *E*/*Z* ratio, however it did reveal a method to access pure *E*-isomer **23**. Another way to isomerise alkenes is to first epoxidise, with retention of stereochemistry, then deoxygenate with inversion of stereochemistry, which will lead to overall isomerisation (Scheme 78). The epoxidation is stereospecific, so pure *E*-alkene will react with retention of the alkene configuration and will give pure *trans*-epoxide. It is then thought that this *trans*-epoxide can be opened by a nucleophile, such as triphenylphosphine, and this happens with inversion of stereochemistry to form the *Z*-isomer.



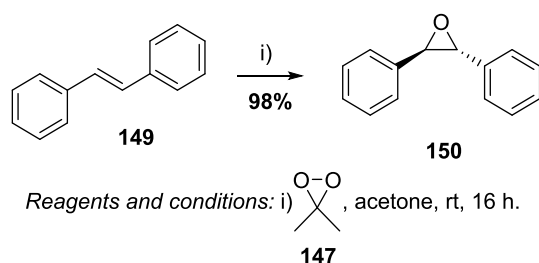
Scheme 78: *E*/*Z* isomerisation through epoxidation then deoxygenation.

Pure *E*-CA1-TBS **23** was first treated with *meta*-chloroperoxybenzoic acid in dichloromethane. However this returned a complex mixture with multiple products and the desired *trans*-stilbene oxide **148** was not observed in the crude ^1H NMR spectrum. Therefore another oxidising reagent was tried, dimethyldioxirane **147** (DMDO), which was freshly prepared from acetone and Oxone®. This reagent has the advantage that the only by-product is acetone which can be removed by evaporation under reduced pressure. But, unfortunately no reaction occurred when *E*-TBS-CA1 **23** was treated with DMDO **147** in acetone at room temperature for 16 hours.



Scheme 79: Attempts at epoxidation of *E*-CA1-TBS **23** with DMDO **147**.

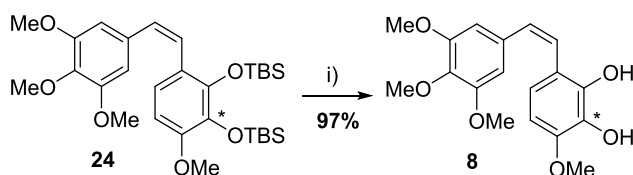
As it was surprising that the epoxidation of *E*-CA1-TBS **23** did not occur when using DMDO **147**, the quality of the DMDO **147** was investigated. Unfortunately DMDO **147** was synthesised at a low concentration in acetone solution and needed to be kept under argon in the freezer, therefore could not be characterised by conventional methods. Consequently, the DMDO solution **147** was treated with *trans*-stilbene **149**, a substrate that is known to react with DMDO (Scheme 80).¹²⁴ The reaction proceeded with 100% conversion to the *trans*-stilbene oxide **150** which was isolated in a 98% yield, thus confirming the quality of the DMDO solution.



Scheme 80: Epoxidation of *trans*-stilbene **149** to *trans*-stilbene oxide **150** using DMDO.

It therefore appears that the *E*-CA1-TBS **23** substrate is incompatible with the DMDO conditions. To confirm this, a competition reaction was undertaken, where a 50:50 mixture of *E*-CA1-TBS **23** and *trans*-stilbene **149** were treated with DMDO **147**. Analysis of the crude ¹H NMR spectrum showed 100% conversion of *trans*-stilbene **149** to *trans*-stilbene oxide **150** and also showed some loss of *E*-CA1-TBS **23**, and the appearance of new peaks. As some *E*-CA1-TBS **23** had reacted with DMDO, the reaction was repeated but this time heated to 50 °C. The reaction went to completion but unfortunately a number of products were observed, similar to those observed for the reaction using *meta*-chloroperoxybenzoic acid (Scheme 79).

As the attempts at converting the unwanted *E*-CA1-TBS isomer **23** were unsuccessful, either through photoisomerisation (Scheme 77, Table 13), or *via* a *trans*-epoxide (Scheme 79), the synthesis continued with the *Z*-CA1-TBS **24** isolated through recrystallisation from the Wittig reaction (Scheme 71). The *Z*-isomer **24** was deprotected using tetrabutylammonium fluoride in tetrahydrofuran which yielded CA1 **8** in a 97% yield after flash column chromatography (Scheme 81).



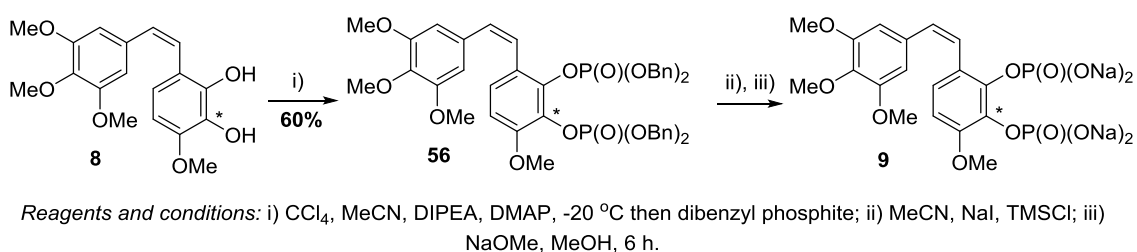
Reagents and conditions: i) TBAF (1 M), THF, rt.

Scheme 81: Deprotection of TBS-protected CA1 **24** to Combretastatin A1 **8**.

CA1 **8** proved to be unstable over long periods of time, with degradation being observed if CA1 **8** was left at room temperature, in air for longer than 72 hours. For both stability and pharmacokinetic reasons, CA1 **8** needs to be converted into its tetrasodium phosphate prodrug CA1P **9**. The prodrug **9** can be synthesised following the route established in the US patent by Pettit and Lippert, where CA1 **8** is first converted to the tetrabenzyl-protected phosphate **56**, and then debenzylated and converted to the tetrasodium phosphate **9**.²⁴ During their investigations, Pettit and Lippert also attempted numerous debenzylation conditions including; Raney nickel, ferric chloride, trimethylphenylthiosilane, chromium trioxide, DDQ, triphenylcarbenium, tin(IV) chloride, and lithium hydroxide, all of which resulted in either incomplete benzylation,

E/Z isomerisation or reduction of the alkene. However, they found success with treatment with chlorotrimethylsilane and sodium iodide followed by treatment with sodium methoxide. Pettit and Lippert observed that a new bottle of sodium iodide and dilute concentrations were needed for the debenzoylation step otherwise they experienced nearly a 1:1 ratio of *Z*- and *E*- isomers, presumably arising from the electrophilic addition of iodine to the *Z*- isomer to form an iodonium ion, and its subsequent elimination to the *E*- isomer.

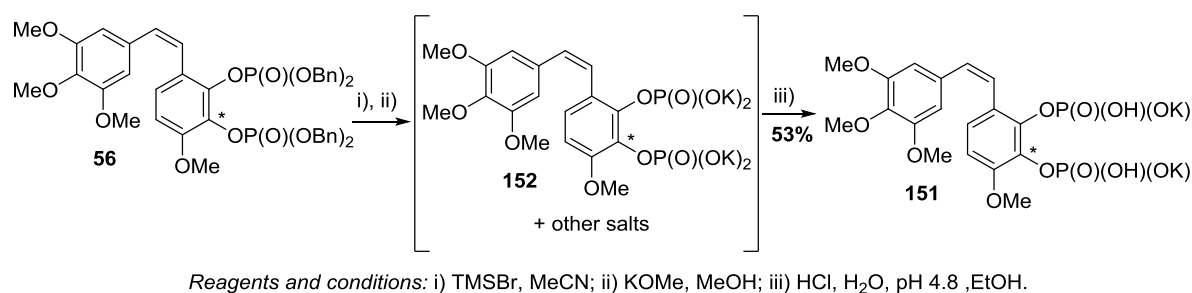
Therefore CA1 **8** was first treated with dibenzyl chlorophosphate, which was generated *in situ* from dibenzyl phosphite and carbon tetrachloride, and gave the tetrabenzyl protected phosphate **56** in a 60% yield after flash column chromatography (Scheme 82). Next, the benzylated phosphate **56** was treated with trimethylsilyl iodide generated *in situ* from chlorotrimethylsilane and sodium iodide. The subsequent acid was treated with sodium methoxide in anhydrous methanol to yield the tetrasodium CA1P **9**. The reaction was performed ensuring a dilute concentration to prevent any *Z-E* isomerisation as observed by Pettit, and fortunately no isomerisation was observed by ¹H NMR spectroscopy.



Scheme 82: Synthesis of CA1P **9** from CA1 **8**.

Unfortunately the tetrasodium salt **9** was found to be unstable over a short time (24 hours) despite the sample being kept at 4 °C and covered in foil to exclude light. The tetrasodium salt **9** also degraded when attempts were made to purify the sample under HPLC conditions. Consequently other salts of CA1P were examined. Oxigene Inc., the company responsible for the clinical development of CA1P, uses the dipotassium salt **151** in their clinical trials as they observed it to be more stable and therefore was of interest to investigate.¹²⁵

The formation of the dipotassium salt **151** has been reported by Brown and co-workers during their work on the carbon-14 radiosynthesis of CA1P.¹²⁶ Like Pettit, they debenzylated the tetrabenzyl-protected CA1 **8** to the tetra-TMS-phosphate ester but instead of quenching with sodium methoxide, Brown used potassium methoxide and carefully adjusted the pH. Therefore the tetrabenzyl phosphate **56** was treated with trimethylsilyl bromide in acetonitrile at -10 °C. This solution was then added dropwise to a solution of excess potassium methoxide in methanol at -10 °C and formed the tetrapotassium salt **152**. To determine the pH where the dipotassium salt is formed, a pH titration curve was generated (Figure 19). The tetrapotassium salt **152** was dissolved in water and 10 mL of 0.1 M HCl acid was added in 0.2 mL increments and the pH measured after each addition.



Scheme 83: Synthesis of dipotassium phosphate salt of CA1P **151**.

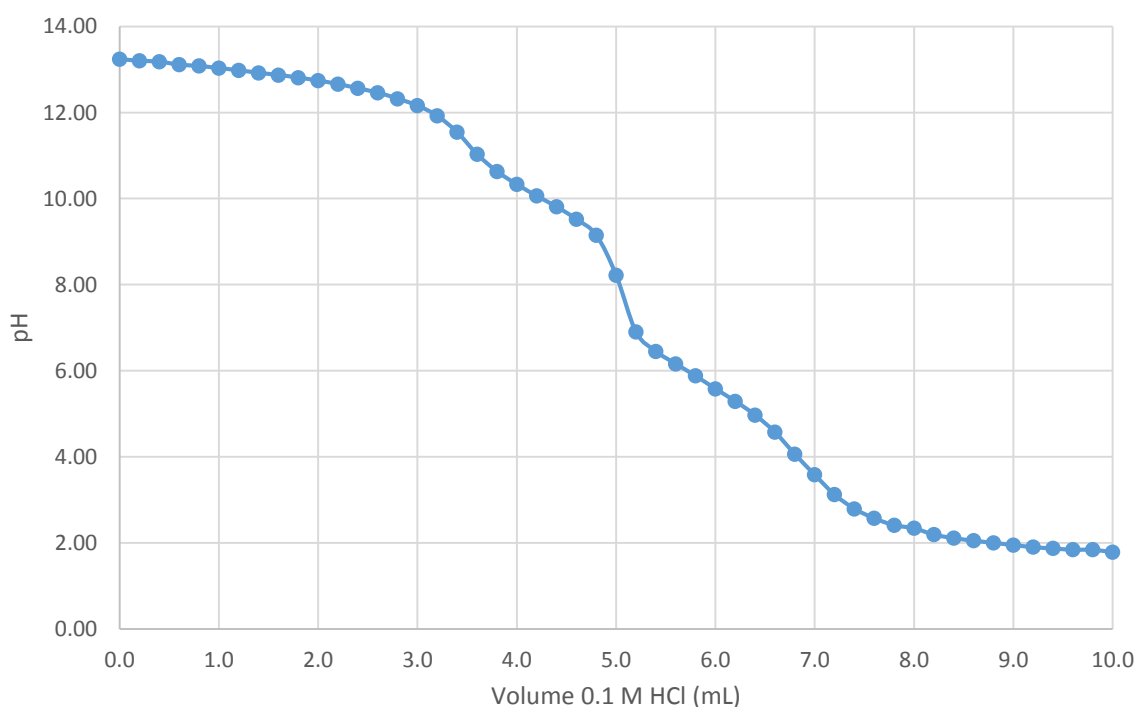


Figure 19: pH Titration curve of tetrapotassium CA1P salt **152** with hydrochloric acid (0.1 M).

The pH was therefore adjusted to pH 7.8, the pH of the second equivalence point, then ethanol was added but only a small amount of precipitate was formed. However when the pH was adjusted to pH 4.8, the pH reported in the literature, a greater quantity precipitate was formed and was isolated in a 45% yield. The ^1H NMR spectrum of the precipitated solid showed the presence desired dipotassium salt **151** but also showed the presence of another product which contained aromatic protons. It was thought this could have arisen from the reaction between benzyl bromide (the by-product from the debenzylation reaction) and the acetonitrile solvent in a Ritter-like reaction. Therefore the reaction was repeated but the acetonitrile solvent was removed immediately after the first step. This time, the ^1H NMR spectrum showed just the desired dipotassium salt **151**, and was isolated in a 58% yield. However, when the reaction was repeated on a smaller scale to replicate the scale that this will later be carried out on ^{13}C material, the precipitate was only formed in a 32% yield.

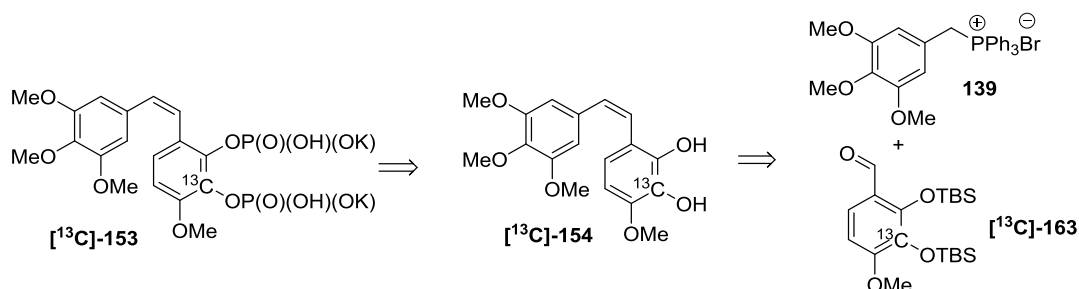
In order to try and increase the yield of CA1P **151** when synthesised on a small scale, the CA1P solution in ethanol was left to precipitate for longer and the temperature reduced to $-20\text{ }^\circ\text{C}$, but unfortunately this failed to increase the yield. Furthermore, all the solvent was removed and the resulting residue was re-dissolved in the minimum amount of water then ethanol was added, but unfortunately the resulting precipitate was formed in the same yield as before. And finally, isopropanol was used as a solvent, but this failed to produce any more dipotassium CA1P **151**.

Despite a low yield observed for the debenzylation of phosphate **56** to CA1P **151** on a small scale at this point, an effective route had been established for the synthesis of CA1P **151**. Therefore, there was confidence that the route established on ^{12}C material can be translated to ^{13}C material for the synthesis of ^{13}C -labelled CA1P [^{13}C]-**153**.

2.5. Synthesis of [^{13}C]-CA1P

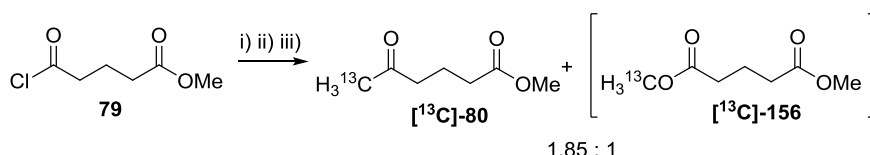
Now that a route for the synthesis of CA1P **151** had been established using unlabelled, ^{12}C material the synthesis was repeated on ^{13}C -labelled material. The dipotassium salt [^{13}C]-**153** can be synthesised from ^{13}C -labelled CA1 [^{13}C]-**154**. The route utilised the

Wittig reaction of TBS-protected aldehyde [^{13}C]-**163** and phosphonium salt **139** (Scheme 84).



Scheme 84: Retrosynthesis of ^{13}C -labelled CA1P [^{13}C]-**153**.

For the first step, the [^{13}C]-labelled Grignard reagent was made by treating commercially available [^{13}C]-methyl iodide with magnesium turnings in diethyl ether. The resulting [^{13}C]-methyl magnesium iodide was added to the acid chloride **79** and formed the ketone [^{13}C]-**80**. The presence of a by-product was also observed in the crude ^1H NMR spectrum. This by-product was also seen, in smaller amounts, in the ^{12}C -synthesis but by using a ^{13}C label the identity was deduced to be diester [1 – ^{13}C]-5-dimethylester pentanedioic acid [^{13}C]-**156**. This deduction was achieved through analysis of the crude ^1H NMR spectrum where a doublet peak was seen in the methoxy region with a large $J_{\text{C-H}}$ value of 146.8, which is caused by the coupling of the three methyl protons with the ^{13}C label.



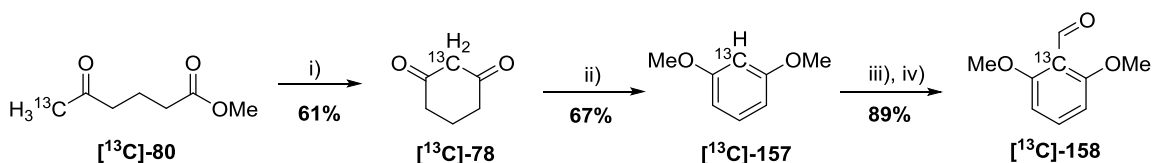
Reagents and conditions: i) Mg^0 , $^{13}\text{CH}_3\text{I}$, Et_2O ; ii) $\text{CuBr}\cdot\text{DMS}$, Et_2O , $-10\text{ }^\circ\text{C}$; iii) glutaric acid monomethyl ester chloride **79**, $-10\text{ }^\circ\text{C}$, 1 h.

Scheme 85: Synthesis of [^{13}C]-labelled ketone [^{13}C]-**80**.

This by-product may have arisen from the hydrolysis of the acid chloride **79** to the acid **83**, followed by methylation from the Grignard reaction or unreacted methyl iodide. An alternative theory is the oxidation of the Grignard reagent to an iodomethoxymagnesium species, which can then react with the acid chloride **79** to form the ester [^{13}C]-**156**. Therefore, the reaction was repeated ensuring anhydrous and deoxygenated conditions, but the percentage of unwanted by-product remained the same. However [^{13}C]-methyl-5-oxohexanoate [^{13}C]-**80** was the major product of the reaction and was isolated in a 55%

yield after column chromatography. The lower yield observed when using the [^{13}C]-labelled material highlights the potential problem of scaling the reaction up; on the 7.4 mmol scale used for ^{12}C -material the ketone **84** was synthesised in a 69% yield, whereas using a 39 mmol scale for the ^{13}C -material gave a 55% yield.

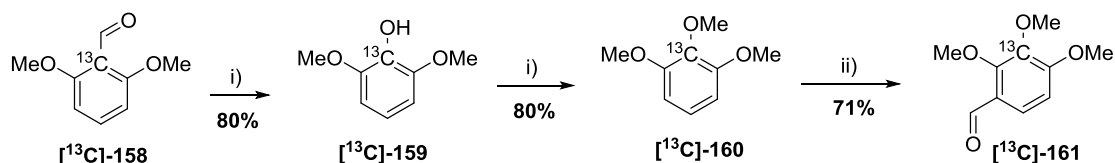
Methyl 5-oxo-[6- ^{13}C]-hexanoate [^{13}C]-**80** was then cyclised to the [2- ^{13}C]-cyclohexane-1,3-dione [^{13}C]-**78** using potassium *tert*-butoxide and was isolated after column chromatography in a 61% yield (Scheme 86). The diketone [^{13}C]-**78** was then aromatised and methylated using iodine in methanol which gave the dimethoxybenzene [^{13}C]-**157** in a 67% yield. Next, an *ortho*-formylation reaction occurred on the dimethoxy benzene [^{13}C]-**157** and this was achieved through selective lithiation with *n*-butyllithium followed by quenching with dimethylformamide. After purification, the benzaldehyde [^{13}C]-**158** was isolated in an 89% yield.



Reagents and conditions: i) KOtBu (2 eq.), THF, reflux, 6 h; ii) I₂, MeOH, reflux; iii) TMEDA, *n*BuLi, THF; iv) DMF.

Scheme 86: Synthesis of [^{13}C]-labelled benzaldehyde [^{13}C]-**158** from ketone [^{13}C]-**80**.

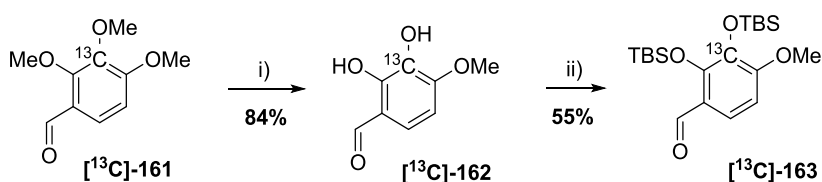
The benzaldehyde [^{13}C]-**158** then underwent a Baeyer-Villiger oxidation using meta-chloroperoxybenzoic acid to form a formate ester which was cleaved under basic conditions to reveal the dimethoxy phenol [^{13}C]-**159** in an 80% yield. The phenol [^{13}C]-**159** was then methylated using methyl iodide, and after flash column chromatography the trimethoxybenzene [^{13}C]-**160** was isolated in an 80% yield. The trimethoxybenzene [^{13}C]-**160** then underwent an *ortho*-formylation reaction using titanium tetrachloride and dichloromethyl methyl ether, and this gave the benzaldehyde [^{13}C]-**161** in a 71% yield.



Reagents and conditions: i) *m*CPBA, DCM; ii) MeI (3 eq.), 18-C-6, acetone; iii) TiCl₄, Cl₂CHOMe, DCM.

Scheme 87: Synthesis of [^{13}C]-labelled benzaldehyde [^{13}C]-**161** from benzaldehyde [^{13}C]-**158**.

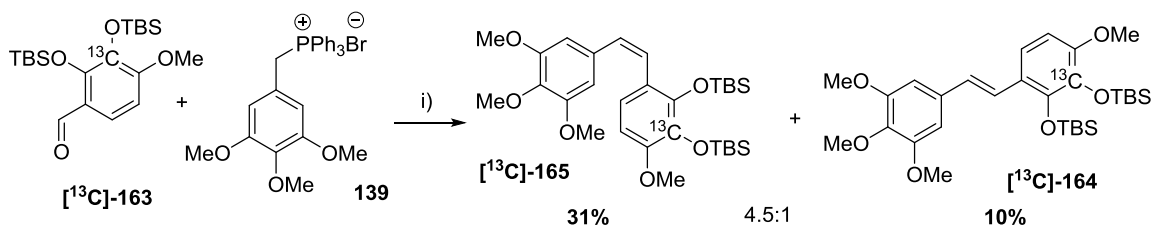
In order to convert the benzaldehyde [^{13}C]-**161** into the Wittig-aldehyde component for the Wittig reaction, the benzaldehyde [^{13}C]-**161** underwent selective double demethylation with boron trichloride, which gave the diphenol [^{13}C]-**162** in an 84% yield (Scheme 88). The two phenol moieties were then protected as *tert*-butyldimethylsilyl ethers to give aldehyde [^{13}C]-**163** which was formed in a 55% yield.



Reagents and conditions: i) BCl_3 , DCM, 16 h; ii) NEt_3 , DMAP, DCM, rt, 10 min then TBSCl, 12 h.

Scheme 88: Synthesis of [^{13}C]-labelled Wittig reagent [^{13}C]-**163** from benzaldehyde [^{13}C]-**161**.

The phosphonium ylide component of the Wittig reaction was derived from the phosphonium salt **139**, and this was synthesised in three steps from the corresponding, commercially available, aldehyde **17** (Scheme 70). The Wittig reaction between the protected aldehyde [^{13}C]-**163** and the phosphonium salt **139** occurred forming the *E* and *Z*-isomers [^{13}C]-**164** and [^{13}C]-**165** in a 1:4.5 ratio (Scheme 89). The mixture of *E*- and *Z*-isomers [^{13}C]-**164** and [^{13}C]-**165** was purified by flash column chromatography, then the *Z*-isomer [^{13}C]-**165** isolated by recrystallisation from ethanol in a 31% yield.

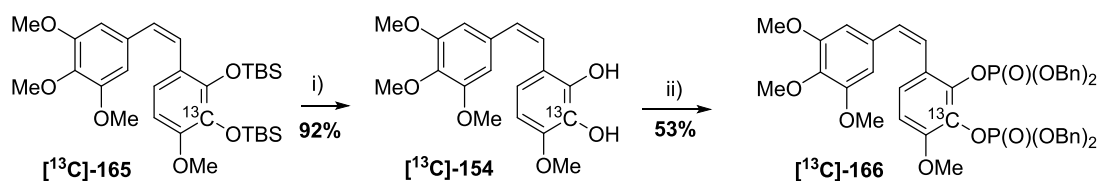


Reagent and conditions: i) $n\text{BuLi}$ (1.9 M, 1 eq.), THF, $-15\text{ }^\circ\text{C}$, then [^{13}C]-**163**, $-78\text{ }^\circ\text{C}$ to $0\text{ }^\circ\text{C}$.

Scheme 89: Wittig reaction between aldehyde [^{13}C]-**163** and phosphonium salt **139**.

The TBS-protected CA1 [^{13}C]-**165** was then deprotected using tetra-*n*-butylammonium fluoride which revealed the [^{13}C]-labelled combretastatin A1 [^{13}C]-**154** in a 92% yield (Scheme 90). Next, [^{13}C]-CA1 [^{13}C]-**154** was converted to its prodrug [^{13}C]-**153**. This was achieved by first forming the tetrabenzyl protected phosphate [^{13}C]-**166** by treatment of CA1 [^{13}C]-**154** with dibenzyl phosphite and carbon tetrachloride. After purification

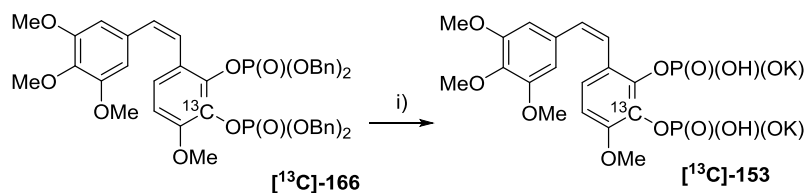
by flash column chromatography the phosphate [^{13}C]-**154** was isolated in a 53% yield (Scheme 90).



Reagents and conditions: i) TBAF (1 M), THF, rt; ii) CCl_4 , MeCN, DIPEA, DMAP, $-20\text{ }^\circ\text{C}$ then dibenzyl phosphite.

Scheme 90: Synthesis of [^{13}C]-labelled dibenzyl phosphate [^{13}C]-**166** from (*Z*)-CA1-TBS [^{13}C]-**165**.

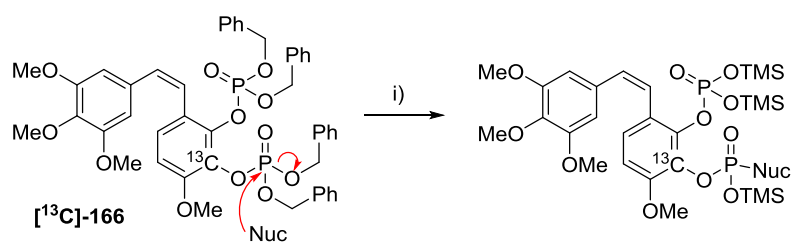
The final step for the synthesis of [^{13}C]-CA1P [^{13}C]-**153** involves the debenylation of the tetrabenzyl phosphate [^{13}C]-**166** using bromotrimethylsilane followed by treatment with potassium methoxide and partial acidification. Subsequent addition of ethanol and filtration of the precipitate revealed an off-white solid. The ^1H NMR spectrum corresponds to the dipotassium salt [^{13}C]-**153**, however multiple peaks were observed in the ^{31}P NMR spectrum. Initially this was thought to be due to the presence of other potassium salts. However when the sample was re-dissolved in water and the pH checked, multiple peaks still remained in the ^{31}P NMR.



Reagents and conditions: i) TMSBr , MeCN; ii) KOMe , MeOH; iii) HCl , H_2O , pH 4.8, EtOH.

Scheme 91: Synthesis of [^{13}C]-labelled CA1P [^{13}C]-**153**.

Another theory is that incomplete benzylation occurred on some of the phosphate [^{13}C]-**166**. However, this was ruled out due to the absence of any benzyl peaks in the ^1H NMR spectrum. Therefore it was hypothesised that the bromotrimethylsilane or a degraded product thereof could be acting as a nucleophile and attacking the phosphorus centre (Scheme 92). This would account for the lack of benzyl groups in the ^1H NMR spectrum and the presence of multiple peaks in the ^{31}P NMR spectrum.



Reagents and conditions: i) TMSBr, MeCN.

Scheme 92: Possible nucleophilic attack at the phosphorus centre on tetrabenzyl phosphate [^{13}C]-**166**.

Therefore the debenylation step was repeated using a new bottle of bromotrimethylsilane which was also freshly distilled over calcium hydride. Unfortunately, no improvement in the yield was observed and multiple peaks were still seen in the ^{31}P NMR spectrum. The range of the peaks in the ^{31}P NMR spectrum for CA1P [^{13}C]-**153** were -4.18 to -2.36. As the peaks assigned in the ^{31}P NMR spectrum for unlabelled CA1P **151** are -3.0 and -3.7, it is possible that the dipotassium CA1P salt [^{13}C]-**153** was formed. The additional peaks could have arisen due to the presence of other potassium CA1P salts or the presence of inorganic phosphates.

2.6. Synthesis of [$^{13}\text{CD}_3$]-CA1P

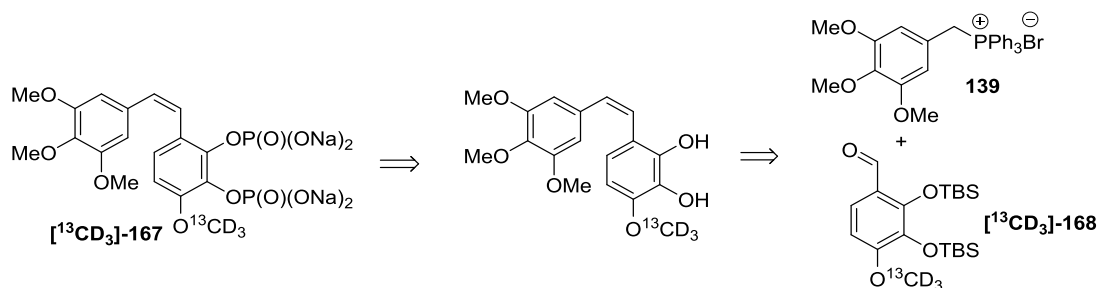
Another ^{13}C -labelled CA1 analogue [$^{13}\text{CD}_3$]-**167** was synthesised involving a shorter synthesis. A methoxy group would be the easiest target as it can be inserted at a later stage in the synthesis and will be more economical in regards to the label. Brown and co-workers have successfully achieved the radiosynthesis of combretastatin A1 with a 14-carbon label in the methoxy group in the 6-position of Ring A.¹²⁶ However this synthesis cannot be applied to a hyperpolarised ^{13}C synthesis as the location of the label is thought to be too far away from the expected site of metabolism in Ring B. Therefore the methoxy group on Ring B was chosen. The T_1 relaxation time for this position of the unlabelled material is 1.6 s (Figure 15, Table 5, Entry 15) and this would only allow for a very small imaging window ($3 - 5 \times T_1$). However deuterium enrichment is known to increase the T_1 times of ^{13}C substrates dramatically. This was recently shown by Sando and co-workers when they used a deuterated ^{13}C methoxy group ($^{13}\text{CD}_3\text{O}$) in the development of hyperpolarised ^{13}C probes.¹²⁷ The hyperpolarised substrate used was [^{13}C , $^2\text{H}_3$]-*p*-anisidine (Figure 20b), where the carbon-13 atom in the methoxy group was found to

have a T_1 value of 44.4 s which is significantly higher than a T_1 time of 6.3 s for the corresponding carbon atom in the non-deuterated *p*-anisidine (Figure 20b).



Figure 20: a) *p*-anisidine b) [^{13}C , $^2\text{H}_3$]-*p*-anisidine.

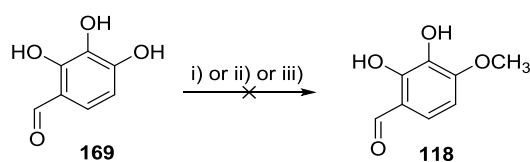
It was therefore envisioned that deuterium enrichment would sufficiently increase the T_1 time of the target CA1P molecule. The synthesis of [$^{13}\text{CD}_3$]-CA1P [$^{13}\text{CD}_3$]-**167** can follow the previously established Wittig route where triphenyl-[(3,4,5-trimethoxyphenyl)methyl]phosphonium bromide **139** is treated with a TBS-protected aldehyde [$^{13}\text{CD}_3$]-**168**. Unlike the previous synthesis of [^{13}C]-combretastatin [^{13}C]-**153** where the ^{13}C – label was embedded in the aromatic ring of the benzaldehyde, this new synthesis targeted the ^{13}C label at the methoxy group in Ring B.



Scheme 93: Retrosynthesis of [$^{13}\text{CD}_3$]-CA1P [$^{13}\text{CD}_3$]-**167**.

The synthesis of the $^{13}\text{CD}_3$ -labelled aldehyde [$^{13}\text{CD}_3$]-**168** component of the Wittig reaction requires insertion of the label using a methylation step with methyl iodide, due to [^{13}C , d_3]-labelled methyl iodide being the most accessible commercially available source of the $^{13}\text{CD}_3$ unit. This method for synthesising the $^{13}\text{CD}_3$ -labelled aldehyde was developed and synthesised by Dr. Ed Cochrane (from the Jones group). Like the development of the route for the synthesis of [^{13}C]-CA1P [^{13}C]-**153**, the route was first established on unlabelled ^{12}C material. His synthesis started with attempts at selective methylation of 2,3,4-trihydroxybenzaldehyde **169** to 2,3-dihydroxy-4-methoxybenzaldehyde **118** (Scheme 94). The benzaldehyde **169** was first treated with potassium carbonate followed by addition of methyl iodide; unfortunately this resulted in a mixture of mono-, di- and tri-methylated products. Next the potassium carbonate was replaced

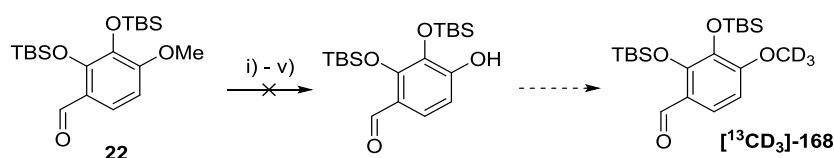
with sodium hydride, but this again failed to yield the desired mono-methylated species, instead primarily giving the di-methylated species. Pettit and co-workers have shown the selective methylation of 2,3,4-trihydroxybenzaldehyde **169** *via* a 2,3-borate; the benzaldehyde **169** was treated with borate to selectively form the 2,3-borate ester which allows the specific methylation by dimethylsulfate. However when these conditions were attempted using methyl iodide instead of dimethylsulfate, which was used due to the commercial availability of [¹³C,₃]-methyl iodide, no methylation occurred.



Reagents and conditions: i) K₂CO₃, CH₃I (1 eq.), dry acetone, reflux; ii) NaH, DMSO, THF, CH₃I, reflux; iii) sodium borate-decahydrate, H₂O; iii) NaOH, H₂O, CH₃I.

Scheme 94: Attempted methylation of 2,3,4-trihydroxybenzaldehyde **169** to 2,3-dihydroxy-4-methoxybenzaldehyde **118**.

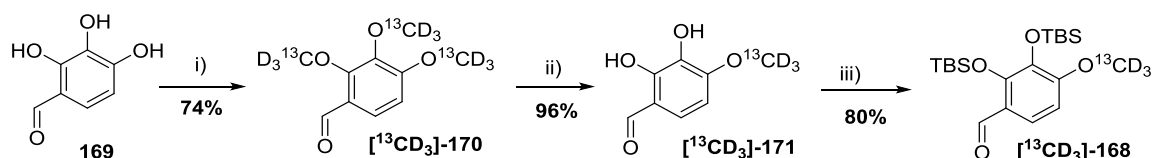
Due to the difficult nature of selectively methylating 2,3,4-trihydroxybenzaldehyde **169** the next approach looked at demethylating the TBS-protected aldehyde **22** (Scheme 95). The first demethylating reagent attempted was boron tribromide, which is known to cleave aryl methyl ethers. However, when one equivalent of boron tribromide was treated with the TBS-protected aldehyde **22**, one of the TBS groups was removed and the methoxy group was left intact. Next, the less reactive boron trichloride was used as the demethylating reagent however this again removed one of the TBS protecting groups rather than cleaving the methyl ether. Other demethylating conditions were tried including; diphenyl phosphide with *n*-butyllithium, titanium isopropoxide with tetra-*n*-butylammonium bromide, and titanium isopropoxide with boron trichloride; unfortunately these all failed to cause demethylation.



Reagents and conditions: i) BBr₃, DCM; ii) BCl₃, DCM; iii) Ph₂P, *n*BuLi, THF; iv) Ti(O*i*Pr)₄, DCM, Bu₄NBr; v) Ti(O*i*Pr)₄, BBr₃, DCM.

Scheme 95: Attempts at demethylation of TBS-protected benzaldehyde **22**.

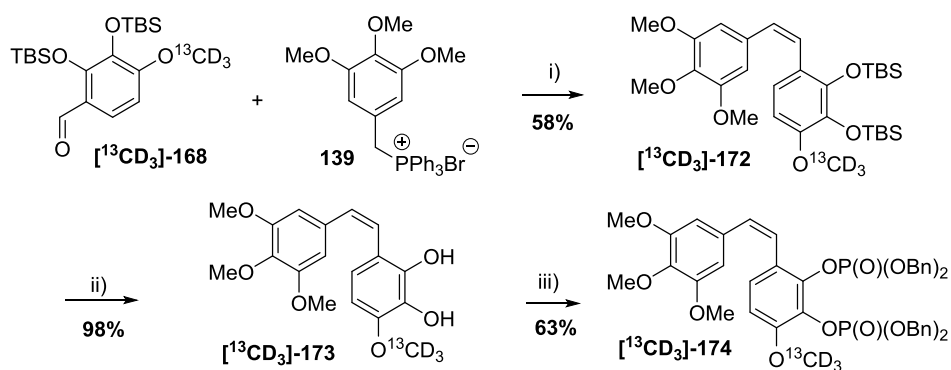
As both the selective methylation route and the demethylation route were unsuccessful it was decided to first do a non-selective tri-methylation on the 2,3,4-trihydroxybenzaldehyde **169** followed by selective demethylation (Scheme 96). First 2,3,4-trihydroxybenzaldehyde **169** was treated with caesium carbonate and [¹³C,^d3]-methyl iodide in dry acetone which gave the trimethylated-labelled aldehyde [¹³CD₃]-**170** in a 74% yield after flash column chromatography. Demethylation of the methylated aldehyde [¹³CD₃]-**170** with boron trichloride selectively removed the methoxide groups from the *ortho* and *meta* positions in a 96% yield after recrystallisation. The resulting free phenols in aldehyde [¹³CD₃]-**171** were protected using *tert*-butyldimethylsilyl chloride with triethylamine and 4-dimethylaminopyridine, after purification by flash column chromatography the TBS-protected aldehyde [¹³CD₃]-**168** was formed in an 80% yield.



Reagents and conditions: i) Cs₂CO₃, dry acetone, ¹³CD₃I, reflux, 3 h; ii) BCl₃, DCM, 16 h; iii) NEt₃, DMAP, DMF, TBSO, 16 h.

Scheme 96: Synthesis of [¹³CD₃]-labelled aldehyde [¹³CD₃]-**172**.

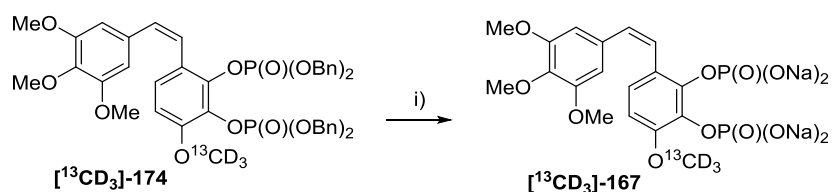
Now with the ¹³CD₃-labelled aldehyde [¹³CD₃]-**168** (which was synthesised by Dr. Ed Cochrane) in hand, this aldehyde [¹³CD₃]-**168** was then employed in the Wittig strategy which was already established for the synthesis for ¹³C-CA1P [¹³C]-**153**. The aldehyde [¹³CD₃]-**168** was treated with the ylide formed *in situ* by the reaction of 3,4,5-trimethoxybenzyl phosphonium bromide **139** and *n*-butyllithium and gave the *E* and *Z* isomers in a 85% yield after flash column chromatography (Scheme 97). The *E/Z* mixture was recrystallised with ethanol to reveal pure *Z*-isomer [¹³CD₃]-**172** in a 58% yield. The *Z*-isomer [¹³CD₃]-**172** was then deprotected using tetrabutylammonium fluoride in THF, revealing [¹³CD₃]-CA1 [¹³CD₃]-**173** in a 98% yield after flash column chromatography. [¹³CD₃]-Combretastatin A1 [¹³CD₃]-**173** was then treated with dibenzyl chlorophosphate, which was generated *in situ* from dibenzyl phosphite and carbon tetrachloride, and gave the tetrabenzyl protected phosphate [¹³CD₃]-**174** in a 63% yield after flash column chromatography.



Reagents and conditions: i) a) phosphonium salt **139**, *n*BuLi, THF, -20 °C; b) aldehyde [**¹³CD₃**]-**168**, 2 h; ii) TBAF, THF, 30 min; iii) CCl₄, DIPEA, DMAP, MeCN, -20 °C, 5min then dibenzyl phosphite, 2 h.

Scheme 97: Synthesis of phosphate [**¹³CD₃**]-**174** from protected benzaldehyde **168**.

The protected phosphate [**¹³CD₃**]-**174** was then converted to the tetrasodium salt [**¹³CD₃**]-**167**. Unfortunately over a few days the sample of CA1P [**¹³CD₃**]-**167**, which was left in the fridge and wrapped in foil to exclude light, decomposed. The sample also degraded when it was put immediately on to a HPLC reverse phase column.

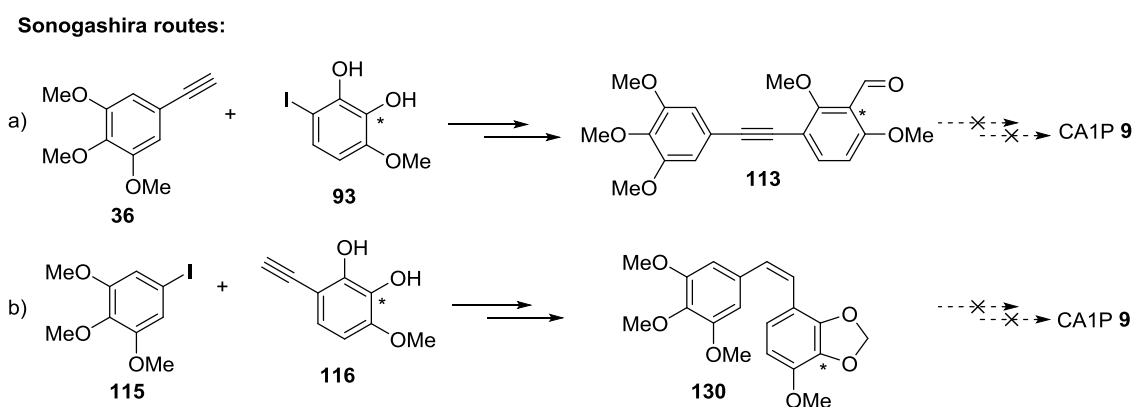


Reagents and conditions: i) MeCN, NaI, TMSCl; iii) NaOMe, MeOH, 6 h.

Scheme 98: Synthesis of [**¹³CD₃**]-labelled CA1P [**¹³CD₃**]-**167**.

3. Conclusions

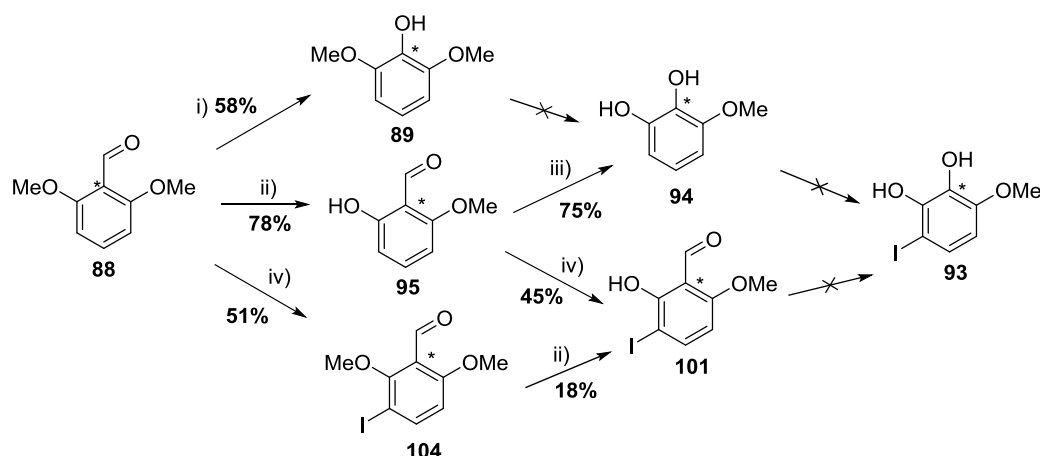
A method had been established for the synthesis of [^{13}C]-labelled combretastatin A1P [^{13}C]-**153**. The method was first carried out using unlabelled ^{12}C -material and then applied using ^{13}C starting material. The site of the ^{13}C -labelled was chosen to be carbon-13 on Ring B as it has a long T_1 time and is on the metabolically active ring. A route was then developed for the synthesis of a 1,2,3-trioxygenated species with the regioselective placement of the ^{13}C label (Scheme 102). This was achieved by developing the work initially done by Botting and co-workers.⁸⁴ The addition of a methylcuprate to the acid chloride **79**, resulted in a ketone **84** which was then cyclised and aromatised. To insert an oxygen on to the 2-position of 2,6-dimethoxybenzene **87** a formylation first occurred, which underwent a Baeyer-Villiger oxidation to reveal a 1,2,3-trioxygenation species with the correct placement of the ^{13}C label.



Scheme 99: The two Sonogashira strategies for the synthesis of CA1P 9.

There have been a number of syntheses in the literature of combretastatins. The selective reduction of a diarylalkyne, synthesised *via* a Sonogashira reaction, was initially chosen as it was believed to be the most economic route with a high *Z*-selectivity. One of the components of the Sonogashira reaction needed to be derived from the 1,2,3-trioxygenated aromatic species which will contain the ^{13}C label. Unfortunately the synthesis of the iodoarene **93** for the Sonogashira reaction proved problematic (Scheme 100). Since the iodoarene **93** was unable to be isolated, the Sonogashira reaction between other iodoarenes was investigated. The Sonogashira reactions using iodoarenes **101** and **110** resulted in unexpected benzofuran formation and deprotection respectively.

However the Sonogashira reaction using iodoarene **104** which formed diarylalkyne **113** was successful but unfortunately the subsequent deprotection was non-selective.

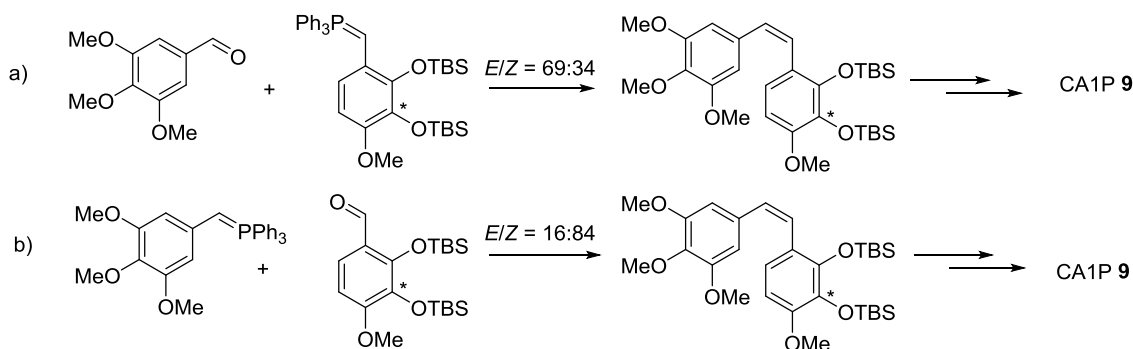


Reagents and conditions: i) a) *m*CPBA, DCM; b) KOH; ii) BCl₃, DCM, rt; iii) a) H₂O₂, MeOH, H₂SO₄, rt; b) NaOH; iv) In(OTf)₃, NIS, MeCN, rt.

Scheme 100: Attempts at synthesising iodoarene **93** from benzaldehyde **88**.

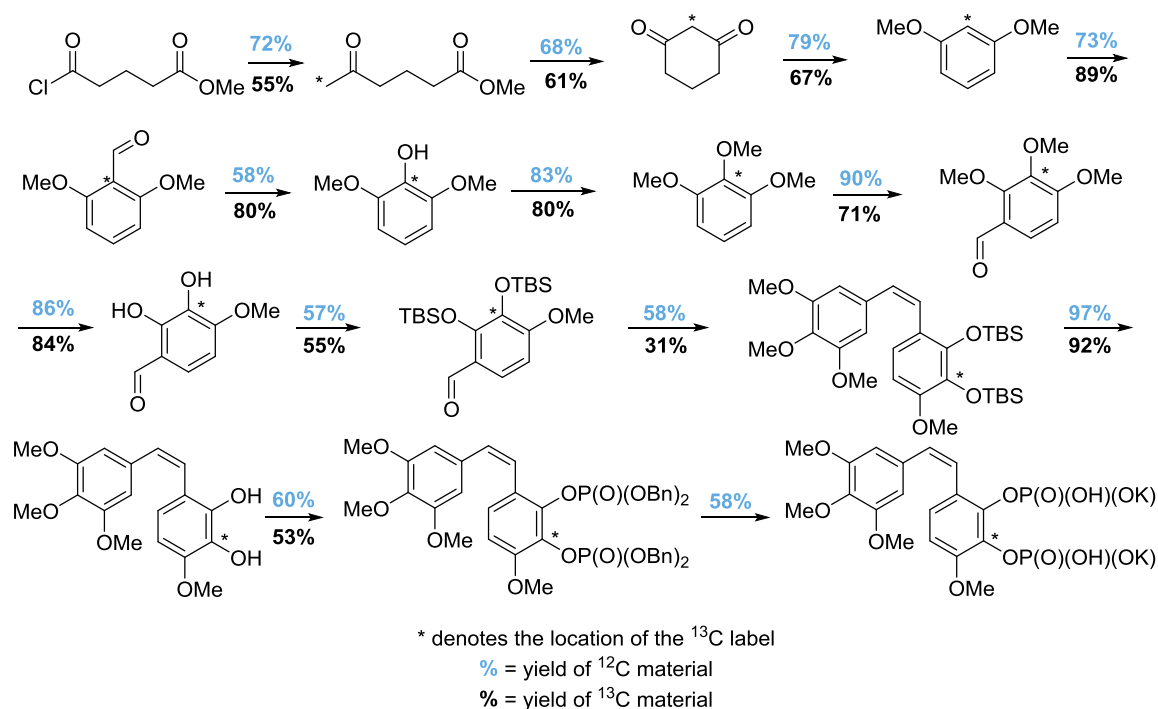
As this route (Scheme 99a) proved not to be viable, the components of the Sonogashira were reversed so that the alkyne was located on ring B, which contains the site for the ¹³C label. The Sonogashira reaction was successful when using a methylene acetal protecting group of the 1,2-diol. Unfortunately initial attempts at the selective reduction of the resulting diarylalkyne **129** using H-cube® conditions was low-yielding as well as over-reduction being observed. Also attempts at the methylene acetal deprotection were unsuccessful. Excluding these last two steps (selective reduction and deprotection) this Sonogashira route (Scheme 99b) already involved 12 steps with an overall yield of 1.9%. As the subsequent two steps showed initial difficulties, a different strategy was investigated (Scheme 101).

Wittig routes:



Scheme 101: The two Wittig strategies for the synthesis of CA1P **9**

Two different Wittig routes were successfully employed for the synthesis of CA1P **9** (Scheme 101). The first has the site of the ^{13}C label on the phosphonium ylide component of the reaction whereas the second had it on the aldehyde component. The *E/Z* selectivity of the two Wittig reactions differed dramatically; one being *E*-selective and the other being *Z*-selective. Therefore the second Wittig reaction was the chosen route. Even though the *E:Z* ratio was in favour of the desired *Z*-isomer **24**, separating the isomers was problematic on a small scale. Attempts were made to separate them through different chromatographic and recrystallisation techniques but on a small scale the *Z*-isomer was isolated in only a 31% yield. Attempts were also made to convert the unwanted *E*-isomer **23** into the *Z*-isomer **24** through photoisomerisation or *via* a *trans*-oxide **148** but this again was fruitless. Nevertheless, the route continued and the *Z*-isomer **24** was deprotected to reveal CA1 **8**. Attempts were made to convert CA1 **8** to CA1P **9**, unfortunately the tetrasodium salt **9** was found to be unstable, degrading over a short period of time and unable to be purified by HPLC. Therefore the CA1 **8** was converted to the dipotassium CA1P salt **151**.



Scheme 102: Summary of route for the synthesis of [^{13}C]-labelled CA1P [^{13}C]-**153** and unlabelled CA1P **151**.

With a route for the synthesis of CA1P **151** in hand using ^{12}C material, the synthesis was repeated using ^{13}C starting material. The yields for the ^{13}C route broadly matched that of the ^{12}C route apart that of the Wittig reaction. This was due to different scales of the reactions, the ^{13}C route was performed on a smaller scale, hence the difficulties in the recrystallisation step. Also due to the small scale of the final debenzoylation step, the ^{13}C -CA1P [^{13}C]-**153** was unable to be isolated cleanly.

Future work includes the isolation then hyperpolarisation of [^{13}C]-CA1P [^{13}C]-**153** (Figure 21). This can be achieved using a HyperSense™ DNP polariser. After finding the optimal conditions for maximum polarisation, the hyperpolarised sample can be transferred to an NMR spectrometer using the dissolution process. An enhanced ^{13}C signal is expected to be seen when compared with a non-hyperpolarised sample.

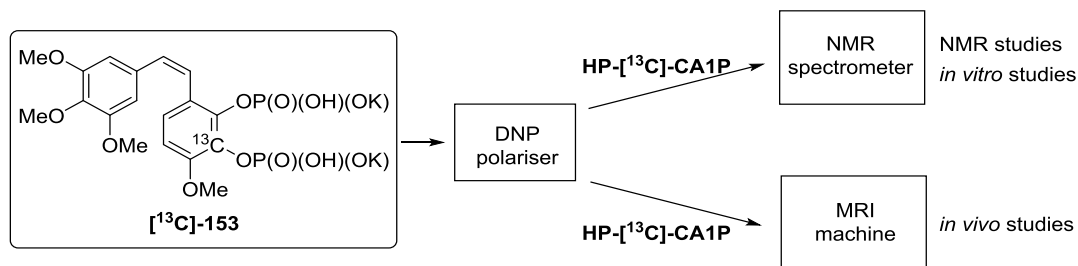


Figure 21: Future hyperpolarisation and MR experiments on [^{13}C]-CA1P [^{13}C]-**153**.

This can be taken on to *in vitro* or *in vivo* studies (Figure 21). Hopefully, not only will a hyperpolarised signal of [^{13}C]-CA1P [^{13}C]-**153** be observed but also that of its metabolites particularly the *ortho*-quinone [^{13}C]-**175**. The concentration and location of these reactive metabolites can be determined giving valuable information on the metabolism and reactivity of CA1 **8**.

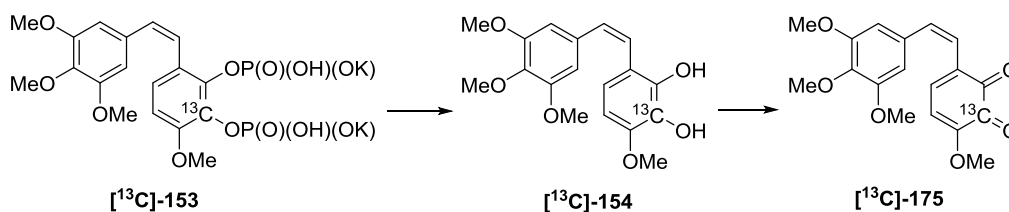


Figure 22: Some of the expected metabolites of [^{13}C]-CA1P [^{13}C]-**153** to be seen in *in vitro* and/or *in vivo* studies.

Chapter 4: Experimental

4.1. General

All reactions were performed under nitrogen at room temperature unless otherwise stated, using glassware, flame-dried under vacuum, with magnetic stirring and if required heated using Dry Syn® blocks. All reagents were obtained from commercial suppliers and were used without further purification unless otherwise stated. 4Å Molecular sieves were activated by flame-drying under vacuum. Reactions that were performed at 0 °C used water/ice baths, -78 °C used acetone/dry ice bath, -10 °C used salt/ice/water bath and -20 °C used acetone/dry ice bath.

Tetrahydrofuran, dichloromethane, acetonitrile, dimethylformamide and diethyl ether solvents used in reactions were obtained from the departmental Grubbs solvent system and stored under a positive pressure of nitrogen. All other solvents were obtained from commercial suppliers and used without prior drying unless otherwise stated. Commercially available Grignard reagents were titrated against a standard solution of (-)-menthol using phenanthroline as an indicator. *n*-Butyllithium was titrated before use against a standard solution of benzophenone tosylhydrazone.

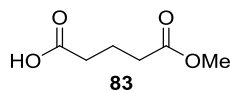
Analytical thin layer chromatography (TLC) was carried out utilising aluminium backed Merck TLC plates (silica gel 60 F254) and visualised with UV light (254 nm) followed by either a potassium permanganate, phosphomolybdic acid or dinitrophenylhydrazine dip then exposed to heat. AgNO₃-coated TLC plates were made by dipping TLC plates in aqueous AgNO₃ solution (12.5% w/v), wrapping in aluminium foil and put in the oven (120 °C) for 2 hours. Flash column chromatography was performed using Flurochem Limited Silica Gel 40 – 60 μ 60Å as the stationary phase. The eluent for each purification is noted within the individual experimental procedures.

All ¹H, ¹³C and ³¹P spectra were obtained using either a Bruker AC 250 or AC 400 spectrometer. ¹³C NMR spectra were recorded using the JMOD method. The NMR solvent used is noted within the individual experimental procedures. Chemical shifts are expressed in parts per million (ppm). All *J*-values (*J*, *J*_{C-H}, *J*_{C-C}, *J*_{C-P}) measured in hertz.

High resolution mass spectrometry was performed by the University of Sheffield Mass Spec department on either a MicroMass LCT spectrometer operating in electrospray mode or a MicroMass Prospec system operating in electron impact mode. Infrared spectra were recorded on a Perkin-Elmer 1600 FT-IR using a Universal diamond ATR top-plate. Melting points were measured on a Gallenkamp melting point apparatus and are uncorrected. Elemental analysis was performed on a Perkin-Elmer 2400 CHNS/O Series II apparatus. The pH was measured using pH indicator paper except for the synthesis of CA1P **151** or [^{13}C]-**153** where a pH meter was used which had previously been calibrated with calibration buffers. UV radiation was achieved through exposure of sample to a UV lamp used for visualising TLC plates equipped with both short-wave (254 nm) and long-wave (366 nm) lamps. H-cube[®] reactions were conducted using a ThalesNano H-cube[®] continuous-flow hydrogenation reactor with a pre-packed CatCart[®] cartridge.

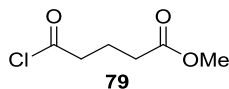
4.2 Synthesis towards [^{12}C]-CA1P

Pentandioic acid monomethyl ester (**83**)⁸⁶



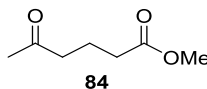
Glutaric anhydride (20.0 g, 175 mmol) and methanol (7.1 mL, 175 mmol) was added to chloroform (200 mL) and heated at reflux for 5 hours. The solvent was removed under reduced pressure affording the title compound **83** (25.6 g, 100%) as a colourless oil which was used without further purification; ^1H NMR (400 MHz, CDCl_3) δ 1.99 (pent., 2H, J 7.3, $\text{CH}_2\text{CH}_2\text{CH}_2$), 2.43 (t, 2H, J 7.3, COCH_2), 2.47 (t, 2H, J 7.3, COCH_2), 3.68 (s, 3H, OCH_3); ^{13}C NMR (101 MHz, CDCl_3) δ 19.8 (CH_2), 32.9 ($2 \times \text{CH}_2$), 51.7 (OCH_3), 173.3 ($\text{C}=\text{O}$), 178.5 ($\text{C}=\text{O}$). ^1H NMR data in accordance with the literature.¹²⁸

Glutaric acid monomethyl ester chloride (79)⁸⁶



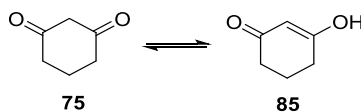
Thionyl chloride (25.6 mL, 350 mmol) was added dropwise to neat pentandioic acid monomethyl ester **83** (25.6 g, 175 mmol) and left for 10 minutes. Purification by distillation at atmospheric pressure (110 °C) gave the title compound **79** (25.3 g, 88%) as a colourless oil; ¹H NMR (400 MHz, CDCl₃) δ 2.02 (pent, 2H, *J* 7.2, CH₂CH₂CH₂), 2.41 (t, 2H, *J* 7.1, CH₂CO₂CH₃), 3.01 (t, 2H, *J* 7.1, CH₂COCl), 3.69 (s, 3H, OCH₃); ¹³C NMR (101 MHz, CDCl₃) δ 20.2 (CH₂), 32.1 (CH₂), 46.0 (CH₂), 51.8 (OCH₃), 172.8 (C=O), 173.4 (C=O). ¹H NMR data in accordance with the literature.⁸⁶

Methyl 5-oxohexanoate (**84**)



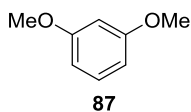
Magnesium turnings (0.18 g, 7.40 mmol) were dry stirred for 5 min and diethyl ether (8 mL) was then added. Methyl iodide (0.44 mL, 7.05 mmol) was added drop-wise to the reaction mixture at a rate to induce heating at a steady reflux. The resulting methyl magnesium iodide was added dropwise to a solution of freshly recrystallised copper bromide dimethyl sulphide complex (1.52 g, 7.40 mmol) in diethyl ether (12 mL) at -10 °C and left for 30 minutes. The resulting solution was added dropwise to a solution of glutaric acid monomethyl ester chloride **79** (0.97 mL, 7.0 mmol) in diethyl ether (12 mL) and the reaction mixture and left stirring overnight. The reaction was quenched with a saturated solution of ammonium chloride (20 mL). The precipitate was filtered under suction and the filtrate was extracted with diethyl ether (3 × 15 mL). The combined organic layers were washed with brine (50 mL) and dried over magnesium sulfate. After filtration and removal of the solvent under reduced pressure, the crude material was purified by flash column chromatography on silica gel using an eluent of 20% ethyl acetate: 40 – 60 °C petroleum ether to afford the title compound **84** as pale yellow oil (0.696 g, 69%); ¹H NMR (400 MHz, CDCl₃) δ 1.89 (pent, 2H, *J* 7.2, CH₂CH₂CH₂), 2.14 (s, 3H, CH₃), 2.35 (t, 2H, *J* 7.2, CH₂), 2.51 (t, 2H, *J* 7.2, CH₂), 3.67 (s, 3H, OCH₃); ¹³C NMR (101 MHz, CDCl₃) δ 18.8 (CH₂), 29.9 (CH₃), 33.0 (CH₂), 42.5 (CH₂), 51.6 (OCH₃), 173.6 (CH₃C=O), 208.0 [(CH₃O)C=O]. NMR data in accordance with the literature.¹²⁹

1,3-Cyclohexanedione (**75**)⁸³



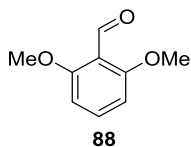
Potassium *tert*-butoxide (1.40 g, 12.5 mmol) was dissolved in tetrahydrofuran (15 mL) to which methyl 5-oxohexanoate **84** (0.36 g, 2.5 mmol) was added. The reaction was heated at reflux for 7 hours. The organic solvents were removed under reduced pressure and the residue was dissolved in water (15 mL) and acidified to pH 1 with concentrated hydrochloric acid. The aqueous layer was extracted with ethyl acetate (10 × 15 mL) and the combined organic layers dried over magnesium sulfate. After filtration the solvent was removed under reduced pressure and yielded the crude product which was purified by flash column chromatography on silica gel using an eluent of 100% ethyl acetate giving the title compound **75** (0.967 g, 68%) as a yellow solid; mp 106 – 108 °C; ¹H NMR (400 MHz, CDCl₃) δ 1.97 [pent, 2H, *J* 6.4, CH₂ (keto) and CH₂ (enol)], 2.38 [t, 2.5H, *J* 6.4, 2 × CH₂ (keto) and CH₂ (enol)], 2.59 [t, 1.5H, *J* 6.4, CH₂ (enol)], 3.41 [s, 0.5H, CH₂ (keto)], 5.48 [s, 0.75H, =CH (enol)], 10.51 [s, 0.75H, OH (enol)]; ¹³C NMR (101 MHz, CDCl₃) δ 18.2 [CH₂ (keto)], 21.0 [CH₂ (enol)], 32.3 [CH₂ (enol)], 39.8 [CH₂ (enol) and 2 × CH₂ (keto)], 58.4 [CH₂ (keto)], 104.2 [=CH (enol)], 192.8 [C=O and C-O (enol)], 204.4 [C=O (keto)]. NMR data was in accordance with the literature.¹³⁰

1,3-Dimethoxybenzene (**87**)⁸⁹



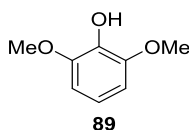
1,3-Cyclohexandione **75** (5.00 g, 44.6 mmol) was dissolved in methanol (100 mL). Iodine (22.6 g, 89.2 mmol) was added and the reaction mixture was heated at reflux for 1.5 hours. The methanol was removed under reduced pressure and the residue dissolved in dichloromethane (60 mL). The organic layer was washed with sodium hydrogen carbonate (20 mL), 10% aq. sodium thiosulfate (20 mL) and 5% sodium hydroxide (20 mL). The combined aqueous layers were then extracted with dichloromethane (3 × 30 mL) and the resulting combined organic layers were dried over magnesium sulfate, filtered and the solvent was removed under reduced pressure. Purification of the crude material by flash column chromatography using an eluent of 5% ethyl acetate: 40 – 60 °C petroleum ether afforded the title compound **87** as a colourless oil (4.88 g, 79%); ¹H NMR (400 MHz, CDCl₃) δ 3.80 (s, 6H, 2 × OCH₃), 6.48 (t, 1H, *J* 2.4, Ar*H*), 6.52 (dd, 2H, *J* 8.2, 2.4, 2 × Ar*H*), 7.19 (t, *J* 8.2, Ar*H*); ¹³C NMR (101 MHz, CDCl₃) δ 55.3 (2 × OCH₃), 100.5 (ArCH), 106.2 (2 × ArCH), 129.9 (ArCH), 160.9 (2 × ArC). NMR data in accordance with the literature.¹³¹

2,6-Dimethoxybenzaldehyde (**88**)⁹²



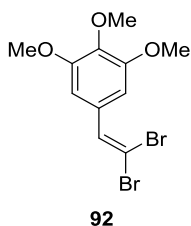
1,3-Dimethoxybenzene **87** (4.94 g, 35.7 mmol) and *N,N,N',N'*-tetramethylethylenediamine (6.0 mL, 40.3 mmol) was dissolved in tetrahydrofuran (60 mL). The reaction mixture was cooled to 0 °C and *n*-butyllithium (21 mL, 2.0 M in hexanes, 42.8 mmol) was added and the reaction left stirring for 30 minutes. Dimethylformamide (4.1 mL, 53.5 mmol) was added dropwise and the solution stirred for a further 1 hour. The reaction was quenched with hydrochloric acid (1 M, 40 mL) whilst maintaining the temperature below 25 °C. The organic solvent was removed under reduced pressure. The aqueous layer was then extracted with diethyl ether (3 × 20 mL) and the combined organic layers were washed with brine (40 mL), dried over magnesium sulfate, filtered and the solvent removed under reduced pressure. The crude material was purified by flash column chromatography on silica using an eluent of 20% ethyl acetate: 40 – 60 °C petroleum ether to afford the title compound **88** (4.34 g, 73%) as a white solid; mp 95 – 98 °C (lit.¹³² 96 – 98 °C); ¹H NMR (400 MHz, CDCl₃) δ 3.89 (s, 6H, 2 × OCH₃), 6.57 (d, *J* 8.4, 2H, 2 × ArH), 7.44 (t, *J* 8.4, 1H, ArH), 10.50 (s, 1H, CHO); ¹³C NMR (101 MHz, CDCl₃) δ 56.1 (2 × OCH₃), 103.9 (2 × ArCH), 114.3 (ArC), 135.9 (ArCH), 162.2 (2 × ArC), 189.5 (CHO). All NMR data was in accordance with the literature.¹³³

2,6-Dimethoxyphenol (**89**)



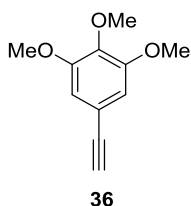
2,6-Dimethoxy-benzaldehyde **88** (0.250 g, 1.50 mmol) was dissolved in dichloromethane (5 mL) and cooled to 0 °C. *meta*-Chloroperbenzoic acid ($\leq 77\%$, 0.674 g, 3.00 mmol) was added dropwise as a dichloromethane solution (3 mL) and the reaction was left at 0 °C for 3 hours. The organic layer was washed with sodium sulfite solution (5 mL) then sodium hydrogen carbonate (5 mL). The combined aqueous layers were extracted with dichloromethane (3×10 mL) then the combined organic layers were washed with brine (20 mL), dried over magnesium sulfate, filtered, and the solvent removed under reduced pressure. The resulting formate ester was dissolved in methanol (5 mL) and cooled to 0 °C. Potassium hydroxide (0.295 g, 5.23 mmol) in methanol (10 mL) was added dropwise and the reaction left for 45 minutes. Water (10 mL) was added and the solution was acidified to pH 2 using concentrated hydrochloric acid. The aqueous layer was extracted with diethyl ether (6×10 mL) and the combined organic layers were washed with brine, dried over magnesium sulfate, filtered and the solvent removed under reduced pressure. The crude reaction material was purified by flash column chromatography using an eluent of 20% ethyl acetate: 40 – 60 °C petroleum ether and afforded the title compound **89** as a white solid (0.135 g, 58%); mp 52 – 53 °C (lit.¹³⁴ 52 – 56 °C); ¹H NMR (400 MHz, CDCl₃) δ 3.89 (s, 6H, 2 \times OCH₃), 5.52 (s, 1H OH), 6.59 (d, *J* 8.4, 2H, 2 \times ArH), 6.80 – 6.83 (m, 1H, ArH); ¹³C NMR (101 MHz, CDCl₃) δ 56.3 (2 \times OCH₃), 104.9 (2 \times ArCH), 119.1 (ArCH), 134.8 (COH), 147.3 (2 \times COCH₃). All data in accordance with the literature.¹³⁴

1,1-Dibromo-2-(3,4,5-trimethoxyphenyl)-ethylene (**92**)¹³⁵



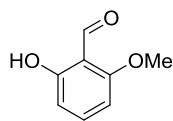
Carbon tetrabromide (2.54 g, 7.65 mmol) was dissolved in dichloromethane (20 mL) and cooled to 0 °C. Triphenylphosphine (4.01 g, 15.3 mmol) was added at 0 °C and the reaction was stirred for 15 minutes. 3,4,5-Trimethoxybenzaldehyde (1.00 g, 5.10 mmol) was dissolved in dichloromethane (6 mL) and added dropwise to the reaction vessel. The reaction was stirred at 0 °C for 5 minutes, then the solvent was removed under reduced pressure to yield a brown oil. Purification of the crude material by flash column chromatography on silica gel using an eluent of 15% ethyl acetate: 40 – 60 °C petroleum ether afforded the title compound **92** as a pale yellow oil (1.71 g, 95%). ¹H NMR (400 MHz; CDCl₃) δ 3.86 (s, 6H, 2 × OCH₃), 3.87 (s, 3H, OCH₃), 6.80 (s, 2H, 2 × ArH), 7.41 (s, 1 H, CH); ¹³C NMR (101 MHz, CDCl₃) δ 56.2 (2 × OCH₃), 60.9 (OCH₃), 88.8 (Br₂C=), 105.8 (2 × ArCH), 130.6 (ArC), 136.6 (=CH), 138.3 (ArCOCH₃), 153.0 (2 × ArCOCH₃); ¹H NMR data in accordance with the literature apart from peaks at 3.86 and 3.87 were reported as a single peak rather than two peaks.¹³⁵

5-Ethynyl-1,2,3-trimethoxybenzene (**36**)¹³⁶



1,1-Dibromo-2-(3,4,5-trimethoxyphenyl)-ethylene **92** (1.25 g, 3.54 mmol) was dissolved in tetrahydrofuran (25 mL) and cooled to $-78\text{ }^{\circ}\text{C}$. *n*-Butyllithium (6.5 mL, 1.9 M in hexanes, 12.4 mmol) was added dropwise to the reaction mixture and left stirring at $-78\text{ }^{\circ}\text{C}$ for 30 minutes. Ammonium chloride (25 mL) was added to the reaction mixture and warmed to room temperature. The organic layer was removed under reduced pressure and the aqueous layer was extracted with ethyl acetate ($3 \times 20\text{ mL}$). The combined organic layers were washed with brine (50 mL), dried over magnesium sulfate, filtered and the solvent removed under reduced pressure. Purification of the crude material by flash column chromatography on silica gel using an eluent of 10% ethyl acetate: 40 – 60 $^{\circ}\text{C}$ petroleum ether afforded the title compound **36** as a white crystalline solid (0.551 g, 81%); mp $56 - 59\text{ }^{\circ}\text{C}$; ^1H NMR (400 MHz, CDCl_3) δ 3.03 (s, 1H, $\equiv\text{CH}$), 3.85 (s, 9H, $3 \times \text{OCH}_3$), 6.73 (s, 2H, $2 \times \text{ArH}$); ^{13}C NMR (101 MHz, CDCl_3) δ 56.2 ($2 \times \text{OCH}_3$), 61.0 (OCH_3), 76.2 ($\text{C}\equiv\text{CH}$), 83.7 (ArC), 103.3 ($\text{C}\equiv\text{CH}$), 109.4 ($2 \times \text{ArCH}$), 117.0 ($2 \times \text{ArC}$), 153.1 (ArC). NMR data in accordance with the literature apart from in the ^1H spectrum where only one singlet (9H) was observed at 3.85 whereas two singlets at 3.83 (6H) and 3.84 (3H) and were reported. Also in the ^{13}C spectrum, only one singlet was observed at 56.2 whereas two singlets were reported at 56.1 and 56.2. In the literature the ^1H and ^{13}C spectra were recorded at 500 and 125 MHz respectively.¹³⁶

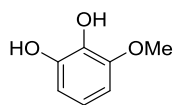
2-Hydroxy-6-methoxybenzaldehyde (**95**)



95

2,6-Dimethoxybenzaldehyde **88** (4.34 g, 26.1 mmol) was dissolved in dichloromethane (50 mL). Boron trichloride (26 mL, 1 M, 26.1 mmol) was added dropwise to the reaction mixture. The reaction was left stirring at room temperature for 18 hours which was then quenched with the dropwise addition of sat. sodium bicarbonate solution (50 mL) at 0 °C. The mixture was then acidified to pH 2 concentrated hydrochloric acid. The aqueous layer was separated and extracted with dichloromethane (3 × 40 mL). The combined organic layers were washed with brine (100 mL), dried over magnesium sulphate, filtered and the solvent removed under reduced pressure. The crude material was purified by flash column chromatography on silica gel using an eluent of 5% ethyl acetate: 40 – 60 °C petroleum ether and afforded the title compound **95** as colourless crystals (3.09 g, 78%); mp 75 – 76 °C (lit.¹³⁷ 73.5 – 74.5 °C); ¹H NMR (400 MHz, CDCl₃) δ 3.90 (s, 3H, OCH₃), 6.37 (d, 1H, *J* 8.4, ArH), 6.52 (d, 1H, *J* 8.4, ArH), 7.41 (t, 1H, *J* 8.4, ArH), 10.34 (s, 1H, HC=O), 11.98 (s, 1H, OH); ¹³C NMR (101 MHz, CDCl₃) δ 55.8 (OCH₃), 101.0 (ArCH), 109.9 (ArCH), 110.8 (ArC), 138.4 (ArCH), 162.2 (ArC), 163.7 (ArC), 194.4 (HC=O); NMR data was in accordance with the literature apart from in the ¹H NMR spectrum the peak observed at 7.41 (app. t, 1H, *J* 8.4) was reported as 7.41 (dd, 1H, *J* 8.5, 8.0).¹³⁷

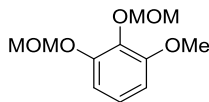
3-Methoxy-1,2-benzenediol (**94**)



94

2-Hydroxy-6-methoxybenzaldehyde **95** (3.09 g, 20.3 mmol) was dissolved in methanol (50 mL). Hydrogen peroxide (2.7 mL, 30%, 26.4 mmol) was added dropwise followed by a few drops of conc. sulfuric acid. The reaction mixture was stirred at room temperature for 18 hours then quenched with 1M sodium hydroxide (30 mL). The mixture was acidified to pH 2 with concentrated hydrochloric acid and the aqueous layer separated then extracted with ethyl acetate (10 × 20 mL). The combined organic layers were washed with brine (50 mL), dried over magnesium sulfate, filtered then the solvent removed under reduced pressure. The crude sample was purified by flash column chromatography on silica gel using an eluent of 25% ethyl acetate: 40 – 60 °C petroleum ether to afford the title compound **94** (2.59 g, 75%) as a colourless oil. ¹H NMR (400 MHz, CDCl₃) δ 3.87 (s, 3H, OCH₃), 5.68 (s, 1H, OH), 5.71 (s, 1H, OH), 6.49 (dd, 1H, *J* 8.3, 1.2, ArH), 6.63 (dd, 1H, *J* 8.3, 1.2, ArH), 6.77 (t, 1H, *J* 8.3, ArH); ¹³C NMR (101 MHz, CDCl₃) δ 56.2 (OCH₃), 103.3 (ArCH), 109.0 (ArCH), 119.9 (ArCH), 132.6 (ArC), 144.1 (ArC), 147.2 (ArC); ¹H NMR data in accordance with the literature apart from the aromatic region was reported as multiplet at 6.77 – 6.49 ppm (m, 3H) and the phenols were reported as a singlet (at 5.30) rather than 2 singlets.¹³⁸

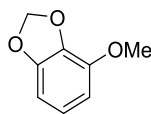
5,6-Bis(methoxymethoxy)phenol (**96**)¹³⁹



96

Sodium hydride (0.180 g, 4.50 mmol, 60% dispersed in mineral oil) was suspended in tetrahydrofuran (10 mL) and cooled to 0 °C. 3-Methoxy-1,2-benzenediol **94** (0.420g, 3.00 mmol) was added dropwise (in 2 mL tetrahydrofuran) and the reaction stirred at 0 °C for 15 minutes, warmed to room temperature and left stirring for 30 minutes. The reaction was then cooled to 0 °C and chloromethyl methyl ether (0.41 mL, 5.39 mmol) was added dropwise and the reaction stirred for 3 hours. The reaction mixture was washed saturated ammonium chloride solution (3 × 10 mL) and the combined aqueous layers extracted with ethyl acetate (3 × 10 mL). The combined organic layers were washed with brine (30 mL), dried over magnesium sulfate, filtered and the solvent removed under reduced pressure. The crude reaction material was purified by flash column chromatography on silica with an eluent of 10% ethyl acetate: 40 – 60 °C petroleum ether to afford the title compound **96** (0.424 g, 62%) as a white solid; mp 29 – 30 °C; ν_{\max} (ATR)/ cm^{-1} 2904 (C-H), 1599 (aromatic); Found: C, 57.89; H 7.06; $\text{C}_{11}\text{H}_{16}\text{O}_5$ requires C, 57.89; H, 7.07; ^1H NMR (400 MHz, CDCl_3) δ 3.50 (s, 3H, OCH_3), 3.62 (s, 3H, OCH_3), 3.85 (s, 3H, OCH_3), 5.14 (s, 2H, CH_2), 5.20 (s, 2H, CH_2), 6.63 (dd, J 8.4, 1.2, 1H, ArH), 6.79 (dd, J 8.4, 1.2, 1H, ArH), 6.99 (t, J 8.4, 1H, ArH); ^{13}C NMR (101 MHz, CDCl_3) δ 56.0 (OCH_3), 56.2 (OCH_3), 57.1 (OCH_3), 95.3 (CH_2), 98.4 (CH_2), 106.3 (ArCH), 109.3 (ArCH), 124.1 (ArCH), 135.6 (ArC), 151.1 (ArC), 153.6 (ArC); m/z (ESI) 246 (38%, $\text{M}+\text{H}_2\text{O}$), 229.1073 (59, MH^+). $\text{C}_{11}\text{H}_{16}\text{O}_5$ requires 229.1071, 197 (95), 165 (100).

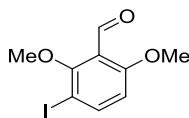
4-Hydroxy-1,3-benzodioxole (**100**)¹⁴⁰



100

3-Methoxy-1,2-benzenediol **94** (0.250 g, 1.78 mmol) was dissolved in dimethylformamide (4 mL) under nitrogen. Caesium fluoride (0.813 g, 5.35 mmol) was added followed by dibromomethane (0.13 mL, 1.78 mmol) and the reaction mixture heated to 120 – 130 °C with stirring and left for 6 hours. Water (10 mL) was added and the aqueous layer extracted with diethyl ether (3 × 10 mL). The combined organic layers were washed with water (20 mL), sodium hydroxide (1M, 20 mL) and brine (20 mL), then dried over magnesium sulfate and filtered. The solvent was removed under reduced pressure and afforded the title compound **100** (0.209 g, 77%) as a yellow solid which was used without further purification; mp 41 – 42 °C (lit.¹⁴¹ 39 – 41 °C); ¹H NMR (400 MHz, CDCl₃) δ 3.89 (s, 3H, OCH₃), 5.94 (s, 2H, OCH₂O), 6.51 – 6.53 (m, 2H, 2 × ArH), 6.77 (t, *J* 8.2, 1H, ArH); ¹³C NMR (101 MHz, CDCl₃) δ 56.5 (OCH₃), 101.2 (CH₂), 102.4 (ArCH), 107.5 (ArCH), 122.1 (ArCH), 135.2 (ArC), 144.1 (ArC), 148.8 (ArC). ¹H NMR data in accordance with the literature apart from the triplet at 6.77 was reported in the literature as a multiplet.¹⁴¹

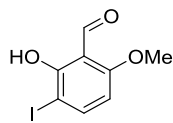
3-Iodo-2,6-dimethoxybenzaldehyde (**104**)



104

2,6-Dimethoxybenzaldehyde **88** (3.11 g, 18.7 mmol) was dissolved in acetonitrile (60 mL). Indium(III) trifluoromethanesulfonate (2.11 g, 3.74 mmol) and *N*-iodosuccinimide (9.29 g, 41.2 mmol) were added to the reaction mixture and left stirring at room temperature for 18 hours. Water (60 mL) was added and the aqueous layer separated then extracted with ethyl acetate (3 × 40 mL). The combined organic layers were washed with brine (80 mL), dried over magnesium sulfate, filtered and the solvent removed under reduced pressure. The crude compound was purified by flash column chromatography on silica gel using an eluent of 10% ethyl acetate: 40 – 60 °C petroleum ether affording the title compound **104** (2.79 g, 51%) as a light orange solid; mp 45 – 47 °C; ν_{\max} (ATR)/ cm^{-1} 1682 (HC=O), 1461 (aromatic); Found: C, 37.31; H 3.15; $\text{C}_9\text{H}_9\text{IO}_3$ requires C, 37.01; H, 3.11; ^1H NMR (400 MHz, CDCl_3) δ 3.87 (s, 3H, OCH_3), 3.91 (s, 3H, OCH_3), 6.61 (d, 1H, J 8.9 ArH), 7.89 (d, 1H, J 8.9, ArH), 10.36 (s, 1H, CHO); ^{13}C NMR (101 MHz, CDCl_3) δ 56.4 (OCH_3), 63.0 (OCH_3), 82.5 (ArCI), 109.9 (ArCH), 120.0 (ArCCHO), 144.6 (ArCH), 161.5 (ArCO), 162.5 (ArCO), 188.6 (HC=O); m/z (ES^+) 292.9686 (100%, M^+ . $\text{C}_9\text{H}_{10}\text{O}_3\text{I}$ requires 292.9675).

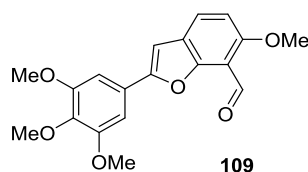
3-Iodo-2-hydroxy-6-methoxybenzaldehyde (**101**)



101

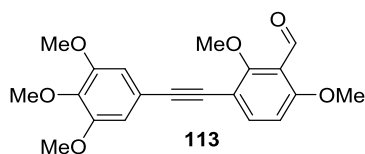
3-Iodo-2,6-dimethoxybenzaldehyde **104** (0.50 g, 1.71 mmol) was dissolved in dichloromethane (25 mL) at room temperature. Boron trichloride (1.70 mL, 1M, 1.71 mmol) was added dropwise to the reaction mixture and left stirring for 12 hours. The solution was acidified to pH 2 with concentrated hydrochloric acid. Water (25 mL) was added and the aqueous layer was extracted with dichloromethane (3×20 mL). The combined organic layers were washed with brine (60 mL), dried over magnesium sulfate, filtered and the solvent removed under reduced pressure to afford the crude product. Purification by flash column chromatography on silica gel using an eluent of 5% ethyl acetate: 40 – 60 °C petroleum ether afforded the title compound **101** (0.094 g, 18%) as a yellow solid; mp 115 – 118 °C; ν_{\max} (ATR)/ cm^{-1} 3208 (OH), 2989 (C-H), 1650 (HC=O), 1602 (aromatics), 1560 (aromatics), 1276 (C-OH); Found: C, 34.52; H 2.30; $\text{C}_8\text{H}_7\text{O}_3$ requires C, 34.56; H, 2.54; ^1H NMR (400 MHz, CDCl_3) δ 3.89 (s, 3H, OCH_3), 6.27 (d, 1H, J 8.8, ArH), 7.82 (d, 1H, J 8.8, ArH), 10.18 (s, 1H, $\text{HC}=\text{O}$), 12.80 (s, 1H, ArOH); ^{13}C NMR (101 MHz, CDCl_3) δ 56.1 (OCH_3), 74.2 (ArCl), 103.8 (ArCH), 110.94 (ArCCHO), 146.9 (ArCH), 162.0 (ArCO), 162.8 (ArCO), 193.7 ($\text{HC}=\text{O}$); m/z (ES^-) 276.9362 (100%, M^- . $\text{C}_8\text{H}_6\text{O}_3\text{I}$ requires 276.9367).

2-(1,2,3-Trimethoxyphenyl)-6-methoxy-7-benzofurancarboxaldehyde (**109**)



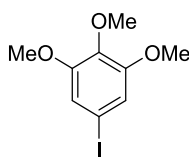
Copper iodide (3.4 mg, 0.018 mmol) and tetrakis(triphenylphosphine)palladium(0) (83.1 mg, 0.071 mmol) were dissolved in piperidine (2 mL). 3-Iodo-2-hydroxy-6-methoxybenzaldehyde **101** (100 mg, 0.36 mmol) was added followed by the dropwise addition of 5-ethynyl-1,2,3-trimethoxybenzene **36** (69 mg, 0.36 mmol, in 0.5 mL piperidine). The reaction was left stirred for 16 hours then saturated ammonium chloride solution (5 mL) was added. The solution was acidified to pH 2 with concentrated hydrochloric acid. The aqueous layer was extracted with diethyl ether (3 × 10 mL). The combined organic layers were washed with brine (20 mL), dried over magnesium sulfate, filtered and the solvent removed under reduced pressure. The crude material was purified by flash column chromatography on silica with an eluent of 30% ethyl acetate: 40 – 60 °C petroleum ether to afford the title compound **109** (55 mg, 45%) as a light yellow solid; ν_{max} (ATR)/ cm^{-1} 2517 [H-C(O)], 1571 (HC=O), 1502 (aromatic); ^1H NMR (400 MHz, CDCl_3) δ 3.92 (s, 3H, OCH_3), 3.99 (s, 6H, 2 × OCH_3), 4.02 (s, 3H, OCH_3), 6.91 (s, 1H, HC=C-O), 6.95 (d, J 8.7, 1H, ArH), 7.13 (s, 2H, 2 × ArH), 7.73 (d, J 8.7, 1H, ArH), 10.71 (s, 1H, HC=O); ^{13}C NMR (101 MHz, CDCl_3) δ 56.3 (2 × OCH_3), 56.7 (OCH_3), 61.0 (OCH_3), 99.8 (ArCH), 102.2 (2 × ArCH), 107.6 (ArCH), 111.1 (ArC), 124.2 (ArC), 125.5 (ArC), 127.4 (ArCH), 138.8 (ArC), 153.6 (ArC), 153.7 (ArC), 156.8 (ArC), 160.1 (ArC), 187.8 (HC=O); m/z (ESI) 343.1176 (100%, MH^+ . $\text{C}_{19}\text{H}_{18}\text{O}_6$ requires 343.1176).

2,6-Dimethoxy-3-(3,4,5-trimethoxyphenyl-1-ethynyl)-benzaldehyde (**113**)



Copper iodide (5 mg, 0.026 mmol) and tetrakis(triphenylphosphine)palladium(0) (0.120 g, 0.10 mmol) were dissolved in piperidine (1 mL) and acetonitrile (1 mL). 3-Iodo-2,6-dimethoxybenzaldehyde **104** (0.145 g, 0.52 mmol) was added followed by the dropwise addition of 5-ethynyl-1,2,3-trimethoxybenzene **36** (0.100 g, 0.52 mmol) in piperidine (1 mL). The reaction heated to 50 °C was left stirred for 16 hours then saturated ammonium chloride solution (5 mL) was added. The aqueous layer was extracted with diethyl ether (3 × 10 mL). The combined organic layers were washed with brine (30 mL), dried over magnesium sulfate, filtered and the solvent removed under reduced pressure. The crude material was purified by flash column chromatography on silica with an eluent of 30% ethyl acetate: 40 – 60 °C petroleum ether to afford the title compound **113** (0.104 g, 56%) as an orange solid; mp 112 – 113 °C; ν_{\max} (ATR)/ cm^{-1} 2932 (C-H), 1686, 1575 (HC=O), 1507 (aromatic); ^1H NMR (400 MHz, CDCl_3) δ 3.87 (s, 3H, OCH_3), 3.88 (s, 6H, 2 × OCH_3), 3.93 (s, 3H, OCH_3), 6.74 (d, J 9.2, 1H ArH), 6.76 (s, 2H, 2 × ArH), 7.65 (d, J 9.2, 1H, ArH), 10.45 (s, 1H, HC=O); ^{13}C NMR (101 MHz, CDCl_3) δ 56.2 (2 × OCH_3), 56.3 (OCH_3), 61.0 (OCH_3), 62.6 (OCH_3), 83.5 ($\text{C}\equiv\text{C}$), 93.5 ($\text{C}\equiv\text{C}$), 107.3 (ArCH), 108.6 (2 × ArCH), 110.2 (ArC), 118.2 (2 × ArC), 119.1 (ArC), 139.4 (ArCH), 153.2 (2 × ArCO), 161.4 (ArCO), 164.1 (ArCO), 189.1 (HC=O); m/z (ESI) 357.1334 (100%, MH^+ . $\text{C}_{20}\text{H}_{20}\text{O}_6$ requires 357.1333).

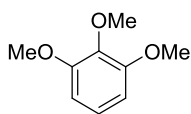
5-Iodo-1,2,3-trimethoxybenzene (**115**)¹⁴²



115

3,4,5-Trimethoxyaniline (1.00 g, 5.46 mmol) was suspended in water (12 mL) and sulfuric acid (conc, 0.8 mL) and cooled to 0 °C. Sodium nitrate (3.77 g, 56.4 mmol) was dissolved in water (6 mL) and added dropwise to the reaction mixture whilst the temperature was maintained at 0 °C. The reaction mixture was then added to a solution of potassium iodide (1.40 g, 8.43 mmol) in water (3 mL) at 50 °C and left for 30 minutes. The reaction was cooled to room temperature, aqueous sodium sulfite (20 mL) was added and the solution was extracted with diethyl ether (3 × 20 mL). The combined organic layers were washed with brine (40 mL), dried over magnesium sulfate, filtered and the solvent removed under reduced pressure which yielded the title compound **115** (1.30 g, 81%) as a yellow solid which was used without further purification; mp 85 – 86 °C (lit.¹⁴³ 83 – 85 °C; ¹H NMR (400 MHz, CDCl₃) δ 3.81 (s, 3H, OCH₃), 3.83 (s, 6H, 2 × OCH₃), 6.88 (s, 2H, 2 × ArH); ¹³C NMR (101 MHz, CDCl₃) δ 56.4 (2 × OCH₃), 60.8 (OCH₃), 86.0 (ArC), 115.1 (2 × ArCH), 138.4 (ArC), 154.0 (2 × ArC). All data in accordance with the literature.¹⁴³

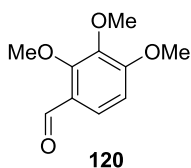
1,2,3-Trimethoxybenzene (**119**)



119

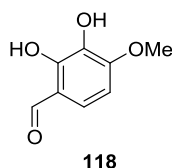
2,6-Dimethoxyphenol **89** (0.53 g, 3.4 mmol) was dissolved in acetone (10 mL) then potassium carbonate (0.71 g, 5.2 mmol) was added and the reaction mixture cooled to 0 °C. 18-Crown-6 (0.1 mL, 0.14 mmol) and iodomethane (0.32 mL, 5.2 mmol) were added at 0 °C and the reaction was allowed to warm to room temperature and stirred overnight. The resulting mixture was poured onto diethyl ether (10 mL), filtered and the filtrate concentrated down under reduced pressure to yield the title compound **119** (0.48 g 83%) as a white solid which was used without further purification; mp 40 – 42 °C (lit.¹⁴⁴ 44 °C); ¹H NMR (400 MHz, CDCl₃) δ 3.85 (s, 3H, OCH₃), 3.86 (s, 6H, 2 × OCH₃), 6.58 (d, *J* 8.3, 2H, 2 × ArH), 6.99 (t, *J* 8.3, 1H, ArH); ¹³C NMR (101 MHz, CDCl₃) 56.1 (2 × OCH₃), 60.8 (OCH₃), 105.4 (2 × ArCH), 123.6 (ArCH), 138.3 (ArC), 153.6 (2 × ArC). All data in accordance with the literature.¹⁴⁴

2,3,4-Trimethoxybenzaldehyde (**120**)¹⁴⁵



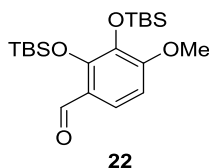
1,2,3-Trimethoxybenzene **119** (6.10 g, 36.2 mmol) was dissolved in dichloromethane (70 mL) and cooled to 0 °C. Titanium (IV) chloride (8.0 mL, 72.5 mmol) was added dropwise followed by dichloromethyl methyl ether (6.60 mL, 72.5 mmol). The reaction mixture was warmed to room temperature and left stirring for 3 hours. Cold water (50 mL) was added to reaction mixture and the aqueous layer extracted with dichloromethane (3 × 50 mL). The combined organic layers were washed with hydrochloric acid (1M, 100 mL), saturated aqueous sodium bicarbonate (100 mL) and brine (100 mL), then dried over magnesium sulfate. After filtration and removal of solvent under reduced pressure the title compound **120** (6.38 g, 90%) was obtained as a white solid which was used without further purification; mp 32 – 33 °C (lit.¹⁴⁶ 30 – 31 °C) ¹H NMR (400 MHz, CDCl₃) δ 3.88 (s, 3H, OCH₃), 3.93 (s, 3H, OCH₃), 4.02 (s, 3H, OCH₃), 6.75 (d, *J* 8.8, 1H, ArH), 7.60 (d, *J* 8.8, 1H, ArH), 10.24 (s, 1H, CHO); ¹³C NMR (101 MHz, CDCl₃) δ 56.2 (OCH₃), 61.0 (OCH₃), 62.3 (OCH₃), 107.4 (ArCH), 123.3 (ArC), 124.2 (ArCH), 141.6 (ArC), 156.9 (ArC), 159.3 (ArC), 188.8 (CHO). All data in accordance with the literature.¹⁴⁶

2,3-Dihydroxy-4-methoxybenzaldehyde (**118**)



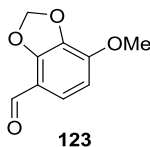
2,3,4-Trimethoxybenzaldehyde **120** (0.25 g, 1.3 mmol) was dissolved in dichloromethane (7 mL) and boron trichloride (1M in dichloromethane, 1.3 mL, 1.3 mmol) was added dropwise. The reaction was left stirring for 2 hours before another equivalent of boron trichloride (1M in dichloromethane, 1.3 mL, 1.3 mmol) was added dropwise and the reaction was left stirring for 24 hours. The reaction was quenched with sat. sodium bicarbonate (10 mL) and acidified to pH 2 using concentrated hydrochloric acid. The aqueous layer was then extracted with dichloromethane (3×10 mL) and the combined organic layers washed with brine (20 mL), dried over magnesium sulfate and filtered. The solvent was removed under reduced pressure, and the crude material recrystallised with ethyl acetate/hexane to afford the title compound **118** (0.19 g, 86%) as a white solid; mp 113 – 114 °C (lit.¹¹¹ 115 – 116 °C); ¹H NMR (400 MHz, CDCl₃) δ 3.98 (s, 3H, OCH₃), 5.53 (s, 1H, OH), 6.61 (d, *J* 8.8, 1H, ArH), 7.14 (d, *J* 8.8, 1H, ArH), 9.74 (s, 1H, CHO), 11.12 (s, 1H, OH); ¹³C NMR (101 MHz, CDCl₃) δ 56.4 (OCH₃), 103.6 (ArCH), 116.1 (ArC), 126.1 (ArCH), 133.0 (ArC), 149.1 (ArC), 153.0 (ArC), 195.3 (CHO). All data in accordance with the literature.¹¹¹

2,3-Di[(*tert*-butyldimethylsilyl)oxy]-4-methoxybenzaldehyde (**22**)¹⁴⁷



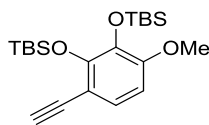
2,3-Dihydroxy-4-methoxybenzaldehyde **118** (2.70 g, 16.1 mmol) was dissolved in dichloromethane (50 mL). Triethylamine (6.7 mL, 48.3 mmol) and DMAP (0.49 g, 4.0 mmol) were added and the mixture was stirred for 10 minutes. *tert*-Butyldimethylsilyl chloride (5.82 g, 38.6 mmol) was added to the reaction mixture in portions and stirred for 12 hours at room temperature. After addition of water (40 mL), the aqueous layer was extracted with dichloromethane (3 × 30 mL) and the combined organic layers were washed with brine (50 mL) and dried over magnesium sulfate. Filtration, followed by the removal of solvent under reduced pressure gave the crude material which was purified by recrystallisation from methanol to afford the title compound **22** (3.64 g, 57%) as pale yellow crystals; mp 72 – 73 °C (lit.¹⁴⁷ 74.5 – 76 °C); ¹H NMR (400 MHz, CDCl₃) δ 0.14 [s, 12H, 2 × OSi(CH₃)₂C(CH₃)₃], 0.99 [s, 9H, OSi(CH₃)₂C(CH₃)₃], 1.04 [s, 9H, OSi(CH₃)₂C(CH₃)₃], 3.84 (s, 3H, OCH₃), 6.62 (d, *J* 8.8, 1H, Ar*H*), 7.48 (d, *J* 8.8, 1H, Ar*H*), 10.22 (s, 1H, CHO); ¹³C NMR (101 MHz, CDCl₃) δ -3.8 [2 × OSi(CH₃)₂C(CH₃)₃], 18.6 [OSi(CH₃)₂C(CH₃)₃], 18.8 [OSi(CH₃)₂C(CH₃)₃], 26.0 [OSi(CH₃)₂C(CH₃)₃], 26.2 [OSi(CH₃)₂C(CH₃)₃], 55.2 (OCH₃), 105.4 (ArCH), 121.4 (ArCH), 123.4 (ArC), 136.8 (ArC), 151.0 (ArC), 157.6 (ArC), 189.3 (CHO). All data in accordance with literature.¹⁴⁷

4-Methoxy-2,3-(methylenedioxy)-benzaldehyde (**123**)¹³⁸



2,3-Dihydroxy-4-methoxybenzaldehyde **118** (0.387 g, 2.3 mmol) and caesium fluoride (1.05 g, 6.9 mmol) were dissolved in dimethylformamide (10 mL). Dibromomethane (0.16 mL, 2.3 mmol) was added dropwise and the reaction heated to 125 °C under nitrogen for 6 hours. Water (10 mL) was added aqueous layer was extracted with diethyl ether (3 × 10 mL). The combined organic layers were washed with sodium hydroxide (1 M, 20 mL) and brine (20 mL) then filtered through Celite[®], dried over magnesium sulfate, filtered and the solvent removed under reduced pressure to afford the title compound **123** (0.267 g, 65%) that was used without further purification; mp 84 – 86 °C (lit.¹⁴¹ 82 – 85 °C); ¹H NMR (400 MHz, CDCl₃) δ 3.98 (s, 3H, OCH₃), 6.13 (s, 2H, CH₂), 6.62 (d, *J* 9.0, 1H, ArH), 7.30 (d, *J* 9.0, 1H, ArH), 9.98 (s, 1H, CHO); ¹³C NMR (101 MHz, CDCl₃) δ 56.8 (OCH₃), 103.0 (CH₂), 107.9 (ArCH), 114.5 (ArC), 123.8 (ArCH), 135.7 (ArC), 148.4 (ArC), 150.3 (ArC), 187.1 (HC=O); *m/z* (ES⁺) 181.0498 (100%, MH⁺. C₉H₉O₄ requires 181.0501). ¹H NMR data in accordance with the literature.¹⁴¹

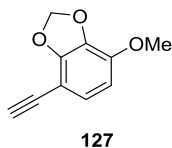
1-Ethynyl-2,3-di[(*tert*-butyldimethylsilyl)oxy]-4-methoxybenzene (**125**)



125

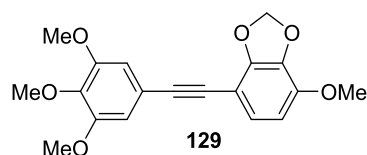
Carbon tetrabromide (0.418 g, 1.26 mmol), triphenylphosphine (0.661 g, 2.52 mmol) and triethylamine (0.18 mL, 1.26 mmol) were dissolved in dichloromethane (3 mL) and stirred under nitrogen for 1 hour at room temperature. The reaction mixture was cooled to 0 °C and 2,3-di[(*tert*-butyldimethylsilyl)oxy]-4-methoxybenzaldehyde **22** (0.250 g, 0.63 mmol) was added. The reaction mixture was allowed to warm to room temperature and left stirring for 16 hours. The resulting precipitate was filtered off and the filtrate concentrated down under reduced pressure. The residue was then stirred in petroleum ether (10 mL) for 10 minutes, filtered and the filtrate concentrated down under reduced pressure. The resulting residue was dissolved in tetrahydrofuran (2 mL) and cooled to -78 °C. *n*-Butyllithium (1.3 mL, 1.8 M in hexanes, 2.21 mmol) was added dropwise to the reaction mixture and left stirring at -78 °C for 30 minutes. Ammonium chloride (5 mL) was added to the reaction mixture and warmed to room temperature. The organic layer was removed under reduced pressure and the aqueous layer was extracted with ethyl acetate (3 × 5 mL). The combined organic layers were washed with brine (15 mL), dried over magnesium sulfate, filtered and the solvent removed under reduced pressure. Purification of the crude material by flash column chromatography on silica gel using an eluent of 5% ethyl acetate: 40 – 60 °C petroleum ether afforded the title compound **125** as a colourless oil (0.178 g, 72%); ¹H NMR (400 MHz, CDCl₃) δ 0.11 [s, 6H, OSi(CH₃)₂C(CH₃)₃], 0.20 [s, 6H, OSi(CH₃)₂C(CH₃)₃], 1.00 [s, 9H, OSi(CH₃)₂C(CH₃)₃], 1.05 [s, 9H, OSi(CH₃)₂C(CH₃)₃], 3.09 (s, 1H, ≡CH), 3.77 (s, 3H, OCH₃), 6.46 (d, *J* 8.4, 1H, Ar*H*), 7.02 (d, *J* 8.4, 1H, Ar*H*); ¹³C NMR (101 MHz, CDCl₃) δ -3.9 [OSi(CH₃)₂C(CH₃)₃], -3.4 [OSi(CH₃)₂C(CH₃)₃], 18.5 [OSi(CH₃)₂C(CH₃)₃], 18.7 [OSi(CH₃)₂C(CH₃)₃], 26.1 [OSi(CH₃)₂C(CH₃)₃], 26.3 [OSi(CH₃)₂C(CH₃)₃], 55.0 (OCH₃), 79.7 (C≡C), 82.2 (C≡C), 104.8 (ArCH), 109.1 (ArC), 126.3 (ArCH), 137.0 (ArCO), 149.2 (ArCO), 153.3 (ArCO). NMR data in accordance with the literature.¹⁴⁸

1-Ethynyl-2,3-(methylenedioxy)-4-methoxybenzene (**127**)



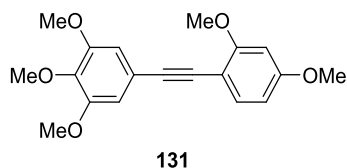
Carbon tetrabromide (0.368 g, 1.11 mmol) and triphenylphosphine (0.582 g, 2.22 mmol) were dissolved in dichloromethane (3 mL) and stirred under nitrogen for 1 hour at room temperature. The reaction mixture was cooled to 0 °C and 4-methoxy-2,3-(methylenedioxy)-benzaldehyde **123** (0.100 g, 0.55 mmol) was added. The reaction mixture was allowed to warm to room temperature and left stirring for 16 hours. The resulting precipitate was filtered off and the filtrate concentrated down under reduced pressure. The residue was then stirred in petroleum ether (10 mL) for 10 minutes, filtered and the filtrate concentrated down under reduced pressure. The resulting residue was dissolved in tetrahydrofuran (2 mL) and cooled to -78 °C. *n*-Butyllithium (1.1 mL, 1.8 M in hexanes, 1.96 mmol) was added dropwise to the reaction mixture and left stirring at -78 °C for 30 minutes. Ammonium chloride (5 mL) was added to the reaction mixture and warmed to room temperature. The organic layer was removed under reduced pressure and the aqueous layer was extracted with ethyl acetate (3 × 5 mL). The combined organic layers were washed with brine (15 mL), dried over magnesium sulfate, filtered and the solvent removed under reduced pressure. Purification of the crude material by flash column chromatography on silica gel using an eluent of 10% ethyl acetate: 40 – 60 °C petroleum ether afforded the title compound **127** (0.177 g, 89%) as a white solid; mp 50 – 52 °C; ν_{\max} (ATR)/ cm^{-1} 3188 (C-H), 2917 (C-H), 2105 ($\equiv\text{CH}$), 1642; ^1H NMR (400 MHz, CDCl_3) δ 3.21 (s, 1H, $\text{C}\equiv\text{CH}$), 3.91 (s, 3H, OCH_3), 6.05 (s, 2H, CH_2), 6.48 (d, J 8.8, 1H, ArH), 6.92 (d, J 8.8, ArH); ^{13}C NMR (101 MHz, CDCl_3) δ 56.6 (OCH_3), 68.2 ($\text{C}\equiv\text{C}$), 80.0 ($\text{C}\equiv\text{C}$), 102.0 (CH_2), 105.3 (ArC), 107.8 (ArCH), 126.1 (ArCH), 132.5 (ArCO), 144.7 (ArCO), 150.3 (ArCO); m/z (ESI) 177.0543 (100%, MH^+ . $\text{C}_{10}\text{H}_8\text{O}_3$ requires 177.0546).

1-[2,3-(methylenedioxy)-4-methoxy-1-ethynyl]-3,4,5-trimethoxybenzene (**129**)



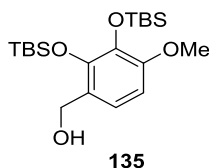
Copper iodide (25 mg, 0.13 mmol) and tetrakis(triphenylphosphine)palladium(0) (0.661 g, 0.50 mmol) was added to a solution of 1-iodo-3,4,5-trimethoxybenzene **115** (0.661 g, 2.50 mmol) in piperidine (5 mL). 1-Ethynyl-2,3-(methylenedioxy)-4-methoxybenzene **127** (0.441 g, 2.50 mmol) in piperidine (2 mL) was added dropwise to the reaction mixture and left stirring for 18 hours. Water (15 mL) was added and the aqueous layer separated and extracted with diethyl ether (3 × 15 mL). The combined organic layers were washed with brine (20 mL), dried over magnesium sulfate, filtered and the solvent removed under reduced pressure. The crude reaction material was purified by flash column chromatography on silica gel using an eluent of 20% ethyl acetate: 40 – 60 °C petroleum ether which gave the title compound **129** (0.265 g, 31%) as a yellow solid; mp 112 – 114 °C; ν_{\max} (ATR)/ cm^{-1} 3005 (C-H), 2159 (C≡C), 1575, 1508 (aromatic); ^1H NMR (400 MHz, CDCl_3) δ 3.86 (s, 3H, OCH_3), 3.86 (s, 6H, 2 × OCH_3), 3.92 (s, 3H, OCH_3), 6.07 (s, 2H, OCH_2O), 6.52 (d, J 8.8, 1H, ArH), 6.76 (s, 2H, 2 × ArH), 6.96 (d, J 8.8, 1H, ArH); ^{13}C NMR (101 MHz, CDCl_3) δ 56.2 (2 × OCH_3), 56.6 (OCH_3), 61.0 (OCH_3), 82.4 (C≡C), 92.2 (C≡C), 98.6 (ArC), 101.9 (CH_2), 107.8 (ArCH), 108.8 (2 × ArCH), 118.2 (ArC), 125.7 (ArCH), 135.0 (ArC), 138.8 (ArC), 144.3 (ArC), 149.4 (ArCO), 153.0 (2 × ArCO); m/z (ES^+) 343.1177 (100%, M^+ . $\text{C}_{19}\text{H}_{19}\text{O}_6$ requires 343.1182).

1-(2,4-Dimethoxyphenyl-1-ethynyl)-3,4,5-trimethoxybenzene (131)



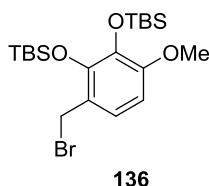
Copper iodide (9 mg, 0.05 mmol) and tetrakis(triphenylphosphine)palladium(0) (0.22 g, 0.19 mmol) was added to a solution of 1-iodo-2,4-dimethoxybenzene (0.25 g, 0.95 mmol) in piperidine (3 mL). 5-Ethynyl-1,2,3-trimethoxybenzene **36** (0.18 g, 0.95 mmol) in piperidine (2 mL) was added dropwise to the reaction mixture and left stirring for 18 hours. Water (10 mL) was added and the aqueous layer separated and extracted with diethyl ether (3×10 mL). The combined organic layers were washed with brine (20 mL), dried over magnesium sulfate, filtered and the solvent removed under reduced pressure. The crude reaction material was purified by flash column chromatography on silica gel using an eluent of 20% ethyl acetate: 40 – 60 °C petroleum ether which gave the title compound **131** (0.212 g, 68%) as a yellow solid; mp 81 – 84 °C; ν_{\max} (ATR)/ cm^{-1} 3014 (C-H), 2935 (C-H), 2840 (C-H), 1571, 1509 (aromatic), 1408 (CH_2); ^1H NMR (400 MHz, CDCl_3) δ 3.84 (s, 3H, OCH_3), 3.86 (s, 3H, OCH_3), 3.87 (s, 6H, $2 \times \text{OCH}_3$), 3.90 (s, 3H, OCH_3), 6.46 – 6.50 (m, 2H, $2 \times \text{ArH}$), 6.78 (s, 2H, $2 \times \text{ArH}$), 7.42 (d, J 8.4, 1H, ArH); ^{13}C NMR (101 MHz, CDCl_3) δ 55.4 (OCH_3), 55.9 (OCH_3), 56.2 ($2 \times \text{OCH}_3$), 60.9 (OCH_3), 84.8 ($\text{C}\equiv\text{C}$), 92.0 ($\text{C}\equiv\text{C}$), 98.5 (ArCH), 105.0 (ArCH), 108.9 ($2 \times \text{ArCH}$), 118.9 ($2 \times \text{ArC}\equiv$), 134.3 (ArCH), 153.0 ($2 \times \text{COCH}_3$), 161.2 (COCH_3), 161.3 ($2 \times \text{COCH}_3$); m/z (ES^+) 329.1382 (100%, MH^+ . $\text{C}_{19}\text{H}_{21}\text{O}_5$ requires 329.1389).

2,3-Di[(*tert*-butyldimethylsilyl)oxy]-4-methoxybenzyl alcohol (**135**)¹⁴⁷



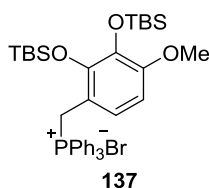
2,3-Di[(*tert*-butyldimethylsilyl)oxy]-4-methoxybenzaldehyde **22** (2.00 g, 5.0 mmol) was dissolved in ethanol (20 mL) and cooled to 0 °C. Sodium borohydride (0.19 g, 5.0 mmol) was added in portions over 5 minutes. The reaction was left stirring at 0 °C for 30 minutes then was quenched with water (20 mL). The organic solvent was removed under reduced pressure and the aqueous phase was extracted with ethyl acetate (3 × 15 mL). The combined organic layers were washed with brine (25 mL), dried over magnesium sulfate and filtered. The solvent was removed under reduced pressure and the crude material was recrystallised from ethanol to afford the title compound **135** (1.99 g, 99%) as off-white solid; mp 73 – 74 °C; ¹H NMR (400 MHz, CDCl₃) δ 0.10 [s, 6H, OSi(CH₃)₂C(CH₃)₃], 0.14 [s, 6H, OSi(CH₃)₂C(CH₃)₃], 0.98 [s, 9H, OSi(CH₃)₂C(CH₃)₃], 1.03 [s, 9H, OSi(CH₃)₂C(CH₃)₃], 1.82 (t, *J* 6.2, 2H, CH₂OH), 3.76 (s, 3H, OCH₃), 4.60 (d, *J* 6.2, 2H, CH₂OH), 6.51 (d, *J* 8.4, 1H, ArH), 6.88 (d, *J* 8.4, 1H, ArH); ¹³C NMR (101 MHz, CDCl₃) δ -3.8 [OSi(CH₃)₂C(CH₃)₃], -3.6 [OSi(CH₃)₂C(CH₃)₃], 18.4 [OSi(CH₃)₂C(CH₃)₃], 18.8 [OSi(CH₃)₂C(CH₃)₃], 26.2 {2 × [OSi(CH₃)₂C(CH₃)₃]}, 54.9 (OCH₃), 61.6 (CH₂OH), 104.9 (ArCH), 120.5 (ArCH), 126.3 (ArC), 136.9 (ArC), 145.3 (ArC), 151.9 (ArC). NMR data in accordance with the literature with the exception for the ¹³C NMR spectrum peak at 26.2 is reported as 2 peaks in the literature (26.16 and 26.15).¹⁴⁷

1-(Bromomethyl)-2,3-bis-[(1,1-dimethylethyl)dimethylsilyl]oxy-4-methoxybenzene (136)¹⁴⁷



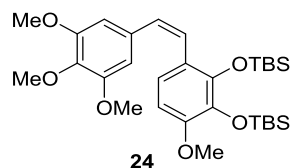
2,3-bis[[1,1-Dimethylethyl)dimethylsilyl]oxy]-4-methoxy-benzenemethanol **135** (1.00 g, 2.51 mmol) was dissolved in dichloromethane (5 mL) and cooled to 0 °C. Phosphorus tribromide (0.24 mL, 2.51 mmol) was added to the reaction mixture and stirred for 6 hours at 0 °C followed by addition of water (10 mL). The aqueous layer was separated and extracted with dichloromethane (3 × 10 mL). The combined organic layers were washed with brine (20 mL), dried over magnesium sulfate and filtered. The solvent was removed under reduced pressure to reveal the title compound **136** (1.07 g, 92%) as a tan-coloured solid which was used without further purification; mp 99 – 100 °C; ¹H NMR (400 MHz, CDCl₃) δ 0.11 [s, 6H, OSi(CH₃)₂C(CH₃)₃], 0.14 [s, 6H, OSi(CH₃)₂C(CH₃)₃], 0.98 [s, 9H, OSi(CH₃)₂C(CH₃)₃], 1.07 [s, 9H, OSi(CH₃)₂C(CH₃)₃], 3.76 (s, 3H, OCH₃), 4.53 (s, 2H, CH₂), 6.50 (d, *J* 8.8, 1H, ArH), 6.94 (d, *J* 8.8, 1H, ArH); ¹³C NMR (101 MHz, CDCl₃) δ -3.8 [OSi(CH₃)₂C(CH₃)₃], -3.6 [OSi(CH₃)₂C(CH₃)₃], 18.6 [OSi(CH₃)₂C(CH₃)₃], 18.8 [OSi(CH₃)₂C(CH₃)₃], 26.2 {2 × [OSi(CH₃)₂C(CH₃)₃]}, 30.8 (CH₂), 55.0 (OCH₃), 105.0 (ArCH), 123.0 (ArC), 123.1 (ArCH), 137.0 (ArC), 145.8 (ArC), 152.7 (ArC). All NMR data in accordance with the literature apart from in the ¹³C NMR spectrum, the peak at 26.2 is reported as 2 peaks in the literature (26.1 and 26.2).¹⁴⁷

[[2,3-bis[[[(1,1-Dimethylethyl)dimethylsilyl]oxy]-4-methoxyphenyl]methyl]triphenyl phosphonium bromide (137)¹⁴⁷



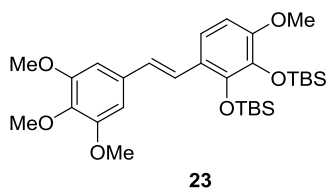
1-(Bromomethyl)-2,3-bis[[[(1,1-dimethylethyl)dimethylsilyl]oxy]-4-methoxy-benzene **136** (0.697 g, 1.51 mmol) was dissolved in dichloromethane (10 mL). Triphenylphosphine (0.436 g, 1.66 mmol) was added to the reaction mixture and was heated at reflux for 24 hours. The solvent was removed under reduced pressure and diethyl ether (20 mL) was added to the resulting residue forming a slurry which was stirred for 1 hour. The solid was filtered and washed with diethyl ether (15 mL) to obtain the title compound **137** (0.918 g, 84%) as a white solid which was used without further purification; mp 190 – 192 °C; ¹H NMR (400 MHz, CDCl₃) δ -0.04 [s, 6H, OSi(CH₃)₂C(CH₃)₃], 0.13 [s, 6H, OSi(CH₃)₂C(CH₃)₃], 0.83 [s, 9H, OSi(CH₃)₂C(CH₃)₃], 0.95 [s, 9H, OSi(CH₃)₂C(CH₃)₃], 3.67 (s, 3H, OCH₃), 5.14 (d, *J*_{H-P} 14.4, 2H, CH₂), 6.31 (d, *J* 8.7, 1H, ArCH), 6.64 (dd, *J*_{H-H} 8.7, *J*_{H-P} 3.0, 1H, ArCH), 7.60 – 7.78 (m, 15H, 3 × C₆H₅); ¹³C NMR (101 MHz, CDCl₃) δ -3.6 [OSi(CH₃)₂C(CH₃)₃], -3.4 [OSi(CH₃)₂C(CH₃)₃], 18.4 [OSi(CH₃)₂C(CH₃)₃], 18.7 [OSi(CH₃)₂C(CH₃)₃], 24.7 (d, *J*_{C-P} 48.8, CH₂), 26.1 [OSi(CH₃)₂C(CH₃)₃], 26.2 [OSi(CH₃)₂C(CH₃)₃], 54.9 (OCH₃), 105.7 (ArCH), 111.3 (d, *J*_{C-P} 8.1, ArCCH₂), 118.1 (ArCOSi), 118.9 (ArCOSi), 123.8 (d, *J*_{C-P} 4.9, ArCH), 130.2 (d, *J*_{C-P} 12.5, 6 × ArCH), 134.1 (d, *J*_{C-P} 9.7, 6 × ArCH), 134.9 (d, *J*_{C-P} 2.7, 3 × ArCH), 137.2 (3 × PCH₂C), 152.5 (d, *J*_{C-P} 3.4, ArCOCH₃); ³¹P NMR (162 MHz, CDCl₃) δ 21.19. ¹H and ³¹P NMR data in accordance with the literature apart from in the ¹H NMR the literature reports the peak at 5.21 as a doublet of doublets (*J*_{H-P} 14, *J*_{H-H} 2.5).¹⁴⁷

2',3'-Bis-[(*tert*-butyldimethylsilyl)-oxy]-(*Z*)-combretastatin A1 (**24**)¹¹



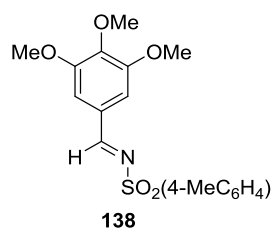
3,4,5-Trimethoxybenzyltriposphonium bromide **139** (1.79 g, 3.4 mmol) was dissolved in tetrahydrofuran (50 mL) at -10 °C. *n*-Butyllithium (1.2 M in hexanes, 2.9 mL, 3.4 mmol) was added dropwise and the reaction left for 30 minutes. The reaction mixture was cooled to -78 °C and 2,3-di[(*tert*-butyldimethylsilyl)oxy]-4-methoxybenzaldehyde **22** (1.36 g, 3.4 mmol) in tetrahydrofuran (7 mL) was added dropwise to the reaction mixture and was left to warm to 0 °C. The reaction was quenched with water (30 mL) and the organic layer removed under reduced pressure. The aqueous layer was extracted with diethyl ether (3 × 20 mL) and the combined organic layers were washed with brine (40 mL), dried over magnesium sulfate, filtered and the solvent removed under reduced pressure. The crude reaction material was purified by flash column chromatography using an eluent of 10% ethyl acetate: 40 – 60 °C petroleum ether and recrystallised from ethanol to yield the *Z*-isomer **24** (1.11 g, 58%) as a white crystals; mp 118 – 120 °C (lit.¹¹ 117 – 118 °C); ¹H NMR (400 MHz, CDCl₃) δ 0.10 [s, 6H, OSi(CH₃)₂C(CH₃)₃], 0.19 [s, 6H, OSi(CH₃)₂C(CH₃)₃], 1.00 [s, 9H, OSi(CH₃)₂C(CH₃)₃], 1.04 [s, 9H, OSi(CH₃)₂C(CH₃)₃], 3.67 (s, 6H, OCH₃), 3.74 (s, 3H, OCH₃), 3.83 (s, 3H, OCH₃), 6.36 (d, *J* 12.2, 1H, HC=C), 6.36 (d, *J* 8.8, 1H, ArH), 6.59 (d, *J* 12.2, 1H, C=CH), 6.62 (s, 2H, 2 × ArH), 6.92 (d, *J* 8.8, 1H, ArH); ¹³C NMR (101 MHz, CDCl₃) δ -3.9 [OSi(CH₃)₂C(CH₃)₃], -3.2 [OSi(CH₃)₂C(CH₃)₃], 18.6 [OSi(CH₃)₂C(CH₃)₃], 18.7 [OSi(CH₃)₂C(CH₃)₃], 26.1 [OSi(CH₃)₂C(CH₃)₃], 26.4 [OSi(CH₃)₂C(CH₃)₃], 55.0 (OCH₃), 55.8 (2 × OCH₃), 60.9 (OCH₃), 104.2 (ArCH), 105.9 (2 × ArCH), 122.2 (ArCH), 123.2 (ArC-C=C), 127.4 (C=), 127.7 (=C), 132.8 (ArC-C=), 136.8 (COSi), 136.9 (COSi), 146.2 (COCH₃), 151.7 (COCH₃), 152.7 (2 × COCH₃). NMR data in accordance with the literature.¹¹

2',3'-Bis-[(*tert*-butyldimethylsilyl)-oxy]-(*E*)-combretastatin A1 (**23**)



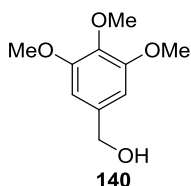
A *E/Z* mixture of 2',3'-Bis-[(*tert*-butyldimethylsilyl)-oxy]-combretastatin A1 **24** (64 mg, 0.11 mmol, *E/Z* ratio: 55:45) was dissolved in hexanes (0.5 mL) then iodine (5.8 mg, 0.023 mmol) was added and the reaction left stirring at room temperature for 16 hours. 5% Aqueous sodium thiosulfate (2 mL) was added and the aqueous layer extracted with diethyl ether (3 × 2 mL). The combined organic layers were washed with brine (5 mL), dried over magnesium sulfate and filtered. The solvent removed under reduced pressure to afford the title compound **23** (64 mg, 100%) as a white solid which required no further purification; mp 138 – 139 °C (lit.¹¹ 139 – 140 °C); ¹H NMR (400 MHz, CDCl₃) δ 0.12 [s, 6H, OSi(CH₃)₂C(CH₃)₃], 0.14 [s, 6H, OSi(CH₃)₂C(CH₃)₃], 1.00 [s, 9H, OSi(CH₃)₂C(CH₃)₃], 1.09 [s, 9H, OSi(CH₃)₂C(CH₃)₃], 3.79 (s, 3H, OCH₃), 3.86 (s, 3H, OCH₃), 3.88 (s, 6H, OCH₃), 6.56 (d, *J* 8.8, 1H, ArH), 6.72 (s, 2H, 2 × ArH), 6.81 (d, *J* 16.4, 1H, HC=C), 7.20 (d, *J* 8.8, 1H, ArH), 7.31 (d, *J* 16.4, 1H, C=CH); ¹³C NMR (101 MHz, CDCl₃) δ -3.8 [OSi(CH₃)₂C(CH₃)₃], -3.5 [OSi(CH₃)₂C(CH₃)₃], 18.7 [OSi(CH₃)₂C(CH₃)₃], 18.8 [OSi(CH₃)₂C(CH₃)₃], 26.1 [OSi(CH₃)₂C(CH₃)₃], 26.5 [OSi(CH₃)₂C(CH₃)₃], 55.0 (OCH₃), 56.0 (2 × OCH₃), 60.9 (OCH₃), 103.3 (=CH), 105.3 (=CH), 117.4 (2 × ArCH), 123.8 (ArC), 124.2 (ArCH), 126.1 (ArCH), 133.8 (ArC), 137.0 (COSi), 137.5 (COSi), 145.6 (COCH₃), 151.9 (COCH₃), 153.4 (2 × COCH₃). ¹H NMR data in accordance with the literature.¹¹

***N*-(3,4,5-Trimethoxybenzylidene)-*p*-toluenesulfonamide (138)**¹⁴⁹



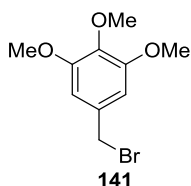
2,3,4-Trimethoxybenzaldehyde (0.50 g, 2.6 mmol), *p*-toluenesulfonamide (0.44 g, 2.6 mmol) and tetraethoxysilane (0.6 mL, 2.68 mmol) was heated to 120 °C for 5 hours then cooled to room temperature. The crude compound was recrystallised from ethyl acetate and petroleum ether to afford the title compound **138** (0.58 g, 65%) as a yellow solid; mp 139 – 141 °C; ¹H NMR (400 MHz, CDCl₃) δ 2.44 (s, 3H, ArCH₃), 3.89 (s, 6H, 2 × OCH₃), 3.93 (s, 3H, OCH₃), 7.16 (s, 2H, 2 × ArH), 7.35 (d, *J* 8.0, 2H, 2 × ArH), 7.88 (d, *J* 8.0, 2H, 2 × ArH), 8.91 (s, 1H, HC=N); ¹³C NMR (101 MHz, CDCl₃) δ 21.7 (ArCH₃), 56.4 (2 × OCH₃), 61.1 (OCH₃), 108.5 (2 × ArCH), 127.4 (ArC), 128.1 (2 × ArCH), 129.8 (2 × ArCH), 135.3 (ArC), 144.2 (ArC), 144.5 (ArC), 153.5 (2 × ArC), 169.8 (HC=N); *m/z* (ESI) 350.1055 (100%, MH⁺. C₁₇H₂₀NO₅S requires 350.1057). ¹H NMR data in accordance with the literature.¹⁴⁹

3,4,5-Trimethoxybenzenemethanol (**140**)



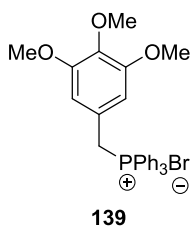
3,4,5-Trimethoxybenzaldehyde (5.00 g, 25.5 mmol) was dissolved in ethanol (100 mL) and cooled to 0°C. Sodium borohydride (0.964 g, 25.5 mmol) was added in portions and the reaction left stirring for 30 minutes. The reaction was quenched with water (100 mL) and the organic solvent removed under reduced pressure. The remaining aqueous layer was extracted with ethyl acetate (3 × 50 mL). The organic layers were combined and washed with brine (100 mL), dried over magnesium sulfate, filtered and the solvent removed under reduced pressure to afford the title compound **140** (4.89 g, 97%) as a colourless oil which was used without further purification; ¹H NMR (400 MHz, CDCl₃) δ 3.64 (s, 6H, 2 × OCH₃), 3.65 (s, 3H, OCH₃), 3.88 (s, 1H, OH), 4.41 (s, 2H, CH₂), 6.41 (s, 2H, 2 × ArH); ¹³C NMR (101 MHz, CDCl₃) δ 56.1 (2 × OCH₃), 60.9 (OCH₃), 65.4 (CH₂), 103.8 (2 × ArCH), 136.7 (ArC), 137.2 (ArC), 153.3 (2 × ArC); All data in accordance with the literature.¹⁵⁰

5-(Bromomethyl)-1,2,3-trimethoxybenzene (**141**)¹⁵¹



3,4,5-Trimethoxybenzenemethanol **140** (4.89 g, 24.7 mmol) was dissolved in dichloromethane (50 mL) and cooled to 0 °C. Phosphorus tribromide (2.3 mL, 24.7 mmol) was added dropwise and the reaction left to stir at 0 °C for 6 hours. Water (50 mL) was added to the reaction mixture and then extracted with dichloromethane (3 × 30 mL). The combined organic layers were washed with brine (50 mL), dried over magnesium sulfate, filtered and the solvent removed under reduced pressure. The crude material was recrystallised from 40 – 60 °C petroleum ether to afford the title compound **141** (4.67 g, 72%) as a white solid; mp 74 – 75 °C (lit.¹⁵² 74 – 75 °C); ¹H NMR (400 MHz, CDCl₃) δ 3.83 (s, 3H, OCH₃), 3.86 (s, 6H, 2 × OCH₃), 4.46 (s, 2H, CH₂), 6.61 (s, 2H, 2 × ArH); ¹³C NMR (101 MHz, CDCl₃) δ 34.3 (CH₂), 56.1 (2 × OCH₃), 60.9 (OCH₃), 106.1 (2 × ArCH), 133.2 (ArC), 138.1 (ArC), 153.3 (2 × ArC). All data in accordance with the literature.¹⁵¹

Triphenyl[(3,4,5-trimethoxyphenyl)methyl]phosphonium bromide (**139**)¹⁵³



5-(Bromomethyl)-1,2,3-trimethoxybenzene **141** (0.40 g, 1.5 mmol) was dissolved in tetrahydrofuran (4.5 mL), triphenylphosphine (0.52 g, 1.9 mmol) was added, and the mixture was heated at reflux for 6 hours. The resulting white solid was filtered and washed with diethyl ether (10 mL) and hexanes (10 mL) to give the title compound **139** (0.64 g, 79%) as a white solid; mp 219 – 220 °C (lit.¹⁵⁴ 222 – 223 °C); ¹H NMR (400 MHz, CDCl₃) δ 3.49 (s, 6H, 2 × OCH₃), 3.74 (s, 3H, OCH₃), 5.40 (d, *J*_{H-P} 14.0, 2H, CH₂), 6.48 (d, *J* 2.4, 2H, 2 × ArH), 7.57 – 7.62 (m, 6H, 6 × ArH); 7.71 – 7.77 (m, 9H, 9 × ArH); ¹³C NMR (101 MHz, CDCl₃) δ 30.8 (d, *J*_{C-P} 46.7, CH₂), 56.2 (2 × OCH₃), 60.8 (d, *J*_{C-P} 2.2, OCH₃), 108.9 (d, *J*_{C-P} 5.7, 2 × ArCH), 117.9 (d, *J*_{C-P} 86.0, 3 × ArCP), 122.5 (d, *J*_{C-P} 9.0, CCH₂P), 130.0 (d, *J*_{C-P} 12.6, 6 × ArCH), 134.7 (d, *J*_{C-P} 9.8, 6 × ArCH), 134.8 (d, *J*_{C-P} 2.8, 3 × ArCH), 137.6 (d, *J*_{C-P} 4.8, COCH₃), 153.0 (d, *J*_{C-P} 3.6, 2 × COCH₃); ³¹P NMR (162 MHz, CDCl₃) 23.3. All NMR data in accordance with the literature apart from in the ¹³C NMR spectrum the doublets at 60.8, 137.6 and 153.0 were reported as singlets in the literature.^{154,155}

Dimethyldioxirane (DMDO) (147)¹⁵⁶



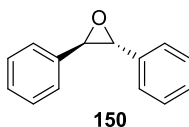
147

A 1 L two-necked round bottom flask was equipped with a U-tube and connected to a 100 mL receiving flask which was also connected to a cold finger condenser filled with dry ice/acetone. The reaction flask was cooled to 0 °C and the receiving flask cooled to -78 °C. The reaction flask was charged with sodium bicarbonate (24 g, 0.29 mol), water (100 mL) and acetone (80 mL, 1.1 mol) and the resulting suspension stirred vigorously through magnetic stirring. Oxone ® (50 g, 0.16 mol) was added to the reaction mixture in five portions at 3 minute intervals. A 125 mbar vacuum was applied 3 minutes after the last addition. The ice/water bath was removed from the reaction vessel and reaction left with vigorous stirring for 80 minutes. The distilled DMDO solution (approx. 40 mL) was collected, dried over potassium carbonate, filtered, and then stored under argon at -20 °C.

Titration of DMDO solution

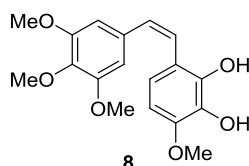
The DMDO solution (0.5 mL) was added to a solution of water (5 mL), potassium iodide (20 mg) and a few drops of acetic acid. The resulting iodine solution was titrated against aq. sodium thiosulfate (0.1 M).

trans-Stilbene oxide (**150**)¹²⁴



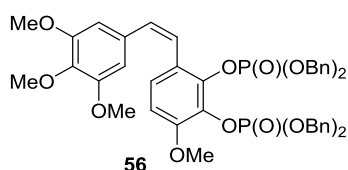
trans-Stilbene (0.100 g, 0.55 mmol) was dissolved in acetone (1 mL) and a solution of DMDO in acetone (0.06 M, 9.2 mL, 0.55 mmol) was added at room temperature. The reaction was left stirring for 18 hours after which the solvent was removed under reduced pressure. The resulting residue was re-dissolved in dichloromethane (2 mL) then dried over magnesium sulfate, filtered and the solvent removed under reduced pressure which yielded the title compound **150** (0.106 g, 98%) as a white solid which required no further purification; mp 67 – 68 °C (lit.¹²⁴ 69 – 70 °C); ¹H NMR (400 MHz, CDCl₃) δ 3.89 (s, 2H, 2 × CH), 7.35 – 7.42 (m, 10H, 10 × ArCH); ¹³C NMR (101 MHz, CDCl₃) δ 62.8 (2 × CH), 125.6 (4 × ArCH), 128.4 (2 × ArCH), 128.6 (4 × ArCH), 137.2 (2 × ArC). All data in accordance with the literature.¹²⁴

(Z)-1-[3',4',5'-Trimethoxyphenyl]-2-[2'',3''-dihydroxy-4''-methoxyphenyl]ethene
(CA1) (**8**)¹¹



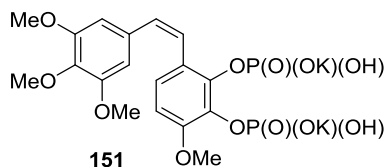
2',3'-Bis-[(*tert*-butyldimethylsilyl)-oxy]-(*Z*)-combretastatin A1 **24** (0.150 g, 0.27 mmol) was dissolved in tetrahydrofuran (1 mL). Tetrabutylammonium fluoride (1M in tetrahydrofuran, 1.1 mL, 1.1 mmol). The mixture was left stirring for 30 minutes after which hydrochloric acid (1M, 5 mL) was added the mixture extracted with ethyl acetate (3 × 5 mL). The combined organic layers were washed with brine (10 mL), dried over magnesium sulfate, filtered and the solvent removed under reduced pressure. The crude material was purified by flash column chromatography on silica with an eluent of 50% ethyl acetate: 40 – 60 °C petroleum ether to reveal the title compound **8** (0.088 g, 97%) as an off-white solid; mp 117 – 118 °C (lit.¹¹ 113 – 115 °C); ¹H NMR (400 MHz, CDCl₃) δ 3.66 (s, 6H, 2 × OCH₃), 3.82 (s, 3H, OCH₃), 3.85 (s, 3H, OCH₃), 5.43 (s, 2H, 2 × OH), 6.38 (d, *J* 8.5, 1H, Ar*H*), 6.52 (s, 2H, 2 × Ar*H*), 6.53 (d, *J* 12.0, 1H, HC=CH), 6.59 (d, *J* 12.0, 1H, HC=CH), 6.76 (d, *J* 8.5, 1H, Ar*H*); ¹³C NMR (101 MHz, CDCl₃) δ 55.9 (2 × OCH₃), 56.2 (OCH₃), 60.9 (OCH₃), 102.9 (ArCH), 105.9 (2 × ArCH), 117.8 (ArC), 120.4 (ArCH), 124.1 (C=C), 130.3 (C=C), 132.5 (ArC), 132.6 (ArC), 137.2 (ArC), 141.6 (ArC), 146.3 (COCH₃), 152.8 (2 × COCH₃). All data in accordance with the literature.¹¹

(Z)-1-(3',4',5'-Trimethoxyphenyl)-2-(2'',3''-di-([bis-(benzyl)oxy]phosphoryloxy)-4''-methoxyphenyl)ethene (**56**)¹²⁶



(Z)-1-[3',4',5'-Trimethoxyphenyl]-2-[2'',3''-dihydroxy-4''-methoxyphenyl]ethene **8** (0.104 g, 0.31 mmol) was dissolved in acetonitrile (1.5 mL) and cooled to -20 °C. Carbon tetrachloride (0.6 mL, 6.26 mmol) was added followed by the addition of *N,N*-diisopropylethylamine (0.09 mL, 0.50 mmol) and 4-dimethylaminopyridine (7.6 mg, 0.06 mmol). The reaction was stirred for 5 minutes then dibenzyl phosphite (0.36 mL, 1.31 mmol) was added and the reaction warmed to 0 °C over 2 hours. Monopotassium phosphate (5 mL, 0.5 M) was added and the aqueous layer extracted with ethyl acetate (3 × 5 mL). The organic layers were combined and washed with brine (10 mL), dried over magnesium sulfate, filtered and the solvent removed under reduced pressure. The crude reaction material was purified by flash column chromatography on silica with an eluent of 50% ethyl acetate: 40 – 60 °C petroleum ether and afforded the title compound **56** (0.158 g, 60%) as a light brown oil; ¹H NMR (400 MHz, CDCl₃) δ 3.64 (s, 6H, 2 × OCH₃), 3.79 (s, 3H, OCH₃), 3.82 (s, 3H, OCH₃), 5.09 (d, *J* 2.8, 2H, CH₂), 5.11 (d, *J* 2.0, 2H, CH₂), 5.19 (d, *J* 7.2, 4H, 2 × CH₂), 6.48 (s, 2H, 2 × ArH), 6.53 (d, *J* 12.0, 1H, HC=C), 6.66 (d, *J* 12.0, 1H, C=CH), 6.69 (d, *J* 9.0, 1H, ArH), 7.03 (d, *J* 9.0, 1H, ArH), 7.24 – 7.31 (m, 10H, 2 × C₆H₅); ¹³C NMR (101 MHz, CDCl₃) δ 55.9 (2 × OCH₃), 56.4 (OCH₃), 60.4 (OCH₃), 69.7 [OP(O)(OCH₂Ph)], 69.8 [OP(O)(OCH₂Ph)], 69.9 [OP(O)(OCH₂Ph)], 70.0 [OP(O)(OCH₂Ph)], 106.3 (2 × ArCH), 109.4 (ArCH), 124.3 (ArCH), 124.6 (=C-C), 126.9 (=C), 127.8 (4 × OCH₂ArCH), 127.9 (4 × OCH₂ArCH), 128.3 (2 × OCH₂ArCH), 128.4 (2 × OCH₂ArCH), 128.4 (8 × OCH₂ArCH), 131.6 (C=), 132.1 (C-C=), 135.6 (2 × OCH₂C), 135.7 (2 × OCH₂C), 135.9 (ArCO), 136.0 (ArCO), 137.7 (ArCO), 151.6 (ArCO), 152.9 (2 × ArCO); ³¹P NMR (162 MHz, CDCl₃) δ -5.56 (d, *J*_{P-P} 1.7), -5.43 (d, *J*_{P-P} 1.7). All data in accordance with the literature apart from in the ¹H NMR data in the literature they reported the 4 × CH₂ peaks as multiplet and the peaks in the ³¹P NMR were reported as singlets.¹⁴⁷

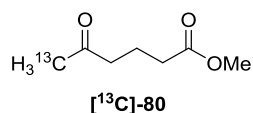
(Z)-1-[3',4',5'-Trimethoxyphenyl]-2-[2'',3''-di[(monopotassium)phosphate]-4''-methoxy phenyl]ethene (151)¹⁴⁷



(Z)-1-[3',4',5'-Trimethoxyphenyl]-2-[2'',3''-di[[bis[(benzyl)oxy]]phosphoryl]oxy]-4''-methoxyphenyl]ethene **56** (0.200 g, 0.234 mmol) was dissolved in acetonitrile (6 mL) and cooled to -10 °C. Trimethylsilyl bromide (0.15 mL, 1.17 mmol) was added dropwise and the reaction left to stir at -10 °C for 1.5 hours. The solvent was then removed under reduced pressure and the residue dissolved in methanol (3 mL) at -10 °C. Potassium methoxide (0.164 g, 2.35 mmol) in methanol (3 mL) was added dropwise to the phosphate solution *via* a syringe pump. The reaction was warmed to room temperature over 15 minutes then the solvent removed under reduced pressure at 30 °C. The residue was dissolved in water (5 mL) and the pH adjusted to pH 4.8 using hydrochloric acid (0.1 M). The reaction mixture was then filtered and ethanol (5 mL) added to the filtrate and stirred for 10 minutes. The resulting precipitate was filtered off and washed with ethanol (5 mL) to give the title compound **151** (71 mg, 58%) as a white solid; ν_{\max} (ATR)/ cm^{-1} 3287 (C-H), 2513 (O=P-OH), 2159 (O=P-OH), 1578; ^1H NMR (400 MHz, D_2O) δ 3.68 (s, 6H, 2 \times OCH_3), 3.73 (s, 3H, OCH_3), 3.82 (s, 3H, OCH_3), 6.64 (d, J 12.2, 1H, $\text{C}=\text{CH}$), 6.66 (s, 2H, 2 \times ArH), 6.68 (d, J 8.8, 1H, ArH), 6.75 (d, J 12.0, 1H, $\text{C}=\text{CH}$), 6.87 (d, J 8.8, 1H, ArH); ^{13}C NMR (162 MHz, D_2O) δ 56.0 (2 \times OCH_3), 56.1 (OCH_3), 60.88 (OCH_3), 106.7 (2 \times ArCH), 108.2 (ArCH), 124.0 (ArC), 125.1 (ArCH), 126.1 ($\text{C}=\text{C}$), 129.9 ($\text{C}=\text{C}$), 133.7 (ArC), 134.4 (ArCO), 135.7 (ArCO), 143.6 (ArCO), 151.7 (ArCO), 152.0 (2 \times ArCO); m/z (ES^+) 493.0646 (100%, MH^+). $\text{C}_{18}\text{H}_{23}\text{O}_{12}\text{P}_2$ requires 493.0665). All data in accordance with the literature.¹⁴⁷

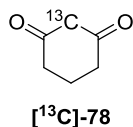
4.3 Synthesis towards [¹³C]-CA1P

Methyl 5-oxo-[6 – ¹³C]-hexanoate ([¹³C]-80)



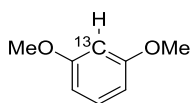
Magnesium turnings (0.938 g, 38.6 mmol) were dry stirred for 5 min and diethyl ether (10 mL) was then added. [¹³C]-Methyl iodide (5.00 g, 35.1 mmol) was added drop-wise to the reaction mixture at a rate to induce heating at a steady reflux. The resulting methyl magnesium iodide was added dropwise to a solution of freshly recrystallised copper bromide dimethyl sulphide complex (10.83 g, 52.6 mmol) in diethyl ether (200 mL) at -10 °C and left for 30 minutes. Glutaric acid monomethyl ester chloride **79** (4.9 mL, 35.1 mmol) was added to the reaction mixture left stirring for 18 hours and the reaction was quenched with a saturated solution of ammonium chloride (100 mL). The precipitate was filtered under suction and the filtrate was extracted with diethyl ether (3 × 100 mL). The combined organic layers were washed with brine (200 mL) and dried over magnesium sulfate. After filtration and removal of the solvent under reduced pressure, the crude material was purified by flash column chromatography on silica gel using an eluent of 20% ethyl acetate: 40 – 60 °C petroleum ether to afford the title compound [¹³C]-**80** as pale yellow oil (2.75 g, 55%); ¹H NMR (400 MHz, CDCl₃) δ 1.91 (pent, *J* 7.2, 2H, CH₂CH₂CH₂), 2.16 (d, *J*_{C-H} 127.2, 3H, CH₃), 2.37 (t, *J* 7.2, 2H, CH₂), 2.53 (t, *J* 7.2, 2H, CH₂), 3.69 (s, 3H, OCH₃); ¹³C NMR (101 MHz, CDCl₃) δ 18.8 (CH₂), 29.9 (enhanced, ¹³CH₃), 33.0 (CH₂), 42.4 (d, *J*_{C-C} 15.4, CH₂), 51.6 (OCH₃), 173.6 [d, *J*_{C-C} 3.1, (CH₃O)C=O], 208.0 (CH₃C=O). All NMR data in accordance with the literature.⁸⁴

[2 – ¹³C]Cyclohexane-1,3-dione ([¹³C]-78)



Potassium *tert*-butoxide (4.25 g, 38.0 mmol) was dissolved in tetrahydrofuran (60 mL) and 5-oxo-[6-¹³C]hexanoate [¹³C]-80 (2.75 g, 19.0 mmol) was added. The reaction was heated at reflux for 7 hours, after which the organic solvents were removed under reduced pressure. The residue was dissolved in water (20 mL) and acidified to pH 2 with concentrated hydrochloric acid. The aqueous layer was extracted with ethyl acetate (3 × 15 mL) and the combined organic layers dried over magnesium sulfate and filtered. Removal of the solvent under reduced pressure yielded the crude product which was purified by flash column chromatography on silica with an eluent of 80% ethyl acetate: 40 – 60 °C petroleum ether to afford the title compound [¹³C]-78 (1.31 g, 61%) as a yellow solid; mp 105 – 108 °C [lit. (¹²C 75) 106 – 108 °C]; ¹H NMR (400 MHz, CDCl₃) δ 1.95 – 2.03 [m, 2H, CH₂ (keto) and CH₂ (enol)], 2.38 [td, 2.4H, *J* 11.2, 3.2, 2 × CH₂ (keto) and CH₂ (enol)], 2.60 [t, 1.6H, *J* 6.4, CH₂ (enol)], 3.42 [d, 0.4H, *J* 130.4, CH₂ (keto)], 5.48 [d, 0.8H, *J* 160.0, =CH (enol)], 10.61 [s, 0.8H, OH (enol)]; ¹³C NMR (101 MHz, CDCl₃) δ 18.5 [d, *J* 11.7, CH₂ (keto)], 21.0 [CH₂ (enol)], 32.2 [d, *J* 7.7, CH₂ (enol)], 39.8 [d, *J* 11.7, CH₂ (enol) and 2 × CH₂ (keto)], 58.4 [enhanced ¹³CH₂ (keto)], 104.3 [enhanced, =¹³CH (enol)], 192.6 [d, *J* 63.0, C=O and C-O (enol)], 204.4 [d, *J* 40.1, C=O (keto)]. NMR data in accordance with the literature.⁸⁴

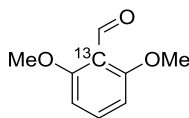
1,3-Dimethoxy-[2-¹³C]benzene ([¹³C]-157)



[¹³C]-157

[2-¹³C]Cyclohexan-1,3-dione [¹³C]-78 (1.22 g, 10.8 mmol) was dissolved in methanol (20 mL). Iodine (8.19 g, 32.4 mmol) was added and the reaction mixture was heated at reflux for 1.5 hours. The methanol was removed under reduced pressure and the residue dissolved in dichloromethane (20 mL). The organic layer was washed with sodium hydrogen carbonate (20 mL), 10% aq. sodium thiosulfate (20 mL) and 5% sodium hydroxide (20 mL). The combined aqueous layers were then extracted with dichloromethane (3 × 30 mL) and the resulting combined organic layers were dried over magnesium sulfate, filtered and the solvent was removed under reduced pressure. Purification of the crude material by flash column chromatography using an eluent of 5% ethyl acetate: 40 – 60 °C petroleum ether afforded the title compound [¹³C]-157 as a pale yellow oil (1.013 g, 67%); ¹H NMR (400 MHz, CDCl₃) δ 3.70 (s, 6H, 2 × OCH₃), 6.50 (dt, *J*_{C-H} 158.0, *J* 2.4, 1H, ¹³CH), 6.56 – 6.52 (m, 2H, 2 × ArH), 7.21 (td, *J*_{H-H} 8.2, *J*_{C-H} 1.2, 1H, ArH); ¹³C NMR (101 MHz, CDCl₃) δ 55.3 (d, *J*_{C-C} 4.4, 2 × OCH₃), 100.5 (enhanced, ¹³C), 106.2 (d, *J*_{C-C} 2.8, 2 × ArCH), 129.9 (d, *J*_{C-C} 4.8, ArCH), 160.8 (d, *J*_{C-C} 60.3, 2 × ArC). NMR data in accordance with the literature apart in the ¹H NMR spectrum the peak at 3.70 was reported as 3H in the literature and the triplet of doublets at 7.21 was reported as a doublet of triplets.⁸⁴

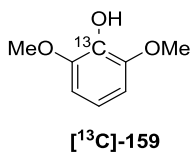
2,6-Dimethoxy-[1-¹³C]benzaldehyde ([¹³C]-158)



[¹³C]-158

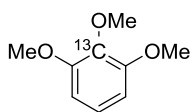
1,3-Dimethoxy-[2-¹³C]benzene [¹³C]-157 (1.42 g, 10.1 mmol) and *N,N,N',N'*-tetramethylethylene diamine (1.7 mL, 11.5 mmol) dissolved in tetrahydrofuran (20 mL) and cooled to 0 °C. *n*-Butyllithium (4.9 mL, 2.5 M in hexanes, 12.2 mmol) was added and the mixture was stirred for 30 minutes. Dimethylformamide (1.2 mL, 15.2 mmol) was added dropwise and the solution stirred for a further 1 hour. The reaction was then quenched with 1 M hydrochloric acid (20 mL) whilst maintaining the temperature below 25 °C and the organic solvent was removed under reduced pressure. The aqueous layer was extracted with diethyl ether (3 × 15 mL) and the combined organic layers were washed with brine (30 mL), dried over magnesium sulfate, filtered and the solvent removed under reduced pressure. The residue was washed with 40 – 60 °C petroleum ether (25 mL) then filtered to afford the title compound [¹³C]-158 (1.51 g, 89%) which was used without further purification; mp 96 – 98 °C [lit. (¹²C **88**) 95 – 98 °C]; ν_{\max} (ATR)/ cm^{-1} 2980 (C-H), 1673 (HC=O), 1586 (aromatic), 1570 (aromatic); Found: C, 64.82; H 6.10; ¹²C₈¹³CH₁₀O₃ requires C, 65.26; H, 6.03; ¹H NMR (400 MHz, CDCl₃) δ 3.86 (s, 6H, 2 × OCH₃), 6.55 (dd, $J_{\text{H-H}}$ 8.5, $J_{\text{C-H}}$ 5.2, 2H, 2 × ArH), 7.42 (td, $J_{\text{H-H}}$ 8.5, $J_{\text{C-H}}$ 1.3, 1H, ArH), 10.48 (d, $J_{\text{C-H}}$ 22.4, 1H, CHO); ¹³C NMR (101 MHz, CDCl₃) δ 56.1 (d, $J_{\text{C-C}}$ 2.4, 2 × OCH₃), 103.0 (d, $J_{\text{C-C}}$ 2.3, 1 × ArCH), 114.3 (enhanced, ¹³C), 136.0 (d, $J_{\text{C-C}}$ 4.8, 2 × ArCH), 162.2 (d, $J_{\text{C-C}}$ 70.2, 2 × ArC), 189.5 (d, $J_{\text{C-C}}$ 54.3, HC=O); m/z (ES⁺) 168.0746 (100%, MH⁺. C₈¹³CH₁₁O₃ requires 168.0742). NMR data corresponds with ¹²C NMR data.

[1 – ¹³C]2,6-Dimethoxyphenol ([¹³C]-159)



2,6-Dimethoxy-[1 – ¹³C]benzaldehyde [¹³C]-158 (1.00 g, 5.98 mmol) was dissolved in dichloromethane (10 mL) and cooled to 0 °C. *meta*-Chloroperbenzoic acid (2.68 g, 12.0 mmol) was added dropwise as a dichloromethane solution (10 mL) and the reaction was left at 0 °C for 3 hours. The organic layer was washed with sodium sulfite solution (10 mL) then sodium hydrogen carbonate (10 mL). The combined aqueous layers were extracted with dichloromethane (3 × 15 mL). The combined organic layers were washed with brine (20 mL), dried over magnesium sulfate, filtered, and the solvent removed under reduced pressure. The resulting formate ester was dissolved in methanol (10 mL) and cooled to 0 °C. Potassium hydroxide (1.22 g, 21.7 mmol) in methanol (10 mL) was added dropwise and the reaction left for 45 minutes. Water (15 mL) was added and the solution was acidified to pH 2 using concentrated hydrochloric acid. The aqueous layer was extracted with diethyl ether (6 × 10 mL) and the combined organic layers were washed with brine, dried over magnesium sulfate, filtered and the solvent removed under reduced pressure. The crude reaction material was purified by flash column chromatography using an eluent of 20% ethyl acetate: 40 – 60 °C petroleum ether and afforded the title compound [¹³C]-159 (0.77 g, 80%) as a white solid; mp 54 – 55 °C [lit. (¹²C **89**) 52 – 53 °C]; ν_{\max} (ATR)/ cm^{-1} 3491 (O-H), 3004 (C-H), 2837 (C-H), 1573 (aromatics), 1260 (C-OH); ¹H NMR (400 MHz, CDCl₃) δ 3.89 (s, 6H, 2 × OCH₃), 5.53 (d, *J* 2.8, 1H OH), 6.59 (t, *J* 8.2, 2H, 2 × ArH), 6.81 (td, *J*_{H-H} 8.2, *J*_{C-H} 1.6, 1H, ArH); ¹³C NMR (101 MHz, CDCl₃) δ 56.3 (d, *J*_{C-C} 2.7, 2 × OCH₃), 104.9 (d, *J*_{C-C} 5.2, 2 × ArCH), 119.1 (d, *J*_{C-C} 6.4, ArCH), 134.8 (enhanced, ¹³C), 147.2 (d, *J* 80.1, 2 × COCH₃); *m/z* (ES⁺) 178 (34%, MNa⁺), 156.0743 (100, MH⁺. ¹²C₇¹³CH₁₁O₃ requires 156.0742), 124 (36). NMR data corresponds with ¹²C NMR data.

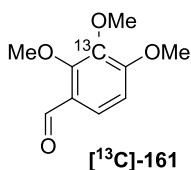
[2 – ¹³C]-1,2,3-Trimethoxybenzene ([¹³C]-160)



[¹³C]-160

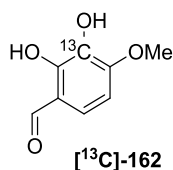
2,6-Dimethoxy-[1 – ¹³C]phenol [¹³C]-**159** (0.958 g, 6.17 mmol) was dissolved in acetone (20 mL), potassium carbonate (1.28 g, 9.26 mmol) was added and the reaction mixture cooled to 0 °C. 18-Crown-6 (0.2 mL) and methyl iodide (0.58 mL, 9.26 mmol) were added at 0 °C and the reaction was stirred overnight. after which the resulting mixture was poured in diethyl ether (20 mL), filtered and the filtrate concentrated under reduced pressure to yield the title compound [¹³C]-**160** (0.836 g 80%) as a white solid which was used without further purification; mp 43 – 44 °C [lit. (¹²C **119**) 40 – 42 °C]; ν_{\max} (ATR)/ cm^{-1} 2991 (C-H), 2965 (C-H), 2940, 2836, (aromatics); Found: C, 64.34; H 7.35; ¹²C₈¹³CH₁₃O₃ requires C, 64.48; H, 7.15; ¹H NMR (400 MHz, CDCl₃) δ 3.85 (d, $J_{\text{C-H}}$ 3.6, 3H, OCH₃), 3.86 (s, 6H, 2 × OCH₃), 6.58 (dd, J 8.3, $J_{\text{C-H}}$ 7.4, 2H, 2 × ArH), 6.99 (td, J 8.3, $J_{\text{C-H}}$ 2.0, 1H, ArH); ¹³C NMR (101 MHz, CDCl₃) δ 56.1 (d, $J_{\text{C-C}}$ 2.7, 2 × OCH₃), 60.8 (d, $J_{\text{C-C}}$ 3.5, OCH₃), 105.2 (d, $J_{\text{C-C}}$ 4.8, 2 × ArCH), 123.6 (d, $J_{\text{C-C}}$ 6.3, ArCH) 138.1 (enhanced, ¹³C), 153.5 (d, $J_{\text{C-C}}$ 80.2, 2 × ArC); m/z (ES⁺) 170.0902 (100%, MH⁺). ¹²C₈¹³CH₁₃O₃ requires 170.0898). NMR data corresponds with ¹²C NMR data.

[3 – ¹³C]-2,3,4-Trimethoxybenzaldehyde ([¹³C]-161)



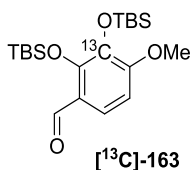
[2 – ¹³C]-1,2,3-Trimethoxybenzene [¹³C]-160 (0.451 g, 2.67 mmol) was dissolved in dichloromethane (5 mL) at 0 °C. Titanium (IV) chloride (0.58 mL, 5.33 mmol) was added dropwise followed by dichloromethyl methyl ether (0.48 mL, 5.33 mmol). The reaction mixture was warmed to room temperature and left stirring for 3 hours. Cold water (5 mL) was added to reaction mixture and the aqueous layer extracted with dichloromethane (3 × 5 mL). The combined organic layers were washed with hydrochloric acid (1 M, 10 mL), saturated aqueous sodium bicarbonate (10 mL) and brine (15 mL). The organic layers were combined, dried over magnesium sulfate, filtered and the solvent removed under reduced pressure. The crude reaction material was purified by flash column chromatography using an eluent of 10% ethyl acetate: 40 – 60 °C petroleum ether and afforded the title compound [¹³C]-161 (0.372 g, 71%) as a white solid; mp 31 – 32 °C [lit. (¹²C **120**) 32 – 33 °C]; ν_{\max} (ATR)/ cm^{-1} 2949 (C-H), 2978 (C-H), 1671 (HC=O), 1586 (aromatics); ¹H NMR (400 MHz, CDCl₃) δ 3.89 (d, $J_{\text{C-H}}$ 3.6, 3H, ¹³COCH₃), 3.94 (s, 3H, OCH₃), 4.03 (s, 3H, OCH₃), 6.76 (dd, $J_{\text{H-H}}$ 8.6, $J_{\text{C-H}}$ 7.6, 1H, ArH), 7.61 (dd, $J_{\text{H-H}}$ 8.6, $J_{\text{C-H}}$ 1.6, 1H, ArH), 10.25 (d, $J_{\text{C-H}}$ 0.4, 1H, CHO); ¹³C NMR (101 MHz, CDCl₃) δ 56.2 (d, $J_{\text{C-C}}$ 2.8, OCH₃), 61.0 (d, $J_{\text{C-C}}$ 3.4, OCH₃), 62.4 (OCH₃), 107.4 (d, $J_{\text{C-C}}$ 5.2, ArCH), 123.3 (d, $J_{\text{C-C}}$ 6.3, ArC), 124.3 (d, $J_{\text{C-C}}$ 4.7, ArCH), 141.6 (enhanced, ¹³C), 157.0 (d, $J_{\text{C-C}}$ 78.9, ArC), 159.3 (d, $J_{\text{C-C}}$ 77.2, ArC), 188.9 (d, $J_{\text{C-C}}$ 3.4, CHO); m/z (ES⁺) 198.0851 (100%, M⁺. ¹²C₉¹³CH₁₃O₄ requires 198.0847). NMR data corresponds with ¹²C NMR data.

[3 – ¹³C]-2,3-Dihydroxy-4-methoxybenzaldehyde ([¹³C]-162)



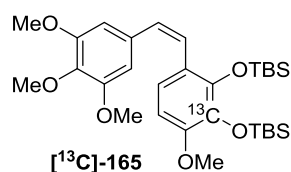
[3 – ¹³C]-2,3,4-Trimethoxybenzaldehyde [¹³C]-161 (0.152 g, 0.77 mmol) was dissolved in dichloromethane (2 mL) and boron trichloride (1M in dichloromethane, 0.77 mL, 0.77 mmol) was added dropwise. The reaction was left stirring for 2 hours before another equivalent of boron trichloride (1M in dichloromethane, 0.77 mL, 0.77 mmol) was added dropwise and the reaction was left stirring for 24 hours. The reaction was quenched with NaHCO₃ (5 mL) and acidified to pH 2 using concentrated hydrochloric acid. The aqueous layer was then extracted with dichloromethane (3 × 5 mL) and the combined organic layers washed with brine (10 mL), dried over magnesium sulfate and filtered. The solvent was removed under reduced pressure, and the crude material recrystallised with ethyl acetate/hexane to afford the title compound [¹³C]-162 (0.109 g, 84%) as a white solid; mp 113 – 114 °C [lit. (¹²C **118**) 113 – 114 °C]; ν_{\max} (ATR)/ cm⁻¹ 3363 (O-H), 2950 (C-H), 1644 (HC=O), 1503 (aromatic); ¹H NMR (400 MHz, CDCl₃) δ 3.98 (s, 3H, OCH₃), 5.49 (d, *J* 3.2, 1H, OH), 6.62 (dd, *J*_{H-H} 8.8 *J*_{C-H} 7.2, 1H, ArH), 7.14 (dd, *J*_{H-H} 8.8 *J*_{C-H} 1.2, 1H, ArH), 9.75 (d, *J*_{C-H} 2.8, 1H, CHO), 11.12 (d, *J*_{C-H} 6.0, 1H, OH); ¹³C NMR (101 MHz, CDCl₃) δ 56.4 (d, *J*_{C-C} 2.7, OCH₃), 103.6 (d, *J*_{C-C} 5.6, ArCH), 116.1 (d, *J*_{C-C} 4.8, ArC), 126.1 (d, *J*_{C-C} 4.9, ArCH), 133.0 (enhanced, ¹³C), 149.1 (d, *J*_{C-C} 80.6, ArC), 153.0 (d, *J*_{C-C} 80.4, ArC), 195.2 (d, *J*_{C-C} 3.6, CHO); *m/z* (ES⁺) 170.0528 (100%, M⁺. ¹²C₇¹³CH₈O₄ requires 170.0529). NMR data corresponds with ¹²C NMR data.

[3 – ^{13}C]-2,3-Di[(*tert*-butyldimethylsilyl)oxy]-4-methoxybenzaldehyde ([^{13}C]-163)



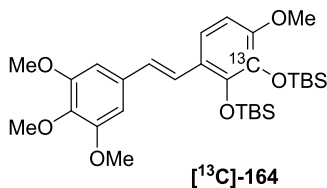
[3 – ^{13}C]-2,3-Dihydroxy-4-methoxybenzaldehyde [^{13}C]-162 (0.119 g, 0.70 mmol) was dissolved in dichloromethane (2 mL). Triethylamine (0.29 mL, 2.11 mmol) and 4-dimethylaminopyridine (18 mg, 0.021 mmol) were added and the mixture was stirred for 10 minutes. *tert*-Butyldimethylsilyl chloride (0.254 g, 1.69 mmol) was added to the reaction mixture in portions and stirred for 12 hours at room temperature. After addition of water (5 mL), the aqueous layer was extracted with dichloromethane (3×5 mL) and the combined organic layers were washed with brine (20 mL) and dried over magnesium sulfate. Filtration, followed by the removal of solvent under reduced pressure gave the crude material which was purified by recrystallisation from methanol to afford the title compound [^{13}C]-163 (0.154 g, 55%) as colourless crystals; mp 74 – 75 °C [lit. (^{12}C 22) 72 – 73 °C]; ν_{max} (ATR)/ cm^{-1} 2928 (C-H), 2856 (C-H), 1679 (HC=O), 1579 (aromatic); ^1H NMR (400 MHz, CDCl_3) δ 0.13 [s, 12H, $2 \times \text{OSi}(\text{CH}_3)_2\text{C}(\text{CH}_3)_3$], 0.98 [s, 9H, $\text{OSi}(\text{CH}_3)_2\text{C}(\text{CH}_3)_3$], 1.04 [s, 9H, $\text{OSi}(\text{CH}_3)_2\text{C}(\text{CH}_3)_3$], 3.83 (s, 3H, OCH_3), 6.62 (t, J 8.0, 1H, Ar-*H*), 7.48 (dd, $J_{\text{H-H}}$ 8.0, $J_{\text{C-H}}$ 1.8, 1H, Ar-*H*), 10.21 (s, 1H, CHO); ^{13}C NMR (101 MHz, CDCl_3) δ -3.8 [$2 \times \text{OSi}(\text{CH}_3)_2\text{C}(\text{CH}_3)_3$], 18.6 [$\text{OSi}(\text{CH}_3)_2\text{C}(\text{CH}_3)_3$], 18.7 [$\text{OSi}(\text{CH}_3)_2\text{C}(\text{CH}_3)_3$], 26.0 [$\text{OSi}(\text{CH}_3)_2\text{C}(\text{CH}_3)_3$], 26.2 [$\text{OSi}(\text{CH}_3)_2\text{C}(\text{CH}_3)_3$], 55.2 (d, $J_{\text{C-H}}$ 2.8, OCH_3), 105.4 (d, $J_{\text{C-H}}$ 5.6, ArCH), 121.4 (d, $J_{\text{C-H}}$ 4.7, ArCH), 123.4 (d, $J_{\text{C-H}}$ 7.4, ArC), 136.8 (enhanced, ^{13}C), 151.0 (d, $J_{\text{C-H}}$ 80.5, ArC), 157.5 (d, $J_{\text{C-H}}$ 77.8, ArC), 189.2 (d, $J_{\text{C-H}}$ 3.6, CHO); m/z (ESI) 398.2258 (100%, MH^+ . $^{12}\text{C}_{19}^{13}\text{CH}_{36}\text{O}_4\text{Si}_2$ requires 398.2258). NMR data corresponds with ^{12}C NMR data.

(Z)-1-(3',4',5'-Trimethoxyphenyl)-2-[2'',¹³C – 3'']-di(*tert*-butyldimethylsilyl)oxy]-4''-methoxyphenyl]ethene ([¹³C]-165)



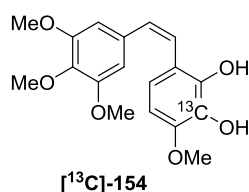
3,4,5-Trimethoxybenzyltriposponium bromide **139** (0.132 g, 0.25 mmol) was dissolved in tetrahydrofuran (1 mL) and cooled to -10 °C. *n*-Butyllithium (1.9 M in hexanes, 0.13 mL, 0.25 mmol) was added dropwise and the reaction left for 30 minutes. The reaction mixture was cooled to -78 °C and [3 – ¹³C]-2,3-di[(*tert*-butyldimethylsilyl)oxy]-4-methoxybenzaldehyde [¹³C]-**163** (0.100 g, 0.25 mmol) in tetrahydrofuran (1 mL) and cooled to (0.5 mL) was added dropwise to the reaction mixture and was left to warm to 0 °C. The reaction was quenched with water (5 mL) and the organic layer removed under reduced pressure. The aqueous layer was extracted with diethyl ether (3 × 5 mL) and the combined organic layers were washed with brine (15 mL), dried over magnesium sulfate, filtered and the solvent removed under reduced pressure. The crude reaction material was purified by flash column chromatography using an eluent of 10% ethyl acetate: 40 – 60 °C petroleum ether and recrystallised from ethanol to yield the *Z*-isomer [¹³C]-**165** (44 mg, 31%) as white crystals; mp 120 – 121 °C [lit. (¹²C **24**) 118 – 120 °C]; ν_{\max} (ATR)/ cm^{-1} 2829 (C-H), 2856 (C-H), 1580 (C=C), 1500 (aromatic); ¹H NMR (400 MHz, CDCl₃) δ 0.10 [s, 6H, OSi(CH₃)₂C(CH₃)₃], 0.19 [s, 6H, OSi(CH₃)₂C(CH₃)₃], 1.00 [s, 9H, OSi(CH₃)₂C(CH₃)₃], 1.04 [s, 9H, OSi(CH₃)₂C(CH₃)₃], 3.67 (s, 6H, OCH₃), 3.74 (s, 3H, OCH₃), 3.83 (s, 3H, OCH₃), 6.36 (d, *J* 12.6, 1H, HC=C), 6.37 (d, *J* 8.3, 1H, ArH), 6.58 (d, *J* 12.6, 1H, C=CH), 6.62 (s, 2H, 2 × ArH), 6.91 (dd, *J*_{H-H} 8.3, *J*_{C-H} 1.4 1H, ArH); ¹³C NMR (101 MHz, CDCl₃) δ -3.9 [OSi(CH₃)₂C(CH₃)₃], -3.2 [OSi(CH₃)₂C(CH₃)₃], 18.6 [OSi(CH₃)₂C(CH₃)₃], 18.7 [OSi(CH₃)₂C(CH₃)₃], 26.1 [OSi(CH₃)₂C(CH₃)₃], 26.4 [OSi(CH₃)₂C(CH₃)₃], 54.9 (OCH₃), 55.8 (2 × OCH₃), 60.9 (OCH₃), 104.2 (d, *J*_{C-C} 5.6, ArCH), 105.9 (2 × ArCH), 122.2 (d, *J*_{C-C} 4.9, ArCH), 123.2 (d, *J*_{C-C} 7.9, ArC-C=), 127.4 (C=), 127.7 (=C), 132.8 (ArC-C=), 136.8 (enhanced, ¹³C), 137.0 (COSi), 146.5 (COCH₃), 151.3 (COCH₃), 152.7 (2 × COCH₃); *m/z* (ESI) 584 (69%, MNa⁺), 562.3097 (100, MH⁺. C₂₉¹³C₁H₄₈O₆Si₂ requires 562.3096). NMR data in accordance with ¹²C NMR data.

(E)-1-(3',4',5'-Trimethoxyphenyl)-2-[2'',¹³C – 3'']-di(*tert*-butyldimethylsilyl)oxy]-4''-methoxyphenyl]ethene (¹³C]-164)



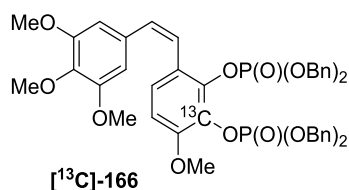
3,4,5-Trimethoxybenzyltriposponium bromide **139** (0.132 g, 0.35 mmol) was dissolved in tetrahydrofuran (1 mL) and cooled to -10 °C. *n*-Butyllithium (1.9 M in hexanes, 0.13 mL, 0.25 mmol) was added dropwise and the reaction left for 30 minutes. The reaction mixture was cooled to -78 °C and [3 – ¹³C]-2,3-di[(*tert*-butyldimethylsilyl)oxy]-4-methoxybenzaldehyde [¹³C]-**163** (0.100 g, 0.25 mmol) in tetrahydrofuran (0.5 mL) was added dropwise to the reaction mixture and was left to warm to 0 °C. The reaction was quenched with water (5 mL) and the organic layer removed under reduced pressure. The aqueous layer was extracted with diethyl ether (3 × 5 mL) and the combined organic layers were washed with brine (15 mL), dried over magnesium sulfate, filtered and the solvent removed under reduced pressure. The crude reaction material was purified by flash column chromatography using an eluent of 10% ethyl acetate: 40 – 60 °C petroleum ether and recrystallised from ethanol to yield the *Z*-isomer [¹³C]-**164** (14 mg, 10%) as a white solid; mp 135 – 136 °C [lit. (¹²C **23**) 138 – 139 °C]; ν_{\max} (ATR)/ cm^{-1} 2928 (C-H), 2855 (C-H), 1594 (C=C), 1500 (aromatic); ¹H NMR (400 MHz, CDCl₃) δ 0.11 [s, 6H, OSi(CH₃)₂C(CH₃)₃], 0.13 [s, 6H, OSi(CH₃)₂C(CH₃)₃], 1.00 [s, 9H, OSi(CH₃)₂C(CH₃)₃], 1.09 [s, 9H, OSi(CH₃)₂C(CH₃)₃], 3.79 (s, 3H, OCH₃), 3.86 (s, 3H, OCH₃), 3.88 (s, 6H, 2 × OCH₃), 6.56 (app. t, *J* 8.5, 1H, *ArH*), 6.72 (s, 2H, 2 × *ArH*), 6.81 (d, *J*_{H-H} 16.4, 1H, *HC=C*), 7.20 (dd, *J*_{H-H} 8.5, *J*_{C-H} 1.6, 1H, *ArH*), 7.31 (d, *J*_{H-H} 16.4, 1H, *C=CH*); ¹³C NMR (101 MHz, CDCl₃) δ 137.0 (enhanced, ¹³C); *m/z* (ESI) 584 (8%, MNa⁺), 562.3091 (100, MH⁺. C₂₉¹³CH₄₈O₆Si₂ requires 562.3096). NMR data corresponds with ¹²C NMR data.

(Z)-1-(3',4',5'-Trimethoxyphenyl)-2-(2'',[3'' - ¹³C]-dihydroxy-4''-methoxyphenyl) ethene ([¹³C – CA1) ([¹³C]-154)



(Z)-1-(3',4',5'-Trimethoxyphenyl)-2-[2'',[¹³C-3'']-di(*tert*-butyldimethylsilyl)oxy]-4''-methoxy phenyl]ethene [¹³C]-165 (0.144 g, 0.26 mmol) was dissolved in tetrahydrofuran (1 mL). Tetrabutylammonium fluoride (1M in THF, 1.0 mL, 1.0 mmol). The mixture was left stirring for 30 minutes after which hydrochloric acid (1M, 3 mL) was added the mixture extracted with ethyl acetate (3 × 5 mL). The combined organic layers were washed with brine (15 mL), dried over magnesium sulfate, filtered and the solvent removed under reduced pressure. The crude material was purified by flash column chromatography on silica with an eluent of 50% ethyl acetate: 40 – 60 °C petroleum ether to reveal the title compound [¹³C]-154 (79 mg, 92%) as an off-white solid; mp 111 – 112 °C [lit. (¹²C **8**) 113 – 115 °C]; ν_{\max} (ATR)/ cm^{-1} 3366 (O-H), 2960 (C-H), 2925 (C-H), 1580, 1505 (aromatic); ¹H NMR (400 MHz, CDCl₃) δ 3.67 (s, 6H, 2 × OCH₃), 3.83 (s, 3H, OCH₃), 3.86 (s, 3H, OCH₃), 5.37 (s, 1H, OH), 5.38 (s, 1H, OH), 6.38 (t, *J* 8.5, 1H, *ArH*), 6.52 (s, 2H, 2 × *ArH*), 6.54 (d, *J* 11.8, 1H, HC=CH), 6.59 (d, *J* 11.8, 1H, HC=CH), 6.76 (dd, *J*_{H-H} 8.5, *J*_{C-H} 1.2 1H, *ArH*); ¹³C NMR (101 MHz, CDCl₃) δ 132.6 (enhanced, ¹³C); *m/z* (ESI) 334.1366 (100%, MH⁺. C₁₇¹³C₁H₂₀O₆ requires 334.1366). NMR data corresponds with ¹²C NMR data.

(Z)-1-(3',4',5'-Trimethoxyphenyl)-2-(2'',[3'' - ¹³C]-di-({[bis-(benzyl)oxy]phosphoryl oxy} -4''-methoxyphenyl)ethene ([¹³C]-166)



(Z)-1-(3',4',5'-Trimethoxyphenyl)-2-(2'',[3''-¹³C]-dihydroxy-4''-methoxyphenyl)ethene ([¹³C - CA1] [¹³C]-154 (85 mg, 0.256 mmol) was dissolved in acetonitrile (1 mL) and cooled to -20 °C. Carbon tetrachloride (0.49 mL, 5.13 mmol) was added followed by the addition of *N,N*-diisopropylethylamine (0.07 mL, 0.41 mmol) and 4-dimethylaminopyridine (6.3 mg, 0.051 mmol). The reaction was stirred for 5 minutes then dibenzyl phosphite (80%, 0.281 g, 1.07 mmol) was added and the reaction warmed to 0 °C over 2 hours. Monopotassium phosphate (1 mL, 0.5 M) was added and the aqueous layer extracted with ethyl acetate (3 × 2 mL). The organic layers were combined and washed with brine (5 mL), dried over magnesium sulfate, filtered and the solvent removed under reduced pressure. The crude reaction material was purified by flash column chromatography on silica with an eluent of 50% ethyl acetate: 40 – 60 °C petroleum ether and afforded the title compound [¹³C]-166 (0.115 g, 53%) as a light brown oil; ν_{\max} (ATR)/ cm^{-1} 2924 (C-H), 2851 (C-H), 1579 (aromatic); ¹H NMR (400 MHz, CDCl₃) δ 3.62 (s, 6H, 2 × OCH₃), 3.76 (s, 3H, OCH₃), 3.79 (s, 3H, OCH₃), 5.07 (d, *J* 2.8, 2H, CH₂), 5.09 (d, *J* 2.4, 2H, CH₂), 5.17 (d, *J* 76.8, 4H, 2 × CH₂), 6.45 (s, 2H, 2 × ArH), 6.50 (d, *J* 12.2, 1H, HC=C), 6.64 (d, *J* 12.2, 1H, C=CH), 6.66 (d, *J* 8.6, 1H, ArH), 7.00 (d, *J* 8.6, 1H, ArH), 7.28 – 7.20 (m, 20H, 4 × C₆H₅); ¹³C NMR (101 MHz, CDCl₃) δ 55.9 (2 × OCH₃), 56.4 (d, *J*_{C-C} 2.6, OCH₃), 60.8 (OCH₃), 69.7 [OP(O)(OCH₂Ph)], 69.8 [OP(O)(OCH₂Ph)], 69.9 [OP(O)(OCH₂Ph)], 70.0 [OP(O)(OCH₂Ph)], 106.1 (2 × ArCH), 109.2 (ArCH), 124.3 (ArCH), 124.6 (=C-C), 126.8 (=C), 127.8 (4 × OCH₂ArCH), 127.9 (4 × OCH₂ArCH), 128.3 (2 × OCH₂ArCH), 128.4 (2 × OCH₂ArCH), 128.4 (8 × OCH₂ArCH), 131.6 (C=), 132.1 (C-C=), 132.94 (enhanced, dd, *J* 7.5, 3.8, ¹³C) 135.6 (2 × OCH₂C), 135.7 (2 × OCH₂C), 135.8 (ArCO), 136.0 (ArCO), 151.7 (ArCO), 152.8 (2 × ArCO); ³¹P NMR (162 MHz, CDCl₃) δ -5.60 – -5.44 (m); *m/z* (ESI) 854.2571 (100%, MH⁺. C₄₅¹³CH₄₆O₁₂P₂ requires 854.2571). NMR data corresponds with ¹²C NMR data.

5. References

1. J. Ferlay, I. Soerjomataram, M. Ervik, R. Dikshit, S. Eser, C. Mathers, M. Rebelo, D. M. Parkin, D. Forman and F. Bray, *GLOBOCAN 2012 v1.0, Cancer Incid. Mortality. Worldw. IARC CancerBase No.11 [Internet]. Lyon, Fr. Int. Agency Res. Cancer; 2013. Available from <http://globocan.iarc.fr>. accessed 12/09/15.*
2. D. Hanahan and R. A. Weinberg, *Cell*, 2011, **144**, 646–674.
3. J. Denekamp, *Br. J. Cancer*, 1982, **45**, 136–139.
4. M. A. Jordan and L. Wilson, *Curr. Opin. Cell Biol.*, 1998, **10**, 123–130.
5. A. Eberhard, S. Kahlert, V. Goede, B. Hemmerlein, K. H. Plate and H. G. Augustin, *Cancer Res.*, 2000, **60**, 1388–1393.
6. M. Kavallaris, *Nat. Rev. Cancer*, 2010, **10**, 194–204.
7. M. A. Jordan and L. Wilson, *Nat. Rev. Cancer*, 2004, **4**, 253–265.
8. D. G. I. Kingston, *J. Nat. Prod.*, 2009, **72**, 507–515.
9. R. L. Noble, C. T. Beer and J. H. Cutts, *Ann. N.Y. Acad. Sci.*, 1958, **76**, 882–894.
10. P. D. Davis, G. J. Dougherty, D. C. Blakey, S. M. Galbraith, G. M. Tozer, A. L. Holder, M. A. Naylor, J. Nolan, M. R. L. Stratford, D. J. Chaplin and S. A. Hill, *Cancer Res.*, 2002, **62**, 7247–7253.
11. G. R. Pettit, S. B. Singh, M. L. Niven, E. Hamel and J. M. Schmidt, *J. Nat. Prod.*, 1987, **50**, 119–131.
12. K. A. Monk, R. Siles, M. B. Hadimani, B. E. Mugabe, J. F. Ackley, S. W. Studerus, K. Edwardsen, M. L. Trawick, C. M. Garner, M. R. Rhodes, G. R. Pettit and K. G. Pinney, *Bioorg. Med. Chem.*, 2006, **14**, 3231–3244.
13. G. R. Pettit, H. J. Rosenberg, R. Dixon, J. C. Knight, E. Hamel, J.-C. Chapuis, R. K. Pettit, F. Hogan, B. Sumner, K. B. Ain and B. Trickey-Platt, *J. Nat. Prod.*, 2012, **75**, 385–393.

14. G. R. Pettit, M. P. Grealish, D. L. Herald, M. R. Boyd, E. Hamel and R. K. Pettit, *J. Med. Chem.*, 2000, **43**, 2731–2737.
15. S. Banerjee, Z. Wang, M. Mohammad, F. H. Sarkar and R. M. Mohammad, *J. Nat. Prod.*, 2008, **71**, 492–496.
16. R. Chen, D. M. Brady, D. Smith, A. W. Murray and K. G. Hardwick, *Mol. Biol. Cell*, 1999, **10**, 2607–2618.
17. C. Kanthou, O. Greco, A. Stratford, I. Cook, R. Knight, O. Benzakour and G. Tozer, *Am. J. Pathol.*, 2004, **165**, 1401–1411.
18. C. Kanthou and G. M. Tozer, *Blood*, 2002, **99**, 2060–2069.
19. G. M. Tozer, V. E. Prise, J. Wilson, M. Cemazar, S. Shan, M. W. Dewhurst, P. R. Barber, B. Vojnovic and D. J. Chaplin, *Cancer Res*, 2001, **61**, 6413–6422.
20. G. M. Tozer, C. Kanthou and B. C. Baguley, *Nat. Rev. Cancer*, 2005, **5**, 423–435.
21. S. E. Holwell, P. A. Cooper, K. Grosios, J. W. Lippert III, G. R. Pettit, S. D. Shnyder and M. C. Bibby, *Anticancer Res.*, 2002, **22**, 707–711.
22. G. G. Dark, S. A. Hill, V. E. Prise, G. M. Tozer, G. R. Pettit and D. J. Chaplin, *Cancer Res.*, 1997, **57**, 1829–1834.
23. S. A. Hill, G. M. Tozer and D. J. Chaplin, *Anticancer Res.*, 2002, **22**, 1453–1458.
24. 2004, US Pat., US 7 078 552 B2, 2006.
25. J. A. Woods, J. A. Hadfield, G. R. Pettit, B. W. Fox and A. T. McGown, *Br. J. Cancer*, 1995, **71**, 705–711.
26. M. E. Eichhorn, S. Strieth and M. Dellian, *Drug Resist. Updat.*, 2004, **7**, 125–138.
27. K. Ohsumi, R. Nakagawa, Y. Fukuda, T. Hatanaka, Y. Morinaga, Y. Nihei, K. Ohishi, Y. Suga, Y. Akiyama and T. Tsuji, *J. Med. Chem.*, 1998, **41**, 3022–3032.
28. T. J. Kim, M. Ravoori, C. N. Landen, A. A. Kamat, L. Y. Han, C. Lu, Y. G. Lin,

- W. M. Merritt, N. Jennings, W. A. Spannuth, R. Langley, D. M. Gershenson, R. L. Coleman, V. Kundra and A. K. Sood, *Cancer Res.*, 2007, **67**, 9337–9345.
29. K. Hori and S. Saito, *Br. J. Cancer*, 2003, **89**, 1334–1344.
 30. G. R. Pettit, S. B. Singh, M. R. Boyd, E. Hamel, R. K. Pettit, J. M. Schmidt and F. Hogan, *J. Med. Chem.*, 1995, **38**, 1666–1672.
 31. G. R. Pettit, S. B. Singh and G. M. Cragg, *J. Org. Chem.*, 1985, **50**, 3404–3406.
 32. S. B. Singh and G. R. Pettit, *J. Org. Chem.*, 1989, **54**, 4105–4114.
 33. K. Gaukroger, J. A. Hadfield, L. A. Hepworth, N. J. Lawrence and A. T. McGown, *J. Org. Chem.*, 2001, **66**, 8135–8138.
 34. V. P. Bui, T. Hudlicky, T. V Hansen and Y. Stenstrom, *Tetrahedron Lett.*, 2002, **43**, 2839–2841.
 35. K. Odlo, J. Klaveness, P. Rongved and T. V. Hansen, *Tetrahedron Lett.*, 2006, **47**, 1101–1103.
 36. A. Fürstner and K. Nikolakis, *Liebigs Ann.*, 1996, 2107–2113.
 37. Y. Malysheva, S. Combes, A. Fedorov, P. Knochel and A. Gavryushin, *Synlett*, 2012, **23**, 1205–1208.
 38. O. Petrov, M. Gerova, C. Chaney and K. Petrova, *Synthesis (Stuttg.)*, 2011, 3711–3715.
 39. F. Lara-Ochoa and G. Espinosa-Pérez, *Tetrahedron Lett.*, 2007, **48**, 7007–7010.
 40. G. C. Nwokogu, *Tetrahedron Lett.*, 1984, **25**, 3263–3266.
 41. J. Li, R. Hua and T. Liu, *J. Org. Chem.*, 2010, **75**, 2966–2970.
 42. A. Giraud, O. Provot, A. Hamzé, J.-D. Brion and M. Alami, *Tetrahedron Lett.*, 2008, **49**, 1107–1110.
 43. S. B. Bedford, C. P. Quarterman, D. L. Rathbone, J. A. Slack, R. J. Griffin and

- M. F. G. Stevens, *Bioorg. Med. Chem. Lett.*, 1996, **6**, 157–160.
44. I. G. Kirwan, P. M. Loadman, D. J. Swaine, D. A. Anthoney, G. R. Pettit, J. W. Lippert III, S. D. Shnyder, P. A. Cooper and M. C. Bibby, *Clin. Cancer Res.*, 2004, **10**, 1446–1453.
45. R. P. Tanpure, B. L. Nguyen, T. E. Strecker, S. Aguirre, S. Sharma, D. J. Chaplin, B. G. Siim, E. Hamel, J. W. Lippert, G. R. Pettit, M. L. Trawick and K. G. Pinney, *J. Nat. Prod.*, 2011, **74**, 1568–1574.
46. R. P. Tanpure, T. E. Strecker, D. J. Chaplin, B. G. Siim, M. L. Trawick and K. G. Pinney, *J. Nat. Prod.*, 2010, **73**, 1093–1101.
47. J. L. Bolton, M. A. Trush, T. M. Penning, G. Dryhurst and T. J. Monks, *Chem. Res. Toxicol.*, 2000, **13**, 135–160.
48. L. K. Folkes, M. Christlieb, E. Madej, M. R. L. Stratford and P. Wardman, *Chem. Res. Toxicol.*, 2007, **20**, 1885–1894.
49. G. R. Pettit, A. J. Thornhill, B. R. Moser and F. Hogan, *J. Nat. Prod.*, 2008, **71**, 1561–1563.
50. S. Aprile, R. Zaninetti, E. Del Grosso, A. A. Genazzani and G. Groso, *J. Pharm. Biomed. Anal.*, 2013, **78-79**, 233–242.
51. L. Rice, C. Pampo, S. Lepler, A. M. Rojiani and D. W. Siemann, *Microvasc. Res.*, 2011, **81**, 44–51.
52. E. M. DeFeo, C.-L. Wu, W. S. McDougal and L. L. Cheng, *Nat. Rev. Urol.*, 2011, **8**, 301–311.
53. J. M. N. Duarte, H. Lei, V. Mlynárik and R. Gruetter, *Neuroimage*, 2012, **61**, 342–362.
54. G. J. Kemp and K. M. Brindle, *Diabetes*, 2012, **61**, 1927–1934.
55. C. Boesch, *J. Magn. Reson. Imaging*, 2007, **25**, 321–338.
56. M. ten Hove and S. Neubauer, *Heart Fail. Rev.*, 2007, **12**, 48–57.

57. T. Roussel, P. Giraudeau, H. Ratiney, S. Akoka and S. Cavassila, *J. Magn. Reson.*, 2012, **215**, 50–55.
58. K. Golman, L. E. Olsson, O. Axelsson, S. Månson, M. Karlsson and J. S. Petersson, *Br. J. Radiol.*, 2003, **76**, S118–S127.
59. P. Dutta, G. V. Martinez and R. J. Gillies, *Biophys. Rev.*, 2013, **5**, 271–281.
60. M. Karlsson, A. Gisselsson, S. K. Nelson, T. H. Witney, S. E. Bohndiek, G. Hansson, T. Peitersen, M. H. Lerche and K. M. Brindle, 2009, **106**, 19801–19806.
61. F. A. Gallagher, M. I. Kettunen, S. E. Day, D.-E. Hu, J. H. Ardenkjaer-Larsen, R. Zandt, P. R. Jensen, M. Karlsson, K. Golman, M. H. Lerche and K. M. Brindle, *Nature*, 2008, **453**, 940–944.
62. S. J. Nelson, J. Kurhanewicz, D. B. Vigneron, P. E. Z. Larson, A. L. Harzstark, M. Ferrone, M. van Criekinge, J. W. Chang, R. Bok, I. Park, G. Reed, L. Carvajal, E. J. Small, P. Munster, V. K. Weinberg, J. H. Ardenkjaer-Larsen, A. P. Chen, R. E. Hurd, L.-I. Odegardstuen, F. J. Robb, J. Tropp and J. A. Murray, *Sci. Transl. Med.*, 2013, **5**, 198ra108.
63. K. Brindle, *Nat. Rev. Cancer*, 2008, **8**, 94–107.
64. S. B. Duckett and R. E. Mewis, *Acc. Chem. Res.*, 2012, **45**, 1247–1257.
65. T. Trantzsche, J. Bernarding, M. Plaumann, D. Lego, T. Gutmann, T. Ratajczyk, S. Dillenberger, G. Buntkowsky, J. Bargon and U. Bommerich, *Phys. Chem. Chem. Phys.*, 2012, **14**, 5601–5604.
66. S. Kadlec, V. Vahdat, T. Nakayama, D. Ng, K. Emami and R. Rizi, *NMR Biomed.*, 2011, **24**, 933–942.
67. A. W. Overhauser, *Phys. Rev.*, 1953, **92**, 411–415.
68. A. B. Barnes, G. De Paëpe, P. C. A. van der Wel, K.-N. Hu, C.-G. Joo, V. S. Bajaj, M. L. Mak-Jurkauskas, J. R. Sirigiri, J. Herzfeld, R. J. Temkin and R. G. Griffin, *Appl. Magn. Reson.*, 2008, **34**, 237–263.
69. K. Brindle, *Br. J. Radiol.*, 2012, **85**, 697–708.

70. K. Golman and J. S. Petersson, *Acad. Radiol.*, 2006, **13**, 932–942.
71. J. H. Ardenkjaer-Larsen, B. Fridlund, A. Gram, G. Hansson, L. Hansson, M. H. Lerche, R. Servin, M. Thaning and K. Golman, *Proc. Natl. Acad. Sci. U. S. A.*, 2003, **100**, 10158–10163.
72. L. Lumata, M. E. Merritt, C. R. Malloy, A. D. Sherry and Z. Kovacs, *J. Phys. Chem. A*, 2012, **116**, 5129–5138.
73. C. Gabellieri, S. Reynolds, A. Lavie, G. S. Payne, M. O. Leach and T. R. Eykyn, *J. Am. Chem. Soc.*, 2008, **130**, 4598–4599.
74. M. C. Cassidy, H. R. Chan, B. D. Ross, P. K. Bhattacharya and C. M. Marcus, *Nat. Nanotechnol.*, 2013, **8**, 363–368.
75. M. E. Merritt, C. Harrison, Z. Kovacs, P. Kshirsagar, C. R. Malloy and A. D. Sherry, *J. Am. Chem. Soc.*, 2007, **129**, 12942–12943.
76. S. Kambourakis, K. M. Draths and J. W. Frost, *J. Am. Chem. Soc.*, 2000, **122**, 9042–9043.
77. H. Yoshida and H. Yamada, *Agric. Biol. Chem.*, 1985, **49**, 659–663.
78. Jap. Pat., JP 1997–291053, 1997.
79. C. A. Hansen and J. W. Frost, *J. Am. Chem. Soc.*, 2002, **124**, 5926–5927.
80. Jap. Pat., JP 11158099A, 1999.
81. M. T. Shipchandler, C. A. Peters and C. D. Hurd, *J. Chem. Soc., Perkins Trans. I*, 1975, 1400–1401.
82. H. H. Wasserman and J. E. Pickett, *Tetrahedron*, 1985, **41**, 2155–2162.
83. M. F. Oldfield, L. Chen and N. P. Botting, *Tetrahedron*, 2004, **60**, 1887–1893.
84. L. J. Marshall, K. M. Cable and N. P. Botting, *J. Label. Compd. Radiopharm.*, 2010, **53**, 601–604.

85. S. D. Boyce, A. C. Barefoot and J. F. Hornig, *J. Label. Compd. Radiopharm.*, 1983, **20**, 243–256.
86. H. Oda, T. Kobayashi, M. Kosugi and T. Migita, *Tetrahedron*, 1995, **51**, 695–702.
87. Y. Tamura and Y. Yoshimoto, *Chem. Ind.*, 1980, 888–889.
88. A. S. Kotnis, *Tetrahedron Lett.*, 1991, **32**, 3441–3444.
89. J. M. Kim, K. Y. Lee and J. N. Kim, *Bull. Korean Chem. Soc.*, 2003, **24**, 1057–1058.
90. E. H. Sessions, M. Smolinski, B. Wang, B. Frackowiak, S. Chowdhury, Y. Yin, Y. T. Chen, C. Ruiz, L. Lin, J. Pocas, T. Schröter, M. D. Cameron, P. LoGrasso, Y. Feng and T. D. Bannister, *Bioorg. Med. Chem. Lett.*, 2010, **20**, 1939–1943.
91. G. Casiraghi, G. Casnati, M. Cornia, A. Pochini, G. Puglia, G. Sartorti and R. Ungaro, *J. Chem. Soc., Perkins Trans. 1*, 1978, 318–321.
92. A. R. Haight, A. E. Bailey, W. S. Baker, M. H. Cain, R. R. Copp, J. A. Demattei, K. L. Ford, R. F. Henry, M. C. Hsu, R. F. Keyes, S. A. King, M. A. McLaughlin, L. M. Melcher, W. R. Nadler, P. A. Oliver, S. I. Parekh, H. H. Patel, L. S. Seif, M. A. Staeger, G. S. Wayne, S. J. Wittenberger and W. Zhang, *Org. Process Res. Dev.*, 2004, **8**, 897–902.
93. M. Matsumoto, H. Kobayashi and Y. Hotta, *J. Org. Chem.*, 1984, **49**, 4740–4741.
94. US pat., US 7 973 185 B2, 2011.
95. U. Wriede, M. Fernandez, K. F. West, D. Harcourt and H. W. Moore, *J. Org. Chem.*, 1987, **52**, 4485–4489.
96. M. C. Carreño, J. L. G. Ruano, G. Sanz, M. A. Toledo and A. Urbano, *Tetrahedron Lett.*, 1996, **37**, 4081–4084.
97. T. Yamamoto, K. Toyota and N. Morita, *Tetrahedron Lett.*, 2010, **51**, 1364–1366.
98. J. Qi, H. Deng and D. Cao, *Sci. China Chem.*, 2010, **53**, 2547–2550.

99. A. S. Castanet, F. Colobert and P.-E. Broutin, *Tetrahedron Lett.*, 2002, **43**, 5047–5048.
100. G. Olah and Q. Wang, *J. Org. Chem.*, 1993, **58**, 3194–3195.
101. G. K. S. Prakash, T. Mathew, D. Hoole, P. M. Esteves, Q. Wang, G. Rasul and G. A. Olah, *J. Am. Chem. Soc.*, 2004, **126**, 15770–15776.
102. Y. Zhang, K. Shibatomi and H. Yamamoto, *Synlett*, 2005, 2837–2842.
103. C.-Y. Zhou, J. Li, S. Peddibhotla and D. Romo, *Org. Lett.*, 2010, **12**, 2104–2107.
104. B. W. Carlson and L. L. Miller, *J. Am. Chem. Soc.*, 1985, **107**, 479–485.
105. T. Takata, R. Tajima and W. Ando, *J. Org. Chem.*, 1983, **20**, 4764–4766.
106. S. Yamaguchi, M. Nedachi, H. Yokoyama and Y. Hirai, *Tetrahedron Lett.*, 1999, **40**, 7363–7365.
107. N. J. Lawrence, F. A. Ghani, L. A. Hepworth, J. A. Hadfield, A. T. McGown and R. G. Pritchard, *Synthesis (Stuttg.)*, 1999, 1656–1660.
108. M. Shigeta, J. Watanabe and G. Konishi, *Tetrahedron Lett.*, 2013, **54**, 1761–1764.
109. H. Lütjens and P. J. Scammells, *Tetrahedron Lett.*, 1998, **39**, 6581–6584.
110. O. García, E. Nicolás and F. Albericio, *Tetrahedron Lett.*, 2003, **44**, 4961–4963.
111. G. R. Pettit, A. Thornhill, N. Melody and J. C. Knight, *J. Nat. Prod.*, 2009, **72**, 380–388.
112. J. J. Eisch and J. N. Gitua, *Organometallics*, 2003, **22**, 24–26.
113. S. Andersson, *Synthesis (Stuttg.)*, 1985, 437–439.
114. S. Cabiddu, A. Maccioni, P. P. Piras and M. Secci, *J. Organomet. Chem.*, 1977, **136**, 139–146.

115. D.-J. Dong, H.-H. Li and S.-K. Tian, *J. Am. Chem. Soc.*, 2010, **132**, 5018–5020.
116. H. Yamataka, K. Nagareda, K. Ando and T. Hanafusa, *J. Org. Chem.*, 1992, **57**, 2865–2869.
117. E. Vedejs and C. F. Marth, *J. Am. Chem. Soc.*, 1988, **110**, 3948–3958.
118. P. A. Byrne and D. G. Gilheany, *J. Am. Chem. Soc.*, 2012, **134**, 9225–9239.
119. M. Schlosser and K. F. Christmann, *Angew. Chemie Int. Ed.*, 1966, **5**, 126.
120. A. B. Reitz, S. O. Nortey, A. D. Jordan, M. S. Mutter and B. E. Maryanoff, *J. Org. Chem.*, 1986, **51**, 3302–3308.
121. P. Lupattelli, M. D’Auria, N. Di Blasio and F. Lenti, *European J. Org. Chem.*, 2009, 141–145.
122. S. Yamashita, *Bull. Chem. Soc. Jpn.*, 1961, **34**, 972–976.
123. W. J. Muizebelt and R. J. F. Nivard, *J. Chem. Soc.*, 1968, 913–920.
124. R. W. Murray and M. Singh, *Org. Synth.*, 1997, **74**, 91–96.
125. Correspondence with David Chaplin at OXiGENE Inc.
126. R. T. Brown, V. L. Murrell, A. McMordie, M. Sriram, K. G. Pinney, S. Sharma and D. J. Chaplin, *J. Label. Compd. Radiopharm.*, 2009, **52**, 567–570.
127. T. Doura, R. Hata, H. Nonaka, K. Ichikawa and S. Sando, *Angew. Chemie - Int. Ed.*, 2012, **51**, 10114–10117.
128. A. Bianchi and A. Bernardi, *J. Org. Chem.*, 2006, **71**, 4565–4577.
129. R. B. Boers, P. Gast, A. J. Hoff, H. J. M. De Groot and J. Lugtenburg, *Eur. J. Org. Chem.*, 2002, 189–202.
130. A. Gryff-Keller and P. Szczeciński, *J. Mol. Struct.*, 2010, **967**, 94–98.
131. L. J. Gooßen, C. Linder, N. Rodríguez, P. P. Lange and A. Fromm, *Chem.*

- Commun. (Camb)*., 2009, 7173–7175.
132. U. Azzena, T. Denurra, G. Melloni and A. M. Piroddi, *J. Org. Chem.*, 1990, **55**, 5386–5390.
 133. L. F. Tietze, L. Ma, R. Reiner, S. Jackenkroll and S. Heidemann, *Chem. Eur. J.*, 2013, **19**, 8610–8614.
 134. A. Sharma, R. Kumar, N. Sharma, V. Kumar and A. K. Sinha, *Adv. Synth. Catal.*, 2008, **350**, 2910–2920.
 135. H. Sai, T. Ogiku, H. Ohmizu and A. Ohtani, *Chem. Pharm. Bull.*, 2006, **54**, 1686–1693.
 136. P. M. Pelphrey, V. M. Popov, T. M. Joska, J. M. Beierlein, E. S. D. Bolstad, Y. A. Fillingham, D. L. Wright and A. C. Anderson, *J. Med. Chem.*, 2007, **50**, 940–950.
 137. E. Yoshioka, S. Kohtani and H. Miyabe, *Org. Lett.*, 2010, **12**, 1956–1959.
 138. W. Fleischhacker, B. Richter and E. Urban, *Monatshefte für Chemie*, 1989, **120**, 765–769.
 139. M. Dal Molin, G. Gasparini, P. Scrimin, F. Rastrelli and L. J. Prins, *Chem. Commun.*, 2011, **47**, 12476–12478.
 140. M. A. Rizzacassa and M. V. Sargent, *J. Chem. Soc., Perkins Trans. I*, 1987, 2017–2022.
 141. B. A. McKittrick and R. Stevenson, *J. Chem. Soc. Perkin Trans. I*, 1984, 709 – 712.
 142. T. Cardolaccia, Y. Li and K. S. Schanze, *J. Am. Chem. Soc.*, 2008, **130**, 2535–2545.
 143. M. G. Banwell, E. Hamel, D. C. R. Hockless, P. Verdier-Pinard, A. C. Willis and D. J. Wong, *Bioorganic Med. Chem.*, 2006, **14**, 4627–4638.
 144. S. Bhadra, W. I. Dzik and L. J. Goossen, *J. Am. Chem. Soc.*, 2012, **134**, 9938–9941.

145. T. Asakawa, A. Hiza, M. Nakayama, M. Inai, D. Oyama, H. Koide, K. Shimizu, T. Wakimoto, N. Harada, H. Tsukada, N. Oku and T. Kan, *Chem. Commun. (Camb)*., 2011, **47**, 2868–2870.
146. R. Prebil, G. Stavber and S. Stavber, *European J. Org. Chem.*, 2014, 395–402.
147. A. Shirali, M. Sriram, J. J. Hall, B. L. Nguyen, R. Guddneppanavar, M. B. Hadimani, J. F. Ackley, R. Siles, C. J. Jelinek, P. Arthasery, R. C. Brown, V. L. Murrell, A. McMordie, S. Sharma, D. J. Chaplin and K. G. Pinney, *J. Nat. Prod.*, 2009, **72**, 414–421.
148. T. M. Beale, P. J. Bond, J. D. Brenton, D. S. Charnock-Jones, S. V. Ley and R. M. Myers, *Bioorganic Med. Chem.*, 2012, **20**, 1749–1759.
149. D. J. Dong, H. H. Li and S. K. Tian, *J. Am. Chem. Soc.*, 2010, **132**, 5018–5020.
150. M. Baumert, M. Albrecht, H. D. F. Winkler and C. A. Schalley, *Synthesis (Stuttg)*., 2010, 953–958.
151. D. Imperio, T. Pirali, U. Galli, F. Pagliai, L. Cafici, P. L. Canonico, G. Sorba, A. A. Genazzani and G. C. Tron, *Bioorganic Med. Chem.*, 2007, **15**, 6748–6757.
152. A. F. Barrero, M. M. Herrador, J. F. Quílez del Moral, P. Arteaga, M. Akssira, F. El Hanbali, J. F. Arteaga, H. R. Diéguez and M. Sánchez, Elena, *J. Org. Chem.*, 2007, **76**, 2251–2254.
153. Y. Lu, C.-M. Li, Z. Wang, J. Chen, M. L. Mohler, W. Li, J. T. Dalton and D. D. Miller, *J. Med. Chem.*, 2011, **54**, 4678–4693.
154. F. Alonso, P. Riente and M. Yus, *European J. Org. Chem.*, 2009, 6034–6042.
155. R. Siles, J. F. Ackley, M. B. Hadimani, J. J. Hall, B. E. Mugabe, R. Guddneppanavar, K. A. Monk, J. C. Chapuis, G. R. Pettit, D. J. Chaplin, K. Edvarlsen, M. L. Trawick, C. M. Garner and K. G. Pinney, *J. Nat. Prod.*, 2008, **71**, 313–320.
156. V. Kikelj, S. Grosjean, J. C. Meslin, K. Julienne and D. Deniaud, *Synthesis (Stuttg)*., 2010, 2811–2815.